Dissertation
submitted to the
Combined Faculties for the Natural Sciences and for Mathematics
of the Ruperto-Carola University of Heidelberg, Germany
for the degree of
Doctor of Natural Sciences

Presented by Rūta Veinalde, M.Sc.
born in: Riga, Latvia
Oral examination: May 30, 2017

Unraveling Determinants of Efficacy in Measles Immunovirotherapy

Referees:
Prof. Dr. Ralf Bartenschlager
Prof. Dr. Christof von Kalle

Abstract

Replicating oncolytic viruses (OVs) that are able to selectively destroy malignant cells are emerging as clinically relevant cancer therapeutics. Along with direct tumor cell lysis, activation of specific anti-tumor immune responses contributes to efficacy of virotherapy, allowing to consider it for a type of cancer immunotherapy. Combinations with different immunomodulation strategies have been shown to enhance the immunostimulatory effects of OVs and contribute to increased therapeutic efficacy. Based on the hypothesis that certain immunomodulation types might more efficiently contribute to efficacy of virotherapy in a given tumor type, this study compared efficacy of oncolytic measles vectors encoding immunomodulators from different classes. Furthermore, to identify immune effector mechanisms associated with successful therapeutic strategies, analysis of the tumor immune environment was performed following treatment with the most promising vectors.

Measles Schwarz vaccine strain vectors (MeVac) encoding immunomodulators to target the main phases in establishment of an anti-tumor immune response were developed. Therapeutic efficacy of the novel vectors was compared in a fully immunocompetent murine colon adenocarcinoma model, MC38cea. MeVac vectors encoding an antibody against the negative T cell regulator PD-L1 (anti-PD-L1) and a fusion protein of murine interleukin-12 (FmIL-12), respectively, were identified as the most promising in terms of increased survival of animals. Importantly, MeVac encoding FmIL-12 was the most effective, ensuring complete tumor remissions in 90% of the treated animals. After MeVac therapy, long-term survivors rejected secondary tumor engraftments, indicating establishment of a systemic anti-tumor immune response. Profiling of the tumor environment four days after the last treatment with the anti-PD-L1 encoding vector revealed a slight benefit for cell mediated immune responses, as observed by a slight upregulation of the effector cytokines IFN-γ and TNF-α as well as an increase in the intratumoral T cell population. More pronounced modulation of the tumor immune environment was observed following treatment with the FmIL-12 encoding vector. One day after treatment with MeVac encoding FmIL-12 an increase of effector cytokines IFN-γ and TNF-α was observed, suggesting activation of a cell mediated immune response. Analysis of tumor infiltrating lymphocytes revealed an increase in the T cell population, a massive decrease in the natural killer (NK) cell population and upregulation of an activation marker on NK cells. These results indicated early activation of the immune effector cells following treatment with MeVac encoding FmIL-12, which in case of the NK cells could be associated with activation induced cell death. Furthermore, immune cell depletion experiments revealed that the $CD4^+$ T cells and NK cells do not importantly contribute to the therapeutic efficacy of the MeVac encoding FmIL-12 in this model, but that the cytotoxic $CD8^+$ T cells are essential.

This study presents MeVac encoding FmIL-12 as an effective therapeutic for activation of cell mediated anti-tumor immune responses. Furthermore, the MeVac vector is established as a flexible platform for targeted local delivery of immunomodulators. The tumor immune profiling data provide a basis for further rational vector modifications to develop immunomodulation strategies tailored to the individual tumor immune environment.

Zusammenfassung

Replizierende onkolytische Viren (OVs), die selektiv maligne Zellen zerstören, gewinnen zunehmend klinische Bedeutung in der Behandlung verschiedener Tumorerkrankungen. Neben der unmittelbaren Lyse von Tumorzellen trägt die Aktivierung einer Tumor-spezifischen Immunantwort zur therapeutischen Effizienz bei. Entsprechend kann die Virotherapie als eine Form der Tumor-Immuntherapie betrachtet werden. Kombinationen verschiedener Immunmodulatoren mit OVs können die immunstimulatorischen Effekte verstärken und zu einer besseren Wirksamkeit beitragen. Ausgehend von der Hypothese, dass bestimmte Immunmodulatoren in bestimmten Tumorarten stärker zur Wirksamkeit der onkolytischen Virotherapie beitragen, wurden in dieser Arbeit onkolytische Masernviren verglichen, die verschiedene Klassen von Immunmodulatoren kodieren. Um immunologische Mechanismen zu identifizieren, die mit einer erfolgreichen Behandlung assoziiert sind, wurde nach Applikation der vielversprechendsten Vektoren das immunologische Mikromilieu der Tumoren analysiert. Vom Schwarz-Impfstamm abgeleitete Masern-Viren (MeVac) wurden entwickelt, um die wesentlichen Phasen der Induktion einer Anti-Tumor-Immunantwort zu verstärken. Die therapeutische Effizienz der neuen Vektoren wurde in einem immunkompetenten Mausmodell des Kolonadenokarzinoms, MC38cea, verglichen. MeVac-Vektoren, welche einen Antikörper gegen den T-Zell-inhibitorischen Faktor PD-L1 (anti-PD-L1) beziehungsweise ein murines Interleukin-12-Fusionsprotein (FmIL-12) kodieren, wurden als die vielversprechendsten Vektoren identifiziert, basierend auf einem verlängerten Überleben der behandelten Tiere. Der MeVac-Vektor, der FmIL-12 kodiert, zeigte eine herausragende therapeutische Effizienz: Die Behandlung mit MeVac FmIL-12 führte bei 90% der behandelten Tiere zu einer kompletten Remission. Nach MeVac-Behandlung stießen überlebende Tiere sekundär implantierte Tumoren ab, ein Hinweis auf die Induktion einer systemischen Anti-Tumor-Immunantwort. Vier Tage nach Behandlung mit den anti-PD-L1 kodierenden Vektoren wies das Tumor-Immunprofil auf eine leicht verstärkte zelluläre Immunantwort hin, erkennbar an einer Hochregulation der Effektor-Zytokine IFN-γ und TNF-α sowie einer Zunahme der intratumoralen T-Zell-Population. Nach Behandlung mit dem FmIL-12 kodierenden Vektor wurde eine durchgreifendere Änderung des Tumormilieus beobachtet. Einen Tag nach der Behandlung mit MeVac FmIL-12 wurde ein Anstieg der Effektor-Zytokine IFN-γ und TNF-α gemessen, ein Hinweis auf eine zelluläre Immunantwort. Die Analyse der Tumorinfiltrierenden Lymphozyten zeigte eine Zunahme der T-Zell-Population, eine drastisch verringerte Anzahl der natürlichen Killer (NK)-Zellen sowie Hochregulation eines Aktivierungs-Markers auf den NK-Zellen. Diese Ergebnisse weisen auf eine frühe Aktivierung dieser Immun-Effektorzellen nach Behandlung mit MeVac FmIL-12 hin, wobei dies im Fall der NK-Zellen mit einem Aktivierungs-induzierten Zelltod einhergehen könnte. Desweiteren zeigte Depletions-Experimente, dass $CD4^+$ T-Zellen und NK-Zellen nicht wesentlich zur therapeutischen Effizienz von MeVac FmIL-12 in diesem Tumormodell beitragen, während zytotoxische $CD8^+$ T-Zellen essentiell sind. Diese Arbeit präsentiert MeVac FmIL-12 als effektive Therapie zur Aktivierung zellulärer Anti-Tumor-Immunantworten. Darüber hinaus wurden MeVac-Vektoren als flexible Plattform zur gezielten, lokalen Darreichung von Immunmodulatoren etabliert. Die Tumor-Immunprofil-Daten bilden die Basis für eine rationale Vektor-Modifikation zur Entwicklung immunmodulatorischer Therapie-Ansätze, die auf das individuelle Tumormilieu zugeschnitten sind.

Kopsavilkums

Replicēties spējīgi onkolītiskie vīrusi (OV), kas specifiski iznīcina ļaundabīgas šūnas, ieņem vietu starp jauniem, klīniski nozīmīgiem vēža terapijas veidiem. Viroterapijas efektivitāte ir balstīta ne tikai uz tiešu vēža šūnu iznīcināšanu, bet arī uz specifiskas pretvēža imūnās atbildes aktivāciju, kas ļauj to uzskatīt par audzēju imūnterapijas veidu. Pētījumi rāda, ka dažādu veidu imūnmodulatori spēj paaugstināt OV imūnstimulatorās īpašības, uzlabojot terapijas efektivitāti. Balstoties uz hipotēzi, ka konkrēti imūnmodulācijas veidi ir vairāk piemēroti viroterapijas efektivitātes uzlabošanai konkrētā audzēja veidā, šajā pētījumā tika salīdzināti onkolītiska masalu vīrusa vektori, kuros iekodēti imūnomodulatori no dažādām klasēm. Turklāt, lai noteiktu imūnās sistēmas efektoros mehānismus, kas saistīti ar veiksmīgākajām terapijas stratēģijām, tika veikta audzēja imūno profilu analīze pēc terapijas ar daudzsološākajiem vektoriem.

Tika izveidoti masalu *Schwarz* vakcīnas vīrusa (MeVac) vektori, kuros iekodēti imūnmodulatori, kas atbalsta dažādas pretvēža imūnās atbildes veidošanās fāzes. Jauno vektoru terapeitiskā efektivitāte tika salīdzināta imūnkompetentā peļu kolorektālās adenokarcinomas modelī MC38cea. Kā daudzsološākie tika noteikti vektori, kuri spēja palielināt dzīvnieku izdzīvotību. Tie bija vektori, kuros iekodēta antiviela pret T šūnu inhibitoro faktoru PD-L1 (MeVac anti-PD-L1), kā arī peļu interleikīna-12 proteīna veids (MeVac FmIL-12). Nozīmīgi, ka MeVac FmIL-12 parādīja augstāko efektivitāti, nodrošinot pilnīgu audzēju remisiju 90% no terapiju saņēmušajiem dzīvniekiem. Izārstētie dzīvnieki atgrūda sekundāru audzēju veidošanos, norādot uz sistēmiskas pretvēža imūnās atbildes klātbūtni. Audzēja imūnās vides analīze četras dienas pēc pēdējās anti-PD-L1 kodējošā vektora devas atklāja nedaudz paaugstinātu efektoro citokīnu IFN-γ un TNF-α koncentrāciju un nelielu T šūnu populācijas pieaugumu, norādot uz vieglu šūnu mediētās imūnatbildes pastiprināšanos. Pēc terapijas ar MeVac FmIL-12 tika novērota izteiktāka audzēja imūnās vides modulācija. Vienu dienu pēc pēdējās MeVac FmIL-12 devas tika novērots efektoro citokīnu IFN-γ un TNF-α koncentrācijas pieaugums, norādot uz šūnu mediētās imūnatbildes aktivāciju. Analizējot galvenās audzējos infiltrējušos limfocītu subpopulācijas, tika atklāts T šūnu populācijas pieaugums, liels dabīgo galētājšūnu (NK) populācijas samazinājums, kā arī aktivācijas marķiera ekspresijas pieaugums NK šūnu populācijā. Šie rezultāti norāda uz agrīnu imūno efektoru aktivāciju pēc MeVac FmIL-12 terapijas, kas attiecībā uz NK šūnām varētu būt saistīta ar aktivācijas ierosinātu šūnu nāvi. Tālāki imūno šūnu populāciju izslēgšanas eksperimenti parādīja, ka šajā modelī $CD4^+$ T šūnām un NK šūnām nav nozīmīgas ietekmes uz MeVac FmIL-12 terapijas efektivitāti, bet ka $CD8^+$ T šūnu klātbūtne ir īpaši būtiska.

Šis pētījums atklāj MeVac FmIL-12 kā efektīvu terapijas veidu šūnu mediētās pretvēža imūnatbildes aktivēšanai un demonstrē MeVac vektora sistēmu kā elastīgu platformu mērķētai, lokālai imūnmodulatoru piegādei. Turklāt iegūtie audzēju imūnās profilēšanas rezultāti veido pamatu turpmākai racionālai vektoru izstrādei, lai attīstītu imūnmodulācijas stratēģijas, kas ir individuāli piemērotas konkrētā audzēja imūnajai videi.

Contents

Abstract **III**

Zusammenfassung **V**

Kopsavilkums **VII**

Abbreviations **XIII**

1 Introduction **1**

1.1 The Immune System — a Sentinel of Homeostasis 1
1.2 Cancer — Evasion from Immune Surveillance 1
1.3 Cancer Immunotherapy 2
1.3.1 Classification and Principles of Immunotherapies 2
1.3.2 Cytokine Therapies 3
1.3.3 Immune Checkpoint Blockade 5
1.4 Oncolytic Viruses as a Type of Immunotherapy 7
1.4.1 Principles of virotherapy 7
1.4.2 Immunomodulatory Properties of Virotherapy 8
1.4.3 Combinations with Other Immunotherapies 8
1.5 Measles Virus 10
1.5.1 Biology of Measles Virus 10
1.5.2 Measles Vaccine Strain Viruses 11
1.5.3 Measles as an Oncolytic Virus 12

2 Aim of the Study **15**

3 Materials and Methods **17**

3.1 Materials 17
3.1.1 Chemicals 17
3.1.2 Buffers 17
3.1.3 Growth Media for Bacterial and Cell Culture 18
3.1.4 Oligonucleotides 18
3.1.5 Antibodies 21
3.1.6 DNA Plasmids 22
3.1.7 Cell Lines 28
3.1.8 Recombinant Measles Viruses 29
3.2 Methods 30

3.2.1 Standard DNA and RNA Molecular Biology Methods 30
3.2.2 Cell culture 32
3.2.3 Recombinant Measles Viruses 33
3.2.4 Cell Viability Assay 35
3.2.5 Detection of MeVac Encoded Transgene Expression 35
3.2.6 Functional Assays for MeVac Encoded Immunomodulators 37
3.2.7 *In vivo* Experiments 38
3.2.8 Experiments with Murine Tissues 39
3.2.9 Immune Profiling of Tumor Environment 40
3.2.10 Statistical Analyses 41

4 Results **43**
4.1 Construction and Characterization of Recombinant MeVac *in vitro* 43
4.1.1 Additional Transcription Unit Behind the *Hemagglutinin* Gene 43
4.1.2 Construction of MeVac Encoding Immunomodulators 44
4.1.3 Retargeting of MeVac Hemagglutinin 47
4.1.4 Replication Kinetics and Cytotoxic Effects 48
4.1.5 Transgene Expression and Functionality 51
4.2 Evaluation of Therapeutic Efficacy *in vivo* 55
4.2.1 Identification of the Most Promising Vectors 56
4.2.2 Therapeutic Efficacy of the Most Promising Vectors 57
4.2.3 Assessment of anti-tumor immune response in long-term survivors of MeVac therapy 60
4.3 Analysis of MeVac induced Anti-Tumor Immune Effector Mechanisms 62
4.3.1 Quantification of Transcription Factor Expression 63
4.3.2 Cytokine Expression Profiling 64
4.3.3 Analysis of Tumor Infiltrating Lymphocyte Subpopulations 65
4.3.4 Identification of Immune Effectors Crucial for the Efficacy of the MeVac encoding FmIL-12 69
4.4 Consideration of the Translational Potential 70
4.4.1 MeVac Encoding a Human IL-12 Fusion Protein 71
4.4.2 Potential of Oncolytic MV for Treatment of Colorectal Cancer 73

5 Discussion **77**
5.1 Perspectives of Immunovirotherapy 77
5.2 Construction and Characterization of Recombinant Oncolytic Measles Vectors 78
5.3 Immunomodulation for Enhanced Efficacy of Oncolytic Measles Virus 82
5.4 Immune Effector Mechanisms in Measles Immunovirotherapy 86
5.5 Translational Potential 90
5.6 Conclusions and Outlook 92

Appendix **95**

Bibliography **115**

Publications **143**

Congress Contributions **145**

Acknowledgements **147**

Thesis Declaration **149**

Abbreviations

Ab	Antibody
ACK	Ammonium-Chloride-Potassium
AdV	Adenovirus
ANOVA	Analysis of variance
APC	Antigen presenting cell or allophycocyanine
ATU	Additional transcription unit
BiTE	Bispecific T cell engager
bp	Basepairs
C_q	Quantification cycle
CD80-Fc	Protein CD80 and IgG1-Fc fusion protein
cDNA	Complementary DNA
CEA	Carcinoembryonic antigen
ciu	Cell infectious units
CRC	Colorectal cancer
CTLA-4	Cytotoxic T-lymphocyte-associated protein 4
Cy	Cyanine
DAPI	4',6-diamidino-2-phenylindole
DC	Dendritic cell
DIs	Defective interfering particles
DLTs	Dose limiting toxicities
DMEM	Dulbecco's Modified Eagle's medium
DNA	Deoxyribonucleic acid
D-PBS	Dulbecco's Phosphate-Buffered Saline
E. coli	*Escherichia coli*
EDTA	Ethylenediaminetetraacetic acid
eGFP	Enhanced green fluorescent protein

ELISA	Enzyme-linked immunosorbent assay
F	Measles virus fusion protein
FC	Flow cytometry
FCS	Fetal calf serum
FDA	The Food and Drug Administration of the United States of America
FhIL-12	Human IL-12 fusion protein
FITC	Fluorescein isothiocyanate
FmIL-12	Murine IL-12 fusion protein
FSC-A	Forward scatter-area
GM-CSF	Granulocyte macrophage colony-stimulating factor
H	Measles virus hemagglutinin
Hbl	"Blinded" measles H
HSV	Herpesvirus
i.p.	Intraperitoneal
i.t.	Intratumoral
i.v.	Intravenous
IFN	Interferon
IL	Interleukin
IP-10	Interferon-γ-inducible protein 10
kbp	Kilobase pairs
L	Measles virus polymerase
LB	Lysogeny broth
ld	Measles leader
M	Measles virus matrix protein
mAb	Monoclonal antibody
MeV	Wild-type measles virus
MeVac	Measles Schwarz vaccine strain virus
MFI	Median fluorescence intensity
MHC-I	Major histocompatibility class I
Mig	Monokine induced by interferon-γ

MOI	Multiplicity of infection
mRNA	Messenger RNA
MV	Measles vaccine strain virus
MV-EZ	Measles Edmonston-Zagreb vaccine strain virus
N	Measles virus nucleoprotein
NDV	Newcastle disease virus
NEB	New England Biolabs
NIS	Sodium iodide symporter
NK	Natural killer
NSCLC	Non-small cell lung cancer
NSe	Edmonston B derived measles vaccine strain virus (*Nar-Spe* eliminated)
NTC	No template control
ORF	Open reading frame
OV	Oncolytic virus
P	Measles virus phosphoprotein
P/S	Penicillin-Streptomycin
PCR	Polymerase chain reaction
PD-1	Programmed cell death protein 1
PE	Phycoerythrin
PerCP	Peridinin chlorophyll protein complex
PD-L1	Programmed death-ligand 1
PMA	Phorbol 12-myristate 13-acetate
PRR	Pathogen recognition receptor
PVDF	Polyvinylidene difluoride
PVRL-4	Poliovirus receptor-like 4
RCC	Renal cell carcinoma
RNA	Ribonucleic acid
RPMI	Roswell Park Memorial Institute medium
RT-PCR	Reverse transcription PCR
RT-qPCR	Reverse transcription-quantitative PCR

scAb	Single chain antibody
SDS-PAGE	Sodium dodecyl sulfate-polyacrylamide gel electrophoresis
SLAM	Signaling lymphocyte activation molecule
SSC-A	Side scatter-area
$\mathbf{T_{reg}}$	T regulatory cell
TAA	Tumor-associated antigen
TBS-T	Tris-buffered saline-Tween
TCR	T cell receptor
Tg	Transgene
$\mathbf{Th_{1/2/17}}$	T helper type 1/2/17
TIL	Tumor infiltrating lymphocyte
TNF-α	Tumor necrosis factor-α
tr	Measles trailer
T-VEC	Talimogene laherparepvec
U.S.	The United States of America
v/v	Volume/volume
VSV	Vesicular stomatitis virus
VV	Vaccinia virus
WB	Western blot
XTT	2,3-Bis-(2-Methoxy-4-Nitro-5-Sulfophenyl)-2H-Tetrazolium-5-Carboxanilide

1 Introduction

1.1 The Immune System — a Sentinel of Homeostasis

The existence of any developed multicellular organism relies on its ability to maintain a status of relative stability, homeostasis, despite constant encounters with environmental threats. Immune system is a set of complex defense mechanisms that provides an organism with a protection against exogenous and endogenous threats, including foreign and potentially harmful microorganisms, as well as altered and dying cells of the organism itself. The immune system of a human body has evolved into an extremely powerful defense system that involves mechanisms to respond to a given threat in a specific, adaptive manner and even form an immunological memory[1]. The power of an activated immune response is immense, ensuring a rapid and effective clearance of an invader, and is therefore constantly tightly regulated to avoid harm for normal tissues in the body and allow restoration of the steady state[2]. Thus, failures and errors in immune responses or their regulation disrupt the homeostatic balance in the organism and can result in dangerous conditions, including persistent bacterial and viral infections[3], autoimmune responses[4] and also development of cancer[5].

1.2 Cancer — Evasion from Immune Surveillance

The idea that the immune system plays a role in protection against development of cancer arose in the middle of the 20th century and became known as the cancer immmunosurveillance hypothesis[6]. However, convincing proof for this concept was delivered not until decades later, when appropriate mouse models with disrupted components of the immune system became available. For instance, mice which lack the recombination activating gene 2 (RAG-2) and are therefore unable to generate mature lymphocytes, have been shown to develop higher rates of chemically induced as well as spontaneously arising tumors in comparison to wild-type animals[7]. Later on, a dual role of the immune system in the development of cancer was recognized and the immunosurveillance hypothesis was followingly expanded to the theory of "cancer immunoediting"[8]. The cancer immunoediting theory proposes three stages during the development of cancer in the presence of a functional immune system, also known as the "three E's" — "elimination", "equilibrium" and "escape"[8]. During the "elimination" phase the immune system is able to destroy transformed cells, hindering establishment of a pre-malignant lesion. In "equilibrium" the immune response acts as a selective pressure, promoting development of less immunogenic tumor cells. In the "escape" phase variants of non-immunogenic tumor cells evade immune recognition and establish an aggressively growing tumor[8]. A great amount of data supporting the cancer immunoediting theory has

been obtained, establishing the concept of immunoediting as a paradigm in current cancer research[9].

1.3 Cancer Immunotherapy

1.3.1 Classification and Principles of Immunotherapies

The evidence for the crucial role of the immune system in the development of cancer formed the basis for investigation of therapeutic interventions in anti-tumor immune response mechanisms. Cancer immunotherapy is the term used for therapeutic strategies that either involve the use of immunological agents with intrinsic anti-tumor properties — passive immunotherapy — or that aim at modulating and activating anti-tumor immune responses in the body — active immunotherapy[10]. A classical example for passive immunotherapy is the use of monoclonal antibodies (mAbs) that, for instance, block receptors providing survival signals for malignant cells[11] or bind to and activate cell-death inducing receptors on tumor cells[12]. Another intensely investigated strategy of passive immunotherapy is adoptive cell transfer which aims at introducing a cell population that is enriched in potentially tumor reactive immune effector cells into the body[13]. Although passive immunotherapy strategies, mainly different anti-tumor mAbs, have demonstrated efficacy in certain tumor types and have successfully entered routine clinical use[14], active immunotherapy approaches offer more possibilities to take advantage of the power of the immune system.

Active immunotherapeutic strategies can be classified as unspecific — aiming at immune activation in general, and specific — aiming at inducing a response against defined antigens[15]. However, such stringent classification is difficult as with both approaches, specific and unspecific, ultimately an adaptive immune response, *ergo*, specific response against the individual tumor, can be elicited. Stimulation of the innate immune response with agonists of the pattern recognition receptors (PRRs) can be considered an example for an unspecific active immunotherapy. PRRs are proteins that recognize various bacterial and viral products that are collectively described as "danger signals"[16]. Activation of PRR signaling results in an inflammatory response that can provide unspecific by-stander anti-tumoral effects, as well as set the stage for activation of a specific adaptive anti-tumor immune response[17]. Several PRR agonists which mostly include different bacteria-derived products or synthetic molecules mimicking such products have been approved for treatment of cancer either as standalone therapies or adjuvants to other immunotherapeutics[17]. One of the best-known PRR agonists is an attenuated variant of *Mycobacterium bovis*, Bacillus Calmette-Guérin, which is among the oldest cancer immunotherapies currently in use and is a therapy option for superficial bladder cancer since the middle of the 1980s[18]. In contrast, therapeutic cancer vaccination with defined tumor-associated antigens (TAAs) represents a specific active immunotherapy. The currently investigated vaccination approaches represent a wide spectrum of methods, including use of cell-based strategies, whole proteins or peptides, of

the specific TAAs, as well as gene therapy approaches for administration of DNA, RNA or viral vectors encoding the respective TAA peptides along with some immunostimulatory adjuvant[19]. If successful, these vaccination methods are able to provide TAAs to antigen presenting cells (APCs) which are simultaneously activated by an adjuvant and can therefore present the peptides to effector cells to prime a TAA-specific immune response[19]. The only therapeutic cancer vaccine that has been approved for clinical application up to now is sipuleucel-T (trade name Provenge) for treatment of castration-resistant prostate cancer[20]. Sipuleucel-T represents a personalized immunotherapeutic approach as it contains *ex vivo* expanded APCs from the individual patient. After activation with a fusion protein consisting of prostatic acid phosphatase and granulocyte macrophage colony-stimulating factor the APCs are reinfused into the patient[20]. Although the approach seemed promising and could provide survival benefit for patients[20], this sophisticated procedure did not enter routine clinical application[21]. Active immunotherapeutic approaches that currently are more clinically relevant will be discussed in the next sections. These include immunostimulatory cytokine therapies and antibodies blocking the "immune checkpoints".

1.3.2 Cytokine Therapies

Cytokines are a family of secreted or membrane-bound proteins that coordinate intercellular communication in most physiological processes, including inflammation, cell differentiation, chemotaxis, immune responses and cell death[22]. As intercellular messengers, cytokines have a central role in the development of immune responses, including immune cell activation, suppression, differentiation and migration[23]. Given their powerful immunoregulatory properties, the role of cytokines in the development of cancer and their potential for stimulating anti-tumor immune responses have been investigated for a long time[24]. The first cytokine to enter routine clinical use as a single agent for cancer therapy was interleukin-2 (IL-2). IL-2 is a powerful T cell growth and activation factor, which was approved for treatment of renal cell carcinoma (RCC) and melanoma in the United States of America (U.S.) in 1992 and 1998, respectively[25]. However, the overall benefit of IL-2 therapy for patients has been modest. Although complete tumor regressions that can last for years have been achieved in individual patients, a durable response after a high dose IL-2 therapy in both melanoma and RCC is observed in 5 – 7% of cases[26]. The importance of IL-2 therapy is therefore more the proof of concept for the potential of an immunostimulatory cytokine in treatment of cancer and encouragement for further studies with other candidates.

IL-12 is a cytokine that, in the early 1990's, was initially met with a great excitment for its robust anti-tumor properties in different animal tumor models. In physiological conditions IL-12 is mainly produced by activated APCs and induces a cell-mediated immune response through activation of cytotoxic $CD8^+$ T cells and natural killer (NK) cells and determines differentiation of $CD4^+$ T cells towards a T helper type 1 (Th_1) phenotype[27]. Accordingly, the anti-tumor activity of the IL-12 in murine tumor models has been demonstrated to depend

on activation of tumor-infiltrating immune cells[28] and on additional anti-angiogenic effects exerted through induction of the interferon-γ-inducible protein 10 (IP-10)[29,30]. However, up to now, attempts to translate IL-12 into clinical application have not been particularly successful. Despite that, the history of clinical trials with IL-12 exemplifies gain of clinical experience with cytokine therapies that is used for generation of promising sophisticated cytokine-based immunotherapy approaches currently explored in pre-clinical and clinical settings.

In most of the early clinical trials IL-12 treatment failed to demonstrate meaningful efficacy and was associated with severe toxicities[31,32]. Nevertheless, these studies also revealed the crucial role of the dosing schedule, as pre-treatment with IL-12 was decisive to reduce IL-12-induced IFN-γ production upon further consecutive IL-12 injections and to minimize the adverse side effects[32]. Reduction of the treatment-associated toxicities and enhancement of the therapeutic efficacy was necessary if the IL-12 was to remain a candidate for clinical application, therefore clearly calling for more targeted application strategies than the intravenous (i.v.)[31], subcutaneous (s.c.)[33] or intraperitoneal (i.p.)[34] administration of a recombinant IL-12 used in most of the early studies. Targeted IL-12 delivery approaches that are currently being tested in clinical studies include intratumoral (i.t.) administration of IL-12 encoding DNA plasmid via electroporation (NCT01502293*, NCT01579318), i.t. injections with an adenovirus (AdV) vector encoding IL-12 (NCT02555397, NCT02026271) and administration of an IL-12 conjugated with a tumor-antigen-specific mAb (NCT01417546). These approaches have been successful at reducing the treatment-related toxicities. Also, at least for the gene therapy approaches with electroporation and AdV, the therapeutic efficacy has been encouraging, demonstrating the possibility to induce sytemic responses in non-injected lesions after local application[35,36].

There are many more cytokines that have been shown to stimulate anti-tumor immune responses and are investigated pre-clinically or have already entered clinical studies. To name just a few — the T and NK cell activation factors IL-15 (NCT01021059), IL-18[37] and interferon-γ (IFN-γ)[38], the APC maturation factor GM-CSF (granulocyte macrophage colony-stimulating factor)[39] and the chemotactic cytokines for recruitment of activated T and NK cells, IP-10 and MIG (monokine induced by IFN-γ)[40]. The number of studies investigating potential therapeutic benefits of cytokines as cancer therapeutics has been and continues to be tremendous. Yet, up to now, aside from IL-2, only two other cytokines have been approved for cancer treatment as monotherapies. Both of these are closely related molecules from the family of IFN-α which possess broad immunomodulatory properties, including activation of cytotoxic T and NK cells, induction of dendritic cell (DC) maturation and enhancement of tumor cell recognition by DCs and also have cytostatic and apoptotic effects in tumor cells and tumor-supporting cells[41]. The current, relatively modest output in clinically relevant therapeutics from the vast amount of the studied cytokines, as well limited

*Here and further, "NCT" followed by an eight digit number is a registry number for a clinical trial on ClinicalTrials.gov. `https://clinicaltrials.gov/`

benefit from the ones already approved, is mainly associated with similar problems as those described in the case of IL-12, namely much lower therapeutic efficacy than expected based on pre-clinical studies and treatment-associated toxicities[42]. Therefore, identification of appropriate dosing schedules, administration routes and vehicles as well as biomarkers predicting response to the therapy are the problems that will need to be addressed to guarantee success of clinical translation of immunomodulatory cytokines for cancer treatment. Furthermore, it is possible that with increasing understanding of the individual immunomodulatory properties, the activities of cytokines will be best taken advantage of in rational combinations with one another, as well as with other immunotherapeutic strategies.

1.3.3 Immune Checkpoint Blockade

The power of an activated T cell response is so potent that, if uncontrolled, it can manifest in autoimmune disorders[43]. Therefore, during all phases of the T cell-mediated immune responses, the extent and duration of T cell activity is tightly regulated by a balance of stimulatory and inhibitory signals that are collectively named "immune checkpoints"[44]. Many human tumor types take advantage of this immunoregulatory system by dysregulating the balance of the stimuli to favor the inhibitory signals and, thus, evade recognition and destruction by immune cells[45]. Disruption of this inhibitory signaling represents a novel strategy in cancer immunotherapy that is known as "immune checkpoint" blockade[44]. In contrast to most other immunotherapeutic strategies that aim at directly stimulating anti-tumor immune response, the checkpoint blockade aims at indirectly releasing the power of the immune response already in place by arresting the inhibitory signaling[44].

Antibodies that aim at modulating the so-called "second signal" for T cell activation are currently clinically the most relevant checkpoint blockade therapeutics. The "two signal" model (a simplified model for T cell activation) proposes that activation of a T cell occurs when the T cell receptor (TCR) recognizes the respective antigen in the context of major histocompatibility complex and receives a second, co-stimulatory signal through a co-receptor[46]. A myriad of stimulatory and inhibitory co-receptors is actually present on the surface of a T cell to allow context-dependent modulation of the fate of a T cell after antigen recognition[47]. Antibodies that block signaling through two inhibitory T cell co-receptors, cytotoxic T-lymphocyte-associated protein 4 (CTLA-4 or CD152) and programmed cell death protein 1 (PD-1 or CD279), have currently entered the clinic as cancer therapeutics. CTLA-4 and PD-1 both belong to the family of CD28 receptors[48]. CD28 itself is one of the best-characterized stimulatory T cell co-receptors, which provides an activation signal to the TCR through interaction with its ligands CD80 and CD86 that are expressed on the surface of APCs[48]. CTLA-4 also binds CD80 and CD86 and therefore mainly opposes the stimulatory signals provided by CD28[48]. Expression of CTLA-4 is upregulated on T cells shortly after initial antigen recognition, but it is constitutively expressed on the immunosuppressive T regulatory cell (T_{reg}) population and is crucial for the immunosuppressive capacity

of T_{regs}[49,50]. Mice with a *Ctla-4* knockout have a lethal phenotype due to severe systemic autoimmune responses, demonstrating the central role of CTLA-4 in self-tolerance[51]. The clinical relevance for CTLA-4 blockade was initially doubted due to the lethality of *Ctla-4* knockout mice, but a partial CTLA-4 blockade with an antibody in murine tumor models later demonstrated anti-tumor efficacy without significant toxicities[52]. A series of clinical studies followed to demonstrate safety of CTLA-4 blockade in humans, until a fully humanized antibody against CTLA-4, ipilimumab, was finally approved for treatment of metastatic melanoma in 2011. The approval was based on a randomized, three-arm phase III clinical study which showed survival benefit for patients treated with either ipilimumab alone or in combination with a peptide vaccine for the melanoma-specific antigen gp100 over the gp100 vaccine alone[53].

In contrast to CTLA-4, PD-1 is involved in regulation of self-tolerance in peripheral tissues. PD-1 expression is upregulated on activated T cells[54], it is constitutively expressed in conditions of persistent TCR activation and it is associated with an exhausted T cell phenotype[55]. There are two PD-1 ligands, programmed death-ligand 1 and 2 (PD-L1 or CD274 and PD-L2 or CD273), that upon engagement with PD-1 negatively regulate T cell activation[56,57]. The regulatory activities of PD-1 are much broader than those of CTLA-4, as aside from T cells it is upregulated also on activated B and NK cells[54,58]. The fact that PD-1 can also bind CD80 further adds to the complexity of its signaling[59]. Thus, it is advantegous for tumor cells to upregulate expression of the PD-1 ligands as an immune evasion mechanism. Although both, PD-L1 and PD-L2, can be upregulated in different tumor types, PD-L1 expression is more relevant[60,61,62]. PD-L1 expression on tumor cells can be induced by activated immune effector cells, mainly as a response to IFN-γ secretion[63,64]. Alternatively, PD-L1 expression can be also induced by constitutive oncogenic signaling[65,66]. The importance of PD-1 signaling in cancer immune evasion is further underlined by evidence for correlation of PD-L1 expression with poor prognosis in different types of human cancer[67,68,69]. PD-1/PD-L1 blockade has therefore emerged as a very promising therapeutic option in different tumor entities with both PD-1 and PD-L1 blocking antibodies. One of the key studies supporting the clinical approval of PD-1 blockade was a randomised, dose comparison cohort of a phase I study in heavily pre-treated metastatic melanoma patients refractory to ipilimumab, in which anti-PD-1 at 2 mg/kg and 10 mg/kg demonstrated 26% overall response rates[70]. Soon after publication of these results, two PD-1 blocking antibodies, pembrolizumab and nivolumab, were granted an accelerated approval for treatment of metastatic melanoma[71]. Since then, PD-1 blockade has also been approved for treatment of non-small cell lung cancer (NSCLC), RCC, classical Hodgkin lymphoma as well as head and neck squamous cell carcinoma[71]. Aside from the PD-1 targeting antibodies, also the first PD-L1 blocking antibody, atezolimumab, was recently approved for treatment of urothelial carcinoma and NSCLC[71]. Although treatment-associated-toxicities such as dermatitis, hepatitis, colitis and pneumonitis are observed with PD-1/PD-L1 blockade, these events are less frequent than in the case of CTLA-4 blockade[72]. These differences are observed due

to the distinct mechanisms of action of both approaches. As PD-1/PD-L1 is involved in the regulation of peripheral tolerance, immune activation is more targeted than in the case of anti-CTLA-4. Furthermore, besides a more favorable safety profile, in a direct head-to-head comparison with ipilimumab in advanced melanoma patients, PD-1 blockade has been also more effective in terms of higher response rates, extended progression free and overall survival[72].

Despite the rapid advancement of checkpoint blockade antibodies in the clinic, many types of cancer remain unresponsive for this type of therapy and in the responsive tumor types only a fraction of patients can experience the benefits. Therefore the main challenges in further development of checkpoint blockade strategies will include identification of reliable biomarkers to predict response to the therapy and allow selection of patients most likely to benefit from the treatment[73], as well as development of rational combination strategies to increase the therapeutic efficacy[74].

1.4 Oncolytic Viruses as a Type of Immunotherapy

1.4.1 Principles of virotherapy

Oncolytic viruses (OVs) are a class of cancer therapeutics that are able to selectively infect and replicate in malignant cells while sparing normal tissues[75]. This property is referred to as oncotropism[76]. The field of OV research has seen a renewed interest and major advancements during the last two decades, but the idea of using viruses for cancer therapy can be considered to be more than a century old, stemming from multiple case reports of tumor regressions after acquisition of infectious diseases[77,78]. Many wild-type as well as attenuated laboratory strain viruses, for instance AdV[79], herpesviruses (HSV)[80], parvoviruses[81], reoviruses[82], measles vaccine strain viruses (MV)[83], Newcastle disease virus (NDV)[84], vaccinia virus (VV)[85] and vesicular stomatitis virus (VSV)[86], have been shown to possess oncotropic properties.

After recognition of a virus, a normal cell strives to induce an antiviral state, shutting down the machinery of protein synthesis and inducing apoptosis to limit the replication and spread of the virus[87]. However, during the process of malignant transformation a cell undergoes major changes in its biology that frequently involve sacrifice of natural innate immune response mechanisms to avoid induction of apoptosis and to sustain growth advantage for the cancerous cells[5]. Mutations in pathways that prevent apoptosis, induce protein synthesis or interfere with innate immune signaling have all been shown to provide replication advantages for different OVs[88]. Thus, an enhanced and unrestricted replication of a virus is supported in cancer cells, ultimately leading to destruction of the infected cells. Importantly, in addition to direct tumor cell lysis through virus infection, bystander effects such as tumor vasculature shutdown[89,90,91] or activation of an anti-tumor immune response[92] can greatly contribute to the therapeutic effect of an OV. In particular, the immunostimulatory properties of OVs have been recognized critical for therapeutic efficacy, allowing to consider virotherapy as a

type of cancer immunotherapy[76]. Investigation of the immunostimulatory properties of OVs to enhance the virus-induced anti-tumor immune response and development of combination strategies with other cancer immunotherapies are currently among the major topics in the field of virotherapy[93].

1.4.2 Immunomodulatory Properties of Virotherapy

During their development, most human tumors establish an immunosuppressive environment to avoid recognition and destruction by the immune system[94]. In contrast, viruses, through activation of PRRs, act as very potent stimulators of innate immune responses[95]. Administration of a virus into the tumor therefore brings an immunostimulatory signal into an otherwise mostly immunologically neglected environment. Destruction of the infected tumor cells further releases TAAs under the established immunostimulatory conditions. The TAAs can be taken up by activated APCs that ensure cross-presentation of the antigens to T cells and prime a tumor-specific adaptive immune response[96]. Activation of a systemic anti-tumor immune response after treatment with different OVs has been demonstrated in many pre-clinical[97,98,92] as well as in clinical studies[99,100]. Therefore, virotherapy includes aspects of PRR agonist immunotherapies and therapeutic vaccination approaches and can therefore be classified as an active, unspecific type of cancer immunotherapy.

1.4.3 Combinations with Other Immunotherapies

Given the potent immunostimulatory properties of OVs, combinations with other cancer immunotherapy strategies are being explored to synergistically enhance the therapeutic potential. The strategies investigated for combination with OVs include approaches from generally all classes of currently available immunotherapeutics – immunomodulatory cytokines[101,102], checkpoint blockade antibodies[103,104], bispecific T cell engagers[105], T cell costimulatory ligands[106], adoptive cell transfer[107,108] and vaccination approaches with oncolytic vectors encoding TAAs[109]. An approach that has received a particularly great attention has been engineering of oncolytic vectors encoding different immunostimulatory molecules[93]. The rationale for this strategy is on the one hand to support establishment of an anti-tumor immune response and on the other hand a local expression of the encoded immunomodulator only in the infected tumor cells to avoid toxicities that are frequently associated with systemic administration of immunotherapeutics[110]. Immunomodulators from many classes, including cytokines, T cell co-stimulatory molecules, immune checkpoint blockade antibodies and bispecific T cell engagers, have been engineered for expression from different oncolytic vectors (Table 1.1). In almost all of the studies listed in Table 1.1 the therapeutic efficacy of the OV could be improved by combination with the chosen immunomodulators. Notably, thus far GM-CSF has been used in combination with the most of the known OVs. GM-CSF is a factor mainly known for its ability to promote expansion and maturation of dendritic cells and is therefore able to support the TAA uptake and presentation phase[111]. Impor-

tantly, a herpes simplex vector encoding GM-CSF known also as talimogene laherparepvec (T-VEC)[100] was approved for treatment of metastatic melanoma by the FDA in 2015.

Table 1.1: **Oncolytic viruses encoding immunomodulators.** List of immunomodulators inserted into genomes of oncolytic viruses for local expression from infected cells. Main functional properties of the respective immunomodulator are given under mode of action. AdV — adenovirus; HSV — herpesvirus; MV — measles virus; NDV — Newcastle disease virus; VV — vaccinia virus,; VSV — vesicular stomatitis virus; BiTE — bispecific T cell engager. Adapted from Lichty *et al.*[93]

Immunmodulators	Vectors	Mode of action
GM-CSF	AdV[112]; HSV-1[113]; MV[114]; NDV[115]; VV[116]; VSV[117]	Enhanced maturation of antigen-presenting cells
IL-2	HSV[118]; NDV[115]	Activation of T cells
IL-4	AdV[119]; HSV[120]	Activation of T and NK cells
IL-12	AdV[121]; HSV[122]; VSV[123]	Activation of T and NK cells
IL-15	HSV[124]; Influenza A[125]; VSV[126]	Activation of T and NK cells
IL-18	AdV[127]; HSV[122]	Activation of T and NK cells
TNF-α	NDV[115]	Activation of T and NK cells
IFN-γ	AdV[128]; NDV[115]; VSV[129]	Activation of T and NK cells
Type I IFNs	AdV[130]; MV[131]; VV[132]; VSV[133]	Activation of antigen presenting cells and T cells
CCL3	AdV[134]	Recruitment of polymorphonuclear leukocytes
CCL5	AdV[102]	Recruitment of T cells
CCL21	HSV[120]	Recruitment of T cells
FLT3L	AdV[134]; VSV[135]	Recruitment of T cells
CD80	AdV[121]; HSV[122]	T cell costimulation
CD137 (41BBL)	AdV[136]; VV[137]	T cell costimulation
CD154 (CD40L)	HSV[120]; VSV[138]	T cell costimulation
Anti-CTLA-4	MV[104]	Blockade of negative T cell signaling
Anti-PD-L1	MV[104]	Blockade of negative T cell signaling
BiTE	VV[105]	Activation of target antigen specific T cells

1.5 Measles Virus

1.5.1 Biology of Measles Virus

Measles virus (MeV)* is a spherical virus with a non-segmented, single stranded, negative sense RNA genome belonging to the *Morbillivirus* genus in the *Paramyxoviridae* family[139]. The MeV viral particles are pleomorphic with a size in range of 100 – 300 nm[139]. The genome of MeV is 15894 nt long and contains six genes[140] which encode six structural[141] and two non-structural proteins[142,143] (Figure 1.1). The genome starts and ends with non-coding leader and trailer sequences containing transcription regulatory elements[144]. The virus genome is encapsidated into a flexible, helical nucleocapsid formed by multiple copies of MeV nucleoprotein (N), each binding exactly six nucleotides of the RNA genome[145]. The nucleocapsid interacts with virus polymerase complexes formed by the large protein (L) and the polymerase cofactor, phosphoprotein (P)[146]. The fusion protein (F), hemagglutinin (H) and matrix protein (M) together with the lipid membrane from the host cell form the viral envelope[139]. The F and H proteins on the surface of virus envelope exist in hetero-oligomeric complexes[147] and mediate fusion with the host cell membrane and interaction with the MeV specific cellular receptors, respectively[139]. The F and H complexes are also transported to the surface of an infected cell and cause fusion with the neighboring cell membranes, creating large multinucleated cellular aggregates, syncytia[139]. The two non-structural proteins V and C, which are alternatively translated from the *P* open reading frame (ORF) in infected cells, are involved in the regulation of the host response against measles infection[148,149,150]. Non-coding regions containing gene-end and gene-start transcription regulatory sequences, which guide transcription termination and reinitiation as well as polyadenylation of mRNA, are located between all ORFs of the viral proteins[144]. As the transcription reinitiation before each ORF is not perfect, a transcription gradient exists in the MeV genome with the genes encoded closer to the MeV trailer being transcribed less efficiently than those closer to the MeV leader[151]. All replication stages of MeV take place in the cytoplasm of the host cell[139].

Wild-type MeV is a human-restricted pathogen[152] and mainly uses two receptors for entry into human cells — poliovirus receptor-like 4 (PVRL-4) or nectin-4[153,154] and signaling lymphocyte activation molecule (SLAM) or CD150[155]. The expression patterns of these proteins determine the course of MeV infection in the host. MeV is transmitted via respiratory droplets from an infected person which enter the upper airways of a new host, where the virus infects airway epithelial cells via PVRL-4[156,153]. Further, MeV infection spreads to alveolar macrophages and DCs which transport MeV to local lymphatic tissue where SLAM-positive lymphoid cells, including monocytes, T and B cells, are infected[157,158]. Subsequently, MeV is disseminated throughout the organism and can replicate in many organs including lungs, skin, thymus, spleen, liver and stomach[159]. Clinical manifestation of measles starts after a

*The abbreviation MeV is used for the wild-type measles virus, MV is used for measles vaccine strain viruses and MeVac is used for measles Schwarz vaccine strain viruses.

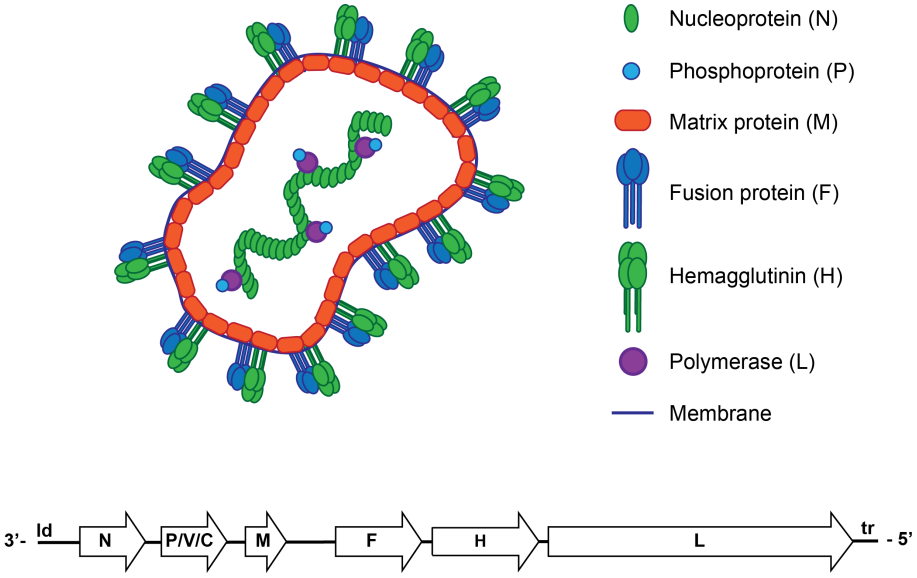

Figure 1.1: **Schematic structure of the measles virus (MeV) virion and genome.** The viral envelope of MeV consists of the plasma membrane from the host cell and is inlined by the measles matrix protein (M). The hemagglutinin (H) and fusion (F) proteins decorate the outer surface of the viral envelope. The MeV genome is a single stranded, negative sense RNA and is tightly packed in a nucleoprotein (N), viral polymerase (L) and a polymerase cofactor, phosphoprotein (P). The *P* open reading frame additionally codes for two alternatively transcribed non-structural proteins V and C. The MeV genome starts and ends with non-coding regions, leader (ld) and trailer (tr), respectively, containing transcription regulatory elements.

10 – 14 day incubation period and includes fever, cough, coryza and conjunctivitis, which is followed by appearance of the characteristic maculopapular rash[139]. The onset of the rash coincides with active adaptive immune responses, including the presence of measles-specific antibodies and activated T cells which clear viremia within a few days[160]. After clearance of the virus, measles-specific antibodies remain in the body and provide lifelong immunity. In rare occassions a persistent measles infection of the nervous system develops, leading to a neurodegenerative disorder, subacute sclerosing panencephalitis[161]. Measles can result in a fatal disease and caused an estimated of 114 900 deaths globally in 2014[162]. The main cause of measles-associated deaths are complications caused by secondary infections due to measles-induced immunosuppression[160]. The mechanisms of immunosuppressive effects caused by MeV are not completely understood, but can involve lymphopenia[163], suppression of Th_1 cytokine responses through upregulation of Th_2 responses[164] and suppression of lymphocyte proliferation[165].

1.5.2 Measles Vaccine Strain Viruses

Wild-type MeV was first isolated in 1954 from the blood of David Edmonston[166] and soon development of a live attenuated vaccine against MeV followed[167]. The measles vaccine turned out to be extremely effective and, although measles remains a health concern in

regions with incomplete vaccination coverage, it is estimated that in the period between 2000 and 2014 alone the vaccine prevented about 17 million measles-associated deaths[162]. The measles vaccine can also be considered one of the safest vaccines in the world, as it has been given to more than one billion people since its development and a conversion to wild-type MeV has never been observed[139]. Today, several different attenuated MeV vaccine strains exist, some of which were derived from the original Edmonston isolate by further passaging in different cell lines and some of which were derived from three other independent isolates[168]. In Europe, the Schwarz measles vaccine strain is used, which was obtained by additional passaging of the Edmonston isolate in chicken embryo fibroblasts[169]. It has been shown that the genome sequence of the Schwarz vaccine strain is identical to that of the Moraten strain which is used as a measles vaccine in the U.S., although both strains were obtained by separate passaging[168]. In addition to CD150 and PVRL-4, the attenuated measles vaccine strain viruses use CD46 as a cellular receptor[170]. This is due to acquisition of a mutation in the *H* gene during virus passaging, changing the amino acid in position 481 of the H protein from asparagine to tyrosine[171]. CD46 is a complement regulatory molecule which has the ability to block the complement cascade at the stage of C3 activation, thereby preserving autologous cells from the complement-induced cell lysis. CD46 is therefore expressed on the surface of most human nucleated cells[172]. As a complement evasion mechanism, CD46 is frequently overexpressed on cells of many different tumor types[173,174,175], thus, as will be discussed further, providing a natural oncotropism for measles vaccine strain viruses.

1.5.3 Measles as an Oncolytic Virus

In the 1970s several cases of tumor remissions in patients with hematological malignancies after measles infection were reported[176,177,178]. These observations led to the idea to apply MeV in cancer therapy. Although these observations actually indicated that wild-type MeV could be an appropriate agent for use in cancer therapy, application of attenuated measles vaccine strains turned out to be a more promising approach regarding safety and efficacy[83]. As mentioned before (subsection 1.5.2), the vaccine strain measles viruses infect CD46-positive cells. However, a critical density of CD46 is necessary for efficient fusion with the cell membrane and formation of syncytia[179]. As a complement evasion mechanism, CD46 expression has been found to be upregulated in many different tumor types including breast[180], renal[181], liver[182], bladder[183], gastrointestinal[184] and hematological[185] malignancies. Taken together, these properties provide measles vaccine strain viruses with a natural oncotropism. Effective tumor growth control of two hematological malignancies, multiple myeloma and lymphoma, could also be demonstrated in the first pre-clinical studies of the oncolytic properties of attenuated measles vaccine strain viruses[186,187].

Development of a reverse genetics system to allow generation of measles virus from cloned DNA[188] opened opportunities for further enhancement of attenuated MV to develop oncolytic MV vectors with increased efficacy and safety. The major directions in MV engi-

neering have focused on development of methods for non-invasive monitoring of virus spread *in vivo*, modulation of viral tropism to enhance specificity of tumor cell infection and generation of viruses that induce more effective anti-tumor immune responses.

Several strategies have been used to modulate the tropism of MV. It was found that the MV attachment protein H tolerates insertion of large polypetides without compromising assembly and replication of the virus[189]. Different tumor cell targeting strategies have been explored since then, including display of tumor marker-specific single chain antibodies[190,191,192] and designed ankyrin repeat proteins (DARPins)[193] or high affinity T cell receptors[194] on the C-terminus of MV H. The "retargeted" H allows MV to enter CD46 negative cells, including non-primate cells, expressing the respective target receptor. Furthermore, to ensure full "retargeting", mutations ablating the H binding to the natural receptors CD46 and CD150 are introduced[195,196]. Another strategy for modulation of MeV tropism includes insertion of micro-RNA target sites into the MV genome, thereby suppressing viral replication in cells expressing the respective microRNA[197]. Multiple tissue-specific microRNA target sites can be inserted into the MV genome to avoid measles replication after systemic application in such sensitive organs as the brain, gastrointestinal tract and liver[198].

MV vectors encoding different immunostimulatory transgenes have been developed to improve vector-induced anti-tumor immunity. Enhanced anti-tumor efficacy in comparison to the parental vector has been demonstrated for an IFN-β encoding MV in a human mesothelioma xenograft in immunodeficient mice[131]. MV encoding a neutrophil-activating protein derived from the *Helicobacter pylori* has been shown to effectively control tumor growth in an advanced human breast cancer xenograft model[199]. MV encoding murine granulocyte macrophage colony-stimulating factor (MV-mGM-CSF) has been shown to have an increased efficacy in an immunodeficient lymphoma xenograft model[200]. Furthermore, efficacy and induction of a more potent anti-tumor immune response by MV-mGM-CSF in comparison to a control vector has been demonstrated also in an immunocompetent murine colon adenocarcinoma model[114]. MV expressing antibodies against the negative regulators of T cells, CTLA-4 and PD-L1, have also been successfully developed and have elicited an enhanced anti-tumor response and a beneficial modulation of the tumor immune environment in a fully immunocompetent murine melanoma model[104]. The immunostimulatory effects of the encoded immunomodulators in the MeV genome synergize with the oncolytic effects of MV, but also addresses delivery and safety issues of these immmunomodulators. Targeted delivery of the immunomodulators to MV-infected cells allows local expression only at the tumor site and avoids toxicities that are frequently associated with systemic administration of immunotherapeutics[201,202].

Development of a feasible non-invasive method for monitoring of viral spread *in vivo* supported advancement of the attenuated MV vaccine vectors into clinical application. Two different strategies for tracking of MV replication have been used until now. The first approach used MV expressing soluble, biologically inert marker peptides – the soluble extracellular domain of the human carcinoembryonic antigen (hCEA) and the human chorionic

gonadotropin β-subunit (βhCG)[203]. Replication of these viruses could be monitored by measuring the concentration of the marker peptides in body fluids[203]. The second approach focused on developing viruses that would allow to also monitor the physical distribution of virus replication sites in the organism. A MV encoding the human thyroidal sodium iodide symporter (NIS) (MV-NIS) was therefore developed[204]. NIS is an ion channel which transports iodide against its concentration gradient. NIS is expressed on the surface of MV-NIS infected cells which are therefore able to concentrate radioactive iodide from the bloodstream, allowing to monitor progress of the infection by single-photon emission computed tomography or positron emission tomography[205].

Several clinical trials for use of attenuated MV vaccine strain viruses for treatment of different cancer types have already been concluded and more are currently ongoing. The first clinical trial administering an unmodified Edmonston-Zagreb measles vaccine strain virus (MV-EZ) in cancer patients was a phase I study for treatment of cutaneous T cell lymphoma. Five patients received intralesional MV-EZ injections which were preceded by IFN-α injections as a safety measure to avoid uncontrolled virus spread. Regressions were observed in five of six injected lesions and improvement of distant, non-injected lesions was observed in two of the patients[206]. The first trial to administer an engineered MV, MV-CEA, was carried out in patients with recurrent ovarian cancer. Twenty-one patients received i.p. injections of escalating doses with MV-CEA up to 10^9 $TCID_{50}$ (50% tissue culture infective dose). No dose-limiting toxicities (DLTs) were observed and, importantly, the observed response rates correlated with the received virus dose[207]. A phase I trial with administration of MV-NIS i.p. in recurrent ovarian cancer patients followed. Also in this trial no significant DLTs were observed and the best objective response was disease stabilization in 13 of 16 patients[208]. In all of these first clinical trials only measles-immune patients were enrolled. In the following, administration of MV-NIS in two measles-seronegative patients with disseminated multiple myeloma has also been reported. Of note, complete remission of the disseminated disease that lasted for nine months was observed in one of these patients[209]. Multiple phase I and II clinical trials investigating MV-CEA or MV-NIS for treatment of different tumor entities, including glioblastoma multiforme (NCT00390299), ovarian, fallopian or peritoneal cancer (NCT02364713), refractory multiple myeloma (NCT00450814), malignant pleural mesothelioma (NCT01503177), malignant peripheral nerve sheath tumor (NCT02700230), recurrent or metastatic squamous cell carcinoma of the head and neck or metastatic breast cancer (NCT01846091) are currently active or recruiting patients.

2 Aim of the Study

Oncolytic viruses (OVs) are emerging as a novel, clinically relevant type of cancer immunotherapy. The ability of different OVs to induce immunogenic death of infected tumor cells, eliciting tumor antigen specific immune responses, has been demonstrated in numerous pre-clinical tumor models and more importantly validated in a clinical situation. Furthermore, it has been recognized that the immunostimulatory properties of OVs can be supported by combination with different immunomodulators to synergistically enhance the therapeutic efficacy. However, understanding of immune effector mechanisms determining success of a particular combination approach and, thus, compatibility with the immunostimulatory effects induced by a particular oncolytic vector remains limited.

Based on the hypothesis that certain immunomodulation types are more suitable for combination with a given oncolytic vector to achieve therapeutic benefit in a given tumor type, the aim of this study was to compare the therapeutic efficacy of oncolytic measles vectors encoding immunomodulators targeting establishment of an anti-tumor immune response at different phases (Figure 2.1).

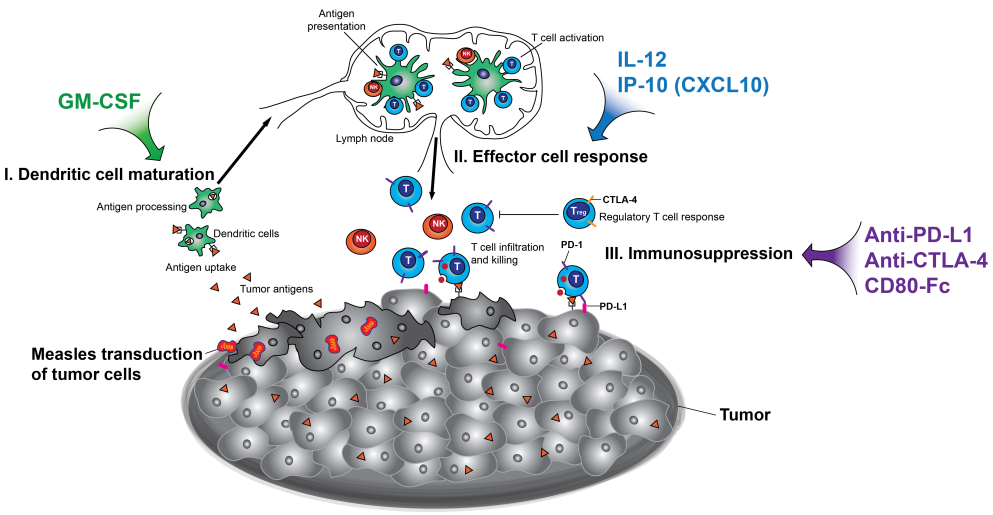

Figure 2.1: **Immunomodulation strategies for oncolytic measles virus therapy.** Transgenes for immunomodulators targeting establishment of anti-tumor immunity at different stages were inserted into the genome of measles Schwarz vaccine strain virus. GM-CSF — granulocyte macrophage colony-stimulating factor; IL-12 — interleukin-12; IP-10 (CXCL10) — interferon-γ-induced protein 10; Anti-PD-L1, anti-CTLA-4 — antibodies against the negative T cell regulators PD-L1 and CTLA-4, respectively. Figure adapted from Mellman *et al.*, 2011[10].

Measles vectors encoding selected immunomodulators were generated: 1) granulocyte macrophage colony-stimulating factor (GM-CSF) — to enhance maturation of antigen-presenting cells; 2) IL-12 and IP-10 (CXCL10) — to enhance immune effector cell responses;

3) antibodies against CTLA-4 and PD-L1 as well as a soluble form of CD80 (CD80-Fc) — to counteract immunosuppression in the tumor microenvironment. The novel vectors were characterized *in vitro* in terms of replication kinetics and cytotoxic potential, as well as transgene expression and functionality. Subsequently, therapeutic efficacy was compared in an immunocompetent murine colon adenocarcinoma model to identify the most promising vectors or vector combinations. As a second objective, the study aimed at identification of immune effector mechanisms associated with efficacy of the most promising novel immunomodulatory measles vectors. To this end, analyses of the tumor immune environment following measles immunovirotherapy were performed. Intratumoral cytokine profiles and the main tumor infiltrating lymphocyte subpopulations were analyzed and the role of the main lymphocyte subpopulations for the therapeutic efficacy of the most promising vector was validated in depletion experiments.

3 Materials and Methods

3.1 Materials

3.1.1 Chemicals

Reagent	Supplier and catalog number
Agarose, molecular biology grade	Sigma-Aldrich, A9539
DAPI (4',6-diamidino-2-phenylindole)	Sigma-Aldrich, D8417
Dimethyl sulfoxide (DMSO)	Sigma-Aldrich, D2438
Ethidium bromide	AppliChem, 1239-45-8
Ethylenediaminetetraacetic acid (EDTA) salt solution	Sigma-Aldrich, E7889-100ML
Glycerol	Sigma-Aldrich, G7757-1L
Ionomycin	Cayman Chemical Company, Cay-11932
Kanamycin	Sigma-Aldrich, K0129
Methanol, > 99.9%	Carl-Roth, 8388.1
Mitomycin-C	Sigma-Aldrich, M4287
NP-40	Abcam, ab142227
Penicillin-Streptomycin	Thermo Fisher Scientific, 15070063
Phorbol 12-myristate 13-acetate (PMA)	Cayman Chemical Company, Cay-10008014
Skim milk powder, blotting grade	Carl-Roth, T145.2
Sodium chloride (NaCl) solution	Sigma-Aldrich, S5150-1L
Trizma® hydrochloride solution (Tris-HCl)	Sigma-Aldrich, T2694

3.1.2 Buffers

Buffer	Supplier and catalog number
Ammonium-Chloride-Potassium (ACK) lysing buffer	Thermo Fisher Scientific, A1049201
Laemmli buffer (4×)	Biorad, 161-0747
Novex® Tris-Glycine Transfer Buffer (25×)	Thermo Fisher Scientific, LC3675

Buffer	Supplier and catalog number
Rotiphorese® 10× SDS-PAGE (Sodium dodecyl sulphate-polyacrylamide gel electrophoresis) running buffer	Carl-Roth, 3060.1
Tris/Borate/EDTA (TBE)	Genaxxon bioscience, M3206.1000
Roti®-Stock 10× Tris-buffered saline-Tween (TBS-T)	Carl Roth, 1061.1

3.1.3 Growth Media for Bacterial and Cell Culture

Medium	Supplier and catalog number
Dulbecco's Phosphate-Buffered Saline (D-PBS) without calcium and magnesium	Thermo Fisher Scientific, 14190250
Dulbecco's Modified Eagle Medium (DMEM)	Thermo Fisher Scientific, 61965026
LB (lysogeny broth) medium	Carl-Roth, X964.1
OptiMEM®	Thermo Fisher Scientific, 51985034
Roswell Park Memorial Institute medium 1640 (RPMI 1640)	Thermo Fisher Scientific, 61870044
SOC Outgrowth Medium (Super Optimal Broth with glucose)	New England Biolabs (NEB), B9020S

3.1.4 Oligonucleotides

Oligonucleotides were designed using Primer-BLAST[210] and synthesized by Eurofins MWG Operon. Primers for RT-PCR and RT-qPCR were designed to span an exon-exon junction. For primers binding in the measles genome (MeV) the genome position of the first complementary nucleotide is given in the primer name. "+" or "rev" indicates primers hybridizing to the "+" strand DNA/RNA; "for" indicates primers hybridizing to the "−" strand DNA/RNA; m — murine; h — human. Restriction enzyme name is given if the respective restriction site is present in the primer sequence.

Name	Sequence 5' → 3'
MeV ld-1	ACCAAACAAAGTTGGGTAAGGATAGT
MeV N-180+	CGGATCCTGATGTAATGGGTGGTT
MeV N-241	TTACCACTCGATCCAGACTTC
MeV N-988	CCACACTTGAGTCCTTGATGAACC
MeV N-1471	GGCCCAGCAGAGCAAGTGATG
MeV P-1967	GGCAGGCAGTTCGGGTCTCAG

Name	Sequence 5' → 3'
MeV P-2769	CTTGGCCAAAATACACGAGGATAA
MeV P-3023+	AGTGCTCGGCCTGAATCTCTGC
MeV P-3287	TTGCCAAGTTCCACCAGATGCT
MeV M-3478+	ATGTCCCATGCCGACTTGTCGAA
MeV M-3831	GGGAGTGTCTTCAACGCAAACCAA
MeV M-4271	GACCTTATGTTACCCGCTGATGGA
MeV F-5129	CACGGCAACCAAACCAGAACC
MeV F-5525+	CCGGTGGGTGTTTGGAGAGTTA
MeV F-5595	GACTCGTTCCAGCCATCAATCAT
MeV F-6094	ATCCTGTCATTATTTGGCCCC
MeV F-7100	GGTCGCTCTGATCCTCTACAACTC
MeV H-7480	CCATAAAAGCCTCAGCACCAATCT
MeV H-7583+	GGCCCACTTCATCACCGATGATT
MeV H-8233	CGTCAAGCTAGGTGTCTGGAAATC
MeV H-9018	GTGTGCTTGCGGACTCAGAATC
MeV L-9249+	CAGATAGCGAGTCCATAACGG
MeV L-9371	TCAGAACATCAAGCACCGCCTAAA
MeV L-9809+	TGTGTGTCTCCTCCTATGGCAAG
MeV L-10045	CACTCGGGAATCCAACTTATCAAA
MeV L-10713	GGTCACGGAGGCTTGTAGATGTT
MeV L-11585	CAGCACATGGCCCTACAACCTTA
MeV L-12004+	TTGTTTGTGAGGAGGGGTATGACT
MeV L-12574	GGATGGTGCTATTGACAGGAAGAA
MeV L-12936+	AGGATCGACTTGGGGCTCTTA
MeV L-13242	ATGCTTCTAGGGTTGGGTGTTTTA
MeV L-13767	GAGCTGTTGTCATCGTTCCTTTCT
MeV L-14505	GGGTTGAACTCATCTGCTTGCTAC
MeV L-15008+	CAAAATCCCCGCTGAAAGGCATAAG
MeV L-15240	GCAATTGTGGGAGACGCAGTTAGT
pJET 1.2 for	CGACTCACTATAGGGAGAGCGGC
pJET 1.2 rev	AAGAACATCGATTTTCCATGGCAG
pCG for	TTGTGCTGTCTCATCATTTTG
pCG rev	GTCCCCATAATTTTTGGCAG
MeVac H-ATU *SpeI*	CTAGTCATCCATCATTGTTATAAAAAACTTAGGAACCAGGTCCACACAGCTC
XbaI for	GAGTCGCGCGCGTT
MeVac H-ATU *SpeI*	CTAGAACGCGCGCGACTCGAGCTGTGTGGACCTGGTTCCTAAGTTTTTTATA
XbaI rev	ACAATGATGGAGTA
saPD-L1 *SalI* rev	TTGTCACAAGATTTGGCCTCGTCGAC
m IP10 *MluI* for	CCCTTTACGCGTGCCACCATGAACCCAAGTGCTGCCGTC

Name	Sequence 5' → 3'
m IP10 *AscI* rev	CCCTTTGGCGCGCCTATTAAGGAGCCCTTTTAGACC
m IL12p40-477 rev	GGAACTGCTACTGCTCTTG
m CD80 for	TTTACGCGTGCCACCATGGCTTGCAATTGTCAGTTG
m CD80-Fc *SalI* rev	TTGTCACAAGATTTGGCCTCGTCGACTTCTCTGCTTGCCTCATTTCTTCTGA
IgG Fc *SalI* for	GTCGACGAGGCCAAATCTTGTGACAA
m CD80-Fc *AscI* rev	AAAGGGGGCGCGCCTAATTCAGATCTTTTTCTGAGATGAG
hsCEA *MluI* for	TTTACGCGTGCCACCATGGAGTCTCCCTCGGCCCCTCC
hsCEA *AscI* rev	TTTGGCGCGCCTATTATGCAGAGACTGTGATGCTCTTGAC
m β2m for	CTGCTACGTAACACAGTTCCACCC
m β2m rev	CATGATGCTTGATCACATGTCTCG
m PD-L1 752 for	GATCATCCCAGAACTGCCTG
m PD-L1 908 rev	TTCAACGCCACATTTCTCCA
m CTLA-4 var1 for	AGGTGGAACTCATGTACCCA
m CTLA-4 var1 rev	CTTCTTTTCTTTAGCATCTTGCTC
m CTLA-4 var2 for	GACGCAGATTTATGTCATTGCTAA
m CTLA-4 var2 rev	AACGGCCTTTCAGTTGATGG
m CXCR3 for	GCCATGTACCTTGAGGTTAGT
m CXCR3 rev	CCAGCAGAACATCGGCTACA
m GAPDH for	TTCACCACCATGGAGAAGGC
m GAPDH rev	GGCATGGACTGTGGTCATGA
m Foxp3 for	GGCCCTTCTCCAGGACAGA
m Foxp3 rev	GCTGATCATGGCTGGGTTGT
m T-bet for	TAAGCAAGGACGGCGAATGTT
m T-bet rev	TGCCTTCTGCCTTTCCACAC
m L13A for	GGCTGCCGAAGATGGCGGAG
m L13A rev	GCCTTCACAGCGTACGACCACC
m β-actin for	AGAGGGAAATCGTGCGTGAC
m β-actin rev	CAATAGTGATGACCTGGCCGT
m 18S for	CTTAGAGGGACAAGTGGCG
m 18S rev	ACGCTGAGCCAGTCAGTGTA
FhIL-12 p40 *MluI* for	CCCGGGACGCGTGCCACCATGTGTCACCAGCAGT
FhIL-12 p40 rev	AGATCCGCCGCCACCGCCACCACTGCAGGGCAC
FhIL-12 p35 for	GGTGGCGGTGGCGGCGGATCTAGAAACCTCCCC
FhIL-12 p35 *PauI* rev	CCCGGGGCGCGCTCACTAGGAAGCATTCAGATAGCTC
h nectin-4 1065 for	CAAAATCTGTGGCACATTGG
h nectin-4 1234 rev	GCTGACATGGCAGACGTAGA
h A33 for	CCTGTCTGGAGGCTGCCAGT
h A33 rev	AGGTGCAGGGCAGGGTGACA
h Cytokeratin-20 for	CAGACACACGGTGAACTATGG

Name	Sequence 5' → 3'
h Cytokeratin-20 rev	GATCAGCTTCCACTGTTAGACG
h Mucin-1 fw	CACTTCTCCCCAGTTGTCTAC
h Mucin-1 rev	GGGTACTCGCTCATAGGATG
h Villin for	TGTTCCTTCCAGCACCTTTG
h Villin rev	CCTGAGTCTCTCCATACGGG
h CEA-810	TTGGTTTGTCAATGGGACTTTC
h CEA-1288+	CTGGACGGTAATAGGTGTATGA
h β-actin Ex6 for	TCATTGCTCCTCCTGAGCGCA
h β-actin Ex6 rev	CTAGAAGCATTTGCGGTGGAC
A1*SnaBI*	GCGCGCTACGTAAAAGCTGGGAATAGAAACTTCG
A2*NotI*	TAGAGAGAGCGGCCGCTCTGGTGTAAGTCTAGTATCAGA
B1	ATGACAGATCTCAAGGCTAAC

3.1.5 Antibodies

Antibodies for western blot (WB), enzyme linked immunosorbent assay (ELISA) and flow cytometry (FC) analyses, as well as *in vivo* immune cell depletions (D) are listed below. The respective antigen and conjugate are given under "Antibody", host, isotype and clone are given under "Description", application and dilution are given under "Application", supplier and catalog number are given under "Supplier". Ab — antibody; PE — phycoerythrin; PerCP-Cy™5.5 — peridinin chlorophyll protein complex with cyanine-5.5; APC — allophycocyanin; Cy™7 — cyanine 7; FITC — fluorescein isothiocyanate.

Antibody	Description	Application	Supplier
Anti-human IgG-Fc-Biotin	Murine IgG2a, clone HP-6017	WB 1:2000, ELISA 1:500	Sigma-Aldrich, B3773
Anti-HA	Murine IgG1, clone HA-7	FC 1:1000	Sigma-Aldrich, H9658
Anti-mouse Ig-PE	Goat, polyclonal	Secondary Ab, FC 0.025 µg/µl	BD Biosciences, 550589
Anti-mouse CD45.2-PerCP-Cy™5.5	Murine (SJL) IgG2a, κ, clone 104	FC 1:100	BD Biosciences, 561096
Anti-mouse CD3 complex-Alexa Fluor® 700	Rat IgG2b, κ, clone 17A2	FC 1:100	BD Biosciences, 561388
Anti-mouse CD8a-APC	Rat IgG2a, κ, clone 53-6.7	FC 1:100	BD Biosciences, 561093
Anti-mouse CD4-APC-Cy™7	Rat IgG2b, κ, clone GK1.5	FC 1:100	BD Biosciences, 561830

Antibody	Description	Application	Supplier
Anti-mouse CD335-FITC	Rat IgG2a, κ, clone 29A1.4	FC 1:50	Biolegend, 137606
Anti-mouse CD69-PE	Armenian Hamster, IgG, clone H1.2F3	FC 1:80	Biolegend, 104507
Mouse IgG2a, κ, PerCP-Cy™5.5	Isotype control, clone MOPC-173	FC 1:100	Biolegend, 400251
Rat IgG2b, κ, Alexa Fluor® 700	Isotype control, clone RTK4530	FC 1:100	Biolegend, 400628
Rat IgG2a, κ, APC	Isotype control, clone R35-95	FC 1:100	BD Biosciences, 553932
Rat IgG2b, κ, APC-Cy™7	Isotype control, clone A95-1	FC 1:100	BD Biosciences, 552773
Rat IgG2a, κ, FITC	Isotype control, clone RTK2758	FC 1:50	Biolegend, 400501
Armenian Hamster, IgG, PE	Isotype control, clone HTK888	FC 1:80	Biolegend, 400907
Anti-mouse CD8	Rat IgG2a, κ, clone 53-6.7	D	Biolegend, 100735
Anti-mouse CD4	Rat IgG2a, κ, clone GK1.5	D	Biolegend, 100435
Anti-mouse NK1.1	Mouse IgG2a, κ, clone PK136	D	Biolegend, 108712
Anti-human CD46-PE	Mouse IgG1, clone TRA-2-10	FC 1:100	Biolegend, 352401
Anti-human CD150-PE	Mouse IgG1, κ, clone A12	FC 1:25	BD Biosciences, 559592
Mouse IgG1, κ, PE	Isotype control, clone MOPC-21	FC 1:100 or 1:25	BD Biosciences, 555749

3.1.6 DNA Plasmids

Plasmid	Description
pUC19	High copy number cloning vector[211]
pJET 1.2	Cloning vector, GenBank accession number: EF694056.1 (Thermo Fisher Scientific)
pcDI dsRed	Eukaryotic expression vector for a variant of the *Discosoma* red fluorescent protein
pcDIMER-N	Eukaryotic expression vector encoding Schwarz measles vaccine strain *N*

Plasmid	Description
pcDIMER-P	Eukaryotic expression vector encoding Schwarz measles vaccine strain *P*
pcDIMER-L	Eukaryotic expression vector encoding Schwarz measles vaccine strain *L*
pJET 1.2 mIP-10	pJET 1.2 vector encoding a murine IP-10 (CXCL10) expression cassette
pCG FmIL-12	Eukaryotic expression vector encoding murine IL-12 fusion protein[212]
pCG anti-CTLA-4	Eukaryotic expression vector encoding an antibody against murine CTLA-4 (CD152)[213]
pCG anti-PD-L1	Eukaryotic expression vector encoding an antibody against murine PD-L1 (CD274)[213]
pCG IgG1-Fc	Eukaryotic expression vector an antibody constant region IgG1-Fc[213]
pCG mCD80	Eukaryotic expression vector encoding murine CD80
pCG MeVac Hbl	Eukaryotic expression vector encoding Schwarz measles vaccine strain *H* which is "blinded" for binding to CD46 and CD150 with Y481, R533A, S548L and F549S mutations
pCG NSe Hbl-αCEA	Eukaryotic expression vector encoding the *H* of measles Edmonston B derived measles vaccine strain vector which is "blinded" for binding to CD46 and CD150 with Y481, R533A, S548L and F549S mutations and fused to a single chain antibody against human CEA with a six-histidine tag at the C terminus
pCG NSe Hbl-αCD20	Eukaryotic expression vector encoding the *H* of measles Edmonston B derived measles vaccine strain vector which is "blinded" for binding to CD46 and CD150 with with Y481, R533A, S548L and F549S mutations and fused to a single chain antibody against human CD20 with a six-histidine tag at the C terminus[212]

Plasmid	Description
pCG MeVac Hbl-αCEA	Eukaryotic expression vector encoding the *H* of measles Schwarz vaccine strain vector which is "blinded" for binding to CD46 and CD150 with with Y481, R533A, S548L and F549S mutations and fused to a single chain antibody against human CEA with a six-histidine tag at the C terminus
pCG MeVac Hbl-αCD20	Eukaryotic expression vector encoding the *H* of measles Schwarz vaccine strain vector which is "blinded" for binding to CD46 and CD150 with with Y481, R533A, S548L and F549S mutations and fused to a single chain antibody against human CD20 with a six-histidine tag at the C terminus
pcMeVac	Measles Schwarz vaccine strain antigenome encoding plasmid[214]; allows rescue with the RNA polymerse II dependent system[215]
pUC19 MeVac *NarI-NarI*	pUC19 vector containing a part of the measles Schwarz vaccine strain antigenome with *F*, *H* and *L* ORFs between two *NarI* restriction sites
pcMeVac ld-ATU	Plasmid with measles Schwarz vaccine strain antigenome encoding an additional transcription unit upstream of the measles leader
pcMeVac P-ATU	Plasmid with measles Schwarz vaccine strain antigenome encoding an additional transcription unit downstream of the measles *P* ORF
pcMeVac H-ATU	Plasmid with measles Schwarz vaccine strain antigenome encoding an additional transcription unit downstream of the measles *H* ORF
pcMeVac Hbl-αCEA	Plasmid with measles Schwarz vaccine strain antigenome in which the *H* is "blinded" for binding to CD46 and CD150 and fused to a single chain antibody against human CEA with a six-histidine tag at the C terminus; allows propagation on Vero-αHis cells
pcMeVac ld-eGFP	Plasmid with measles Schwarz vaccine strain antigenome encoding an ORF for *eGFP* upstream of the measles leader

Plasmid	Description
pcMeVac ld-eGFP Hbl-αCEA	Plasmid with measles Schwarz vaccine strain antigenome encoding an ORF for *eGFP* upstream of the measles leader and with measles *H* "blinded" for binding to CD46 and CD150 and fused to a single chain antibody against human CEA with a six-histidine tag at the C terminus; allows propagation on Vero-αHis cells
pcMeVac H-anti-CTLA-4	Plasmid with measles Schwarz vaccine strain antigenome encoding an ORF for an antibody against murine CTLA-4 (CD152) downstream of the measles *H* ORF
pcMeVac H-anti-CTLA-4 Hbl-αCEA	Plasmid with measles Schwarz vaccine strain antigenome encoding an ORF for an antibody against murine CTLA-4 (CD152) downstream of the measles *H* ORF and with measles *H* "blinded" for binding to CD46 and CD150 and fused to a single chain antibody against human CEA with a six-histidine tag at the C terminus; allows propagation on Vero-αHis cells
pcMeVac H-anti-PD-L1	Plasmid with measles Schwarz vaccine strain antigenome encoding an antibody against murine PD-L1 (CD274) downstream of the measles *H* ORF
pcMeVac H-anti-PD-L1 Hbl-αCEA	Plasmid with measles Schwarz vaccine strain antigenome encoding an ORF for an antibody against murine PD-L1 (CD274) downstream of the measles *H* ORF and with measles *H* "blinded" for binding to CD46 and CD150 and fused to a single chain antibody against human CEA with a six-histidine tag at the C terminus; allows propagation on Vero-αHis cells
pcMeVac H-anti-PD-L1 Hbl-αCD20	Plasmid with measles Schwarz vaccine strain antigenome encoding an ORF for an antibody against murine PD-L1 (CD274) downstream of the measles *H* ORF and with measles *H* "blinded" for binding to CD46 and CD150 and fused to a single chain antibody against human CD20 with a six-histidine tag at the C terminus; allows propagation on Vero-αHis cells

Plasmid	Description
pcMeVac H-IgG1Fc	Plasmid with measles Schwarz vaccine strain antigenome encoding an antibody constant region IgG1-Fc downstream of the measles *H* ORF
pcMeVac H-IgG1Fc Hbl-αCEA	Plasmid with measles Schwarz vaccine strain antigenome encoding an ORF for an antibody constant region IgG1-Fc downstream of the measles *H* ORF and with measles *H* "blinded" for binding to CD46 and CD150 and fused to a single chain antibody against human CEA with a six-histidine tag at the C terminus; allows propagation on Vero-αHis cells
pcMeVac H-IgG1Fc Hbl-αCD20	Plasmid with measles Schwarz vaccine strain antigenome encoding an ORF for an antibody constant region IgG1-Fc downstream of the measles *H* ORF and with measles *H* "blinded" for binding to CD46 and CD150 and fused to a single chain antibody against human CD20 with a six-histidine tag at the C terminus; allows propagation on Vero-αHis cells
pcMeVac H-mCD80-Fc Hbl-αCEA	Plasmid with measles Schwarz vaccine strain antigenome encoding an ORF for a soluble form of murine CD80 downstream of the measles *H* ORF and with measles *H* "blinded" for binding to CD46 and CD150 and fused to a single chain antibody against human CEA with a six-histidine tag at the C terminus; allows propagation on Vero-αHis cells
pcMeVac ld-mIP-10	Plasmid with measles Schwarz vaccine strain antigenome encoding an ORF for murine *Ip-10* (*Cxcl10*) upstream of the measles leader
pcMeVac ld-mIP-10 Hbl-αCEA	Plasmid with measles Schwarz vaccine strain antigenome encoding an ORF for murine *Ip-10* (*Cxcl10*) upstream of the measles leader and with measles *H* "blinded" for binding to CD46 and CD150 and fused to a single chain antibody against human CEA with a six-histidine tag at the C terminus; allows propagation on Vero-αHis cells

Plasmid	Description
pcMeVac ld-mGM-CSF	Plasmid with measles Schwarz vaccine strain antigenome encoding an ORF for murine *Gm-csf* upstream of the measles leader
pcMeVac ld-mGM-CSF Hbl-αCEA	Plasmid with measles Schwarz vaccine strain antigenome encoding an ORF for murine *Gm-csf* upstream of the measles leader and with measles *H* "blinded" for binding to CD46 and CD150 and fused to a single chain antibody against human CEA with a six-histidine tag at the C terminus; allows propagation on Vero-αHis cells
pcMeVac P-FmIL-12	Plasmid with measles Schwarz vaccine strain antigenome encoding an ORF for murine IL-12 fusion protein downstream of the measles *P* ORF
pcMeVac P-FmIL-12 Hbl-αCEA	Plasmid with measles Schwarz vaccine strain antigenome encoding an ORF for murine IL-12 fusion protein downstream of the measles *P* ORF and with measles *H* "blinded" for binding to CD46 and CD150 and fused to a single chain antibody against human CEA with a six-histidine tag at the C terminus; allows propagation on Vero-αHis cells
pcMeVac P-FmIL-12 Hbl-αCD20	Plasmid with measles Schwarz vaccine strain antigenome encoding an ORF for murine IL-12 fusion protein downstream of the measles *P* ORF and with measles *H* "blinded" for binding to CD46 and CD150 and fused to a single chain antibody against human CD20 with a six-histidine tag at the C terminus; allows propagation on Vero-αHis cells
pcMeVac P-FhIL-12	Plasmid with measles Schwarz vaccine strain antigenome encoding an ORF for human IL-12 fusion protein downstream of the measles *P* ORF
pcMeVac H-FhIL-12	Plasmid with measles Schwarz vaccine strain antigenome encoding an ORF for human IL-12 fusion protein downstream of the measles *H* ORF

3.1.7 Cell Lines

Cell line	Description	Medium	Source
Vero	African green monkey *Cercopitheus aethiops* kidney epithelial cell line	DMEM + 10% FCS	ATCC, Manassas, VA
Vero-αHis	Vero cells transduced with a lentiviral vector for stable expression of a single-chain antibody against a six-histidine peptide (His_6)[216]	DMEM + 10% FCS	S. J. Russell, Rochester, MN
MC38	Murine colon adenocarcinoma cell line derived from a chemically induced tumor in a C57BL/6 mouse[217]	DMEM + 10% FCS	R. Cattaneo, Rochester, MN
MC38cea	MC38 cells transduced with a lentiviral vector for stable expression of a human carcinoembryonic antigen (CEA) variant[218]	DMEM + 10% FCS	R. Cattaneo, Rochester, MN
B16	Murine melanoma cell line derived from a spontaneous tumor of a C57BL/6 mouse	RPMI 1640 + 10% FCS	D. M. Nettelbeck, Heidelberg, Germany
B16-CD20	B16 cells transduced with a lentiviral vector for stable expression of human CD20[212]	RPMI 1640 + 10% FCS	C. Großardt, Heidelberg, Germany
COLO 205	Human colorectal carcinoma cell line	RPMI 1640 + 10% FCS	A. Jassowicz, Heidelberg, Germany
DLD-1	Human colorectal carcinoma cell line	RPMI 1640 + 10% FCS	S. Fröhling, Heidelberg, Germany
HCT 116	Human colorectal carcinoma cell line	DMEM + 10% FCS	S. Fröhling, Heidelberg, Germany
HT29	Human colorectal carcinoma cell line	RPMI 1640 + 10% FCS	C. Plass, Heidelberg, Germany
KM12	Human colorectal carcinoma cell line	DMEM + 10% FCS	C. Plass, Heidelberg, Germany

3.1.8 Recombinant Measles Viruses

Virus	Description
MeVac	Measles Schwarz vaccine strain virus[214]
NSe	Measles Edmonston B derived vaccine strain virus
MeVac ld-eGFP Hbl-αCEA	Measles Schwarz vaccine strain virus encoding eGFP in an additional transcription unit upstream the measles leader and with the H fully retargeted to human CEA
MeVac H-anti-CTLA-4 Hbl-αCEA	Measles Schwarz vaccine strain virus encoding an antibody against murine CTLA-4 (CD152) in an additional transcription unit downstream the *H* ORF and with the H fully retargeted to human CEA
MeVac H-anti-PD-L1 Hbl-αCEA	Measles Schwarz vaccine strain virus encoding an antibody against murine PD-L1 (CD274) in an additional transcription unit downstream the *H* ORF and with the H fully retargeted to human CEA
MeVac H-IgG1Fc Hbl-αCEA	Measles Schwarz vaccine strain virus encoding a constant region of an antibody IgG1-Fc in an additional transcription unit downstream the *H* ORF and with the H fully retargeted to human CEA
MeVac ld-mIP-10 Hbl-αCEA	Measles Schwarz vaccine strain virus encoding murine IP-10 (CXCL10) in an additional transcription unit upstream of the measles leader and with the H fully retargeted to human CEA
MeVac P-FmIL-12 Hbl-αCEA	Measles Schwarz vaccine strain virus encoding a murine IL-12 fusion protein in an additional transcription unit downstream of the measles *P* ORF and with the H fully retargeted to human CEA
MeVac H-mCD80-Fc Hbl-αCEA	Measles Schwarz vaccine strain virus encoding a soluble form of murine CD80 in an additional transcription unit downstream of the measles *H* ORF and with the H fully retargeted to human CEA

Virus	Description
MeVac ld-mGMCSF Hbl-αCEA	Measles Schwarz vaccine strain virus encoding murine GM-CSF in an additional transcription unit upstream of the measles leader and with the H fully retargeted to human CEA
MeVac P-FmIL-12 Hbl-αCD20	Measles Schwarz vaccine strain virus encoding a murine IL-12 fusion protein in an additional transcription unit downstream of the measles *P* ORF and with the H fully retargeted to human CD20
MeVac H-IgG1Fc Hbl-αCD20	Measles Schwarz vaccine strain virus encoding a constant region of an antibody IgG1-Fc in an additional transcription unit downstream the *H* ORF and with the H fully retargeted to human CD20
MeVac H-anti-PDL1 Hbl-αCD20	Measles Schwarz vaccine strain virus encoding an antibody against murine PD-L1 (CD274) in an additional transcription unit downstream the *H* ORF and with the H fully retargeted to human CD20
MeVac P-FhIL-12	Measles Schwarz vaccine strain virus encoding a human IL-12 fusion protein in an additional transcription unit downstream of the measles *P*
MeVac H-FhIL-12	Measles Schwarz vaccine strain virus encoding a human IL-12 fusion protein in an additional transcription unit downstream of the measles *H*

3.2 Methods

3.2.1 Standard DNA and RNA Molecular Biology Methods

Polymerase chain reaction

DNA fragments were amplified in a polymerase chain reaction (PCR) with One*Taq*® standard buffer (NEB, M0480L), 200 nM deoxynucleotide triphosphates (dNTPs, Thermo Fisher Scientific, R0192), 200 nM respective forward and reverse primers, 0.625 U One*Taq*® DNA polymerase (NEB, M0480L) and sterile water. For cloning, DNA fragments were amplified in a PCR with Phusion HF buffer (NEB, M0530S), 200 nM dNTPs, 200 nM respective forward and reverse primers, 0.01 U Phusion® High Fidelity DNA polymerase (NEB, M0530S) and sterile water. The PCR conditions are given in the Table 3.1. The PCR reactions were perfomed in a T1 PCR cycler (Biometra, Göttingen).

Table 3.1: **Polymerase chain reaction (PCR) conditions.** Conditions for PCR with a One*Taq*® DNA polymerase (One*Taq*) or Phusion® High Fidelity DNA polymerase (Phusion). The annealing temperature (**x**) was determined individually for each primer pair. The extension time (**y**) was calculated based on the size of the expected product — 60 s per kbp for One*Taq* and 15 s per kbp for Phusion. t°C — temperature, degrees Celsius.

	One*Taq*		**Phusion**		
	t°C	Time, s	t°C	Time, s	
Initial denaturation	94	120	98	30	
Denaturation	94	30	98	10	} 25 – 35×
Annealing	**x**	30	**x**	30	
Extension	68	**y**	72	**y**	
Final extension	68	120	72	120	

Agarose gel electrophoresis

For separation in a gel electrophoresis, a DNA gel loading dye (Thermo Fisher Scientific, R0611) was added to the DNA fragments and the mixture was loaded on a 1% agarose gel with ethidium bromide. As a molecular weight standard, 100 bp or 1 kbp DNA Ladder (SM0321 or SM0311, Thermo Fisher Scientific) was used. Horizontal electrophoresis was performed in a 1× TBE buffer at 140 V for approximately 30 min and gels were visualized under ultraviolet light of 265 nm wavelength.

DNA fragment cloning

DNA was fragmented via restriction enzyme digest in appropriate buffers as suggested by the manufacturer (NEB or Thermo Fisher Scientific). Vector backbones were dephosphorylated using the Rapid DNA Dephos & Ligation Kit (Sigma-Aldrich, 04 898 117 001) according to instructions of the manufacturer. Inserts were separated in an agarose gel electrophoresis as described above and the band of interest was excised from the gel with a scalpel. Subsequently, the insert fragment was purified using the Qiaquick Gel Extraction Kit (Qiagen, 28704) according to the instructions of the manufacturer. Insert fragments generated via PCR were purified using the Qiaquick PCR purification Kit (Qiagen, 28104). To generate inserts from synthetic oligonucleotides, a double-stranded oligonucleotide (dsOligo) was created by mixing 1 nmol (10 µl) of each complementary oligonucleotide with 80 µl 50 mM NaCl in a buffer EB (Qiagen, 19086), denaturing the mix at 95°C for 10 min and slowly cooling to room temperature. The generated dsOligo was phosphorylated with T4 Polynucleotide Kinase (Thermo Fisher Scientific, EK0031) as suggested by manufacturer. Vector and insert ligation was performed using the Rapid DNA Dephos & Ligation Kit at a molar ratio 1:3 according to the instructions of the manufacturer. Transformation competent *Escherichia coli* (*E. coli*) (NEB, C3019H) bacteria were transformed with 2 µl ligation products as described further.

Plasmid DNA preparation and quality control

Transformation competent *E. coli* bacteria were thawed on ice. DNA was added to the bacterial suspension and incubated on ice for 30 min. Subsequently, a heat shock for exactly 40 s was performed and afterwards the suspension was incubated on ice for another 5 min. Next, 450 µl of SOC outgrowth medium was added and the cell suspension was incubated at 37°C with shaking at 900 rpm (rounds per minute) for 1 h. Further, 200 – 300 µl of the bacterial suspension was uniformely plated on an agar plate with selection antibiotics and the plate was incubated at 37°C overnight. On the next day, single colonies were picked with a sterile toothpick and added to round bottom tubes with 2 – 8 ml LB medium. The inoculated LB medium mini cultures were incubated at 37°C with shaking at 800 rpm overnight. On the next day, plasmid DNA was isolated from the mini cultures using the QIAprep Spin Miniprep Kit (Qiagen, 27104) according to the instructions of the manufacturer. DNA concentration in the resulting samples was determined using a Nano-Drop ND-1000 spectrophotometer (Thermo Fisher Scientific) by measuring absorbance at 260 nm wavelength. Further, the correct plasmid preparations were identified by restriction enzyme digestion analysis and the sequence in the correct samples was finally controlled by Sanger sequencing (GATC Biotech, Konstanz).

RNA isolation and quality control

Total RNA was isolated using the RNeasy Mini Kit (Qiagen, 74104) according to the instructions of the manufacturer. To remove potential genomic DNA contamination, cleanup with RNAse-free DNAse set (Qiagen, 79254) according to the instructions of the manufacturer was included. RNA concentration in the resulting samples was determined with a Nano-Drop ND-1000 spectrophotometer by absorbance measurments at 260 nm wavelength. The integrity of the isolated RNA was assessed in a horizontal agarose gel electrophoresis. The RNA integrity was considered intact if two clear bands corresponding the 18S and 28S ribosomal RNA could be detected.

Complementary DNA synthesis and reverse transcription PCR

Complementary DNA (cDNA) synthesis was performed using the Maxima H Minus First Strand cDNA Synthesis Kit (Thermo Fisher Scientific, K1681) using 1 µg total RNA and oligo(dT) primers according to the instructions of the manufacturer. Subsequently, digestion with Ribonuclease H (RNAse H, NEB, M0297L) for 20 min at 37°C was included. Reverse transcription PCR (RT-PCR) was performed using One*Taq*® DNA polymerase as described before (subsection 3.2.1).

3.2.2 Cell culture

Cultivation of cell lines

All cell lines were cultivated at 37°C in a humidified atmosphere with 5% CO_2. Cells were cultivated in Nunc cell culture treated flasks with filter caps (Thermo Fisher Scientific).

When reaching confluency of 80 – 100%, cells were split for subcultivation. For that, medium was removed, cell layer was gently washed with D-PBS, a 0.05% Trypsin-EDTA solution with phenol-red (Thermo Fisher Scientific, 25300054) was added and the culture flask was returned to incubator. After detachment of the cell layer (5 – 15 min), the respective cell culture medium (see before subsection 3.1.7) was added and cells were split at a ratio 1:10 – 1:20. The subcultivation procedure was performed once or twice per week, depending on the cell line. To determine cell number, cell suspension was mixed with 0.4% Trypan blue solution (Sigma-Aldrich, T8154) for cell viability staining and cells were counted using a Neubauer hemocytometer (Marienfeld, Lauda-Königshofen). All cell lines were routinely tested for *Mycoplasma* contamination using the Venor® GeM mycoplasma detection kit (Sigma-Aldrich, MP0025). Fetal calf serum (FCS) (Biosera) used for supplementation of the cell culture media, was heat-inactivated at 56°C for 30 min and filtrated through a 0.22 µm pore-size EMD Millipore Stericup™ Sterile Vacuum Filter Unit (SCGPU05RE, Thermo Fisher Scientific).

Cryopreservation and storage of cell lines

To prepare cells for cryopreservation they were pelleted at 300×g for 5 min and pellets were resuspended with the respective cell culture medium supplemented with 20% (v/v) FCS and 10% (v/v) DMSO and aliquoted into Nunc® CryoTubes® (Thermo Fisher Scientific, 375418). The tubes were kept into Stratagene Cryo 1°C Freezing Container (Agilent, Waldbronn) at −80°C for 24 h and then transferred to liquid nitrogen. For resuscitation of frozen cell lines, the vials were thawed in a 37°C water bath and the cell suspension was transferred into a cell culture flask with the respective culture medium. After cultivation at 37°C 5% CO_2 for 24 h the culture medium was removed and supplemented with a fresh respective medium.

3.2.3 Recombinant Measles Viruses

Rescue of viral particles

Rescue of recombinant measles virus particles was performed using the RNA polymerase II-dependent system[215]. Vero-αHis cells were seeded into 6-well plates 6 – 12 h prior to preparation of a rescue. Plasmid encoding a measles antigenome (5 µg) and expression plasmids encoding MeVac N, P and L proteins, pcDIMER-N (500 ng), pcDIMER-P (100 ng) and pcDIMER-L (500 ng), respectively, were added to ≈180 µl unsupplemented DMEM. For use as a transfection efficieny control, 0.1 µg of a plasmid encoding a red fluorescent protein, pcDI dsRed, was added to the mix. Followingly, 3 µl/µg FuGENE® HD (Promega, E2311) was slowly added to the plasmid mix and the mixture was incubated for 25 min at room temperature to allow formation of transfection complexes. During incubation of the transfection mixture, Vero-αHis cells were washed twice with unsupplemented DMEM and afterwards cultivation medium was changed to DMEM + 2% FCS + 50 µg/ml kanamycin. Subsequently, the previously prepared transfection mixture was evenly distributed per one well with Vero-αHis and cells were cultivated at 37°C in a humidified atmosphere with 5%

CO_2. Cells were monitored daily for formation of syncytia.

Virus propagation and storage

After rescue, the recombinant virus particles were propagated on Vero-αHis cells. For first two to three passages, 1.5×10^6 Vero-αHis cells were seeded into 10 cm cell culture dishes 8 – 16 h prior infection. Before the first passage, cells with the newly rescued viral particles in the 6-well plate well were scraped in the rescue medium with a cell lifter, the cell suspension was transferred to a 2 ml tube and vortexed vigorously. In parallel, culture medium was removed from the prepared 10 cm dish with Vero-αHis cells and replaced with 3 ml OptiMEM®. Followingly, the whole rescue cell suspension was added to the Vero-αHis in the 10 cm dish and cells were cultivated at 37°C. After 2 – 4 h 6 ml DMEM + 10% FCS was added to the culture dish. Cultivation was continued at 37°C for up to 96 h. Subsequently, culture medium was removed, up to 1 ml OptiMEM® was added, cells were scraped with a cell lifter, transferred to a 2 ml tube, vortexed vigorously, snap-frozen in liquid nitrogen and stored at −80°C. Followingly, the initial virus preparations were thawed at 37°C in water-bath and centrifuged for 5 min at 6000×g 4°C to remove cellular debris. The cleared virus suspension was aliquoted and stored at −80°C. For virus propagation in the second and following passages, Vero-αHis cells were infected with a multiplicity of infection (MOI) of 0.03. For large scale virus propagation, $4.5 - 5\times10^6$ Vero-αHis were seeded into 15 cm cell culture dishes 12 – 16 h prior to infection. Inoculation with virus suspension at MOI = 0.03 was performed in 8 ml OptiMEM. After 8 – 12 h of incubation at 37°C, 8 ml DMEM + 10% FCS was added per plate and cultivation at 37°C was continued for up to 45 h. For harvest of the viral particles, the culture medium was completely removed and cells were scraped with a cell lifter. The cell suspension was collected and a clear virus suspension was further prepared as described above.

Virus titration

The amount of viral particles in a virus suspension was determined in a serial dilution titration assay. Serial dilutions of the virus suspension stocks in octuplicates (virus propagation) or quadruplicates (one-step growth curves) were performed at 1:10 with a DMEM + 10% FCS in 100 µl total volume per well in 96-well plates. Subsequently, 1×10^4 Vero-αHis cells in 100 µl were seeded in each well and plate was incubated at 37°C. After 72 h, individual syncytia were counted and titer was calculated as cell infectious units per milliliter (ciu/ml).

One-step growth curves

Vero-αHis (1×10^5) or MC38cea (1.5×10^5) cells were seeded into 12-well cell culture plates. After 12 h cell culture medium was removed and cells were inoculated with the respective viruses at an MOI = 3 in 300 µl OptiMEM in triplicates for each time point. After allowing adsorption for 2 h, the inoculum was removed and substituted with 1 ml DMEM + 10% FCS per well. Cells were scraped in the culture medium at the designated time points, 300 µl cell suspension from each of the triplicate infections per time point was pooled in one 2 ml tube

and snap-frozen in liquid nitrogen. The amount of viral particles was determined by serial dilution titration assay as described above.

3.2.4 Cell Viability Assay

Target cells were seeded into 6-well plates and cultivated for 12 h to allow adherence of the cells. Afterwards, the culture medium was removed and cells were inoculated with the respective viruses at an MOI = 5 in 800 µl total volume of OptiMEM. After adsorption for 2 h, the inoculum was removed and substituted with the respective cell culture medium. At the designated time points cell viability was determined using an XTT (2,3-Bis-(2-Methoxy-4-Nitro-5-Sulfophenyl)-2H-Tetrazolium-5-Carboxanilide) assay. The XTT assay allows to monitor cell viability based on the ability of metabolically active cells to convert the water-soluble XTT reagent into an orange-colored formazan product. The amount of of the converted formazan product in the medium can be quantified with a spectrophotometer. XTT assays were performed using the Colorimetric Cell Viability Kit III (PromoKine, PK-CA20-300-1000) according to the instructions of the manufacturer.

3.2.5 Detection of MeVac Encoded Transgene Expression

Enzyme-linked immunosorbent assays

Expression of the MeVac encoded immunomodulators was detected by enzyme-linked immunosorbent assays (ELISAs). All samples were cleared of cellular debris by centrifugation at 300×g prior to analysis. Commercially available ELISA kits were used for detection of mGM-CSF, FmIL-12 (murine IL-12p70), mIP-10 (R&D Systems, MGM00, M1270, MCX100, respectively), CD80-Fc (Boster Biological Technology, EK0708), murine IFN-γ (eBioscience, 88-7314-22) and FhIL-12 (human IL-12p70) (eBioscience, 88-7126-22) according to the instructions of the manufacturer. Anti-CTLA-4 and anti-PD-L1 were detected by binding to the respective murine proteins by ELISA as described previously[104]. In detail, Nunc Maxisorp 96-well plates (Thermo Fisher Scientific, 439454) were coated with 100 µg recombinant murine CTLA-4 or PD-L1 (Sinobological, 50503-M08H-100 and 50010-M08H, respectively) in 100 µl D-PBS by incubating 2 h at room temperature or over night at 4°C. Protein solution was removed and wells were washed twice with 200 µl D-PBS per well. To block unspecific binding, 200 µl blocking buffer consisting of D-PBS + 5% FCS + 0.05% Tween20 (Biotium, 22002) was added per well and incubated for 1 h at room temperature. Subsequently, plate was washed three times with 200 µl D-PBS per well, 100 µl of the cleared sample per well was added and incubated for 2 h at room temperature or at 4°C over night. After incubation, samples were removed and plate was washed four times with 200 µl washing buffer per well consisting of D-PBS supplemented with 0.05% Tween20. Biotin-labeled antibody against the HA-tag was diluted 1:500 in blocking buffer, 100 µl of the prepared solution was added per well and incubated for 1 h at room temperature. Afterwards, antibody solution was removed and plate was washed four times with 200 µl washing buffer per well.

Horseradish peroxidase-coupled Streptavidin (Dianova, 016-030-084) (1 mg/ml) was diluted 1:500 in blocking buffer and 100 µl of the solution was added per well. After incubation for 10 min at room temperature, the Streptavidin containing solution was removed and plate was washed five times with 200 µl washing buffer per well. Further, 100 µl 1-Step™ Ultra TMB-ELISA Substrate Solution (Thermo Fisher Scientific, 34028) was added and after incubation for 5 – 20 min at room temperature the reaction was stopped with Stop Solution for ELISA (Takara, MK021). Absorbance was read at 450 nm wavelength with an Infinite M200 Plate reader and i-control Software (Tecan, Männedorf).

Immunoprecipitation

To concentrate MeVac expressed anti-PD-L1 and IgG1-Fc from supernatants of transduced cells, immunoprecipitation with Sepharose-A beads (Biocat, 6520-1-BV) was performed. Approximately 20 µl of the beads were prepared for 2 ml supernatant sample. The beads were washed three times with D-PBS and following resuspension in D-PBS added to the samples. The samples were incubated for 1 h at room temperature with constant rotation. Afterwards, the beads were pelleted at 300×g for 5 min and washed twice with D-PBS.

Sodium dodecyl sulphate-polyacrylamide gel electrophoresis

For further separation of the IgG1-Fc and anti-PD-L1 by sodium dodecyl sulphate-polyacrylamide gel electrophoresis (SDS-PAGE), the immunoprecipitated samples were supplemented with 1× Laemmli buffer and incubated at 95°C for 5 min. Subsequently, the samples were loaded onto a 12% precast polyacrylamide protein gel (Mini-PROTEAN® TGX™; Biorad, 4561041) in SDS-Running buffer. Prestained protein ladder (Thermo Fisher Scientific, 26616) was used as a molecular weight standard. The electrophoresis was performed for ≈ 30 min at 200 V.

Western blot analysis

After SDS-PAGE electrophoresis, the proteins were transferred onto a methanol activated Immobilon-P polyvinylidene difluoride (PVDF) membrane, 0.45 µm (Merck Millipore, IPVH-07850) in a Mini-PROTEAN® Tetra Cell wet-chamber with 1× Novex® Tris-Glycin Transfer Buffer. After the transfer, the PVDF membrane was incubated in a 5% skim-milk in a TBS-T buffer for blocking of the unspecific binding sites. After blocking, the skim-milk was substituted with 10 ml of fresh 5% skim-milk, a biotin-coupled antibody against the human IgG-Fc was added at a dilution 1:2000 and the membrane was incubated for 2 h at room temperature. Subsequently, the membrane was washed three times with 10 ml TBS-T buffer. After washing, 10 ml fresh 5% skim-milk was added, 4 µl (1 mg/ml) horseradish peroxidase-coupled Streptavidin (Dianova, 016-030-084) was added and the membrane was incubated 10 min at room temperature. Afterwards, the membrane was washed three times with 10 ml TBS-T buffer. For detection of the bound antibodies, SuperSignal West PICO Chemiluminescent Substrate (Thermo Fisher Scientific, 10177533) was added and signals were recorded using a ChemiDOC XRS Imaging System (Biorad, Munich).

3.2.6 Functional Assays for MeVac Encoded Immunomodulators

Production of MeVac encoded immunomodulators

Vero-αHis cells were seeded in 15 cm cell culture dishes and infected with MeVac encoding the respective transgenes at MOI = 0.03. Supernatants were collected (15 ml per plate) when syncytia had spread across the whole cell layer (ca. 36 h – 44 h post infection). Supernatants were snap-frozen in liquid nitrogen, stored at −80°C and sterile filtered before use. Expression and concentration of the immunomodulators was determined by ELISA as described before (subsection 3.2.5).

Anti-PD-L1 binding to MC38cea cells

To assess MeVac expressed anti-PD-L1 binding to the surface of PD-L1 positive cells, MC38cea cell line was used. 1×10^6 MC38cea cells were incubated with anti-PD-L1 or IgG1-Fc containing supernatant previously collected from a one fully infected 15 cm dish for 1 h with rotation at room temperature. After incubation, cells were washed once with 1 ml D-PBS and resuspended in 100 µl D-PBS. For detection of the bound anti-PD-L1, cells were stained with an antibody against the HA-tag at a 1:1000 dilution and incubated for 30 min at RT. Afterwards, cells were washed with 1 ml D-PBS and pellet was resuspended in 100 µl D-PBS. Further, 2.5 µg of a secondary PE-coupled antibody against the mouse IgG1-Fc was added per sample and incubated for 30 min at RT in dark. After incubation, cells were washed with 1 ml D-PBS and resuspended in 500 µl D-PBS with 0.2 µg/ml DAPI. The samples were directly acquired on an LSRII flow cytometer (BD Biosciences) with FACS Diva software version 8.0.1 (BD Biosciences) and at least 10000 events per sample were recorded. Results were analyzed with FlowJo V10 (Tree Star Inc., La Jolla, CA).

Functional assay for anti-PD-L1, anti-CTLA-4 and CD80-Fc

MC38cea cells (2×10^5) were incubated with 15 ml medium containing MeVac-encoded anti-PD-L1, anti-CTLA-4, mCD80-Fc or IgG1-Fc. The treated MC38cea cells were resuspended in 100 µl activation medium consisting of RPMI 1640 with 5% FCS, 1% Penicillin-Streptomycin (P/S), 500 nM ionomycin and 5 nM PMA and seeded in a 96-well plate. 2×10^5 freshly isolated splenocytes from a C57BL/6J mouse in 100 µl activation medium were added per well. After 24 h coculture of splenocytes with the treated MC38cea cells supernatants were collected and IFN-γ concentration was determined by ELISA as described before (subsection 3.2.5).

IFN-γ induction assay for murine IL-12 fusion protein

To assess FmIL-12 functionality 2×10^6 freshly isolated splenocytes from a C57BL/6J mouse were resuspended in RPMI 1640 supplemented with 10% FCS, 1% P/S and 50 U/ml recombinant murine IL-2 (mIL-2; Miltenyi, 130-094-05) and varying concentrations of MeVac-encoded FmIL-12 or respective amounts of supernatant from cells infected with MeVac encoding eGFP. Splenocytes were seeded in 12-well plates and incubated for 48 h at 37°C

5% CO2. Supernatants were collected and IFN-γ concentration was determined by ELISA as described before.

Chemotaxis assay for murine IP-10

Freshly isolated C57BL/6J mouse splenocytes were cultivated for 48 h in a medium consisting of RPMI 1640, 10% FCS, 1% P/S, 50 U/ml IL-2. The activated splenocytes were added to the upper part and supernatants from cells infected with MeVac mIP-10 or MeVac eGFP to the lower part of 24-well cell culture plate with transwell migration chambers (6.5 mm, pore size 5 µm) (Corning, 29442-118). Splenocyte migration was allowed for 3 h at 37°C. Supernatants from the lower part of the chamber were collected and cells were counted using trypan blue staining for dead-cell exclusion and a Neubauer hemocytometer.

3.2.7 *In vivo* Experiments

All animal experimental procedures were approved by the Animal Protection Officer at the German Cancer Research Center (Heidelberg, Germany) and by the regional council according to the German Animal Protection Law. Six to eight weeks old C57BL/6J mice bred in Harlan Laboratories (Rossdorf, Germany) or the Central Animal Laboratory of the German Cancer Research Center were used in all experiments.

Implantation of tumor cells

Low passage (up to eight) tumor cells were detached and collected from the cell culture flasks as described before (subsection 3.2.2) when reaching 70 – 80% confluency. The collected cells were washed twice with D-PBS and resuspended in D-PBS to achieve a final concentration of 1×10^7 cells/ml. The cell suspension was kept on ice until use. Right flanks of the animals were shaved and subsequently 100 µl (1×10^6 cells) of the prepared cell suspension per mouse was implanted subcutaneously (s.c.) into the shaved region using 1 ml syringes (VWR, 720-2561) and 26 G needles (Neolab, 194211002).

Monitoring

Tumor volumes were determined every third day by measuring the largest and smallest diameter with a caliper and calculating the volume using the formula: largest diameter×(smallest diameter)$^2\times0.5$. Mice were sacrificed when tumor volumes exceeded 1500 mm^3, ulceration occurred or animals were moribund.

Treatment with recombinant measles viruses

Treatment was initiated when the average tumor volume reached 40 – 70 mm^3 (efficacy experiments) or 120 mm^3 (immune profiling experiments). Before start of the treatment the animals were allocated to the treatment groups as to ensure similar average tumor volume and standard deviation in the groups. The respective virus suspensions were thawed only directly before the treatment and diluted with OptiMEM® to concentrations of 5×10^5 or 1×10^6 cell infectious units per ml depending on experiment. Mice received intratumoral

(i.t.) injections with 100 µl of the respective virus suspensions (1 ml syringes, 26 G needles) on four or five consecutive days (see figure legends for treatment schedules). Mice in the mock group received treatment with 100 µl OptiMEM.

Collection of peripheral blood

Peripheral blood was collected via puncture of the *vena saphena*. The mouse was restrained, the left hind leg was immobilized and shaved with an electrical trimmer until the saphenous vein was visible. The vein was punctured with a 26 G needle and up to 100 µl of the blood was dropwise collected with a capillary blood collection tube. Microvette® CB 300 µl, Lithium Heparin tubes (Sarstedt, 16.443) were used if further plasma separation was intended, Microvette® CB 300 µl, K2 EDTA tubes (Sartstedt, 16.444) were used if analysis of full blood was to follow. The site of the puncture was compressed with a cotton swab to stop the bleeding.

Depletion of immune cell populations

For immune cell depletion experiments mice received intraperitoneal injections with antibodies against CD4 (clone GK1.5), CD8 (clone 2.43) or NK1.1 (clone PK136). The CD4 and CD8 depletion groups received injections of 100 µg antibody in 100 µl three days before s.c. implantation of MC38cea cells, on the day of tumor cell implantation, three days post tumor cell implanatation and followingly once a week. The NK1.1 depletion group received injections with 200 µg of the antibody in 200 µl three and two days before tumor cell implantation, on the day of tumor cell implantation, one and three days post tumor cell implantation and followingly once a week. The depletion efficiency was controlled by flow cytometry of peripheral blood in selected animals from each group once a week as described further (subsection 3.2.8).

3.2.8 Experiments with Murine Tissues

Isolation of murine splenocytes

Aseptically isolated spleens were maintained in RPMI 1640 at 4°C until further processing. Spleens were passed through 100 µm nylon cell strainers (Neolab, 352360) into 10 ml RPMI 1640 and pelleted. The pellets were resuspended in 1 ml ACK lysing buffer for red blood cell lysis, incubated 10 min at room temperature and pelleted. Cells were resuspended in D-PBS and kept on ice until further use.

Tumor-specific IFN-γ immune memory recall

MC38cea, MC38 and B16 cells were treated with 20 µg/ml mitomycin-C for 2 h with shaking at 37°C. Subsequently, cells were washed three times with D-PBS and resuspended in activation medium consisting of RPMI 1640 with 10% FCS, 1% P/S and 50 U/ml mIL-2. Freshly isolated murine splenocytes were resuspended in activation medium. Cocultures were prepared in 24-well plates by seeding 1×10^5 tumor cells with 1×10^6 splenocytes per well in 0.5 ml total volume of activation medium. As controls 1×10^6 splenocytes were cocultivated

with Vero or DLD-1 cell lysates prepared by lysis of 1×10^6 cells per ml with one freeze-thaw cycle. Cells were cocultivated for 48 h, supernatants were collected and IFN-γ concentration was assessed by ELISA as described before (subsection 3.2.5).

Measurement of FmIL-12 concentration in peripheral blood of mice

Peripheral blood from animals was collected for serum separation as described before (subsection 3.2.7) and kept on ice until further use. Plasma separation was performed by centrifuging the tubes at 2000×g for 15 min. The serum fraction was transferred to a sterile tube by pipetting and stored at −80°C until analysis. FmIL-12 concentration in the samples was determined by ELISA as described before (subsection 3.2.5).

Flow cytometry of immune cell populations in peripheral blood

Freshly collected murine peripheral blood (up to 100 µl) was eluted from the collection tubes into 1.5 ml Eppendorf tubes with 700 µl ACK lysing buffer, vortexed briefly and incubated for 5 min at room temperature. Subsequently, 700 µl D-PBS was added and the samples were centrifuged at 300×g for 5 min at room temperature. Supernatant was removed, pellet was resuspended in 700 µl ACK lysing buffer, incubated for 5 min, 700 µl D-PBS was added and centrifuged at 300×g for 5 min. Supernatant was removed and pellet was resuspended in 100 µl D-PBS. Fluorescently labeled antibodies against murine leukocyte subpopulation markers were added — 1 µl anti-CD45.2-PerCP-Cy™5.5, 1 µl anti-CD3 Molecular Complex-Alexa Fluor® 700, 1 µl anti-CD4-APC-Cy™7, 1 µl anti-CD8a-APC, 2 µl anti-CD335-FITC, and samples were incubated for 30 min in dark at room temperature. For washing, 1 ml D-PBS per sample was added and samples were centrifuged at 300×g for 5 min. Pellets were resuspended in 500 µl D-PBS with 1 µg/ml DAPI for dead cell staining and acquired directly on a BD FACS AriaII instrument with FACS Diva software version 8.0.1 (BD Biosciences). Results were analyzed with FlowJo V10 (Tree Star Inc., La Jolla, CA).

3.2.9 Immune Profiling of Tumor Environment

Quantification of transcription factor mRNA levels

Pieces of freshly explanted MC38cea tumors were immersed in RNA*later* (Qiagen) and stored at −20°C until further processing. Total RNA was extracted and cDNA synthesis was carried out as described before (subsection 3.2.1). RT-qPCR was prepared with 1 µl cDNA, 200 nM respective forward and reverse primers, 10 µl Power SYBR® Green PCR Master mix (Thermo Fisher Scientific, 4367659) and water up to 20 µl total reaction volume. The reaction conditions were as follows — 10 min initial denaturation at 95°C, followed by 40 cycles of 15 s denaturation at 95°C, 60 s annealing and extension at 55°C (*T-bet*) or 60°C (*Foxp3* and *L13a*), and 5 s fluorescence detection at 72°C on a Roche LightCycler® 480 System. Melting curve analysis was prepared to identify specific amplification. Minus reverse transcriptase controls and no template controls were run in parallel with the cDNA samples. Stable expression of the reference gene among treatment groups was validated using the

Normfinder Software[219].

Intratumoral cytokine profiling

Protein extraction from freshly harvested MC38cea tumors was performed as described in[220]. In brief, freshly isolated MC38cea tumors were snap-frozen in liquid nitrogen and stored at −80°C until processing. Samples were thawed on ice, minced in small pieces and homogenized with a pestle in lysis buffer with 10 mM Tris–HCl (pH 8.0), 150 mM NaCl, 10% Glycerol, 5 mM EDTA, 1% NP-40 and one cOmplete Mini, EDTA-free Protease Inhibitor Cocktail Tablet (Sigma-Aldrich, 05892791001). Lysates were incubated for 1 h at 4°C with rotation and sonicated afterwards with an intermittent (0.5 min) on and off sonication regimen for 7 min (High intensity) using Diagenode Bioruptor® Standard with a cooling water pump (Diagenode, Seraing, Belgium). Lysates were cleared by centrifugation at 13000×g for 15 min and aliquots of supernatants were stored at −80°C until analysis. Cytokine concentrations were measured with the Mouse Th1/Th2/Th17 Cytokine Bead Array Kit (BD Biosciences, 560485) according to the manufacturer's instructions.

Flow cytometry of tumor infiltrating lymphocytes

Single cell suspensions were prepared from freshly isolated MC38cea tumors. Tumors were minced in small pieces in RPMI 1640 + 10% FCS + 200 U/ml Collagenase Type I and incubated for 30 min at 37°C with gentle vortexing every 10 min. The resulting cell suspensions were passed through 100 µm nylon cell strainers and cells were spun down and resuspended in D-PBS. Subsequently 2×10^6 cells per sample were resuspended in 100 µl D-PBS and stained with the antibodies against murine leukocyte subpopulation markers — 1 µl CD45.2-PerCP-Cy™5.5, 1 µl CD3 Molecular Complex-Alexa Fluor® 700, 1 µl CD4-APC-Cy™7, 1 µl CD8a-APC, 1.25 µl CD69-PE, 2 µl CD335-FITC. For dead cell staining samples were resuspended in D-PBS with 1 µg/ml DAPI before acquisition. Data were acquired on a BD FACS AriaII instrument with FACS Diva software version 8.0.1 and analyzed with FlowJo V10. Only samples with at least 3000 events were included in the analysis.

3.2.10 Statistical Analyses

Statistical analyses were performed using GraphPad Prism software (version 6.01; GraphPad Software). Tumor volume differences in *in vivo* experiments, ELISA results in restimulation experiments, RT-qPCR, flow cytometry and cytokine profiling results were analyzed by one-way analysis of variance (ANOVA) with Tukey's multiple comparison post-hoc-test. Multiplicity adjusted p-values are reported for data analyzed with ANOVA. Results were considered statistically significant if p-values were lower than 0.05. Tumor volume distributions were analyzed for the last day when all animals where alive. Survival curves were analyzed by log-rank (Mantel-Cox) test with Bonferroni correction for multiple comparisons. Results were considered statistically significant if the p-value was lower than the corrected threshold after Bonferroni correction.

4 Results

4.1 Construction and Characterization of Recombinant MeVac *in vitro*

Measles Schwarz vaccine strain viruses (MeVac) encoding different immunomodulators were developed to support establishment of an anti-tumor immune response by application of the oncolytic MeVac vectors. Transgenes encoding the chosen immunomodulators were inserted into different positions of the MeVac genome. Tropism of the novel vectors was modified by displaying a single chain antibody variable fragment on the MeVac Hemagglutinin (H) to allow transduction of target murine cells expressing the corresponding antigen. The novel vectors were characterized in terms of replication kinetics, cytotoxic effects in the target murine cells, expression kinetics of the inserted immunomodulators and their functionality *in vitro*.

4.1.1 Additional Transcription Unit Behind the *Hemagglutinin* Gene

Transgenes of interest can be inserted into the MeV genome in specifically designed additional transcription units (ATUs) with artificial gene-end/gene-start signals harboring unique cloning sites. MeVac genomes with ATUs in the leader position (pcMeVac ld-ATU) and downstream the *P* gene (pcMeVac P-ATU) have been previously constructed by S. Bossow (unpublished). The ld-ATU contains an N→N gene-end/gene-start transit to transgene (Tg) and a unique *AscI* cloning site. The P-ATU contains a P→P transit to Tg and a unique *MauBI* cloning site. Transgenes inserted further upstream of the MeV genome are expressed at higher levels than transgenes inserted further downstream due to the transcription gradient characteristic for MeV[151]. Insertion of a transgene in a position as close as possible to the MeV leader is therefore favorable for higher expression level. However, it is known from previous work with Edmonston B vaccine strain MeV (NSe) that insertion of large transgenes in the leader position may lead to severe inhibition of virus replication, e.g. NSe ld-FmIL-12[212], and rescue of viral particles from certain constructs can even be impossible, e.g. NSe ld-anti-CTLA-4[213].

To allow insertion of large transgenes and to avoid substantial attenuation of virus if using existing MeVac constructs with ATUs closer to leader, a MeVac genome with an ATU behind the *H* gene was constructed. The concept of the H-ATU was identical to that previously used in the Edmonston B genome[104]. The H-ATU was designed as a 66 nt fragment harboring 5'-*SpeI* and 3'-*XbaI* sites. The gene-end/gene-start transit to Tg was designed as

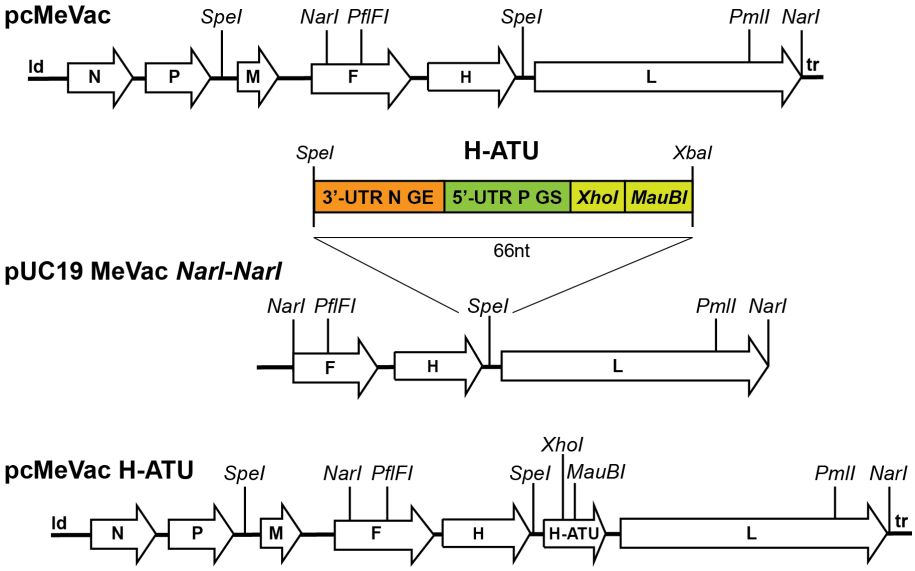

Figure 4.1: **Schematic for cloning of MeVac with an additional transcription unit (ATU) behind the *Hemagglutinin* gene.** The *SpeI-XbaI* cassete containing H-ATU was first inserted into a pUC19 cloning vector containing MeVac *NarI-NarI* subgenome. The *NarI-NarI* fragment containing the H-ATU was then exchanged in the pcMeVac, thereby generating pcMeVac H-ATU. Details in the figure are not depicted to scale. GE — gene-end signal; GS — gene-start signal.

an N→P transit. The 5' sequence in the ATU was slightly modified to exclude the "hidden" start codons. The MeVac genome contains two *SpeI* sites in contrast to the Edmonston B or NSe ("*NarSpe eliminated*") vaccine strain. Therefore the 66 nt H-ATU cassette was first inserted into a 11000 bp *NarI-NarI* MeVac subgenome in a pUC19 cloning vector as a dsOligonucleotide *SpeI-XbaI* fragment via the *SpeI* site unique in the subgenome (constructed by C. E. Engeland). Subsequently, a *PflFI-PmlI* fragment containing the H-ATU was excised from the generated subgenome and exchanged for the *PflFI-PmlI* fragment in pcMeVac yielding pcMeVac H-ATU (Figure 4.1).

4.1.2 Construction of MeVac Encoding Immunomodulators

Transgenes coding for different immunomodulators were inserted into the MeVac genomes with ATU downstream of the MeV leader, downstream the *P* gene or downstream the *H* gene. Construction of the novel MeVac genomes was guided by two general considerations. Firstly, MeV must have a genome length of a multiple of six ("rule of six") to derive replication competent virus particles[188;221]. Secondly, insertion of large transgenes (> 1 kbp) close to the leader position of the genome should be avoided as it may severely impair replication of the virus[212;213].

Transgenes smaller than 1 kbp which included mGM-CSF, mIP-10 and eGFP as a control were inserted into the leader (ld) position of MeVac genome as *MluI-AscI* fragments via the unique *AscI* restriction site (Figure 4.2). MeVac genomes encoding mGM-CSF and

eGFP had previously been constructed by S. Bossow and C. Grossardt (unpublished). Murine IP-10 encoding cassette was designed as an *MluI-AscI* fragment containing the 295 nt ORF of mIP-10 preceded by Kozak sequence (GCCACC) and followed by a two nucleotide spacer (TA) to obtain a 312 nt construct. The mIP-10 (*mCxcl10*) was amplified with primers flanking the novel construct using cDNA obtained from murine splenocytes and cloned into a pJET 1.2/blunt cloning vector. The mIP-10 cassette was excised from the cloning vector as an *MluI-AscI* fragment and inserted into the MeVac ld-ATU via the unique *AscI* restriction site (Figure 4.2.a).

The cassette encoding murine IL-12 was designed for expression of IL-12 as a fusion protein (FmIL-12 – murine IL-12 fusion protein) consisting of the IL-12 p35 and IL-12 p40 protein subunits linked by a $(Gly_3Ser)_4$ linker which had previously been constructed for insertion into the NSe genome by C. Grossardt[212] based on results of Lieschke *et al.*[222]. Systematic experiments with MeV Edmonston B vaccine strain viruses encoding FmIL-12 in ld-ATU, P-ATU and H-ATU positions revealed that P-ATU is the most suitable, ensuring high expression of FmIL-12 without significant attenuation of the virus[212]. The P-ATU was therefore considered the most appropriate position for FmIL-12 insertion also into the MeVac genome. The FmIL-12 cassette was excised from a pCG expression vector as a *PauI-MluI* fragment and inserted into the pcMeVac P-ATU via the unique *MauBI* cloning site (Figure 4.2.a).

Cassettes encoding antibodies against the negative regulators of murine T cells, CTLA-4 and PD-L1, as well as a soluble form of the murine T cell costimulatory molecule CD80 were inserted into the MeVac H-ATU. Also, a cassette encoding the respective antibody constant region in these constructs, IgG1-Fc, for use as a control, was inserted into the MeVac H-ATU. Cassettes encoding antibodies against murine CTLA-4 and PD-L1 and human IgG1-Fc fragment, previously constructed by C. E. Engeland[104], were used as templates. The respective constructs were excised from pCG expression vectors as *MluI-PauI* fragments and inserted into pcMeVac H-ATU via the unique *MauBI* cloning site (Figure 4.2.a).

The murine CD80 molecule, which under physiological conditions is expressed on the cell surface, was inserted for expression from MeVac in a soluble form. CD80 is a known T cell costimulatory molecule participating in activation of T cell receptor (TCR) signaling through interaction with the TCR co-receptor CD28[223]. CD80 has also been shown to interact with the negative T cell regulator PD-L1[59]. Recent data have shown that a soluble form of CD80 constructed from the extracellular domain of the CD80 molecule fused to an IgG-Fc region (CD80-Fc) is functional and can counteract the PD-1/PD-L1 suppression even more efficiently than blockade with anti-PD-1/PD-L1[224]. CD80-Fc was therefore considered a more promising candidate for insertion into the MeVac genome than the native, membrane-bound form of CD80. CD80-Fc was constructed by fusing the extracellular part of murine CD80 with the same human IgG1-Fc region as used in both anti-CTLA-4 and anti-PD-L1 constructs via fusion PCR. The first PCR fragment consisting of the *MluI* restriction site followed by a Kozak sequence (GCCACC), the murine CD80 signal peptide, the extracellular

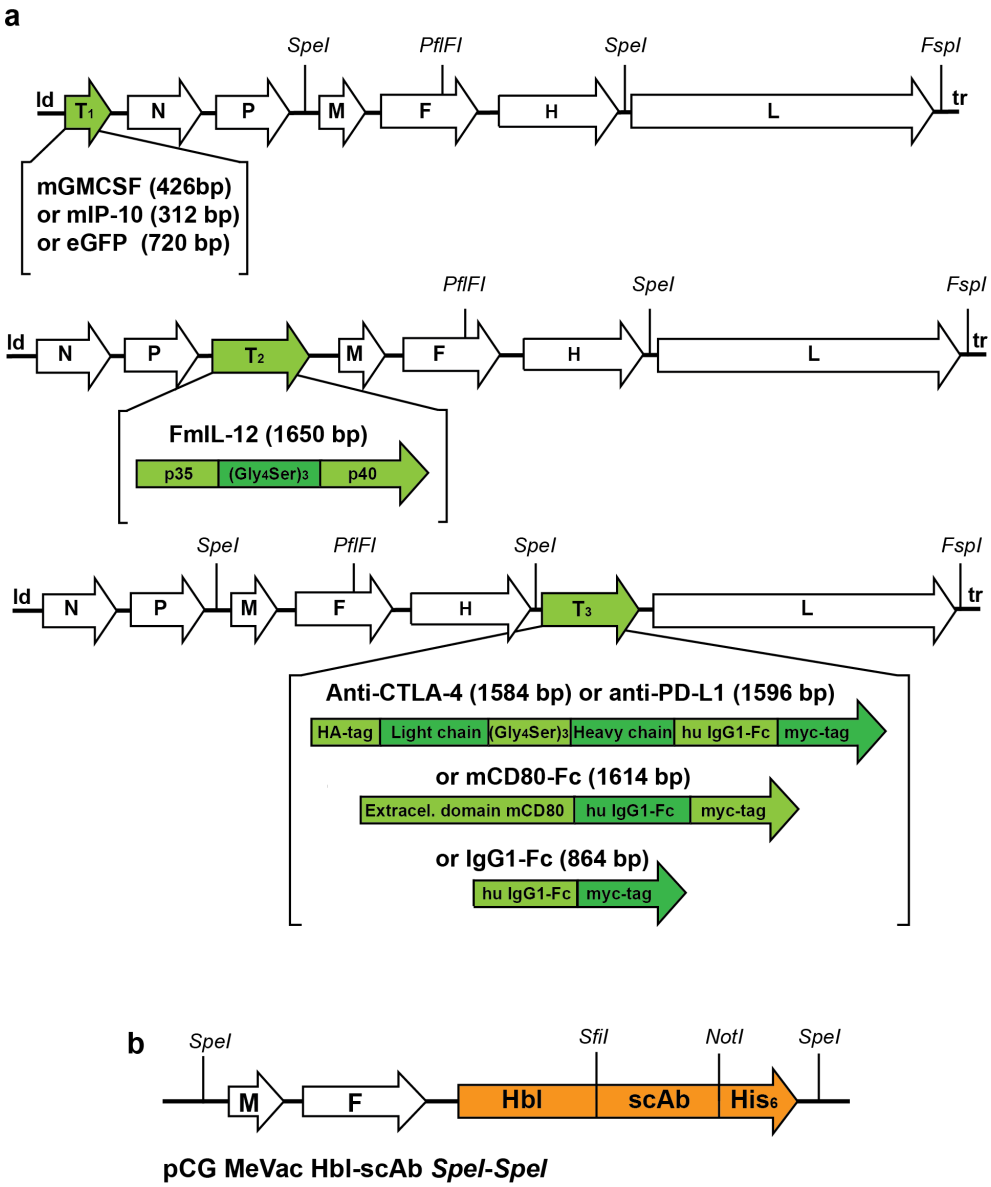

Figure 4.2: **Schematics of the constructed recombinant MeVac genomes and retargeting strategy. a** — transgenes encoding different immunomodulators as well as eGFP and IgG1-Fc as controls were inserted into additional transcription units (ATUs) in different positions of MeVac genome — ld-ATU (T_1), P-ATU (T_2), H-ATU (T_3). **b** — retargeting of the MeVac H protein was achieved by exchanging the authentic *H* gene in the novel constructs for an *H* gene with mutated attachment site to measles receptors CD46 and CD150 ("blinded" H — Hbl) and fused to a variable fragment of single chain antibody (scAb) against human CEA (carcinoembryonic antigen) or CD20 to allow specific transduction of murine MC38cea or B16-CD20 cell lines, respectively. The modified *H* gene contains a six histidine tag (His_6) to allow transduction of Vero cells expressing scAb for His_6. A *SpeI-SpeI* fragment encoding the modified *H* gene was cloned into an expression vector (pCG MeVac Hbl-scAb *SpeI-SpeI*) and inserted into the recombinant MeVac genomes (**a**) via exchange of *SpeI-SpeI* fragments. ld — measles virus leader; tr — measles virus trailer.

part (up to the asparagine in position 246) of murine CD80 and the first 26 nucleotides of the hinge of IgG1-Fc was amplified using a pCG vector encoding murine CD80 (constructed

by C. E. Engeland, unpublished) as a template. The second PCR fragment consisting of the human IgG1-Fc region followed by a myc tag, a stop codon and an *AscI* restriction site was amplified using a pCG vector encoding human IgG1-Fc as a template. The obtained PCR products were fused with flanking primers in an overlap PCR to obtain the mCD80-Fc construct of 1614 bp. The resulting mCD80-Fc was inserted into the pcMeVac H-ATU as an *MluI-AscI* fragment via the unique *MauBI* cloning site (Figure 4.2.a).

4.1.3 Retargeting of MeVac Hemagglutinin

An immunocompetent mouse tumor model is a prerequisite to study effects of immunovirotherapy with the novel MeVac constructs encoding immunomodulators *in vivo*. MeV is however able to naturally transduce only primate cells which express the specific receptors CD150, CD46 or nectin-4[225]. Retargeting of the MeV attachment protein H to a defined surface antigen is possible through different strategies with the most common being display of single chain variable fragments of antibodies[226,227]. Two immunocompetent murine tumor models, syngeneic for C57BL/6 mice, expressing a defined antigen for targeting with a single chain antibody (scAb) on MeV H have previously been created — murine colon adenocarcinoma MC38 expresssing human carcinoembryonic antigen (CEA) (MC38cea)[218,190] and B16 murine melanoma expressing human CD20 (B16-CD20)[212,104]. MC38cea was chosen as the main tumor model for further use in this study. Expression of human *CEA* on mRNA level by the MC38cea cell line maintained in laboratory was confirmed by RT-PCR (Figure 4.3).

In all the novel MeVac constructs the H protein was modified to allow transduction of the target murine MC38cea cells via the human CEA antigen. The natural H attachment sites to CD150 and CD46 were ablated by mutations in the coding region of the *H* gene and a *SpeI-SpeI* subgenomic fragment with the mutated ("blinded") *H* gene was cloned into the pCG expression vector (pCG MeVac Hbl, generated by C. E. Engeland). MeVac Hbl additionally contains a six-histidine (His_6) tag at the 3' end of the mutated H. The His_6 tag

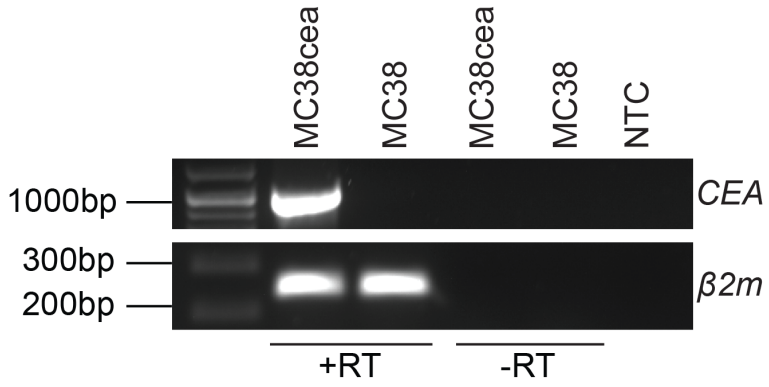

Figure 4.3: **Human carcinoembryonic antigen (CEA) expression in MC38cea cell line.** Human *CEA* expression was assessed in MC38cea and MC38 cell lines by RT-PCR. Murine beta 2 microglobulin (*β2m*) was amplified as a loading control. +RT – cDNA samples; -RT – minus reverse transcriptase controls; NTC – no template control.

allows rescue and propagation of the fully "blinded" MeVac on African green monkey kidney Vero cells transduced for stable expression of a scAb against the His_6 tag (Vero-αHis)[216]. Targeting of the "blinded" MeVac H protein (Hbl) to a desired antigen was further achieved by displaying a respective scAb as an extension to the C terminus of the "blinded" H[190]. The anti-hCEA scAb (clone MFE-23) with a 16 aa spacer between the V_H and V_L chains was used, which had previously been developed in a context of retargeting the H protein of Edmonston B vaccine strain MeV[190]. The scAb fragment was excised from the pCG vector encoding the NSe H protein retargeted to CEA (generated by C. Grossardt) as an *SfiI-NotI* fragment and inserted into pCG MeVac Hbl *SpeI-SpeI* via the respective restriction sites, yielding pCG MeVac Hbl-αCEA *SpeI-SpeI* (Figure 4.2.b). The generated Hbl-αCEA fragment was further inserted into the respective MeVac genomes encoding transgenes (Figure 4.2.a) by exchange of the *SpeI-SpeI* fragment except for the FmIL-12 encoding construct. As the second *SpeI* site is missing in the pcMeVac P-FmIL-12 construct due to the ATU inserted downstream of *P*, in this construct the retargeting was achieved by exchanging the *PflFI-FspI* fragment containing the fully retargeted *H* with pcMeVac ld-eGFP Hbl-αCEA. The retargeting strategy allows a flexible change of the used model as a library of pCG MeVac Hbl-scAb *SpeI-SpeI* fragments targeting different antigens can be created.

To assess the functionality of the retargeted H protein Vero, Vero-αHis, MC38 and MC38cea cells were transduced with MeVac ld-eGFP Hbl-αCEA. No syncytia formation was observed in Vero cells suggesting ablation of the natural tropism of the virus. Also no spread of the infection could be observed in murine MC38 cells which lack the receptors for MeV entry (Figure 4.4). In Vero-αHis syncytia had spread over the whole cell layer within 48 h after infection and most of the cells were lysed 72 h after infection. In MC38cea cells single eGFP positive cells were observed 48 h post infection and syncytia formation was observed 72 h post infection (Figure 4.4). These results therefore illustrate that full retargeting of the virus was achieved, ablating the natural tropism of MeVac and ensuring targeted infection of murine MC38cea cells and Vero-αHis cells through the human CEA and scAb against His_6, respectively.

4.1.4 Replication Kinetics and Cytotoxic Effects

One step growth curves in the producer Vero-αHis and target MC38cea cell lines were generated to characterize replication kinetics of the novel MeVac constructs. In Vero-αHis cells titers for viruses with transgenes in the leader position of the genome (eGFP, mGM-CSF, mIP-10) and with FmIL-12 downstream of the *P* gene peaked 96 h post infection in the range of 4×10^5 ciu/ml and 3.5×10^3 ciu/ml for FmIL-12 and mGM-CSF encoding viruses, respectively (Figure 4.5). Viruses with transgenes downstream of the *H* gene reached highest titers in Vero-αHis cells 36 – 48 h post infection in the range of 2×10^6 ciu/ml and 1×10^4 ciu/ml for anti-CTLA-4 and IgG1-Fc encoding viruses, respectively (Figure 4.5). For the IgG1-Fc encoding virus only a minimal increase in the amount of viral particles was observed in Vero-αHis cells. This could be attributed to the fact that a very rapid destruction of the cell layer

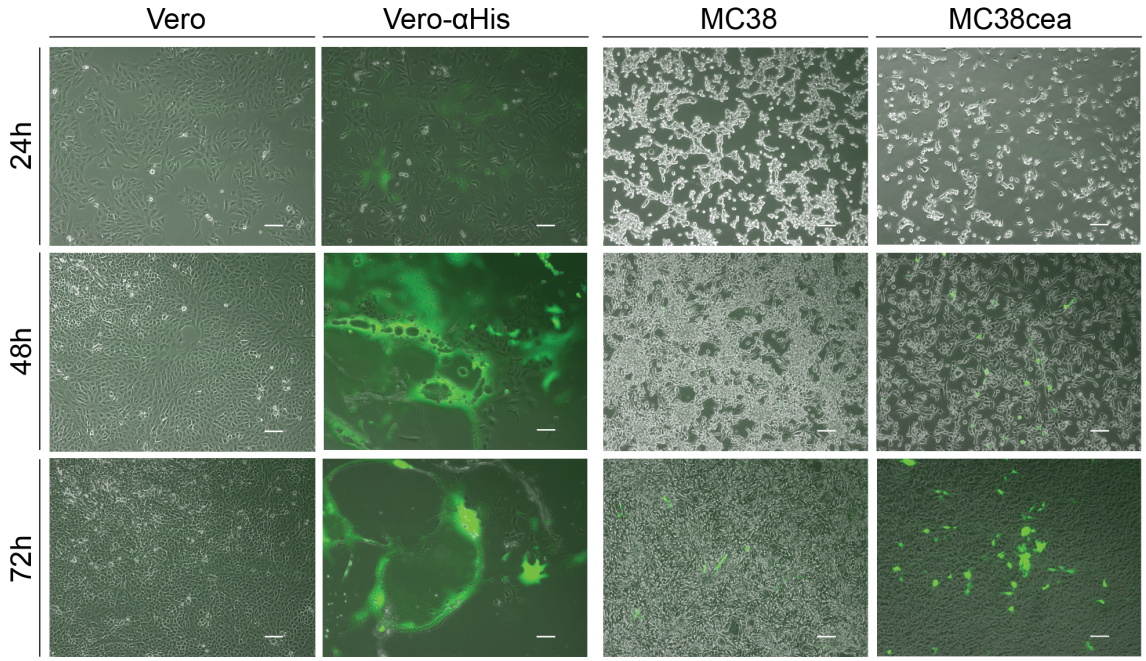

Figure 4.4: **Targeted infection with MeVac.** Cells were inoculated with MeVac ld-eGFP Hbl-αCEA at a multiplicity of infection = 1 and fluorescence microscopy images were taken at the depicted time points. Scale bars: 100 µm.

was observed when using this virus (Figure A.1*). Overall, viruses encoding smaller transgenes in the leader position reached lower titers in Vero-αHis cells than viruses with large transgenes downstream of the *H* gene. Reason for this could be a faster spread and a rapid destruction of cell layer by the less attenuated viruses with smaller transgenes which limits production of viral particles. In the target MC38cea cells titers for all viruses peaked between 36 h and 48 h post infection in the range of 4×10^5 and 2.25×10^3 ciu/ml for anti-CTLA-4 and mGM-CSF encoding viruses, respectively. In contrast to Vero-αHis cells, a steep decline of the virus particle amount after 48 h post infection was observed (Figure 4.5). Maximum titers in MC38cea for all viruses except for MeVac encoding IgG1-Fc were lower than in Vero-αHis cells. The observed peak of virus particle production followed by the decline and the lower amount of the produced viral particles in MC38cea cells in comparison to Vero-αHis cells reflects the host restriction of MeV to primate cells and the inability of MeV to efficiently counteract post-entry barriers in murine cells[228].

Of note is that the mGM-CSF encoding virus reached the lowest titers in both cell lines and it could be clearly observed that the spread of syncytia in Vero-αHis cell layer was markedly slower than for the other viruses (Figure A.2). Also production of this virus to high titers ($>1\times10^7$ ciu/ml) was hindered in comparison to other vectors. Titers in the third and fourth passage of the virus never exceeded 5×10^6 ciu/ml despite the complete fusion of the cell layer in syncytia. Complete genome sequencing was performed for a fourth virus passage of MeVac ld-mGM-CSF Hbl-αCEA and for a fourth virus passage of MeVac P-FmIL-12 Hbl-αCEA construct. One silent mutation within the *H* ORF and three one nucleotide changes

*Here and further, figures numbered as A.1, A.2, *etc.* are included in Appendix.

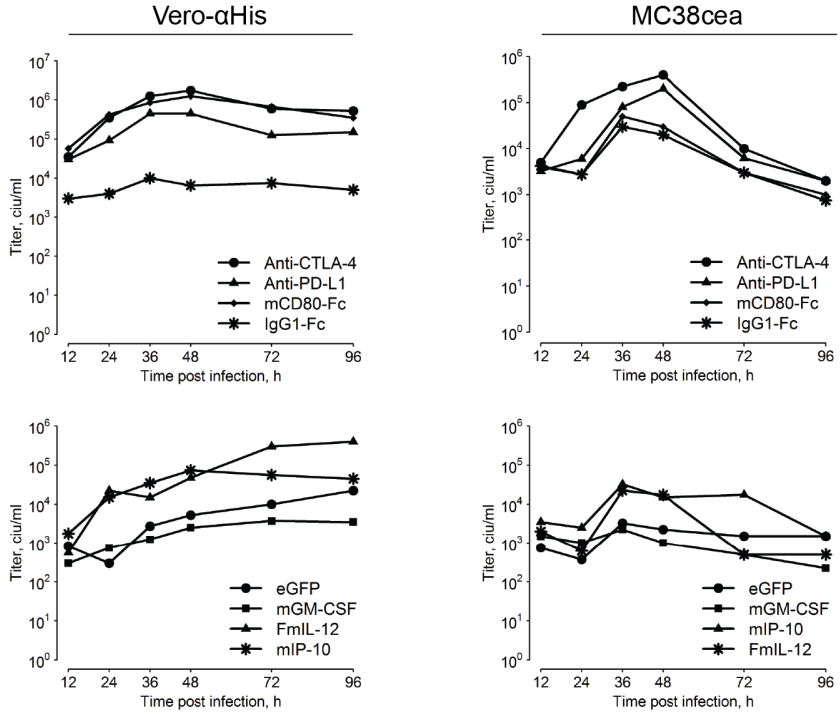

Figure 4.5: **One-step growth curves in Vero-αHis and MC38cea cells.** Cells were transduced with MeVac encoding the respective transgenes at a multiplicity of infection = 3. Cell suspensions were collected by scraping in the culture medium and titers determined at the depicted time points.

in the intergenic regions, that were identical in both constructs, were detected (Table A.1 in Appendix). Thus, mutations in the sequence of the mGM-CSF encoding construct were excluded as the cause for its impaired replication. Accumulation of defective interfering particles (DIs) could also explain an impaired replication of the mGM-CSF encoding vector. DIs are defective, incomplete virus genomes, that arise if the virus polymerase prematurely stops genome synthesis and subsequently, while still bound to the incomplete genome, re-initiates genome synthesis in the opposite direction. In such a manner, a hybrid of a virus genome and anti-genome with complementary ends is being generated. The DIs are known to interfere with virus replication and the frequency of DI generation can depend on virus strain, infected cell type, as well as the history of the virus passage[229]. To assess, if excessive DI generation could explain the impaired replication of MeVac encoding mGM-CSF, a PCR based assay was performed as described by Pfaller *et al.*[230]. Five other virus suspensions of the third or fourth passage were assessed along with the mGM-CSF encoding virus. In all of the tested virus passages, amplification with the two forward primers A1*SnaBI*/A2*NotI* yielded two bands at approximately 600 bp and 800 bp, which could indicate either common DIs species in all of the samples or an unspecific amplification. In the sample prepared from the mGM-CSF encoding virus the common band at 800 bp was missing. Only in the sample prepared from the mGM-CSF encoding virus suspension, a distinct band of approximately 300 bp was detected. This result indicates that, indeed, excessive DIs accumulation could be the cause of the impaired replication of the mGM-CSF encoding MeVac. Furthermore,

in addition to the mGM-CSF encoding MeVac, only in virus passages of MeVac encoding a murine IL-15 protein agonist (FmIL-15) constructed in a different project, which also demonstrated impaired replication, bands additionally to the two common bands could be detected after DIs specific amplification.

Cytotoxic properties of the novel constructs were further assessed. Target MC38cea cells were transduced with the respective viruses at an MOI = 5 and cell viability was determined with an XTT (2,3-Bis-(2-Methoxy-4-Nitro-5-Sulfophenyl)-2H-Tetrazolium-5-Carboxanilide) assay. As expected based on the observed impaired replication in MC38cea cells, only mild cytotoxic effects were detected. Cell viability decreased over the first 48 – 72 h and recovered afterwards (Figure 4.6). The vector encoding anti-PD-L1 caused the greatest decline of cell viability (Figure 4.6).

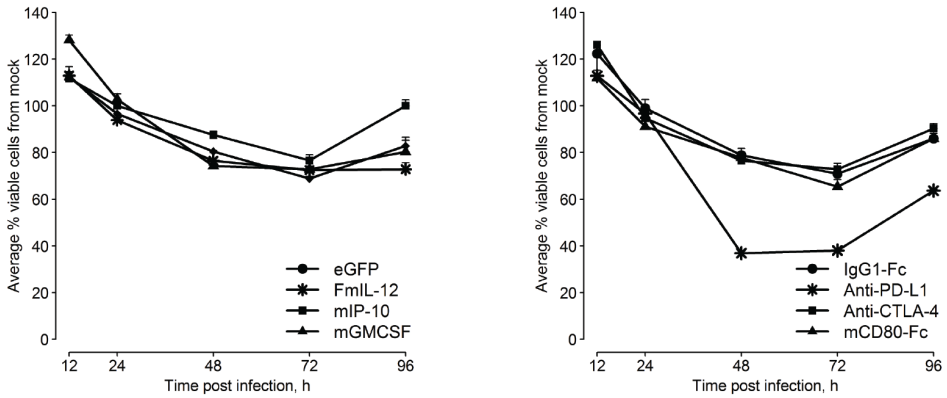

Figure 4.6: **Cytotoxicity in target MC38cea cells.** Cells were transduced with MeVac encoding the respective transgenes at a multiplicity of infection = 5 and cell viability was determined by XTT assay at the depicted time points. Mean results of triplicate infections per time point with standard errors of the mean (not visible for some data points) are shown.

4.1.5 Transgene Expression and Functionality

To assess expression kinetics of the immunomodulators inserted into the MeVac genome, MC38cea cells were transduced with the respective vectors and the concentration of immunomodulators was measured by ELISA at different time points. Expression of the control transgenes eGFP and IgG1-Fc was determined by fluorescence microscopy (Figure A.2) and western blot analysis (Figure A.4), respectively. Different patterns of expression kinetics were observed for the MeVac encoded immunomodulators (Figure 4.7). Anti-CTLA-4 expression reached a peak 36 h post infection and declined afterwards. Anti-PD-L1 and FmIL-12 concentration continuously increased over the course of the experiment reaching the highest level 96 h post infection, but for mCD80-Fc and mGM-CSF the highest concentration was measured in the inoculum at the time point of infection (0 h).

In case of mIP-10, an increase of the specific signal was observed also in the supernatants collected from cells transduced only with the eGFP encoding vector. A barplot depicting mIP-10 concentration in MC38cea transduced with both mIP-10 and eGFP vectors showed

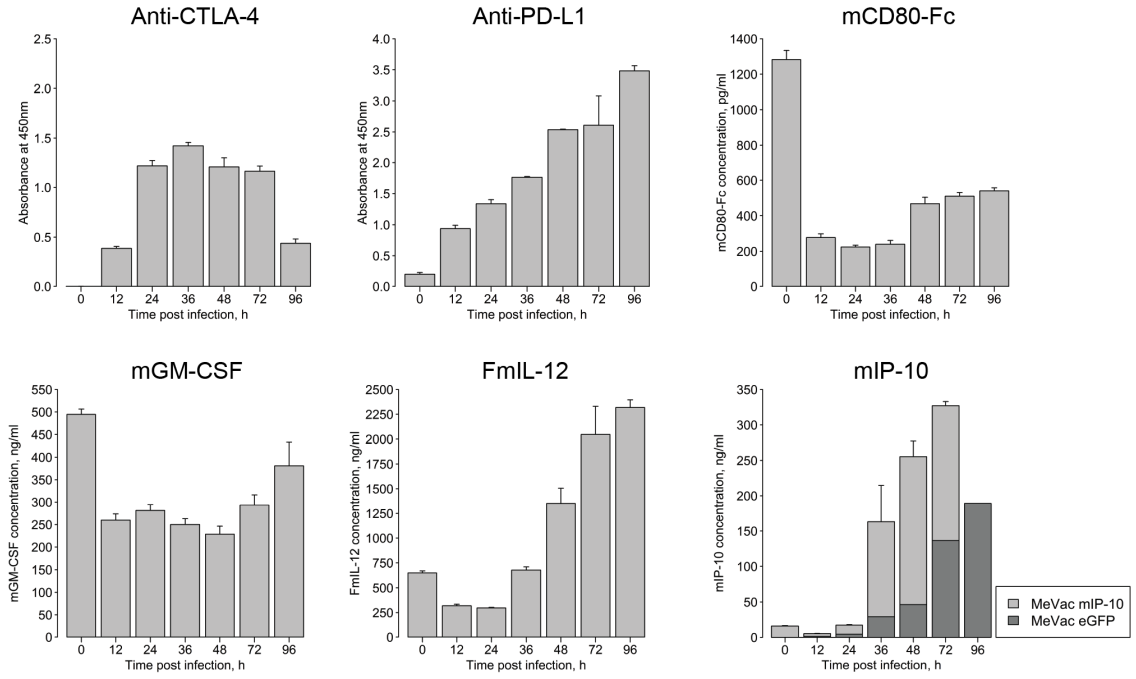

Figure 4.7: **Expression of MeVac encoded immunomodulators.** MC38cea cells were transduced with MeVac encoding the respective immunomodulators and eGFP or IgG1-Fc as control vectors at a multiplicity of infection = 3. Supernatant samples were collected at the depicted time points and transgene expression was detected by ELISA. Unspecific binding was controlled by IgG1-Fc (upper panels) or eGFP (lower panels) supernatants and subtracted from the specific measurements. In case of mIP-10 an increase of the signal was observed in the eGFP controls which was not subtracted from the specific measurements and is depicted accordingly.

that there is a specific expression of MeVac encoded mIP-10 as a markedly higher mIP-10 concentration was detected in cells transduced with mIP-10 encoding vector (Figure 4.7). However, the observed steady increase of the specific signal also in control samples suggested that untransduced MC38cea constitutively express mIP-10. RT-PCR was carried out to examine mIP-10 expression in untransduced MC38cea, parental MC38 and the unrelated B16 murine melanoma cell line on mRNA level. Results confirmed that mIP-10 is expressed in both MC38cea and MC38 cell lines and to a lesser extent also in B16 cells (Figure A.5). Expression of the mIP-10 receptor CXCR3 was also further assessed by RT-PCR in all of these cell lines. Weak bands for the specific product were detected in MC38cea and MC38 lines and a notably more intensive band in the B16 line (Figure A.5). Therefore, the MC38cea model was considered unsuitable for evaluation of mIP-10 in the context of MeV therapy.

Functionality of MeVac-encoded immunomodulators was further evaluated *in vitro*. Measles encoding mGM-CSF has been studied previously [212]. Functionality of MeVac-encoded mIP-10 was assessed in a chemotaxis assay. Supernatants containing MeVac-encoded mIP-10 attracted more splenocytes than supernatants from cells infected with MeVac encoding eGFP (Figure A.6). Cell lines expressing CTLA-4 and PD-L1 were necessary to assess the ability of MeVac encoded anti-CTLA-4, anti-PD-L1 and mCD80-Fc to counteract the

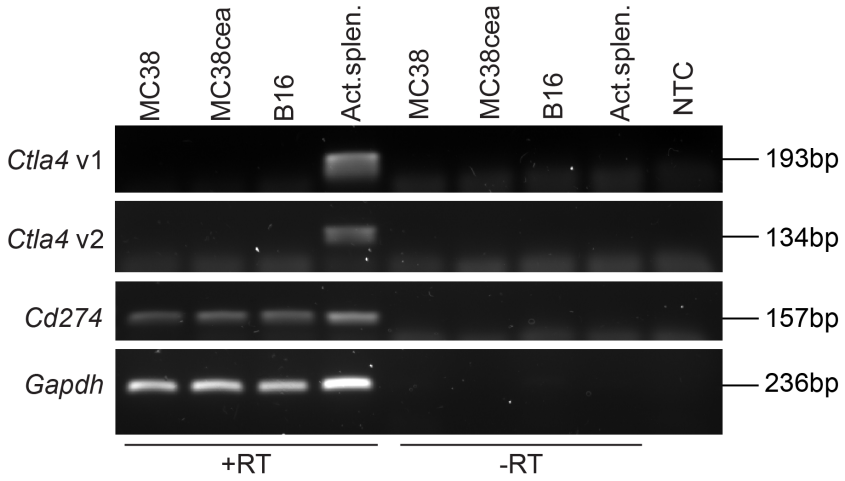

Figure 4.8: **Murine *Ctla4* and *Pd-l1* expression in MC38, MC38cea and B16 cell lines.** RT-PCR for murine *Ctla4* variant 1 (v1) and variant 2 (v2), *Pd-l1* (*Cd274*) and *Gapdh* as a loading control was carried out using cDNA from the indicated cell lines. cDNA from murine splenocytes activated with PMA and ionomycin served as a positive control. +RT — cDNA samples; -RT — minus reverse transcriptase controls; NTC — no template control; Act.splen. — activated splenocytes.

immunosuppressive signaling. The target MC38cea, parental MC38 and B16 cell lines were tested for expression of both CTLA-4 and PD-L1 on mRNA level by RT-PCR. Neither of the two murine CTLA-4 splice variants was detected in any of the tested cell lines (Figure 4.8). PD-L1 expression was however detected in all of the cell lines (Figure 4.8).

Anti-PD-L1 binding to the PD-L1 positive MC38cea cells was assessed by flow cytome-

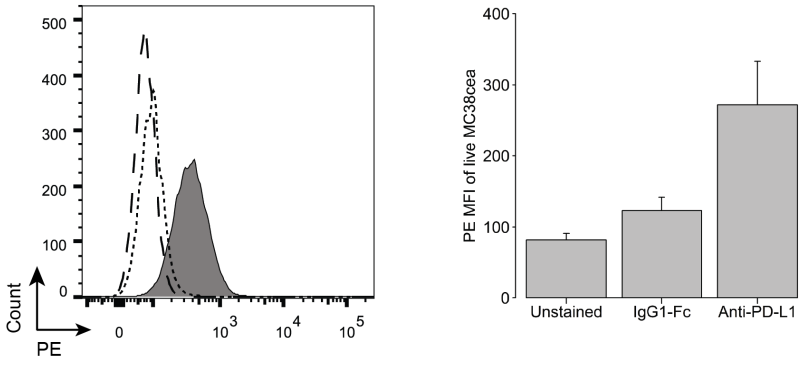

Figure 4.9: **MeVac encoded anti-PD-L1 binding to MC38cea cells.** MC38cea cells were incubated with supernatants from Vero-αHis infected with MeVac encoding anti-PD-L1 or IgG1-Fc. For detection of bound anti-PD-L1 cells were stained with primary Ab specific for the HA tag and secondary Ab coupled to PE. DAPI staining was used to exclude dead cells and samples were analyzed by flow cytometry. Overlay histogram for PE of DAPI$^-$ MC38cea populations from one of three independent experiments is shown in the left panel. Dashed — untreated MC38cea; dotted — MC38cea treated with IgG1-Fc; solid fill — MC38cea treated with anti-PD-L1. Average median fluorescence intensity (MFI) of PE for DAPI$^-$ populations with standard error of the means from the three independent experiments is shown in the right panel.

try. An increase in the fluorescence signal was observed in samples treated with supernatants from Vero-αHis infected with MeVac encoding anti-PD-L1 in comparison to untreated cells or cells treated with supernatant from Vero-αHis infected with MeVac encoding IgG1-Fc (Figure 4.9), indicating specific binding of MeVac encoded anti-PD-L1 to the surface of PD-L1 positive cells.

The ability of MeVac encoded anti-PD-L1 and mCD80-Fc to counteract the immunosuppressive signaling of PD-L1 positive MC38cea cells was further assessed. Cocultivation of activated murine splenocytes with untreated MC38cea cells markedly decreased IFN-γ concentration in culture medium, suggesting that immunosuppressive signaling is taking place. However, IFN-γ concentration increased when activated splenocytes were cocultivated with MC38cea cells treated with supernatants collected from cells infected with MeVac encoding anti-PD-L1, mCD80-Fc or anti-CTLA-4 (Figure 4.10.a). IFN-γ concentration did not increase if MC38cea cells were treated with supernatants containing MeVac encoded IgG1-Fc. These results suggest that the examined MeVac encoded immunomodulators are able to counteract immunosuppression mediated by PD-L1 positive tumor cells.

Functionality of MeVac encoded FmIL-12 was assessed by the ability to induce IFN-γ production in murine splenocytes. Cultivation of murine splenocytes in medium containing different concentrations of MeVac encoded FmIL-12 revealed that the increase in IFN-γ production is dependent on FmIL-12 concentration in the range of 0.01 - 1 ng/ml. IFN-γ concentration decreased when using FmIL-12 concentrations higher than 1 ng/ml, probably due to over-stimulation of the cells and activation induced cell death (Figure 4.10.b).

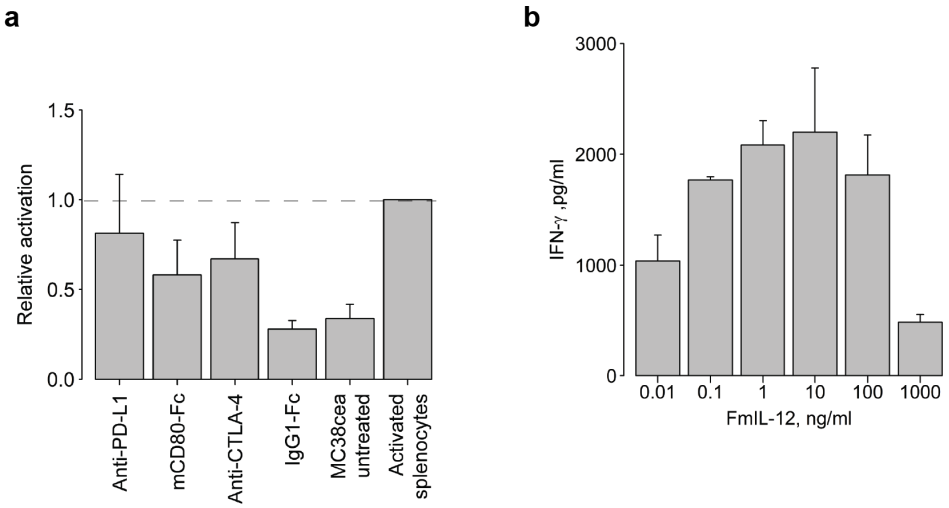

Figure 4.10: **Functionality of MeVac encoded immunomodulators. a** – MC38cea cells were treated with supernatants from Vero-αHis cells infected with MeVac encoding the respective immunomodulators and cocultured at a ratio 2:1 with murine splenocytes in the presence of PMA and ionomycin. After 24 h supernatants were collected and IFN-γ concentrations were measured by ELISA. Relative activation corresponds to the ratio of the optical density (absorbance at 450 nm minus 570 nm) of the respective samples to activated splenocytes. Mean relative activation values with standard errors of the mean from three independent experiments are shown; **b** – murine splenocytes were stimulated with recombinant murine IL-2 and cultivated in the presence of medium from Vero-αHis infected with MeVac encoding FmIL-12 or eGFP. After 48 h supernatants were collected and IFN-γ concentrations were measured by ELISA. Mean IFN-γ concentrations with standard errors of the mean of triplicate splenocyte cultures are shown for each FmIL-12 concentration. IFN-γ concentrations in the eGFP controls were close to background (data not shown). Representative data from one of two independent experiments are shown.

4.2 Evaluation of Therapeutic Efficacy *in vivo*

Therapeutic efficacy of the novel MeVac vectors encoding immunomodulators was evaluated in the immunocompetent subcutaneous (s.c.) murine colon adenocarcinoma model MC38cea[226]. First, screening experiments to identify the most promising vectors in terms of reduction of tumor growth and extension of animal survival were performed. After the screening experiments a head-to-head comparison of the most promising vectors encoding FmIL-12 and anti-PD-L1 was performed in the s.c. MC38cea model. The potential for combination of the MeVac vectors encoding FmIL-12 and anti-PD-L1 was also considered. Therapeutic efficacy of the combination of these two vectors was evaluated in the s.c. MC38cea model and in the more aggressive s.c. murine melanoma B16-CD20 model[104]. Finally, the establishment of systemic anti-tumor immunity in long-term survivors of MeVac therapy was examined in tumor rechallenge experiments *in vivo* and splenocyte restimulation experiments *in vitro*.

4.2.1 Identification of the Most Promising Vectors

First, vectors encoding immunomodulators targeting the immunosuppressive tumor environment (anti-CTLA-4, anti-PD-L1, mCD80-Fc) and selected combinations of these were compared. Statistically significant differences in tumor growth or survival of the animals could not be observed between the treatment groups (Figure 4.11.a). However, a trend towards an extended survival of animals was observed in the group that received treatment with the anti-PD-L1 encoding vector only. Two out of nine animals in the anti-PD-L1 group experienced complete tumor remissions (Figure 4.11.a). It must be noted that a halted tumor growth for a period of approximately 35 days was observed for one mouse receiving treatment with the mCD80-Fc encoding MeVac, indicating a therapeutic effect of the applied vector (Figure A.7).

Vectors encoding immunomodulators targeted at enhancement of antigen presenting cell (mGM-CSF) and immune effector cell functions (FmIL-12 and mIP-10) as well as selected combinations of these were compared in the next experiment. Due to the propagation problems of the mGM-CSF encoding vector (see subsection 4.1.4), a lower virus dose (5×10^6 ciu/injection) was used, treatment was started earlier and carried out for five instead of four consecutive days. Significantly delayed increase of tumor volume in comparison to mock was observed in groups that received MeVac encoding FmIL-12 alone or in combination with both, the GM-CSF and mIP-10 encoding vectors, as well as in the group receiving treatment with the eGFP encoding vector (Figure 4.11.b). Survival of the animals was significantly extended in the groups receiving treatment with the FmIL-12 encoding vector only or in both combination groups in comparison to mock treatment (Figure 4.11.b). Notably, seven out of nine mice in the FmIL-12 only group experienced complete tumor remissions as well as six out of nine and five out nine mice in the combination groups with GM-CSF and mIP-10, respectively. Thus, these screening experiments identified MeVac encoding FmIL-12 and anti-PD-L1, respectively, as having the best therapeutic efficacy in each experiment.

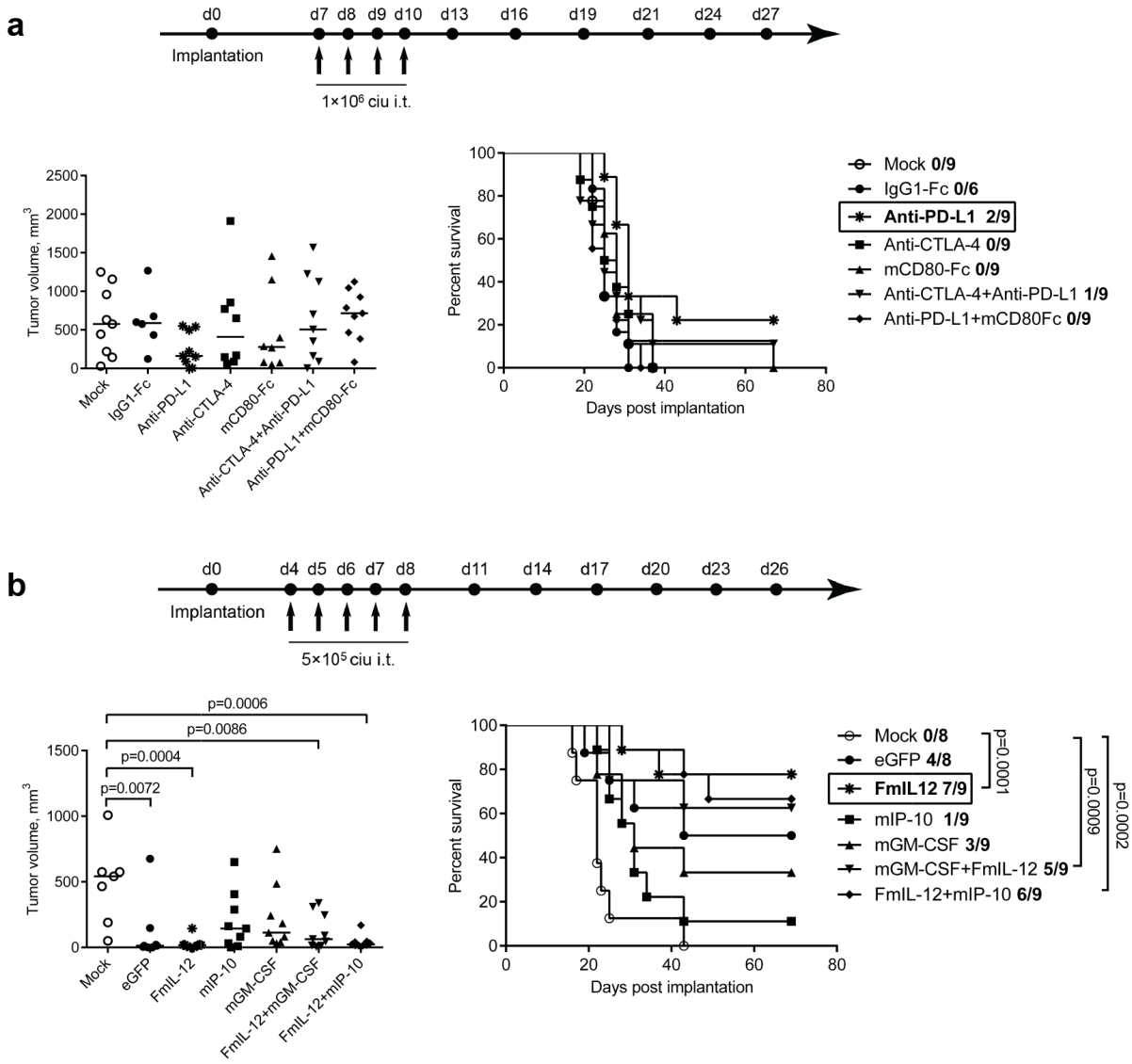

Figure 4.11: **Therapeutic efficacy of immunomodulatory MeVac.** MC38cea cells were implanted subcutaneously (s.c.) into the right flank of C57BL/6J mice (6 – 9 animals per group). When tumors reached an average volume of 40 – 70 mm^3 mice received intratumoral injections (black arrows) with 1×10^6 ciu (**a**) or 5×10^5 ciu (**b**) with MeVac vectors encoding the respective transgenes on four (**a**) or five (**b**) consecutive days in 100 µl virus suspension with carrier fluid (OptiMEM). Mice in mock groups received i.t. injections of 100 µl OptiMEM. Tumor volume distribution on day 19 (**a**) and day 16 (**b**) post implantation with dots representing individual mice and Kaplan-Meier survival analysis are shown. Complete tumor remission rates are shown for each group in Kaplan-Meier plots. ciu — cell infectious units.

4.2.2 Therapeutic Efficacy of the Most Promising Vectors

Therapeutic efficacy of the FmIL-12 and anti-PD-L1 vectors was subsequently directly compared in the s.c. MC38cea tumor model. MeVac encoding IgG1-Fc instead of eGFP was included as a control vector due to more similar genome structure to both FmIL-12 and

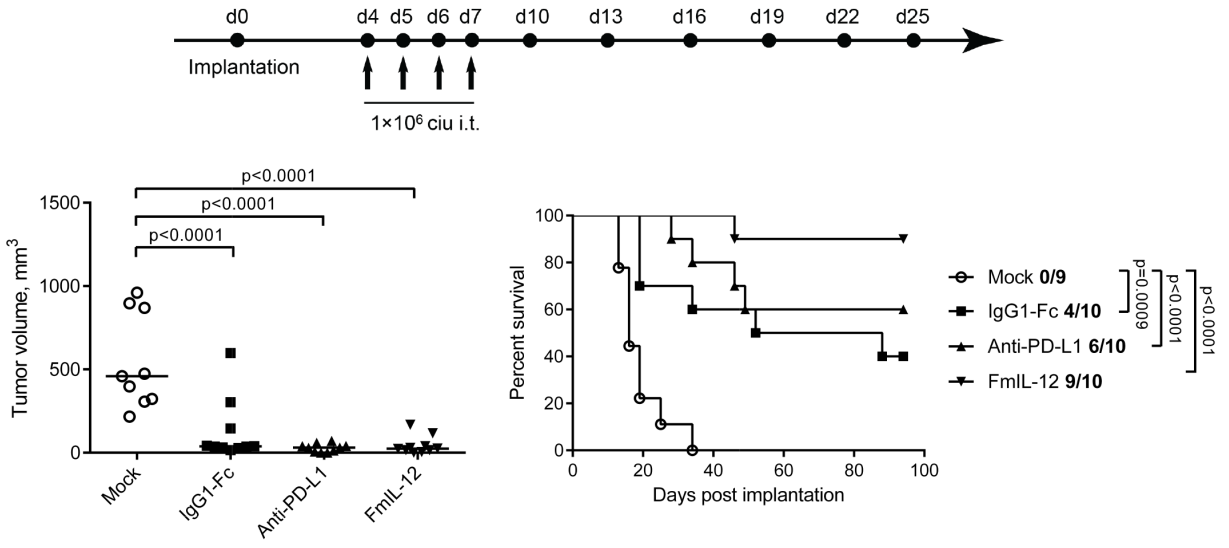

Figure 4.12: **Comparison of therapeutic efficacy of MeVac encoding FmIL-12 and anti-PD-L1.** MC38cea cells were implanted subcutaneously into the right flank of C57BL/6J mice (10 animals per group). When tumors reached an average volume of 40 mm^3 mice received intratumoral (i.t.) injections with 1×10^6 ciu of viruses encoding the respective transgenes on four consecutive days in 100 µl virus suspension with carrier fluid (OptiMEM). Mice in the mock group received i.t. injections of 100 µl OptiMEM. Tumor volume distribution on day 16 post implantation with median for each group and Kaplan-Meier analysis are shown. Dots represent individual mice. Complete tumor remission rates are shown for each group in the Kaplan-Meier plot. ciu — cell infectious units.

anti-PD-L1 encoding vectors. MeVac treatment led to a significant delay in tumor growth and prolonged survival of the animals in comparison to mock treatment, but no significant differences were observed between the virus treatment groups (Figure 4.12). However, frequency of complete tumor remissions indicated differences in efficacy: Four out of ten animals treated with MeVac IgG1-Fc experienced complete tumor remissions, in contrast to six and nine out of ten animals treated with MeVac encoding anti-PD-L1 and FmIL-12, respectively. This result suggested an added therapeutic benefit for anti-PD-L1 and especially FmIL-12 in the context of MeVac therapy.

Interleukin-12 is a known potent activator of immune cells with one of its main properties being induction of IFN-γ production by NK and T cells[27]. It is however also known that IFN-γ upregulates expression of PD-L1 as a negative feedback loop mechanism[231]. This property would warrant combination of IL-12 therapy with blockade of PD-L1 to impede the immunosuppressive signaling upregulated through IFN-γ induction. Furthermore, although application of MeVac encoding FmIL-12 even as a single agent demonstrated a highly beneficial anti-tumor effect in the MC38cea model, the efficacy could be more modest in other less immunogenic and more aggressive tumor models. Given this rationale, experiments evaluating efficacy of combining MeVac vectors encoding FmIL-12 and anti-PD-L1 were performed in the previously used MC38cea model and the more aggresive immunocompetent murine

melanoma B16-CD20 model[104]. Efficacy of the combination of vectors encoding FmIL-12 and anti-PD-L1 was compared with combinations of both vectors with MeVac encoding IgG1-Fc. In the MC38cea tumor model a significantly delayed increase of tumor volume in comparison to mock was observed in the groups receiving treatment with any combination of MeVac vectors, but no differences were observed between the treatment groups (Figure A.10.a). Survival of animals was significantly extended in the groups receiving treatment with the FmIL-12 and anti-PD-L1 combination and the FmIL-12 and IgG1-Fc vector combination in comparison to mock. However, more animals experienced complete tumor remissions in the group receiving treatment with FmIL-12 and IgG1-Fc vector combination (nine of ten) than in the FmIL-12 and anti-PD-L1 (six of ten) combination group (Figure A.10.a). In the B16-CD20 tumor model significantly delayed increase of tumor volume in comparison to mock was observed only in the group receiving treatment with FmIL-12 and IgG1-Fc vector combination (Figure A.10.b). Survival of the animals was extended in comparison to mock in all groups receiving treatment with MeVac vector combinations. The FmIL-12 and anti-PD-L1 as well as the FmIL-12 and IgG1-Fc combination extended survival significantly more than the anti-PD-L1 and IgG1-Fc vector combination. No clear benefit could however be recognized comparing the FmIL-12 and IgG1-Fc with the FmIL-12 and anti-PD-L1 vector combination. No complete tumor remissions could be achieved with the examined treatment strategies in the B16-CD20 tumor model (Figure A.10.b). These results therefore suggested that there is no added therapeutic benefit when applying this combination of MeVac vectors encoding FmIL-12 and anti-PD-L1 over the FmIL-12 in combination with a control vector in this setting.

A certain amount of MeVac encoded transgene that is produced during virus propagation in Vero-αHis cells remains present in the MeVac virus suspension. A non-targeted MeVac encoding FmIL-12 was evaluated in the MC38cea model in comparison to the targeted MeVac FmIL-12 Hbl-αCEA to assess the effects of the FmIL-12 delivered with virus suspension. FmIL-12 could be detected in the serum collected from peripheral blood of mice treated with both non-targeted and targeted constructs on the second day of treatment and two days after the last treatment. The maximal FmIL-12 concentration, 857.5 pg/ml, was detected in the MeVac FmIL-12 Hbl-αCEA group on third day of treatment. Expressed as a dose per kg of body mass, if assuming total blood volume of a mouse ≈1.7 ml and body mass ≈22 g, this equals to ≈66 ng/kg. Mice that received the targeted virus had significantly higher serum levels of FmIL-12 on the second day of treatment than the mice receiving the non-targeted virus (Figure 4.13.b). The FmIL-12 serum level declined to baseline within a week after the last treatment. This implies a *de novo* FmIL-12 production during virus replication in MC38cea cells *in vivo* after treatment with the targeted virus. Regarding efficacy, treatment with both non-targeted and targeted FmIL-12 vectors significantly delayed tumor growth and extended survival of the animals in comparison to mock, but no significant differences could be observed between the treatment groups (Figure 4.13.c, d). This result demonstrated that the delivery of a virus unable to replicate in the tumor cells and containing immunomodulator

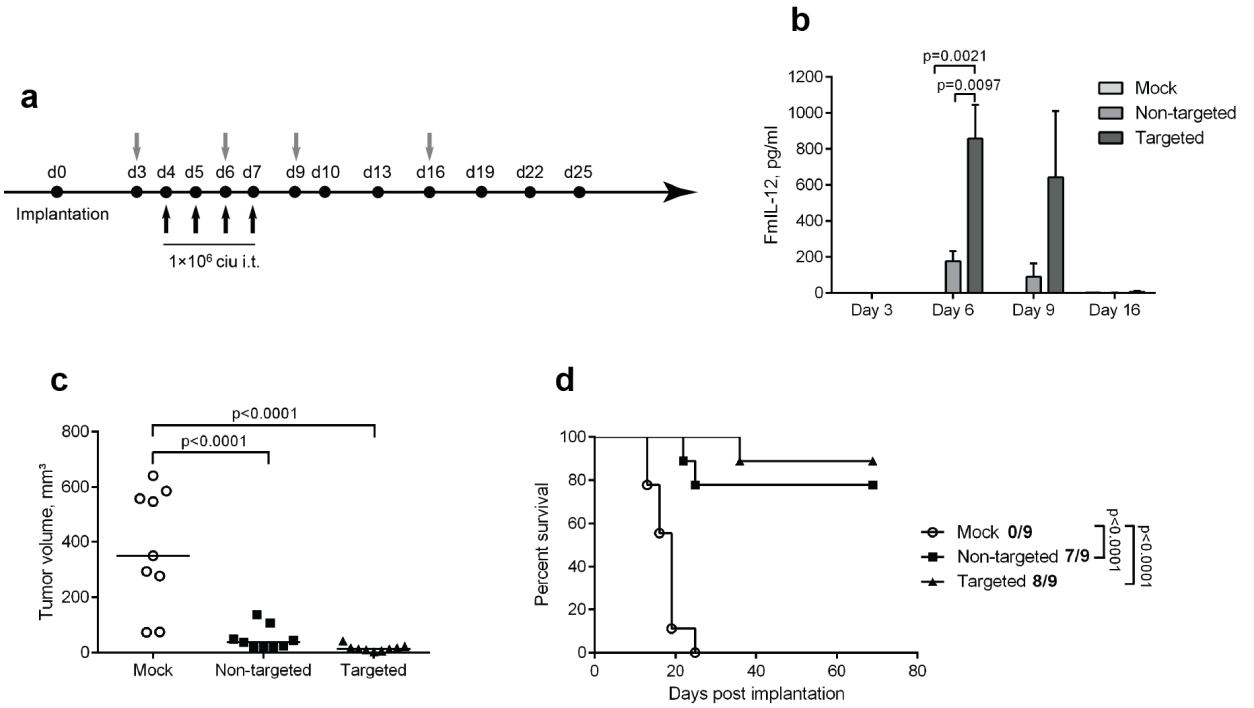

Figure 4.13: **Systemic levels of FmIL-12 after intratumoral application and therapeutic efficacy of a non-targeted MeVac FmIL-12**. **a** — schedule of the experiment. MC38cea cells were implanted subcutaneously (s.c.) into the right flank of C57BL/6J mice (9 animals per group). When tumors reached an average volume of 40 mm^3 mice received intratumoral (i.t.) treatment with 1×10^6 ciu of the respective viruses on four consecutive days (black arrows) in 100 µl virus suspension with carrier fluid (OptiMEM). Mice in the mock group received i.t. injections with 100 µl OptiMEM. **b** — peripheral blood was collected from 3 – 4 animals per group from the *vena saphena* at the time points denoted with grey arrows in **a**. Serum was collected, the concentration of FmIL-12 was measured by ELISA and the results were analysed with one-way ANOVA. Mean values from 2 – 5 individual samples per group with standard errors of the mean are shown. **c** — tumor volume distribution on day 13 post implantation. Dots representing individual mice and a median in each group are shown. **d** — Kaplan-Meier plot. Complete tumor remission rates are shown for each group. ciu — cell infectious units.

only in the virus suspension is sufficient to achieve similar therapeutic benefit as with the replicating virus which ensures also *de novo* production of the immunomodulator *in vivo*.

4.2.3 Assessment of anti-tumor immune response in long-term survivors of MeVac therapy

Animals experiencing complete tumor remissions after MeVac therapy were rechallenged with MC38cea cells six months after the initial tumor cell implantation. Tumor engraftment rejection rates were monitored to assess establishment of protective anti-tumor immunity. All of the mice previously treated with FmIL-12 and anti-PD-L1 encoding vectors from the experiment comparing efficacy of FmIL-12 and anti-PD-L1 encoding MeVac and three

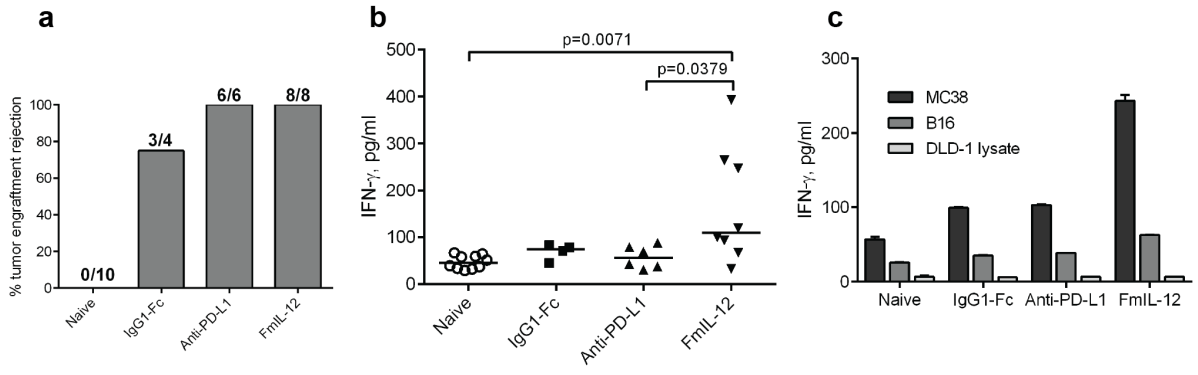

Figure 4.14: **Systemic anti-tumor immunity in long-term survivors of MeVac therapy.** Animals experiencing complete tumor remissions after treatment with MeVac encoding the respective transgenes were rechallenged with subcutaneous (s.c.) MC38cea implantation six months after the initial tumor cell implantation. Naive mice served as a control group. **a** – mice were monitored for tumor engraftment. Tumor rejection rates are shown. Splenocytes were collected from the animals two weeks after rechallenge, stimulated with recombinant murine IL-2 and cocultivated with MC38cea cells (**b**) or with MC38 and B16 cells and DLD-1 cell lysate (**c**) for one mouse from each group at a ratio 10:1. Supernatants were collected after 48 h and IFN-γ concentration was measured by ELISA. Dots representing individual mice and a median in each group are shown in **b**. Mean values with standard errors of the mean from two replicate measurements per sample are shown in **c**.

out of four mice treated with the IgG1-Fc vector rejected secondary tumor engraftment, in contrast to naive control mice, where tumor engraftment was observed in all animals (Figure 4.14.a). The ability to reject secondary tumor engrafment in mice treated with MeVac was confirmed also in other rechallenge experiments. In total, 64 of 71 mice (90.1%) that experienced complete tumor remissions after treatment with different MeVac vectors or vector combinations rejected secondary tumor engraftment in contrast to only 3 of 25 (10.7%) naive mice.

To assess specificity of the induced anti-tumor immune response, splenocytes from the survivors in the experiment comparing efficacy of the FmIL-12 and anti-PD-L1 vectors were stimulated with MC38cea *in vitro* two weeks after tumor rechallenge. A significantly higher IFN-γ production was observed in the group receiving MeVac encoding FmIL-12 compared to naive mice and the anti-PD-L1 group (Figure 4.14.b), suggesting more potent cell mediated immune memory in animals treated with the FmIL-12 encoding MeVac. Stimulation with parental MC38 cells induced a similar IFN-γ production pattern as with MC38cea cells, demonstrating that the response is not CEA restricted (Figure 4.14.c). Only a slight induction of IFN-γ production was detected after stimulation with an unrelated murine tumor cell line, B16, and IFN-γ concentration was close to background after stimulation with human DLD-1 cell lysate (Figure 4.14.c), showing that the observed response is specific for MC38-derived tumor cells. Similarly, a higher IFN-γ memory recall after rechallenge was demonstrated also from survivors of treatment with MeVac encoding FmIL-12 in com-

bination with IgG1-Fc or anti-PD-L1 than from animals treated with the anti-PD-L1 and IgG1-Fc MeVac combination and naive mice (Figure A.11), further strengthening the results described above.

4.3 Analysis of MeVac induced Anti-Tumor Immune Effector Mechanisms

Analysis of the immunological milieu in tumors after MeVac therapy was performed to identify immune effector mechanisms associated with the mechanisms of action of MeVac encoding FmIL-12 or anti-PD-L1. Assuming that FmIL-12 would exert its specific effects earlier after expression than anti-PD-L1, two experiments with different schedules were carried out. To analyze the effects of the vector encoding FmIL-12, tumors were explanted 24 h (Figure 4.15.a), but to analyze the effects of the vector encoding anti-PD-L1 tumor were explanted four days (Figure 4.15.b) after the last treatment. Control group receiving treatment with the IgG1-Fc encoding vector and a mock group were also included in each experiment. After tumor explantation the material was divided for flow cytometry, cytokine bead array and RT-qPCR analyses (Figure 4.15.c). Further, depletions of the main immune effector cell populations were performed to identify their contribution for the therapeutic efficacy of the most promising MeVac vector encoding FmIL-12.

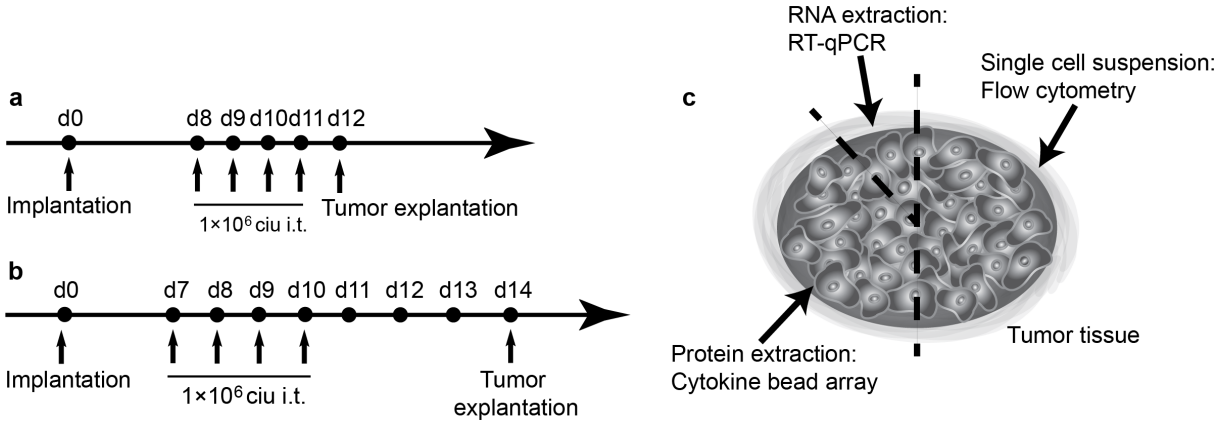

Figure 4.15: **Treatment schedules and schematic for preparation of tumor material for analyses of MeVac induced immune effectors.** MC38cea cells were implanted subcutaneously into the right flank of C57BL/6J mice (12 animals per group). When tumors reached an average volume of 120 mm^3 (**a**) or 100 mm^3 (**b**) mice received intratumoral (i.t.) treatment with 1×10^6 ciu of MeVac encoding FmIL-12 or IgG1-Fc (**a**) or anti-PD-L1 or IgG1-Fc (**b**) on four consecutive days in 100 µl virus suspension with carrier fluid (OptiMEM). Mice in the mock group received i.t. injections with 100 µl OptiMEM. Tumors were explanted one (**a**) or four (**b**) days after the last treatment and tumor material was divided for further analyses as depicted in **c**.

4.3.1 Quantification of Transcription Factor Expression

The mRNA levels of the transcription factors *Foxp3* and *T-bet* were quantified in the tumors after MeVac therapy to assess changes in immunosuppressive and cell mediated immune response mediators, respectively. Complete RNA was extracted from the freshly explanted tumor material (Figure 4.15) and reverse transcriptase quantitative PCR (RT-qPCR) analysis was carried out. RNA integrity was assessed by electrophoresis on an agarose gel and only samples with clear 18S and 28S ribosomal RNA bands were included in the analysis (Figure A.12). mRNA levels of different potential reference genes in representative samples from all treatment groups were evaluated before the analysis. The reference gene *L13a* (*Rpl13a*) had the lowest variation of the mRNA levels between the samples and the treatment groups and was, thus, chosen for further use (Figure A.13).

In the "early" experiment, including the group with the FmIL-12 encoding vector, analysis indicated an increased level of *T-bet* mRNA in the tumors treated with the FmIL-12 encoding vector in comparison to the IgG1-Fc encoding vector and mock groups (Figure 4.16.early). In the "late" experiment, including the treatment group with the anti-PD-L1 encoding vector, only a slight shift towards elevated amount of *T-bet* mRNA in comparison to the IgG1-Fc encoding vector and mock groups could be detected, but the differences were

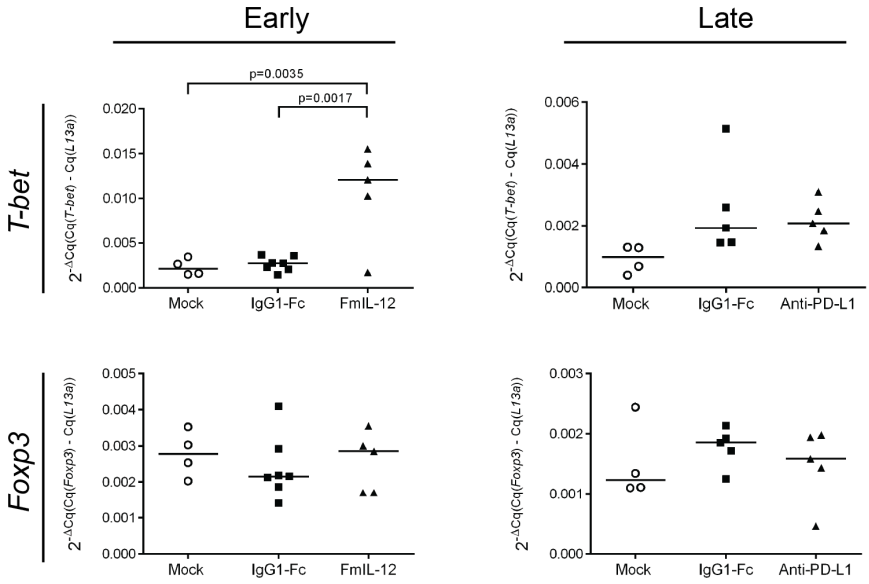

Figure 4.16: **Changes in *T-bet* and *Foxp3* mRNA levels after MeVac therapy.** MC38cea cells were implanted subcutaneously into C57BL/6J mice. When tumors reached an average volume of 120 mm^3 (early) or 100 mm^3 (late) mice received intratumoral treatment with MeVac encoding the respective transgenes or the respective amount of OptiMEM (mock). Reverse transcription quantitative PCR (RT-qPCR) analysis was carried out using RNA from tumors explanted one (early) or four (late) days after the last treatment. Dots representing samples from individual mice and median values are shown. C_q — quantification cycle.

not statistically significant (Figure 4.16.late). No statistically significant differences could be detected in *FoxP3* mRNA levels in either of the experiments between any of the treatment groups.

4.3.2 Cytokine Expression Profiling

Intratumoral cytokine profiles after therapy with MeVac encoding FmIL-12 or anti-PD-L1 were examined with cytokine bead array. Levels of seven different cytokines defining polarization towards Th_1 (IL-2, IFN-γ, TNF (tumor necrosis factor)-α), Th_2 (IL-4, IL-10) or Th_{17} (IL-17) associated immune response types were simultaneously measured in tumor samples prepared as described before (Figure 4.15). Significantly higher IFN-γ and TNF-α concentrations were detected in the group receiving treatment with MeVac encod-

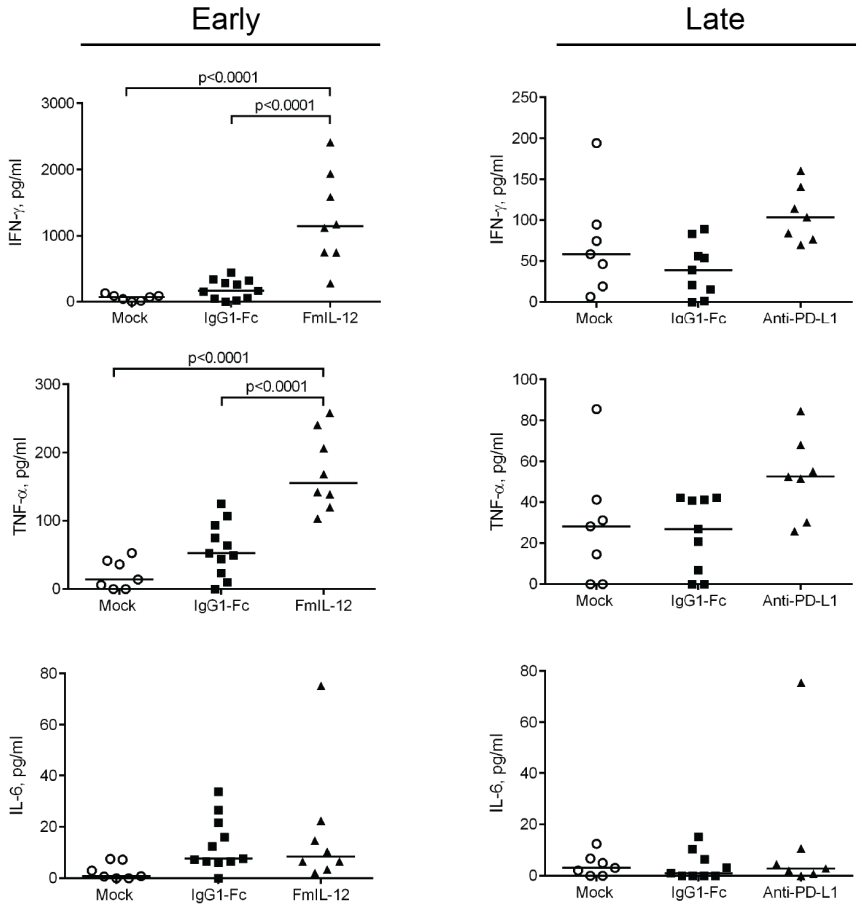

Figure 4.17: **Intratumoral cytokine profiles after MeVac therapy.** MC38cea cells were implanted subcutaneously into C57BL/6J mice. When tumors reached an average volume of 120 mm^3 (early) or 100 mm^3 (late) mice received intratumoral treatment with MeVac encoding the respective transgenes or the respective amount of OptiMEM (mock). Cytokine bead arrays were performed using protein extracts from tumors explanted one (early) or four (late) days after the last treatment. Dots representing tumor samples from individual mice and a median value in each group are shown.

ing FmIL-12 than in the groups receiving treatment with the IgG1-Fc encoding vector and mock (Figure 4.17.early). Also a slightly, but not significantly, higher IL-6 concentration was observed in both the MeVac IgG1-Fc and FmIL-12 treatment groups in comparison to mock (Figure 4.17.early). In the experiment including the treatment group with the anti-PD-L1 encoding vector, no significant differences in cytokine expression could be observed between the treatment groups, except for a slightly higher IFN-γ and TNF-α concentration in the group receiving treatment with the anti-PD-L1 encoding vector in comparison to the IgG1-Fc and mock groups (Figure 4.17.late). The cytokines IL-2, IL-4, IL-10 and IL-17 were close to background in all samples tested (data not shown).

4.3.3 Analysis of Tumor Infiltrating Lymphocyte Subpopulations

Further, changes in tumor infiltrating lymphocyte (TIL) subpopulations after MeVac therapy were evaluated. Single cell suspensions were prepared using tumor material explanted in the previously described experiments (Figure 4.15) and flow cytometry analysis was carried out. The gating strategy for a representative sample is shown in Figure 4.18.

Significant differences in the total amount of the $CD45^+$ cells could not be observed between the treatment groups. Treatment with MeVac encoding FmIL-12 led to a massive decrease of the amount of natural killer (NK) cells ($CD335^+$) (Figure 4.19.early) in comparison to treatment with IgG1-Fc encoding vector and mock. The amount of activated NK cells ($CD335^+CD69^+$) however was significantly higher after treatment with FmIL-12 vector in comparison to the IgG1-Fc and mock groups (Figure 4.19.early). A significant decrease in the amount of NK cells was observed also after treatment with both the IgG1-Fc and anti-PD-L1 encoding vectors in comparison to mock with a slightly greater decrease in the anti-PD-L1 group, but the amount of activated NK cells did not differ between the groups (Figure 4.19.late). The proportion of TIL T cells increased significantly in the "early" experiment after treatment with the FmIL-12 encoding vector in comparison to the IgG1-Fc and mock groups and also in the "late" experiment after treatment with IgG1-Fc and anti-PD-L1 encoding vectors in comparison to mock (Figure 4.19). The size of the cytotoxic T cell subpopulation ($CD3^+CD8^+$) did not differ significantly between treatment groups in neither of the experiments. A slight, but not significant increase of the activated cytotoxic T cell population ($CD3^+CD8^+CD69^+$) could be observed after treatment with the FmIL-12 vector in the "early" experiment. However, treatment with MeVac encoding anti-PD-L1 and IgG1-Fc led to a significant decrease in the activated cytotoxic T cell population in comparison to mock (Figure 4.19). The size of the T helper cell population ($CD3^+CD4^+$) did not differ between treatment groups in the "early" experiment, but in the "late" experiment a slight and significant increase of the population could be observed after treatment with anti-PD-L1 encoding MeVac (Figure 4.19).

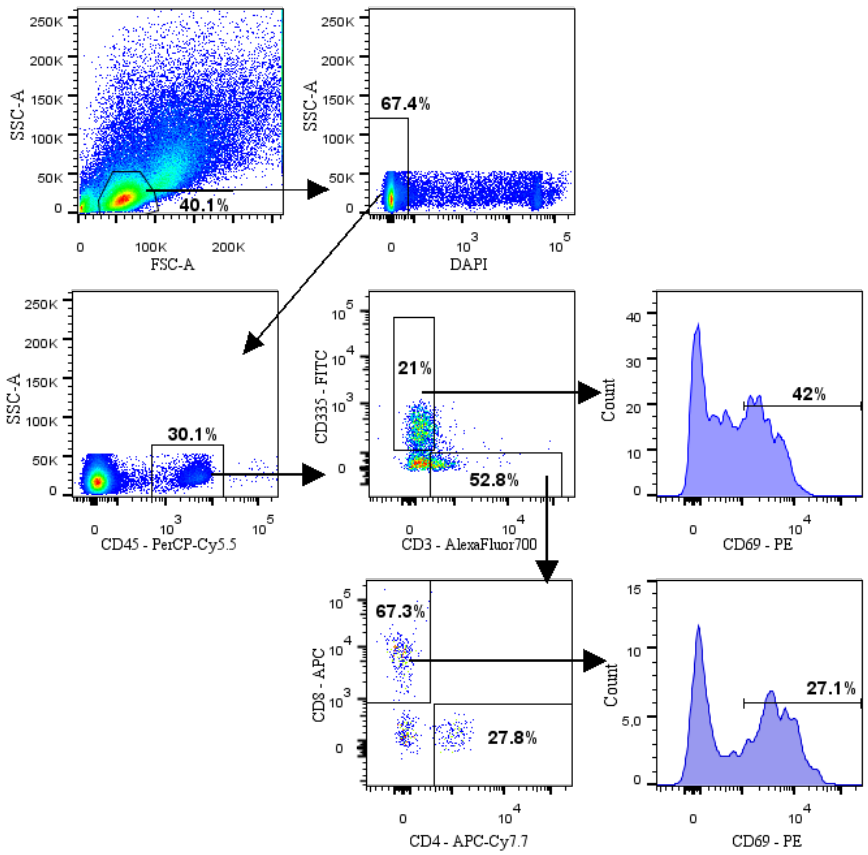

Figure 4.18: **Gating strategy for analysis of tumor infiltrating lymphocyte subpopulations after MeVac therapy.** The cell population of interest was identified using forward (FSC-A) and side scatter (SSC-A) parameters. Dead cells were excluded by gating on the DAPI negative cell population. Within the live cell population the leukocyte population was identified as the $CD45^+$ cells. Within the $CD45^+$ cell population the natural killer (NK) ($CD335^+$) and the T cell ($CD3^+$) populations were identified. Within the T cell population the cytotoxic T cell ($CD8^+$) and the helper T cell ($CD4^+$) populations were discriminated. Activated NK cells and $CD8^+$ cells were identified as $CD69^+$ cells in each population.

To assess the involvement of intratumoral immune effector populations in the therapeutic effect of the MeVac vectors, a relationship between the amount of certain TIL subpopulations with the change of tumor volume after MeVac therapy was examined. The time span of the experiment evaluating effector mechanisms of the anti-PD-L1 and IgG1-Fc encoding vectors (Figure 4.15.b) was considered sufficient to meaningfully compare the impact of treatment on changes in tumor volume. The differences of the tumor volume before the beginning of the treatment and on the day of tumor explantation was calculated and correlated with the size of TIL populations significantly differing between the treatment groups. The proportion of NK cells in the tumor correlated significantly with a smaller increase in the tumor volume in the mock group (Figure 4.20). In the IgG1-Fc group the same correlation was not significant, but in the anti-PD-L1 group a smaller proportion of NK cells significantly correlated with a greater decrease in tumor volume (Figure 4.20). In the mock group

a larger size of the T cell population significantly correlated with a greater increase in tumor volume, while in the IgG1-Fc group there was no significant correlation of these parameters. However, in the anti-PD-L1 group a larger T cell population correlated significantly with a greater decrease in tumor volume (Figure 4.20). The size of the activated cytotoxic T cell population did not correlate significantly with change in tumor volume in the mock group, but in both the IgG1-Fc and anti-PD-L1 groups a smaller activated cytotoxic T cell population correlated significantly with a greater decrease in tumor volume (Figure 4.20).

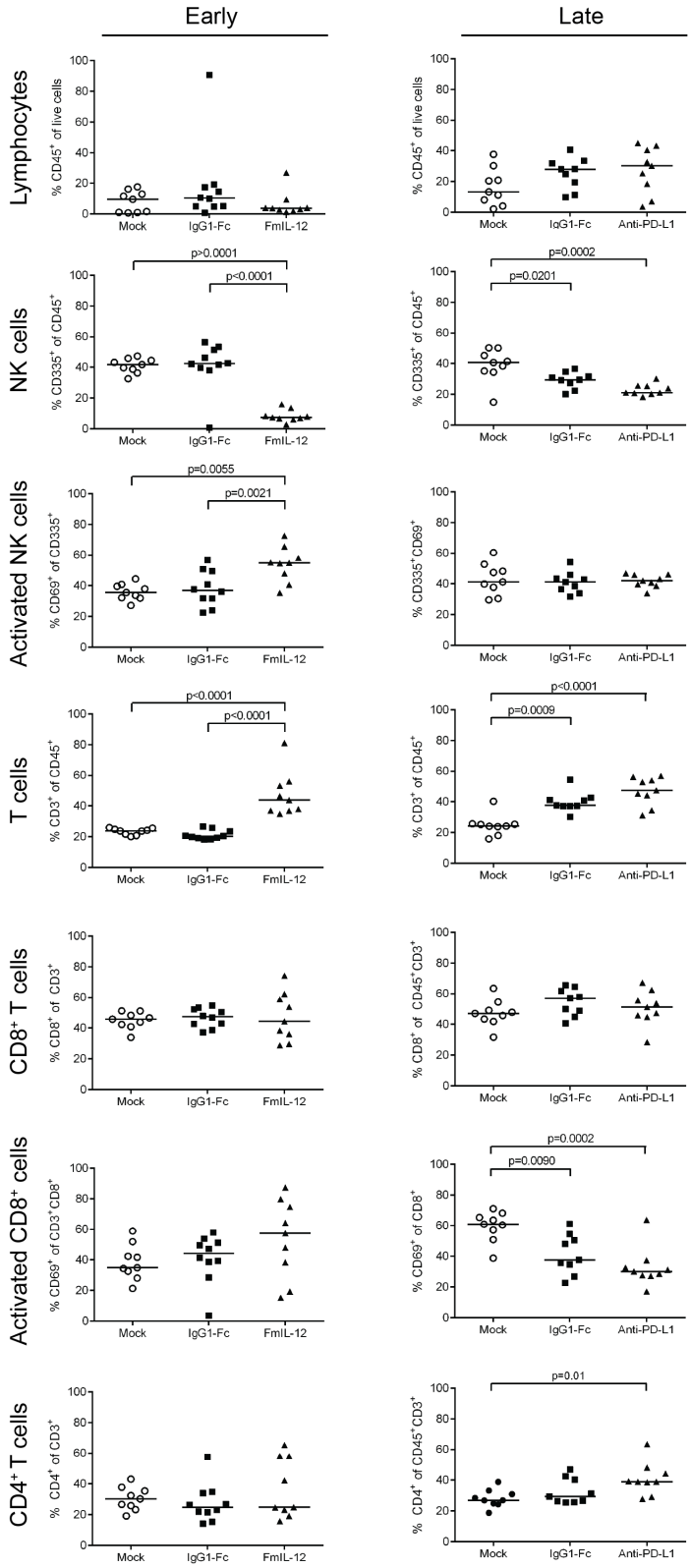

Figure 4.19: **Tumor infiltrating lymphocyte subpopulations after MeVac therapy.** MC38cea cells were implanted subcutaneously into C57BL/6J mice. When tumors reached an average volume of 120 mm^3 (early) or 100 mm^3 (late) mice received intratumoral treatment with MeVac encoding the respective transgenes or the respective amount of OptiMEM (mock). Single cell suspensions from the tumors were prepared and flow cytometry analysis was performed one (early) or four (late) days after the last treatment. Dots representing tumor samples from individual mice and the median value in each group are shown.

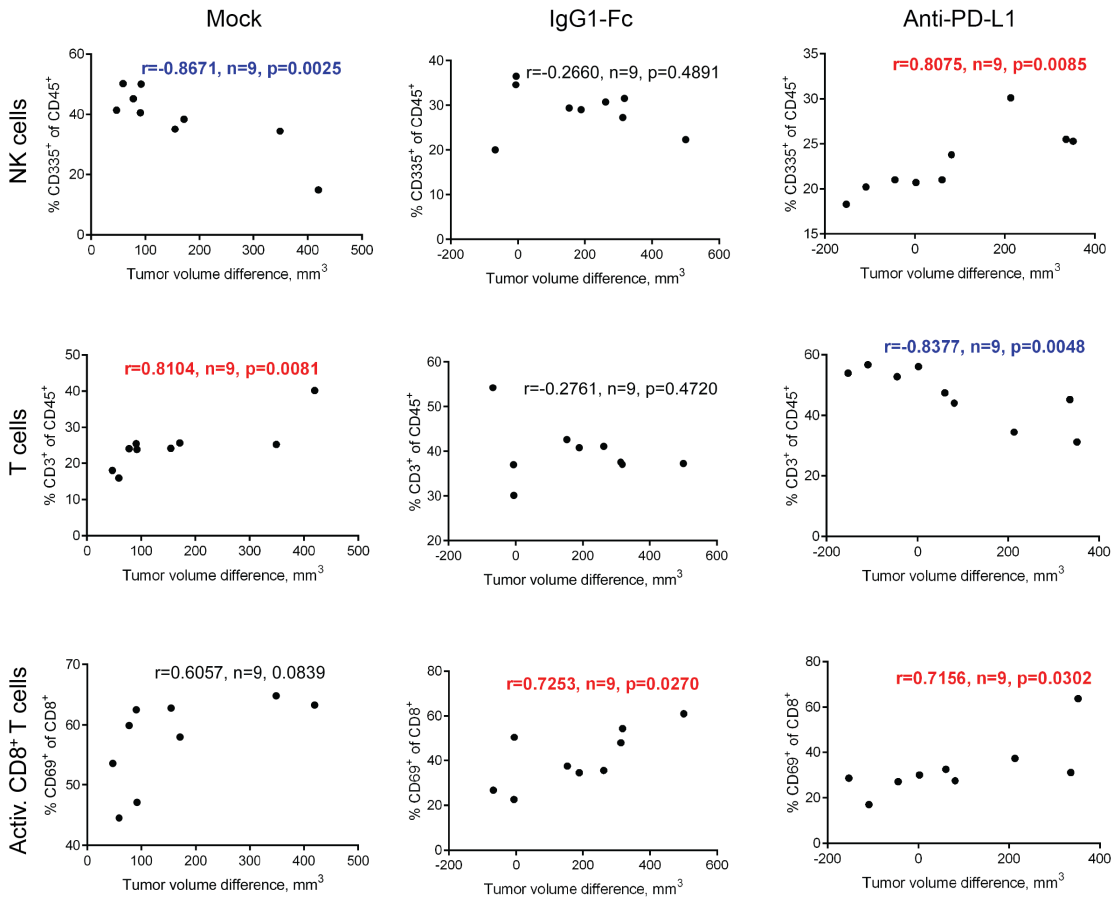

Figure 4.20: **Correlations of the amount of certain tumor infiltrating lymphocyte subpopulations and a change in tumor volume after MeVac therapy.** MC38cea cells were implanted subcutaneously into C57BL/6J mice. When tumors reached an average volume of 100 mm^3 mice received intratumoral treatment with MeVac encoding the respective transgenes or the respective amount of OptiMEM (mock) on four consecutive days. Tumors were explanted four days after the last treatment and flow cytometry analysis was carried out. Differences between the tumor volume on the day before the treatment and four days after the last treatment were calculated and plotted against the proportion of the respective immune cell populations. Pearson product-moment correlation analysis was carried out to assess the correlation between the two factors. Results for significant positive correlations are depicted in red, significant negative correlations in blue and no correlation is shown in black. Dots represent samples from individual mice. r — Pearson's correlation coefficient; n — number of data points; p — p value.

4.3.4 Identification of Immune Effectors Crucial for the Efficacy of the MeVac encoding FmIL-12

Contribution of the main immune effector cell populations to the therapeutic effect of the most effective immunomodulatory vector in the MC38cea tumor model, the MeVac encoding FmIL-12, was further assessed. The NK cells or the $CD8^+$ cytotoxic T cells or the $CD4^+$ T helper cells, were depleted by intraperitoneal antibody injections prior to s.c. implantation of the MC38cea cells and i.t. treatment with the MeVac encoding FmIL-12. Depletion efficiency

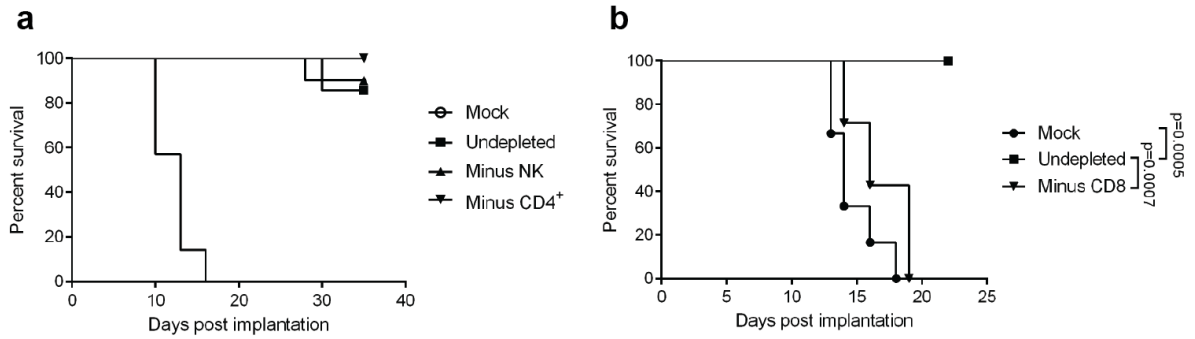

Figure 4.21: **Impact of the main immune effector cell population depletions on the therapeutic efficacy of the MeVac encoding FmIL-12.** C57BL/6J mice were depleted of natural killer cells or $CD4^+$ T cells (minus NK or minus $CD4^+$ in **a**) or $CD8^+$ T cells (minus $CD8^+$ in **b**) by intraperitoneal antibody injections. Two separate experiments are shown in **a** and **b**. Mice with no immune cell depletions served as controls (mock, undepleted). MC38cea cells were implanted subcutaneously and established tumors were treated with intratumoral (i.t.) injections of 1×10^6 cell infectious units MeVac P-FmIL-12 Hbl-αCEA in 100 µl on four consecutive days. Mice in the mock groups received i.t. injections with 100 µl OptiMEM in parallel. Kaplan-Meier survival analyses are shown.

was controlled by flow cytometry in peripheral blood of selected animals from each group (Figure A.15, Figure A.16, Figure A.17). Depletions of the NK and $CD4^+$ T cell populations did not have a significant impact on the survival of animals in comparison to the treated animals with no depletions of the immune cells (Figure 4.21.a). However, depletion of the $CD8^+$ T cell population almost completely abrogated the therapeutic effect of the MeVac encoding FmIL-12 (Figure 4.21.b).

4.4 Consideration of the Translational Potential

The previous chapters described the development of oncolytic measles virus vectors encoding different immunomodulators and the assessment of their immunomodulatory properties in murine tumor models. Experiments in immunocompetent mouse models can give valuable information about the role of immune responses in the mode-of-acion of the oncolytic vectors. However, the previously described MeVac vectors encode only the murine analogs of human immunomodulatory molecules and development of vectors encoding transgenes for the respective human proteins is a prerequisite for development of clinically relevant therapeutics. As MeVac encoding the murine IL-12 fusion protein demonstrated the highest therapeutic efficacy in the previously described experiments in murine tumor models, MeVac vectors encoding human IL-12 fusion protein were further constructed and characterized *in vitro*. Furthermore, as most of the experiments described previously focused on a murine colorectal adenocarcinoma model, colorectal cancer was highlighted as a possible target for oncolytic measles virus. A panel of human colorectal cancer cell lines was evaluated in terms of MV receptor expression levels as well as replication kinetics and cytotoxic properties of both

measles Edmonston B (NSe) and Schwarz (MeVac) vaccine strain viruses were examined *in vitro*.

4.4.1 MeVac Encoding a Human IL-12 Fusion Protein*

MeVac encoding the murine IL-12 fusion protein FmIL-12 demonstrated the highest therapeutic efficacy in the experiments in the MC38cea murine colon adenocarcinoma model described in the previous chapters. Further, the ability to establish a long-term anti-tumor immune response and favorably modulate the tumor immune milieu was revealed, which taken together allows to consider MeVac encoding IL-12 fusion protein a promising candidate for translation into clinical application. MeVac encoding a human IL-12 fusion protein[222] was therefore further developed and characterized *in vitro*.

The cassette encoding a human IL-12 fusion protein (FhIL-12) was designed analogously to FmIL-12 with the exception of using a different linker, as the $(Gly_4Ser)_3$ used in the murine construct had previously been found to be unstable in a human IL-12 construct[222]. The IL-12p40 subunit was fused with the IL-12p35 subunit lacking the secretory leader sequence (Δp35) via a Gly_6Ser linker as in Lieschke *et al.*[222]. The fusion protein was preceded by a Kozak sequence and an extra stop codon was introduced behind Δp35 to obtain a construct complying with the "rule of six" for insertion into the MeVac genome as an *MluI-PauI* fragment. The FhIL-12 cassette (1614 bp) was inserted downstream of the MeVac *P* ORF or *H* ORF yielding MeVac P-FhIL-12 and MeVac H-FhIL-12 genomes, respectively (Figure 4.23). It must be noted that two point mutations in the p40 subunit, both G to C transversions, were revealed when controlling the final FhIL-12 construct by Sanger sequencing. The mutation in the position 717 of the FhIL-12 construct was a missense mutation that has been described as a sequence conflict previously[232], but the second mutation in position 873 did not change the amino acid sequence.

One-step growth curves in the producer Vero cell line were performed to compare replication kinetics of the two novel MeVac constructs encoding FhIL-12. Replication kinetics of both vectors were similar, with titers peaking 48 h post infection and declining only slightly until 96 h post infection (Figure 4.23.a). MeVac H-FhIL-12 reached slightly higher titers than MeVac P-FhIL-12. Expression kinetics of the MeVac encoded FhIL-12 was further assessed in Vero cells transduced with both constructs. The FhIL-12 concentration in the cell culture medium steadily increased after infection over the course of the whole experiment until 96 h post infection. The FhIL-12 concentration after infection with MeVac H-FhIL-12 was markedly lower than when using MeVac P-FhIL-12 at all time points, reaching the maximum difference 96 h post infection (Figure 4.23.b).

Cytotoxic properties of both MeVac constructs encoding FhIL-12 were compared with the parental MeVac vector in the producer cell line, Vero, and a human colorectal adenocarcinoma cell line, DLD-1. In Vero cells MeVac H-FhIL-12 displayed similar cytotoxic activity

*Experiments described in this subsection were carried out by L. Hartmann during a laboratory internship supervised by R. Veinalde.

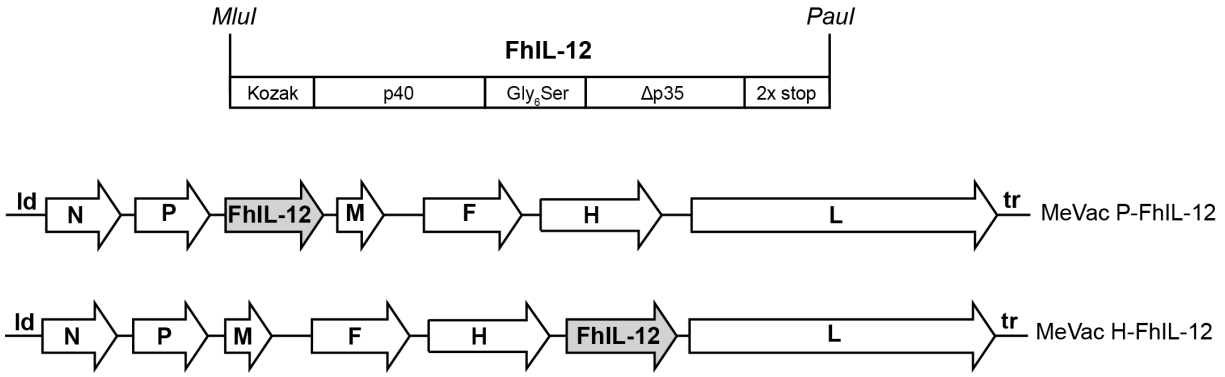

Figure 4.22: **Schematic of human IL-12 fusion protein (FhIL-12) and MeVac genomes encoding FhIL-12.** A human IL-12 fusion protein (FhIL-12) was constructed by fusing the IL-12 p40 and a IL-12 p35 subunit lacking the secretory leader sequence (Δp35) via a Gly_6Ser linker. The fusion protein was preceded by a Kozak sequence and a second stop codon was introduced behind Δp35. The FhIL-12 cassette was inserted into the MeVac genome as an *MluI-PauI* fragment (1614 bp) either downstream of the measles *P* ORF or *H* ORF.

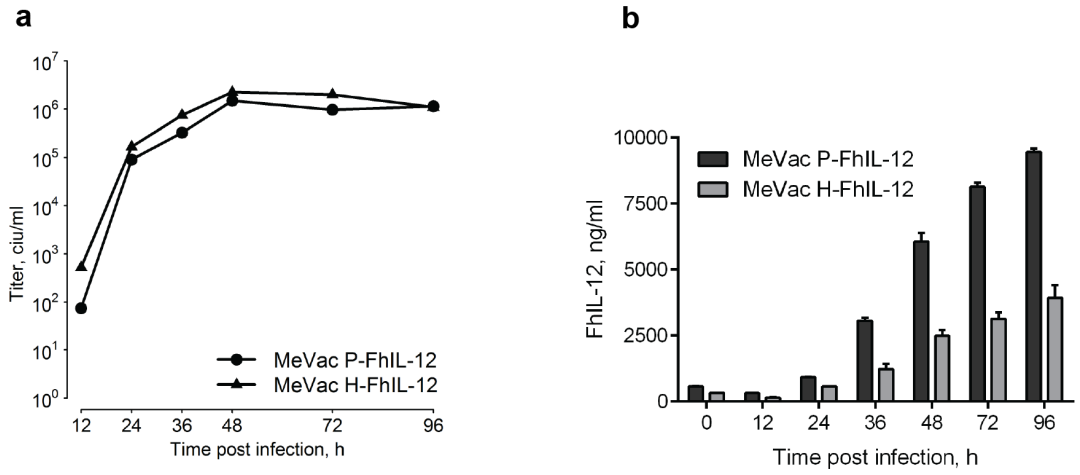

Figure 4.23: **Replication kinetics of MeVac encoding human IL-12 fusion protein (FhIL-12) and expression of FhIL-12. a** – one-step growth curves were constructed by transduction of Vero cells with the respective viruses at a multiplicity of infection (MOI) = 3. Cells were scraped in their medium at the depicted time points and titers were assessed by serial dilution titrations and expressed as cell infectious units (ciu) per ml; **b** – Vero cells were transduced with the respective vectors and with MeVac A as a control at an MOI = 3. Supernatants were collected from the infected cells at the depicted time points and concentrations of FhIL-12 were assessed by ELISA. Supernatants from cells infected with MeVac A served as background controls and were subtracted from the respective specific measurements. Mean values from triplicate infections per time point with standard errors of the mean are shown.

as the parental MeVac vector. However, the MeVac P-FhIL-12 showed a notably lower cytotoxicity, being able to reduce cell viability to 56% compared to mock at 96 h post infection in contrast to 15% and 7% for MeVac and MeVac H-FhIL-12, respectively (Figure 4.24). However, in the DLD-1 cell line all constructs displayed similar cytotoxic properties and at

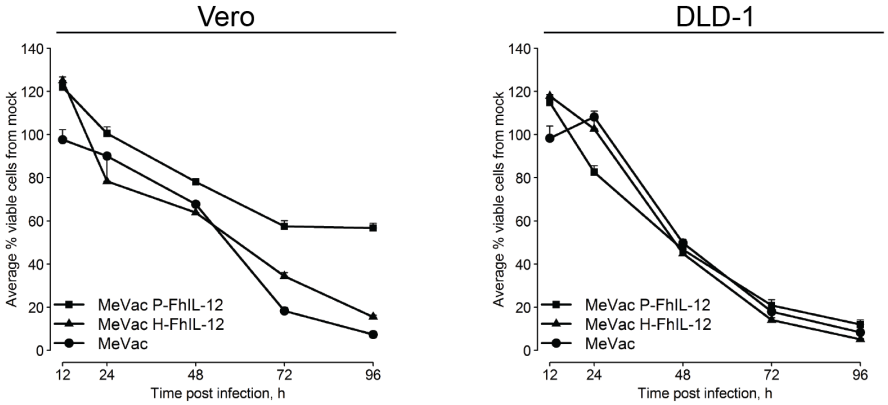

Figure 4.24: **Cytotoxic properties of MeVac encoding human IL-12 fusion protein.** Vero or DLD-1 cells were infected at multiplicity of infection = 1 with the respective MeVac constructs. An XTT cell viability assay was carried out at the depicted time points. Results are presented as a percentage of viable cells compared to mock (= 100%). Mean values from triplicate infections with standard errors of the mean are shown.

96 h post infection cell viability was reduced to a range of 0.74% – 11% compared to mock (MeVac – MeVac P-FhIL-12, respectively) (Figure 4.24).

4.4.2 Potential of Oncolytic MV for Treatment of Colorectal Cancer*

A panel of colorectal cancer cell lines was chosen to examine the expression of MV receptors and to compare MeVac and NSe measles vaccine strain viruses in terms of their replication kinetics and cytotoxic properties. The chosen cell lines were validated by assessing expression of several colon cell specific markers (Figure A.18). Further, expression of the known MeV receptors CD46, CD150 and Nectin-4 (PVRL-4) was examined. All of the tested cell lines expressed CD46 on their surface as determined by flow cytometry (Figure 4.25.a). However, the results indicated differences in the expression intensity of the CD46, as the lowest median fluorescence intensity of the PE labeled antibody was detected on HCT 116, but the highest on DLD-1 cells (Figure 4.25.b). However, none of the tested cell lines were positive for CD150 expression in flow cytometry (data not shown). Expression of the Nectin-4 was assessed by RT-PCR and three of the cell lines, COLO 205, DLD-1 and HT-29, were positive for Nectin-4 on mRNA level (Figure 4.25.c).

MeVac and NSe vectors were tested in terms of replication kinetics and cytotoxic effects in the previously characterized colon cancer cell lines by performing one-step growth curves and XTT assays. In one-step growth curves titers for both vectors reached a peak 36 – 48 h post infection in all cell lines, but the amount of the viral particles produced differed between the vectors and cell lines. As a general pattern, at almost all time points lower titers were

*Experiments described in this subsection were carried out by V. Mitesser during a laboratory internship supervised by R. Veinalde.

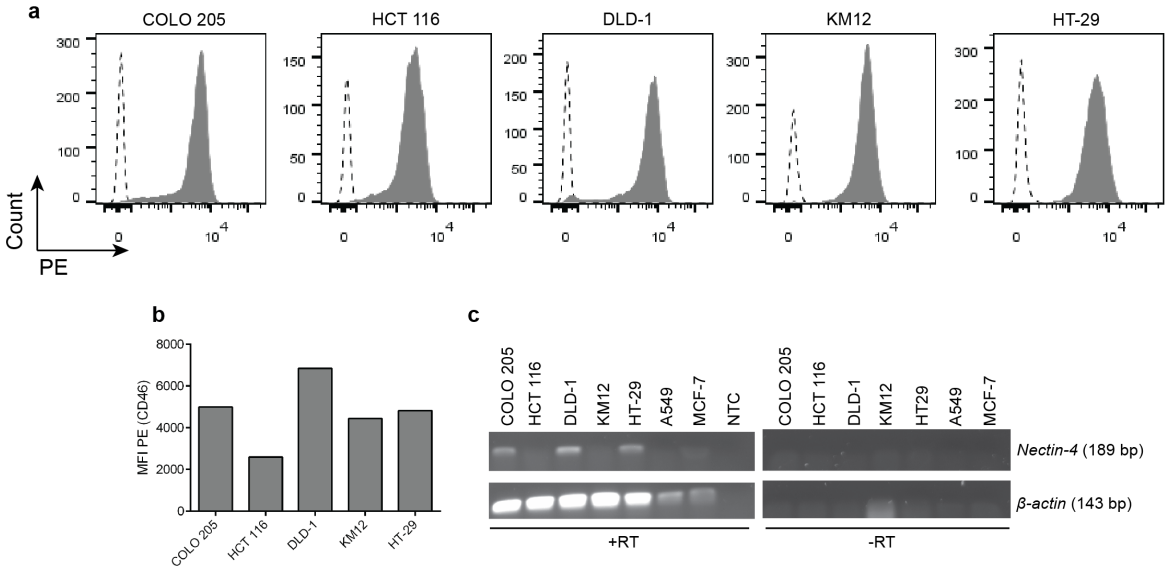

Figure 4.25: **Expression of MV receptors by human colon cancer cell lines. a**, **b** — expression of CD46 by the respective colon cancer cell lines was assessed by flow cytometry. Cells were stained with a PE labeled antibody against human CD46 (anti-hCD46) and DAPI staining was used for exclusion of dead cells. Histograms showing PE signal intensity of the live cell population ($DAPI^-$) of cells stained with the anti-hCD46 (solid fill) in comparison to an isotype control (dashed lines) by the respective cell lines is shown in **a**. Median fluorescence intensity (MFI) of PE (anti-hCD46) by the live population of the respective cell lines is shown in **b**. **c** — mRNA level of *Nectin-4* (*PVRL-4*) was assessed by RT-PCR. *Beta actin* (*β-actin*) was amplified as a loading control. +RT — cDNA samples; -RT — minus reverse transcriptase controls.

reached after infection with the MeVac vector than with the NSe vector in the same cell line (Figure 4.26). Cell lines in which the highest and lowest titers were reached differed between both vectors. After infection with MeVac the highest titer (1.75×10^6 ciu/ml after 48 h) was reached in KM12, but the lowest (8.75×10^4ciu/ml after 36 h) in the COLO 205 cell line. After infection with the NSe vector the highest titer (5×10^6 ciu/ml after 48 h) was reached in DLD-1, but the lowest (7.25×10^5 after 48 h) in the HT-29 cell line (Figure 4.26). Of note, the differences between the peak titers after infection with MeVac were much higher and more dispersed between the cell lines than after infection with the NSe vector.

Cytotoxic effects of MeVac and NSe vectors were assessed in all of the chosen cell lines by XTT assay. Both vectors were able to reduce cell viability in a range of 35 – 0.25% viable cells compared to mock 96 h post infection. The most resistant cell line with the lowest reduction of cell viability after infection with both vectors was the HT-29, with MeVac reducing cell viability to 21.5%, but NSe to 35.5% viable cells compared to mock 96 h post infection (Figure 4.26). For the other cell lines the sensitivity to each of the vector was different. After infection with MeVac the greatest and most rapid decline in cell viability was observed for COLO 205 and KM12, but after infection with NSe for DLD-1 and HCT 116 cell lines (Figure 4.26).

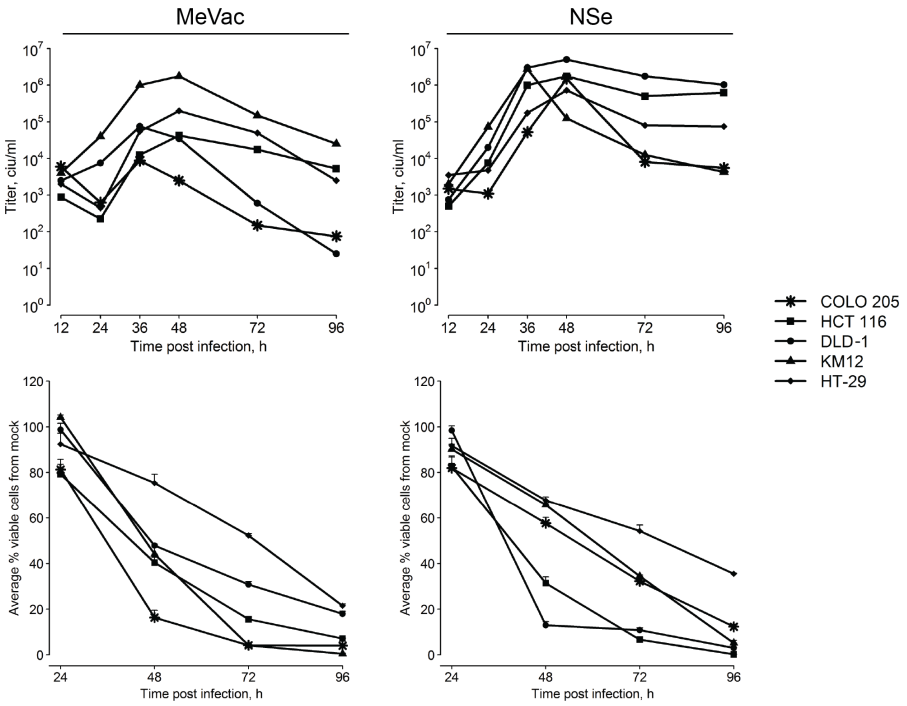

Figure 4.26: **Replication kinetics and cytotoxic effects of measles Schwarz (MeVac) and Edmonston B (NSe) vaccine strain viruses in human colon cancer cell lines.** Upper panels — one-step growth curves were performed by transducing the respective cell lines at a multiplicity of infection = 3. Cells were collected by scraping in their own medium and titers were determined at the depicted time points; lower panels — the respective cell lines were transduced with MeVac or NSe vectors at a multiplicity of infection = 1 and cell viability was determined by XTT assay at the depicted time points. Mean results of triplicate infections per time point with standard errors of the mean are shown (not visible for some data points). ciu — cell infectious units.

5 Discussion

5.1 Perspectives of Immunovirotherapy

Oncolytic viruses (OVs) are emerging as a class of clinically relevant cancer therapeutics and declaring their place among current cancer immunotherapy strategies. The immunomodulatory properties of the OV therapy have been recognized to be an integral part of their mechanism of action, allowing to coin the term "immunovirotherapy"[75]. Early studies of oncolytic properties of different viruses focused on identification and generation of viruses with enhanced cytotoxic potential in malignant cells[233,234]. Since then, the focus in the field of OV research has shifted considerably, with most of the current studies concentrating on the immunomodulatory aspects of virotherapy and development of strategies to support the induction of an anti-tumor immune response[93]. OVs provide a unique mechanism of action among the currently known immunotherapeutics. In virotherapy, the abilities of OVs to selectively infect, replicate and destroy malignant tissues synergize with the immunostimulatory aspects, supporting establishment of a tumor-specific immune response[235]. Furthermore, modification of the immunostimulatory properties of OVs and combination with other immunotherapeutic strategies can result in a significantly enhanced therapeutic efficacy[236,237,107,103]. Particular interest has been given to development of OVs as vehicles for delivery of different immunomodulators to tumor tissues[93]. Such oncolytic vectors encoding immunomodulators frequently demonstrate therapeutic benefits in pre-clinical tumor models[123,126,129]. However, most importantly, this strategy has also been translated into clinical application. The only oncolytic vector currently approved for clinical use in the U.S. and European Union, T-VEC, encodes an immunomodulator, GM-CSF, targeting antigen presenting cell functions[71,238]. Although T-VEC has demonstrated enhanced therapeutic efficacy for patients with advanced malignant melanoma in terms of increased response rates and overall survival in comparison to administration of GM-CSF alone, the majority of patients do not experience benefits from the therapy[100]. Thus, further studies focusing on identification of the most effective immunomodulators for combination with oncolytic vectors as well as elucidation of immune effector mechanisms supporting the therapeutic effects will be important for advancement of immunovirotherapy.

This study focused on the oncolytic measles vaccine strain vectors (MV), which are emerging as promising virotherapeutics in clinical trials[206,207,208]. A great immunostimulatory potential associated with MV-mediated oncolysis has been demonstrated. *In vitro* studies have confirmed induction of immunogenic cell death in MV-infected tumor cells[239,240,241]. More importantly, activation of tumor antigen specific T cell responses after MV therapy has been demonstrated in a clinical trial for treatment of ovarian cancer[208]. Several pre-

clinical studies have demonstrated that the therapeutic efficacy of oncolytic MV vectors can be enhanced by combination with different immunomodulators, including GM-CSF, IFN-β and antibodies against the negative regulators of T cell activation CTLA-4 and PD-L1[200, 114, 131, 104]. However, advantages of different immunomodulation strategies in combination with oncolytic MV vectors have not been compared before. Thus, this study aimed at systematic evaluation of MV vectors encoding immunomodulators from different classes. Furthermore, analyses of the tumor immunomicroenvironment following the most promising MV immunovirotherapy strategies were carried out to deepen understanding of the determinants of therapeutic efficacy.

5.2 Construction and Characterization of Recombinant Oncolytic Measles Vectors

In contrast to the Edmonston B measles vaccine strain derivatives used in previous measles oncolysis studies[226, 114, 104], this study introduces recombinant Schwarz (MeVac) strain vectors. The measles cloning platform was developed based on an Edmonston B-derived vector[188]. However, probably due to mutations that have occured during cloning process and adaptation to propagation in Vero cells, the sequence of the Edmonston B-derived vectors has deviated significantly from the initial vaccine seed[214]. The recombinant MeVac vectors have been developed based on the commercially available measles vaccine Rouvax, which is used for measles immunization in Europe[214]. It has been shown that the MeVac vectors retain an immunogenic potential similar to that of the commercial vaccine, while the recombinant Edmonston B strain is poorly immunogenic[214]. The reduced immunogenicity of the Edmonston B vaccine strain is most probably associated with its lost ability to counteract interferon (IFN) signaling, which, in contrast, is preserved in the MeVac vectors[148]. These properties strongly suggest recombinant MeVac vectors as candidates for further clinical development and, thus, they were chosen for this study to deepen understanding of their immunomodulatory properties in the context of oncolysis.

A panel of MeVac vectors encoding previously selected immunomodulators targeting distinct phases in the establishment of an anti-tumor immune response was created. Additionally, MeVac encoding the enhanced green fluorescent protein (eGFP) and the constant region of an antibody (IgG1-Fc) were generated for use as controls in further experiments. Measles encoding IgG1-Fc has been used as a control vector for anti-CTLA-4 and anti-PD-L1 encoding Edmonston B measles vectors[104]. Thus, the IgG1-Fc encoding MeVac was used as a control in experiments with MeVac encoding anti-CTLA-4, anti-PD-L1, as well as the soluble form of CD80 (CD80-Fc). Measles encoding eGFP has been used as a control vector in a previous study examining therapeutic effects of an Edmonston B strain virus encoding mGM-CSF[114]. Thus, MeVac encoding eGFP was chosen as a control vector for experiments with MeVac vectors encoding cytokines, mGM-CSF, IL-12 fusion protein (FmIL-12) and mIP-10. To appropriately control experiments with oncolytic vectors encoding immunomod-

ulators, an ideal control vector should have a similar genome structure, replication kinetics and cytotoxic potential in the target cells as the vectors in question. Furthermore, it should ensure expression of an immunologically inert molecule from the transduced cells. It must be noted that, mainly in regards to the replication kinetics, selection of such a vector is very challenging. The main factors influencing replication kinetics of recombinant measles vectors are the size and position of the inserted transgene cassette as well as the structure of the inserted sequence itself. Vectors with large transgene inserts (>1 kbp) in genome positions close to the measles leader can be severely attenuated or even impossible to rescue[212,213]. Nevertheless, previous studies have demonstrated that generation of recombinant measles vectors encoding single transgenes up to 3 kbp and multiple transgene cassettes with a total size up to 5 kbp is feasible[242,243]. The sizes of the transgene cassettes for immunomodulators chosen in this study differed significantly (from 312 bp for mIP-10 to 1650 bp for FmIL-12). Thus, to balance attenuation of the generated vectors, it was necessary to insert the transgene cassettes into different positions of the measles genome. A further concern is that the size of the transgene cassettes in control vectors in most cases differed significantly from the size of the cassettes encoding immunomodulators. For instance, the IgG1-Fc cassette was only approximately half of the size of anti-CTLA-4, anti-PD-L1 and CD80-Fc encoding cassettes and the eGFP cassette was more than 1.5 times the size of mIP-10 encoding cassette. It must also be noted that a codon optimization process to exclude sequences that could cause premature interruption of RNA synthesis by measles polymerase during replication (repetitive sequences and sequences resembling regulatory elements in the measles genome) was performed only for the anti-PD-L1 encoding cassette[213]. Nevertheless, as will be discussed further, the replicative potential of the vector plays a secondary role in the models used in this study. Therefore, despite the possibility of different replication efficiencies, the generated vectors encoding immunomodulators and the respective control vectors were considered suitable for further experiments.

Measles replication is restricted to primate cells as hosts and therefore natural transduction of murine cells with MV vectors is not possible. Measles hemagglutinin (H) however tolerates insertion of foreign sequences. This allows alteration of the natural measles tropism at the entry level by, for instance, display of single chain antibodies (scAb) on the C terminus of H[190]. The retargeted vectors are able to enter murine cells expressing the respective antigen via binding of the scAb. Until now, two immunocompetent murine models have been developed in studies with oncolytic Edmonston B strain vectors — MC38cea[226,114] and B16-CD20[104]. To allow further use of both of them, the H protein in the novel MeVac vectors encoding immunomodulators was retargeted by insertion of scAb sequences against CEA or CD20. Full retargeting was achieved by using vectors with point mutations in the H protein that ablate binding to the natural measles receptors CD46 and CD150. The STAR system was used for propagation of the viruses[216]. From a clinical perspective, modification of measles vector tropism is not an absolute necessity, as in most cases measles vaccine strain vectors have a natural oncotropism due to the overexpression of CD46 in many tu-

mor types[179]. The modification of measles tropism would be appealing only in cases with CD46-negative tumors and as a safety measure, to detarget the virus from CD46, which at low levels is expressed also on normal nucleated cells[244], and to ensure targeting of only a specific tumor-associated antigen as an entry receptor. However, until now, clinical trials for measles oncolysis have successfully used only vectors with unmodified tropism. In these trials no critical safety concerns arose[207, 208].

Replication kinetics of the novel retargeted MeVac vectors in the producer cell line Vero-αHis differed significantly, with differences in the maximum measured titers reaching up to two $\log_{10}$. Overall, vectors with smaller transgene inserts tended to reach lower titers than the vectors with larger transgene cassettes. A plausible explanation for this observation would be that, as the vectors with shorter inserts are less attenuated and replicate faster, the virus life cycle is completed more rapidly, resulting in cell lysis. The fast destruction of the cell layer restricts the capacity for production of novel infectious particles and therefore the in fact more attenuated vectors, with the large transgene inserts, are able to produce more infectious particles in a cell before its destruction. Despite this, propagation of the retargeted vectors to high titers ($>10^7$ ciu/ml) in the Vero-αHis cell line was feasible for all of the novel retargeted vectors except for MeVac encoding mGM-CSF. In the previous study with the Edmonston B-derived vector encoding the same mGM-CSF construct in leader position of the genome, the replication of the vector was not impaired[114]. To exclude that mutations introduced during the cloning or propagation process could be the cause of the impaired replication of MeVac encoding mGM-CSF, the whole genome of the construct was sequenced and compared to MeVac encoding FmIL-12. Since only one silent mutation within the *H* ORF and three non-coding sequence variants in intergenic regions that were identical in both constructs were detected, this was excluded as a reason for the impaired replication. Further analysis for accumulation of defective interfering particles (DIs)[230] was carried out in which a distinct, DI amplification-specific band was detected only in samples from the mGM-CSF encoding vector. This indicates that excessive accumulation of the DIs could have caused the impaired replication of the mGM-CSF encoding MeVac. This could probably be associated with the alteration of the genome structure through the insertion of this specific mGM-CSF transgene cassette. As a solution, a vector encoding the mGM-CSF cassette with an alternative codon usage could be assessed or the cassette could be inserted further downstream in the MeVac genome.

Retargeted MeVac vectors were able to transduce the murine target cells, MC38cea, as demonstrated by syncytia formation. Comparison of the replication kinetics in the MC38cea cells *in vitro* confirmed the ability of all vectors to productively replicate in the target cells. The results indicated one productive replication cycle as observed by a peak in the amount of infectious cell units 36 – 48 h post infection. Furthermore, in general all vectors demonstrated only mild cytotoxic effects in the MC38cea cells. Taken together, these results illustrate the limitations for measles studies in mouse cells. Although the retargeted vectors are able to enter murine cells, replication and subsequent oncolytic effect is hindered by the inability

to efficiently counteract post-entry barriers in murine cells[226]. The oncolytic efficiency of measles vectors in immunocompetent mouse tumor models can therefore be considered to be of secondary importance, but the models are suitable for evaluation of the immunological aspects of the therapy.

Further, it was demonstrated that after transduction of the MC38cea target cell line with the respective vectors, the MeVac-encoded immunomodulators are expressed and retain their biological activities. However, patterns of expression kinetics differed considerably between the vectors. The expression kinetics of the inserted transgenes of the immunomodulators can be expected to depend on a complex set of properties, including the replication efficiency of the respective vector in a given cell line and properties of the resulting molecule. Concentration of MeVac expressed FmIL-12 and anti-PD-L1 was observed to accumulate constitutively in the cell culture medium over the course of the experiment. As for both of these vectors a peak of viral particles followed by a decline until the end of the experiment was measured in the one-step growth curve, the transgene expression result suggests both molecules to be relatively stable, allowing their accumulation during the experiment. In contrast to these results, the expression of anti-CTLA-4 presented a peak with a decline at the end of the experiment, consistent with the pattern of virus particle production in the growth curve. Thus, anti-CTLA-4 appears to be less stable than FmIL-12 and anti-PD-L1. MeVac-encoded mCD80-Fc and mGM-CSF appeared to be produced inefficiently in the target cell line, as the highest concentration for both was measured in the inoculum. In case of MeVac-encoded mGM-CSF, this result is in line with the impaired replication of the vector. In the case of mCD80-Fc encoding virus, replication was comparable to the other vectors. It is therefore possible that other factors might play a role in the observed CD80-Fc expression pattern, for instance, instability of the molecule or inefficient secretion from the infected cells.

During vector characterization *in vitro* it was discovered that the untransduced MC38cea cell line as well as the parental cell line MC38 constitutively express mIP-10 and its receptor CXCR3. It has been recognized that in the context of human cancer, IP-10 can either exert an anti-tumoral effects or support tumor growth and formation of metastasis[245]. This controversy can possibly be explained by involvement of different splice forms of the IP-10 receptor CXCR3. Several studies in different human tumor types have indicated that up-regulation of the CXCR3-A splice variant and down-regulation of the CXCR3-B variant on tumor cells is associated with increased metastatic potential[246,247]. However, in murine cells no alternative CXCR3 forms are known[248]. Many studies in murine tumor models, including MC38-derived models, have reported involvement of IP-10 in a variety of anti-tumor actions through its support of immune cell recruitment or its angiostatic activities[40,249,250,251]. Reports of the pro-tumorigenic IP-10 properties in murine tumor models are scarce, but it has recently been demonstrated that the CXCR3/IP-10 interaction in a B16-derived murine melanoma tumor model is associated with increased metastatic potential[252]. It is possible that CXCR3/IP-10 engagement also supports the tumorigenic properties of the MC38cea

cell clone used in this study. Given this, the MC38cea model used in this study cannot be considered suitable to evaluate the therapeutic potential of the MeVac encoding mIP-10. Nevertheless, the *in vitro* characterization data suggested that the MC38cea tumor model will be suitable for evaluation of the properties of all the other novel immunomodulatory MeVac vectors.

5.3 Immunomodulation for Enhanced Efficacy of Oncolytic Measles Virus

For identification of the most promising immunomodulation strategies in the context of oncolytic measles virus, therapeutic potential of the novel MeVac vectors encoding immunomodulators, as well as their combinations was assessed in the fully immunocompetent subcutaneous (s.c.) MC38cea murine tumor model. First, two screening experiments indicated vectors encoding anti-PD-L1 and FmIL-12 to have the best therapeutic efficacy. In a further head-to-head comparison of these most promising vectors, the FmIL-12 encoding vector demonstrated a superior efficacy, reproducibly leading to complete tumor remissions in 90% of the treated animals. Such a high rate of complete tumor remissions has never been achieved in previous pre-clinical measles oncolysis studies in immunocompetent tumor models[226, 114, 104].

Based on its potent anti-tumor activities in different animal tumor models, IL-12 has long been considered a candidate for application in cancer therapy[253]. Clinical translation, however, has been hampered by the modest efficacy and high toxicities observed in early clinical trials. However, given its robust immunostimulatory potential, the studies of IL-12 as a cancer immunotherapeutic have not been abandonded, with recent efforts being focused on finding approaches for more targeted administration strategies to minimize toxicity and increase therapeutic efficacy. The challenge for IL-12 delivery lies in its heterodimeric structure, as expression of both protein subunits, p35 and p40, at a comparable level in the same cell is necessary for generation of the biologically active IL-12 molecule[27]. Several oncolytic vectors encoding both IL-12 protein subunits separated by an internal ribosomal entry site have been previously studied[122, 121, 123]. Administration of both IL-12 subunits separately creates a potential for formation of p40 homodimers which are natural inhibitors of IL-12 functions[27]. Generation of a biologically active single chain IL-12 has previously been demonstrated to be feasible[222]. Furthermore, an optimally designed IL-12 fusion protein has been shown to have even more pronounced anti-tumor activity than the natural heterodimeric molecule, which could be a result of an increased stability of the fusion protein or an increased affinity for the IL-12 receptor[222]. Thus, MeVac encoding a murine IL-12 fusion protein which was developed in this study presents a novel approach for a targeted delivery of this potent cytokine.

The anti-tumoral effects of IL-12 have previously been demonstrated also in MC38-derived murine tumor models. For instance, local administration of a recombinant IL-12

(rIL-12) has been shown to suppress growth of intracutaneous MC38 tumors and systemic rIL-12 administration has reduced formation of liver metastases[254]. Local IL-12 administration with a non-replicating adenovirus (AdV) has demonstrated high efficacy in a s.c. MC38 tumor model, leading to complete tumor remissions in 80% of the treated animals[255]. Evaluation of the transgene expression kinetics from the MeVac vectors used in this study revealed that a large amount of FmIL-12 produced during virus propagation remains present in the virus preparations and is, therefore, administered with initial virus injections. Given the known IL-12 therapeutic benefits in MC38-derived tumor models, an obvious question was, whether the administration of FmIL-12 present in the virus suspension is sufficient for a therapeutic effect. A further experiment including an FmIL-12 encoding MeVac vector with an unmodified tropism which is, thus, not able to enter the MC38cea cells, revealed induction of complete tumor remissions at a rate comparable to that of the targeted FmIL-12 encoding MeVac. This result indicated that the FmIL-12 administered with the virus suspension might be sufficient for the observed therapeutic effect and the *de novo* FmIL-12 production from the transduced MC38cea cells and oncolytic effect might not be essential in this model. Nevertheless, it must be noted that although the non-targeted vector is not able to mediate an oncolytic effect, the virus suspension can still potently activate innate immune responses which could contribute to the therapeutic effect. The administered virus suspension contains a large amount of cellular debris and components of different stages of measles virus replication. Particularly important could be the presence of different RNA species that arise during the virus replication cycle. These can be recognized by RIG-I-like receptors RIG-I (retinoic acid-inducible gene I) and MDA5 (melanoma differentiation-associated protein 5)[256], leading to a potent upregulation of I type IFN expression[257]. IFN-α induction could potentially synergize with the immunostimulatory effects of IL-12, as demonstrated in the MC38 tumor model before[258]. Thus, for a clear dissection of the relative contribution of the oncolytic effect, immunostimulatory properties of FmIL-12 and the virus to the therapeutic efficacy, a further comparison of a recombinant FmIL-12, a non-replicating MeVac and a replicating MeVac encoding FmIL-12 would be needed.

An important concern regarding any new therapeutic approach is safety. After intratumoral injections of MeVac encoding FmIL-12, a peak of FmIL-12 concentration could be observed also in peripheral blood of the treated animals. However, the highest peripheral FmIL-12 dose assessed in this experiment, 66 ng/kg, would be relatively low in comparison to the highest tolerated dose, 500 ng/kg, frequently reported in clinical studies with systemic IL-12 administration[32,33]. Therefore, this result indicates a rather insignificant leakage of FmIL-12 into the periphery after a local administration with the MeVac vector. However, the impaired measles replication in murine cells and, consequently, the relatively low *de novo* production of FmIL-12 *in vivo* must be noted here. It is possible that FmIL-12 leakage into the periphery might be an issue in a clinical situation where FmIL-12 production would increase as the virus would have the ability to constitutively replicate into tumor cells. Further vector optimization strategies could be applied to avoid this. First, the transcription gradient in

the measles genome[151] offers a possibility to modulate the amount of protein produced from an inserted transgene cassette. Thus, the amount of FmIL-12 produced by the transduced cells could be reduced by inserting the FmIL-12 cassette further downstream in the MeVac genome. Second, a system providing a control of virus replication could be introduced in the vector. A feasible approach for conditional control of measles virus replication has previously been developed using artificial riboswitches based on aptazymes[259]. Aptazymes consist of a ribozyme, a self-cleaving RNA sequence and an aptamer, a ligand binding RNA domain[260]. Upon binding of the aptamer-specific ligand, the catalytic activity of the ribozyme can be activated[260]. Thus, insertion of an aptazyme sequence into the measles genome provides an opportunity to induce conditional cleavage of the virus genome by providing the respective aptamer ligand. Ketzer *et al.* demonstrated that activation of aptazyme sequences flanking the measles *F* gene results in inhibition of measles virus gene expression, replication and spread[259]. Furthermore, since the aptazyme sequences are relatively short, around 100 bp, insertion of this safety system should not considerably attenuate the vector[259], and, thus, should be compatible also with recombinant vectors already carrying such large transgene inserts as the IL-12 fusion protein.

Although MeVac encoding PD-L1 was less efficient than the FmIL-12 encoding vector, it also demonstrated a slight therapeutic benefit over the control vector in terms of the frequency of induced complete tumor remissions. Measles encoding anti-PD-L1 was previously studied in the aggressive murine melanoma B16-CD20 model, where the anti-PD-L1 encoding vector treatment extended survival of animals in comparison to control vector, but no complete tumor remissions could be achieved[104]. Therefore, in comparison to the study in the B16-CD20 model, the MC38cea model appears to be more manageable with measles virotherapy. Both MC38- and B16-derived tumor cells, have previously been reported to express PD-L1[261,262]. Thus, both models theoretically represent favorable targets for PD-1/PD-L1 blockade. In a clinical situation, the PD-L1 expression in the tumor microenvironment was revealed as an indicator for a response to the PD-1/PD-L1 blockade already in one of the first clinical studies using the PD-1 blocking antibody nivolumab[263]. Consequently, a lot of effort has been invested in the development of a reliable test for PD-L1 expression to identify patients with the highest chances of benefit from this therapeutic approach[264]. An immunohistochemistry test to accompany the decision for application of PD-1/PD-L1 blockade in non-small-cell lung cancer and melanoma has been approved by the U.S. FDA[71]. However, it must be noted, that stratification of patients for PD-1/PD-L1 blockade according only to PD-L1 expression most probably cannot be considered an absolute measure. There are still many other immune checkpoints and factors that could contribute to resistance against PD-1/PD-L1 blockade[265]. Since only slightly more than half of the animals with MC38cea tumors responded to MeVac encoding anti-PD-L1, this model would be interesting for further study of factors determining resistance to the PD-L1 checkpoint blockade.

In some tumor types PD-L1 expression can be driven by constitutively active oncogenic signaling pathways[65]. In other cases PD-L1 expression on the tumor cell surface can be

induced as a result of an active immune response, in particular in response to IFN-γ, a mechanism that is known as adaptive immune resistance[44]. It has been demonstrated that, upon treatment with IFN-γ, PD-L1 expression is upregulated also in MC38- and B16-derived cell lines[266, 262]. Thus, an increase of PD-L1 expression on the tumor cell surface would be expected during treatment with IL-12, which is a well-known inducer of IFN-γ production[27]. The synergy of PD-1 blockade and an IL-12 encoding Semliki Forest virus vector has been demonstrated in a B16-OVA tumor model[231]. Given these results, therapeutic efficacy of the combination of MeVac vectors encoding anti-PD-L1 and FmIL-12 was also examined. However, synergistic effects could not be observed either in the MC38cea, or the B16-CD20 tumor model. The FmIL-12 encoding vector in combination with a control vector demonstrated slight therapeutic benefit over the combination with the anti-PD-L1 encoding vector in both models. It is possible that the therapeutic efficacy of the combination strategy could be greatly influenced by the administration schedule. Based on the proposed mechanism of synergy, a sequential treatment schedule with administration of the FmIL-12 encoding vector followed by application of the anti-PD-L1 encoding MeVac could be advantageous. It would be expected that treatment with the FmIL-12 encoding vector leads to strong immune activation, inducing IFN-γ production and increasing PD-L1 expression on the tumor cell surface. The following PD-L1 signaling blockade would antagonize the remaining immune suppression. For optimization of the treatment schedule, an experiment assessing the PD-L1 increase on the tumor cells following treatment with MeVac encoding FmIL-12 over time would have to be carried out. After identification of the optimal treatment schedule this combination might offer therapeutic advantages, especially in tumor types that do not respond well to MeVac encoding FmIL-12 alone.

Due to the observed limited efficacy in the initial screening experiments, the potential therapeutic value for other previously developed MeVac vectors encoding anti-CTLA-4, mCD80-Fc, mGM-CSF and mIP-10, as well as the initially examined vector combination strategies, was not further assessed. However, efficacy of these vectors in the current study was compared in only one tumor model. The efficacy of a particular immunovirotherapeutic approach is expected to depend on interactions between the immunostimulatory properties of the used oncolytic vector, the chosen immunomodulation type and the immune environment of the particular tumor. Therefore, in tumors with different immune signatures than the MC38cea, MeVac vectors encoding anti-CTLA-4, mCD80-Fc, mGM-CSF or mIP-10 might offer therapeutic benefits. To this end, the developed panel with MeVac encoding immunomodulators can be considered a flexible platform which could be used for targeted delivery of immunomodulators most suitable for treatment of a certain type of malignancy.

5.4 Immune Effector Mechanisms in Measles Immunovirotherapy

Challenge of the long-term survivors of MeVac therapy with the tumor cells used in initial tumor implantations demonstrated establishment of a protective long-term immune response in most of the treated animals. The anti-tumor vaccination effect following MV immunovirotherapy has been demonstrated before[114]. Further *in vitro* restimulation experiments showed a higher IFN-γ production by splenocytes from mice treated with MeVac encoding FmIL-12, indicating a larger or more potent immune memory response. This result would be in line with the previously reported enhanced memory T cell survival in presence of IL-12[267]. To further explore the immune effector mechanisms associated with response to MeVac therapy in detail, analyses of the tumor immune micorenvironment following treatment were performed. Previous studies of measles vectors in immunocompetent murine tumor models have focused on few immunological parameters and highlighted the role of T cell responses. An increase of $CD3^+$ T cells in the tumor and invasive margin of the MC38cea tumors has been observed after treatment with an mGM-CSF encoding measles vector[114]. Increase in the total amount of T cells and decrease in the amount of T_{reg} cells has been demonstrated in B16-CD20 tumors after treatment with measles encoding anti-CTLA-4 and anti-PD-L1[104]. In the present study, intratumoral cytokine profiling, analyses of the main intratumoral immune cell subpopulations and their activation status as well as validation of the contribution of the immune effector cells to the therapeutic efficacy of measles immunovirotherapy were carried out. Thus, this is the first study providing a broader overview of the immune effector mechanisms associated with measles immunovirotherapy.

Two separate experiments were performed to assess the impact of treatment with MeVac encoding FmIL-12 and anti-PD-L1 on the tumor immune environment. It was expected that MeVac-expressed FmIL-12 would exert its effect early after the expression due to the known IL-12 ability to directly stimulate immune effector cells[27]. Thus, the effects of FmIL-12 encoding MeVac were examined 24 h after the last treatment ("early"). In contrast, the impact of MeVac encoding anti-PD-L1 was examined four days after the last treatment ("late"). The effects observed in the "early" experiment seemed mainly associated with the actions of the MeVac-encoded FmIL-12, as the changes in *T-bet* mRNA level, cytokine profile and the amount and activation status of TIL subpopulations were observed only in the group receiving treatment with the FmIL-12 encoding vector, but not in both control groups. In the "late" experiment changes in immunological parameters were observed in both groups that received treatment with MeVac vectors, the anti-PD-L1 as well as the control IgG1-Fc group, but not in the mock group, suggesting also vector-mediated immunostimulatory effects. The most significant change in cytokine profile after treatment with MeVac encoding FmIL-12 was an increase in IFN-γ and TNF-α concentration. These changes in the cytokine profile are in line with the well-known ability of IL-12 to induce IFN-γ and TNF-α expression, mainly from NK and T cells[27]. Consistently, also an increase of *T-bet*

mRNA level was observed after treatment with MeVac encoding FmIL-12. Taken together these results indicate polarization towards a Th_1-associated immune response, which is also a well-described characteristic of IL-12[27]. Notably, in the "early" experiment a slight increase in IL-6 concentration was observed in both virus treatment groups, which could represent an acute inflammation induced by application of the MeVac vector. It is possible that also infected tumor cells are among the IL-6 producers in the given model. It has been demonstrated that IL-6 is among the cytokines released from measles-infected human mesothelioma and melanoma cells[239,241]. In the "late" experiment, an increase in the mRNA level of the Th_1 response-associated *T-bet* was observed in both groups receiving virus treatment with no significant differences between the anti-PD-L1 and control vectors. Given that in the "early" experiment no increase in *T-bet* mRNA level could be observed after treatment with the control vector, the increase in "late" experiment in both treatment groups could be associated with activation of adaptive immune cell responses as a result of oncolysis. Although one of the best-known functions of T-bet is to determine $CD4^+$ T cell differentiation towards a Th_1 phenotype, this transcription factor is also involved in regulation of many more immunological processes, including regulation of development and effector functions of innate immune cells[268]. Thus, the increase of *T-bet* mRNA level alone only indicates activation of an immune response following MeVac treatment, but the specific meaning of this result needs to be considered in the context of the TIL subpopulation analysis that will be discussed further.

After treatment with the FmIL-12 encoding MeVac, a decrease in the total amount of NK cells and an increase of the early activation marker CD69 on the remaining NK cell population was observed. IL-12 was initially discovered as an NK cell stimulatory factor[269]. The ability of IL-12 to stimulate human NK cell responses, inducing expression of activation markers, including CD69, and increasing the target cell killing capacity has often been reported subsequently[270,271,272]. It is possible that the observed decrease in the NK cell population following treatment with MeVac encoding FmIL-12 was caused by NK cell death due to powerful direct IL-12 stimulation. It is known that a prolonged exposure of human NK cells to IL-12 *in vitro* in combination with IL-2 or IL-15 induces cell death, with higher IL-12 concentrations causing apoptosis in a higher number of NK cells[273]. This effect is considered a control mechanism for excessive NK cell activation[273].

The total number of intratumoral T cells increased after treatment with MeVac encoding FmIL-12. This could result either from proliferation of T cells within the tumor or from *de novo* T cell infiltration. Involvement of both mechanisms would be plausible. Although tumor-infiltrating T cells become functionally suppressed, most of them have been pre-activated and would express the IL-12 receptor[274]. Therefore, IL-12-induced T cell proliferation should be possible. No significant differences were observed between treatment groups in the amount of $CD4^+$ and $CD8^+$ T cell subpopulations from the amount of all T cells. Thus, the extent of the induced proliferation on the $CD4^+$ and $CD8^+$ T cells should have been similar in this experiment. This is in agreement with similar IL-12R expression

level on activated $CD8^+$ and $CD4^+$ T cells[274]. Recruitment of novel T cells to the tumor site following treatment with MeVac encoding FmIL-12 could be supported by the chemokines IP-10 and Mig, which are expected to be upregulated in response to IFN-γ which is induced by IL-12[275]. Both chemokines are known to attract cells expressing the specific receptor CXCR3, mainly activated T and NK cells[275]. It has been demonstrated that blockade of IP-10 and Mig in the murine renal adenocarcinoma model, RENCA, dramatically reduces the amount of $CD8^+$ T cell infiltration observed after systemic treatment with recombinant IL-12[276]. However, further experiments are needed to assess if this mechanism is relevant in the model used in this study.

As the TIL subopulation analysis indicated activation of both NK and T cell populations, both could contribute to therapeutic efficacy of MeVac encoding FmIL-12. Depletion experiments revealed that the NK and $CD4^+$ T cell subpopulations do not significantly influence therapeutic efficacy of MeVac encoding FmIL-12, but that the $CD8^+$ T cells are essential. Discrepant results have been reported regarding the relative contribution of the TIL subpopulations to the therapeutic efficacy of IL-12 in pre-clinical tumor models. The essential role of the $CD8^+$ subpopulation, but not $CD4^+$ or NK cells, for efficacy of IL-12 has been reported in a B16F10 murine melanoma model[253]. In contrast, both $CD8^+$ and $CD4^+$ T cell subpopulations have been shown to contribute to IL-12 efficacy in a methycholanthrene-induced murine sarcoma model, MCA-207[277]. Furthermore, NK cell activity has been shown to be important for the therapeutic effect of IL-12 in a B16 lung metastasis model[28]. These discrepancies can most probably be explained by differences in the dose, treatment schedule and the used tumor model. Smyth *et al.* demonstrated that in the B16F10 lung metastasis model the therapeutic effect of high-dose IL-12 relied on the activity of NK cells, while at low doses the relevance of NKT cells increased[278]. The present study did not specifically assess the effects of NKT cells. It was also suggested that the importance of an immune cell population to the therapeutic efficacy of IL-12 is determined by its overall contribution to tumor control in a given model[278]. Along this line, it could be hypothesized that the critical role of $CD8^+$ T cells in this model is determined by the central role of T cells in the control of MC38 tumors. Furthermore, also the immunostimulatory effects of the vector and the oncolytic effect might contribute to the mechanism of action of MeVac encoding FmIL-12, adding a further layer of complexity.

In the "late" experiment, an increased T cell amount was observed in both MeVac treatment groups, with a slightly higher increase in the MeVac anti-PD-L1 group. This result indicates that treatment with MeVac without an immunomodulator is sufficient for intratumoral T cell expansion or attraction with, as expected, a slight benefit for the anti-PD-L1 group. The restoration of T cell activity and proliferation following PD-1/PD-L1 blockade is well-known and has been demonstrated for human and murine T cells[279, 280]. Since a slightly increased amount of IFN-γ was also observed in the anti-PD-L1 group as discussed before, it is possible that T cell attraction through upregulation of IFN-γ-induced chemokine expression was also involved. It has indeed been shown that IP-10 determines

increased trafficking of adoptively transfered T cells into tumor following PD-1 blockade in a B16 tumor model[249]. Notably, a higher amount of intratumoral T cells in the anti-PD-L1 group correlated with a larger decrease in tumor volume. Increased intratumoral $CD8^+$ T cell proliferation and amount is known to be associated with tumor regressions also in a clinical situation[281]. However, a decrease was observed in the amount of activated $CD8^+$ T cells in both virus treatment groups in the "late" experiment. This could reflect T cell death in the contraction phase of the T cell response which follows target cell killing[282]. Only small amount of T cells survive the contraction phase and form the memory T cell pool[282]. As mentioned before, it must be noted that the differences in the amount of intratumoral T cells after treatment with the control and anti-PD-L1 encoding MeVac vectors were not significant. Activation of T cell responses after treatment with the control vector is probably mostly associated with enhanced T cell priming as a result of immunological cell death of infected tumor cells[239].

In the "late" experiment, decreased amount of NK cells in comparison to mock treated animals was observed after treatment with the control vector and an even slightly greater decrease in the MeVac anti-PD-L1 group. In the MeVac anti-PD-L1 group, a lower amount of NK cells also correlated with a greater decrease in tumor volume during the treatment. This correlation was in a striking contrast to the mock treated animals where a lower amount of NK cells correlated with a larger increase of tumor volume. However, it must be noted that the NK and T cell populations were quantified as a percentage of the $CD45^+$ cells and an increase in one of them, would cause a decrease in the other one or *vice versa*. Since the degree of the decrease in NK cell population was comparable to the increase in T cell population, it is possible, that these results just reflect the relative change in one of these populations in comparison to the other. However, with only these results, it is not possible to explicitly determine which, the increase of the T cell amount or decrease of the NK cell amount, is responsible for the observed effect. It is possible that NK cells contribute to the control of tumor growth in the untreated animals, become activated after treatment with MeVac, gaining a greater target cell killing capacity, but eventually undergo cell death after completion of their effector functions. It has been demonstrated that activated NK cells can engage in serial target cell killing[283], but this capacity is most probably not unlimited. Furthermore, there are also data demonstrating induction of apoptosis in activated NK cells after engaging in their cytolytic function[284,285]. Since recognition and destruction of virus-infected cells is one of the main functions of NK cells[286], solely the infection of the tumor cells by MeVac could trigger their activation. This could explain the decrease of NK cell numbers observed also in the control vector group. NK cells can recognize virus-infected cells via several mechanisms, including recognition of MHC-I (major histocompatibility complex I) class molecule downregulation on the surface of the infected cell, recognition of virus proteins through natural cytotoxicity receptors, recognition of stress-induced ligands through the NKG2D receptor and direct stimulation of TLR receptors on the surface of NK cells by virus associated pathogen-associated molecular patterns[286]. If some of these mechanisms are

relevant in the model used in this study should be assessed in further experiments. A trend for a greater decrease in the amount of NK cells in the anti-PD-L1 group compared to the IgG1-Fc group suggested that PD-L1 blockade could also be of a slight benefit for NK cell activation. The PD-1/PD-L1 axis has indeed been shown to be relevant in regulation of NK cell functions in the context of human multiple myeloma[287]. Clear dissection of the relative contribution of T cells and NK cells to the therapeutic efficacy of the anti-PD-L1 encoding vector would be possible in further immune cell depletion experiments.

The MC38cea tumor model used in this study has a specific immunological signature. It was observed that tumors from animals in the mock group contain large amount of T and NK cells, thus, suggesting an immunogenic environment under immunosuppression. Data obtained in this study allow to propose a model in which the MeVac expressed FmIL-12 strongly activates the pre-existing tumor infiltrating immune effector cells, counteracting the immunosuppressive signaling and inducing rapid killing of the surrounding tumor cells. Therefore, tumors with similar immunological signatures as the MC38cea could be expected to respond well to treatment with MeVac encoding the IL-12 fusion protein.

5.5 Translational Potential

This study revealed the potential to significantly increase therapeutic efficacy of oncolytic MeVac vectors in combination with immunomodulators in a murine tumor model. In particular, MeVac encoding FmIL-12 demonstrated great efficacy in terms of complete tumor remissions. Yet, the ultimate goal of the research of novel strategies for cancer treatment is, of course, not the treatment of a murine, but a human disease. It is a disturbing fact that most of the novel cancer therapeutics demonstrating promising effects in murine tumor models, fail in clinical trials and never reach approvement for clinical use[288]. There are many factors contributing to this unsettling statistic, including the burden of regulatory and financial issues, but frequently the cause of a failure is incompatibility of the used pre-clinical model with the clinical situation. Testing of novel treatment strategies *in vivo* is mandatory for initial assessment of safety and efficacy, but one must be aware of the fact that the broadly used murine tumors models differ from situation in cancer patients in many important aspects. These can include: age of the subject — use of young mice in contrast to mostly elderly human cancer patients; minimal individual variation — use of inbred mouse strains; time frame — use of tumor models that develop a malignancy within days in contrast to human cancer development over decades; tumor microenvironment — use of subcutaneous tumor models that can not be compared with physiology of tumors arising in organs other than skin; immunobiology — differences between mice and humans in functions of some components of the immune system. These limitations must be kept in mind when interpreting the data obtained in this study in terms of implications for further clinical development of MeVac encoding IL-12 fusion protein.

The biology of murine and human IL-12 does not differ significantly, with IL-12 from

both species being involved in activation and enhancement of the cytotoxic potential of T and NK cells[27]. The identity of murine and human IL-12 is 60% for the p35 protein subunits and 70% for p40 protein subunits[289]. Furthermore, it has even been demonstrated that mouse IL-12 remains active in human cells, but that human IL-12 is not active in murine cells[289]. Nevertheless, given the differences in the protein sequence of IL-12 between both species and the possibility for unknown interactions, the use of MeVac encoding FmIL-12 in a human system would not be desirable. Thus, a MeVac vector encoding a human IL-12 fusion protein (FhIL-12), which was constructed based on a previous study by Lieschke *et al.*[222], was generated. Insertion of FhIL-12 in genome positions downstream of the MeVac *P* or *H* gene was demonstrated to be feasible. Replication and cytotoxic potential of the novel vectors were not significantly affected. Expression of FhIL-12 from the inserted transgene cassette could also be demonstrated. With these experiments an appropriate vector for further clinical development of the oncolytic measles virus encoding an IL-12 fusion protein has been generated. However, further functional *in vitro* and *in vivo* experiments would be needed to further pursue a plan for clinical translation.

Most of the experiments performed in this study were carried out using the murine colorectal adenocarcinoma model. However, as mentioned before, the subcutaneous model used here can not be considered to reflect properties of human colorectal cancer (CRC). Although currently no clinical studies for use of MV vectors in CRC therapy have been performed, some pre-clinical data suggest that CRC could be a potential target for oncolytic MV therapy[290]. To further examine CRC as a target for the vector used in this study, five different human CRC cell lines were characterized for expression of MV receptors. Further, replication kinetics and cytotoxic properties of the parental MeVac vector used in this study, as well as the Edmonston B derived vaccine strain derived vector (NSe), used in most of the current clinical studies with oncolytic MV, were assessed in these CRC cell lines. The main MV receptor CD46 was expressed on all the cell lines, although the expression levels slightly differed. Furthermore, three of the cell lines were found to be positive for the epithelial MV receptor Nectin-4 on mRNA level. As expected based on the determined expression of CD46 by all of the cell lines, they were all susceptible to infection with MeVac and NSe viruses. However, further experiments revealed that vector replication efficiency and cytotoxicity differs between the cell lines and between the vectors. The available data set is not large enough to draw any strong conclusions about the correlations of MV receptor expression with the replicative or cytotoxic potential of the vectors or efficiency of virus particle production and cytotoxic properties. Nevertheless, it could be distinguished, that receptor expression is not the only factor influencing the cells' susceptibility to MV infection. For instance, the HT-29 cell line which was found to have one of the highest CD46 expression levels of the tested cell lines and was also positive for nectin-4 on mRNA level, had the lowest decrease in cell viability after infection with both MV vectors, but it was not the cell line with the lowest viral particle production in the one-step growth curve. Differences, mainly in virus particle production efficiency, were detected also between the two vectors, with MeVac reaching lower

titers in most of the cell lines compared to the NSe vector. These data suggest that it would be of further interest to systematically assess the properties of MeVac and NSe vectors in different human CRC cell lines to identify host cell factors influencing replication efficiency and cytotoxic properties. For such an analysis the U.S. National Cancer Institute 60 human cancer cell line panel (NCI60), which includes comprehensively characterized cancer cell lines, could be of interest[291]. Four of the CRC cell lines used in this study are included in the NCI60. The replication efficiency and cytotoxic properties of MeVac and NSe vectors could be screened on all seven of the NCI60 panel CRC cell lines and correlations with the available gene and protein expression data could be performed. Such experiments could give valuable indications about intrinsic host cell factors associated with efficacy of oncolytic MV that could be used for selection of therapy targets and further vector modifications.

5.6 Conclusions and Outlook

This study compared advantages of different immunomodulation strategies in combination with oncolytic MV. Novel MV vectors encoding six different immunomodulators to support different phases in the establishment of an anti-tumor immune response were generated based on the measles Schwarz vaccine strain vectors (MeVac). *In vitro* characterization demonstrated that after transduction of the target cells with the novel MeVac vectors the encoded immunomodulators are expressed and maintain their functionality. MeVac vectors, which are more immunogenic than the Edmonston B derived MV used in previous measles oncolysis studies, have not previously been engineered for expression of immunomodulators. Thus, with the novel recombinant MeVac vectors the armamentarium of available immunomodulatory MV vectors has been significantly expanded. Therapeutic efficacy of the immunomodulatory MeVac vectors was evaluated *in vivo* in a fully immunocompetent murine colon adenocarcinoma model. MeVac encoding an antibody against murine PD-L1 (anti-PD-L1) and a murine IL-12 fusion protein (FmIL-12) were identified as the most promising among the novel vectors in terms of extended survival of animals. MeVac encoding FmIL-12 demonstrated the highest therapeutic efficacy, inducing complete tumor remissions in 90% of the treated animals. MeVac treatment induced a systemic anti-tumor immune response in most of the long-term survivors of the therapy, as demonstrated by tumor engraftment rejections after tumor rechallenge. To analyze immune effector mechanisms contributing to the therapeutic efficacy of the MeVac encoding anti-PD-L1 and FmIL12, analysis of the tumor immune microenvironment following treatment was performed. Analysis four days after the last treatment indicated that MeVac encoding anti-PD-L1 slightly enhances beneficial modulation of the tumor immune environment by supporting activation of cell-mediated immune responses. In contrast, strong modulation of the tumor immune environment was observed after treatment with MeVac encoding FmIL-12, as determined 24 h after the last treatment. Activation of cell-mediated immune responses was indicated by an increase of the concentration of effector cytokines IFN-γ and TNF-α, as well as an increase in the intratumoral T cell

amount and activation status and activation of NK cells. Immune cell depletion experiments revealed that the cytotoxic $CD8^+$ T cell subpopulation is essential for therapeutic efficacy of the MeVac encoding FmIL-12, while $CD4^+$ T cells and NK cells did not appear to be crucial in the given model. The obtained data suggest MeVac encoding FmIL-12 as an effective therapeutic in tumors with high immune effector infiltration under immunosuppression. However, tumors with different immune signatures might benefit from other immunomodulation types and, thus, require vectors encoding other immunomodulators from the MeVac vector panel developed in this study.

Based on the results of this study, rational development of measles immunovirotherapeutic strategies is continued. A study to assess the properties of MeVac encoding murine IL-15 has been started (L. Hartmann, R. Veinalde, C. E. Engeland, unpublished). This project is based on the hypothesis that MeVac encoding the cytokine IL-15 could be more beneficial than the IL-12 encoding vector in tumors with lower immune effector infiltration. In contrast to FmIL-12, along with the activation of immune effector cells, IL-15 is expected to have a proliferative effect, particularly on NK cells[292]. The immunomodulatory effects of MeVac encoding FmIL-12 and MeVac encoding IL-15 will be compared by performing an analysis of the tumor immune environment post treatment, similarly as described in this study. Therapeutic efficacy of both vectors will be compared in the MC38cea tumor model and in a less immunogenic tumor model. With regards to MeVac encoding anti-PD-L1, since only slightly more than a half of the animals responded to the therapy in this PD-L1 positive MC38cea tumor model, it could be used to further study mechanisms associated with resistance to the PD-L1 blockade therapy. Furthermore, the therapeutic efficacy and immunostimulatory properties of MeVac encoding anti-PD-L1 analyzed in this study, should be compared with MeVac encoding anti-PD-1, which is a clinically more widely used approach for PD-1/PD-L1 blockade (C. E. Engeland, R. Veinalde, unpublished). Importantly, to facilitate further clinical translation, development of mouse models with a humanized immune system for studies of safety and efficacy of the immunomodulatory measles vectors, particularly MeVac encoding the human IL-12 fusion protein, would be needed. Lastly, the MeVac vector system can be envisioned as a flexible platform to allow targeted delivery of immunomodulators based on the immune signature of the individual tumor. To approach this, tumor immune profiling following oncolytic measles immunovirotherapy, similar as described in this study, should be included in future clinical studies. Importantly, such an analysis of tumor immune environment will be included in a Phase I clinical trial for oncolytic measles virus which is currently in preparation in the National Center for Tumor Diseases in Heidelberg, Germany.

Appendix

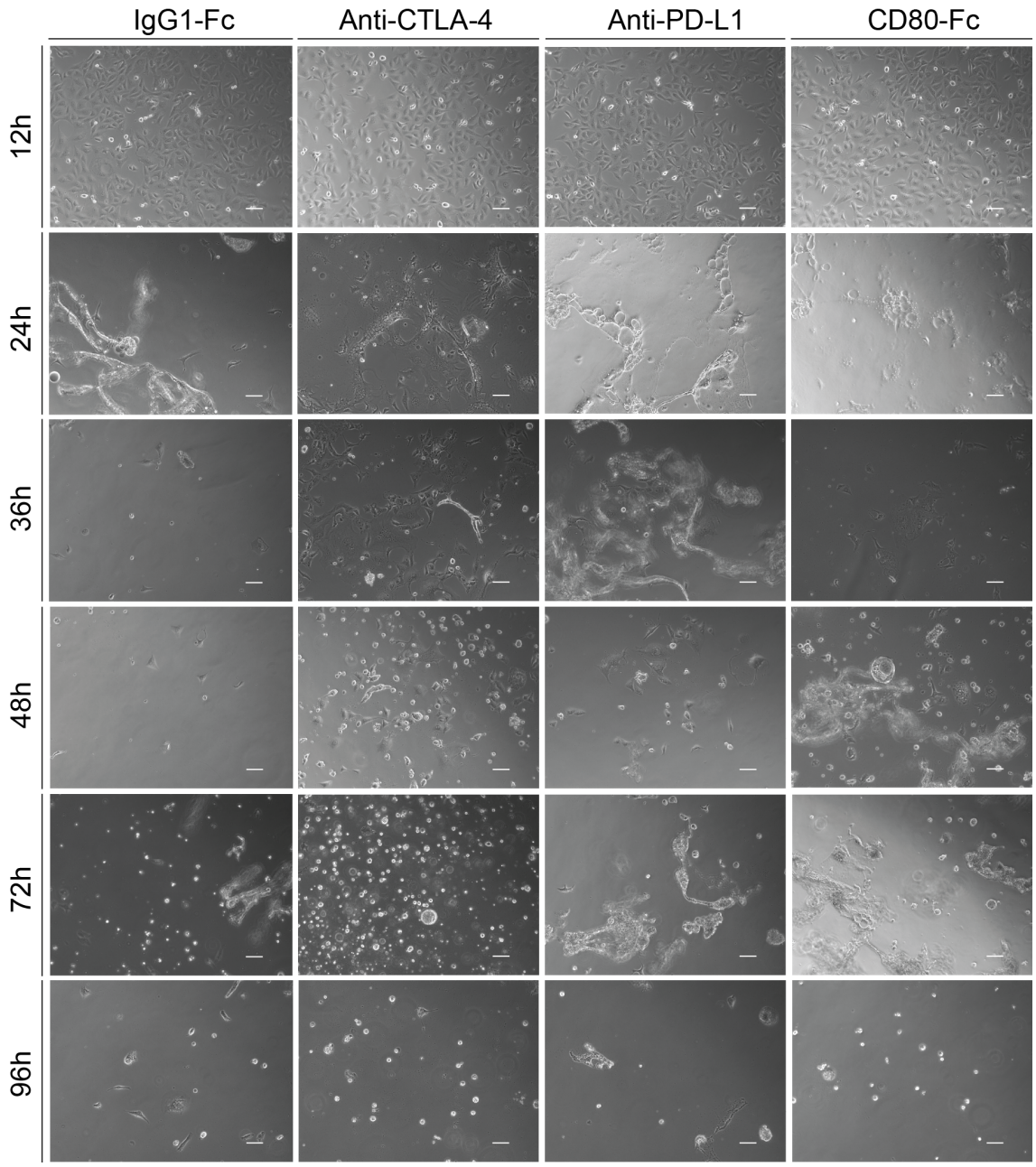

Figure A.1: **One step growth curves in Vero-αHis cells.** Cells were infected with MeVac encoding the respective transgenes at a multiplicity of infection = 3 and fluorescence microscopy images were taken at the depicted time points. Scale bars 100 µm.

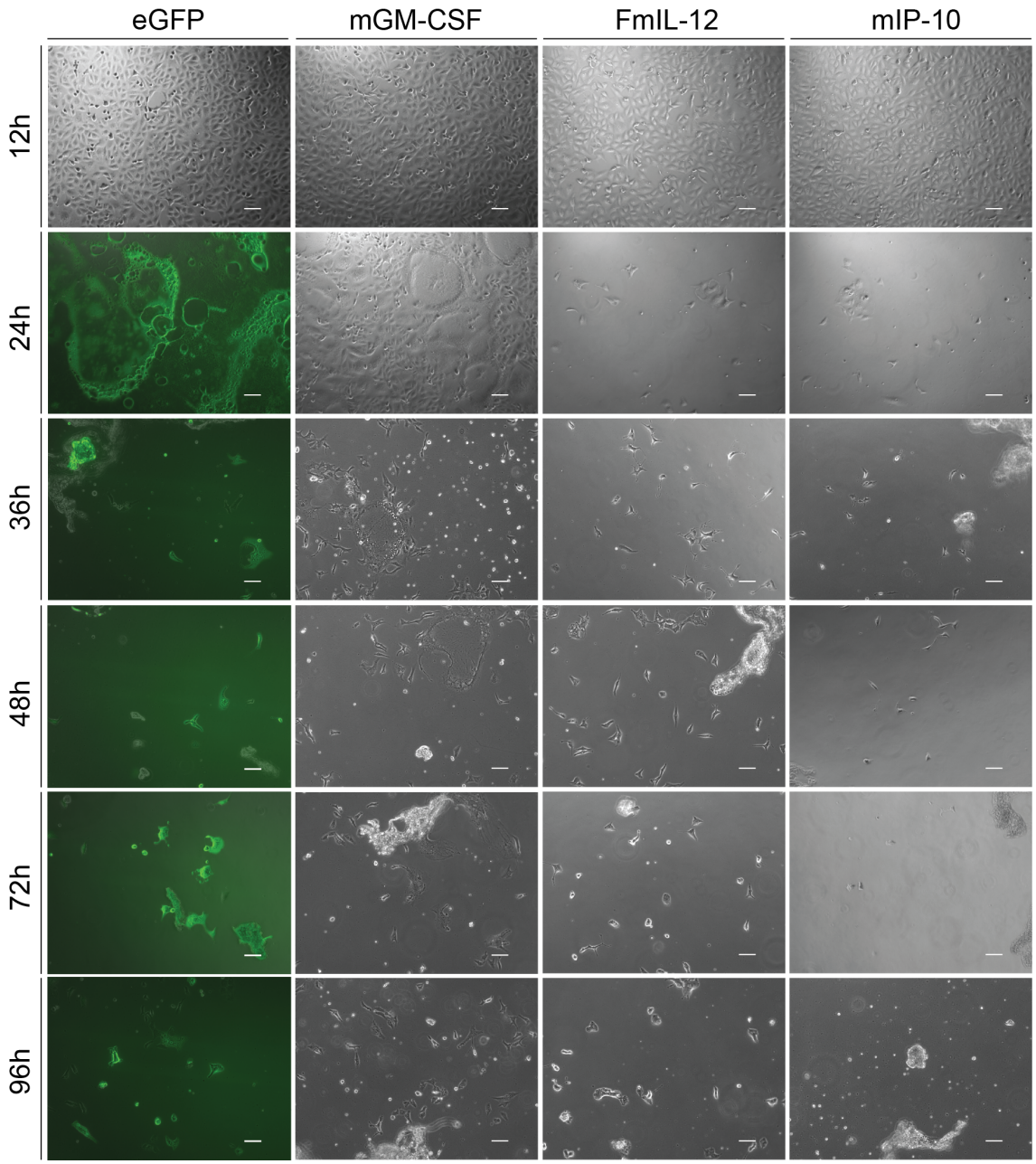

Figure A.2: **One step growth curves in Vero-αHis cells.** Cells were infected with MeVac encoding the respective transgenes at a multiplicity of infection = 3 and fluorescence microscopy images were taken at the depicted time points. Scale bars 100 µm.

Table A.1: **Results for complete genome sequencing of MeVac GM-CSF Hbl-antiCEA.** ORF — open reading frame; *H* — measles hemagglutinin; *F* — measles fusion protein; *L* — measles polymerase.

Position	Region of genome	Change	Type of change
7812	Intergenic region between *F* ORF and *H* ORF	A>G	Change in a non-coding region
8875	*H* ORF	C>T	Silent mutation
10075	Intergenic region between *H* ORF and *L* ORF	G>A	Change in a non-coding region
10129	Intergenic region between *H* ORF and *L* ORF	A>G	Change in a non-coding region

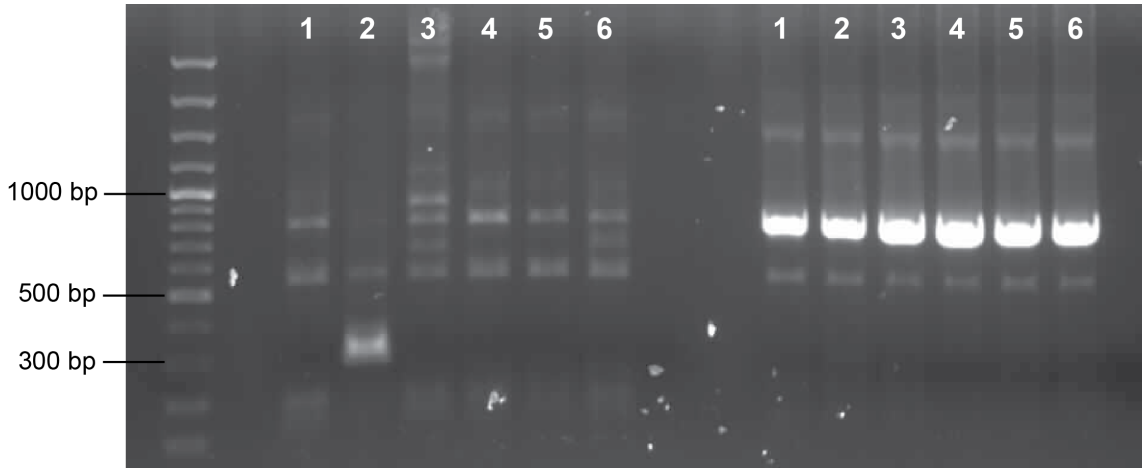

Figure A.3: **Assay for detection of the presence of defective interfering particles (DIs).** Total RNA was isolated from virus suspensions and RT-PCR analysis was carried out for detection of DIs as described by Pfaller *et al.*[230]. 1 — MeVac Hbl-αCEA (VHp4), 2 — MeVac ld-mGM-CSF Hbl-αCEA (VHp4), 3 — MeVac ld-FmIL-15 Hbl-αCEA (VHp3), 4 — MeVac P-FmIL-12 Hbl-αCEA (VHp4), 5 — MeVac ld-eGFP Hbl-αCEA (VHp4), 6 — MeVac ld-FmIL-15 Hbl-αCEA (VHp4). First six sample lines from the left were amplified with two negative polarity primers A1*SnaBI*/A2*NotI* for DI specific amplification, second six sample lines were amplified with a negative and positive polarity primers A1*SnaBI*/B1 as cDNA input controls. VHp3, VHp4 — third and fourth passage on Vero-αHis cells, respectively; FmIL-12 — murine IL-12 fusion protein; FmIL-15 — murine IL-15 agonist.

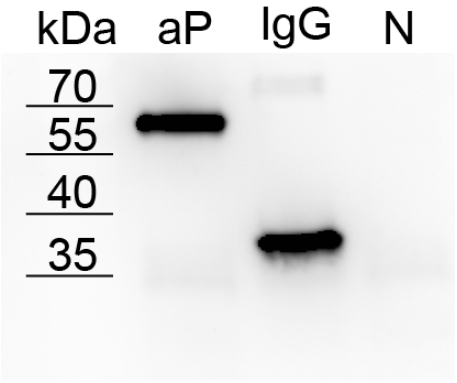

Figure A.4: **Expression of MeVac encoded anti-PD-L1 and IgG1-Fc**. Supernatants were collected from Vero-αHis cells infected with MeVac encoding anti-PD-L1 (aP) and IgG1-Fc (IgG) and western blot analysis was carried out. DMEM+10% FCS was used as a negative control (N).

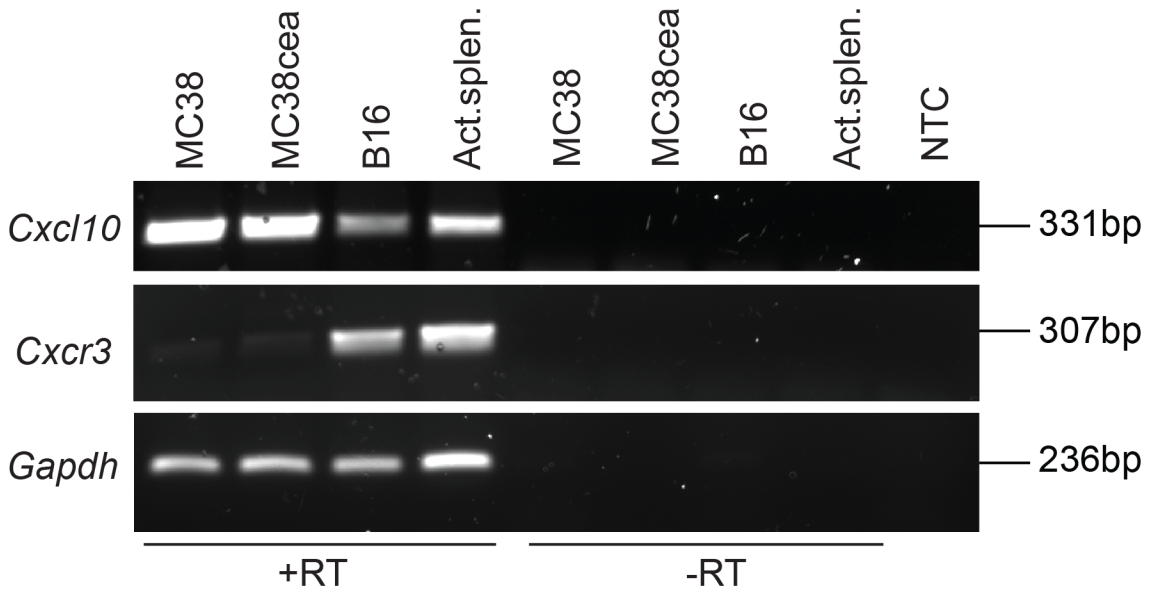

Figure A.5: **RT-PCR for murine *Ip-10* (*Cxcl10*) and *Cxcr3* in MC38, MC38cea and B16 cell lines.** RT-PCR for murine *Cxcl10*, *Cxcr3* genes and *Gapdh* as a loading control was carried out using cDNA from the indicated cell lines. cDNA from murine splenocytes activated with PMA and ionomycin served as a positive control. +RT — cDNA samples; −RT — minus reverse transcriptase controls; NTC — no template control; Act. splen. — activated splenocytes.

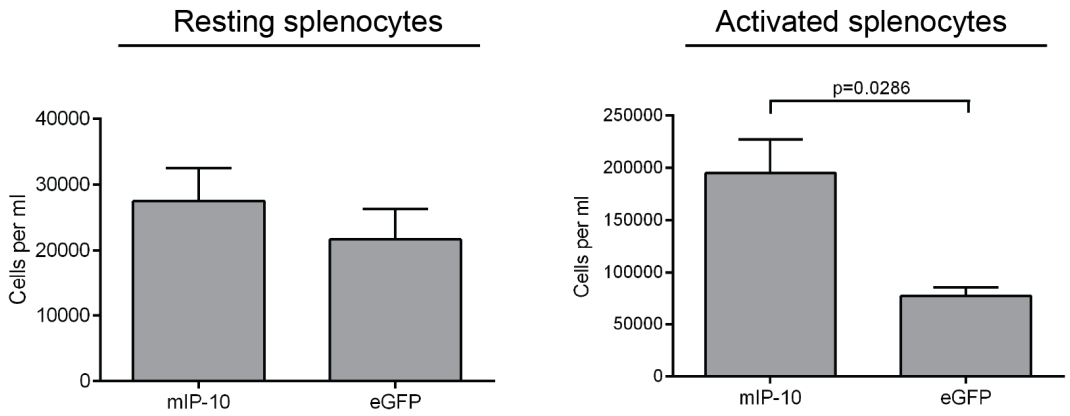

Figure A.6: **Functionality of MeVac encoded mIP-10.** Resting splenocytes or splenocytes stimulated with a recombinant murine IL-2 were added in the upper part and supernatants collected from Vero-αHis cells infected with MeVac encoding mIP-10 or eGFP in the lower part of a transwell insert. Splenocyte migration was allowed for 3 h in 37°C 5 % CO_2 incubator. Cells in the lower part of the chamber were counted using a hemocytometer and Trypan Blue for dead cell exclusion. Mean values from three to four counts per sample with standard errors of the mean are shown. Results were compared using Mann-Whitney U test.

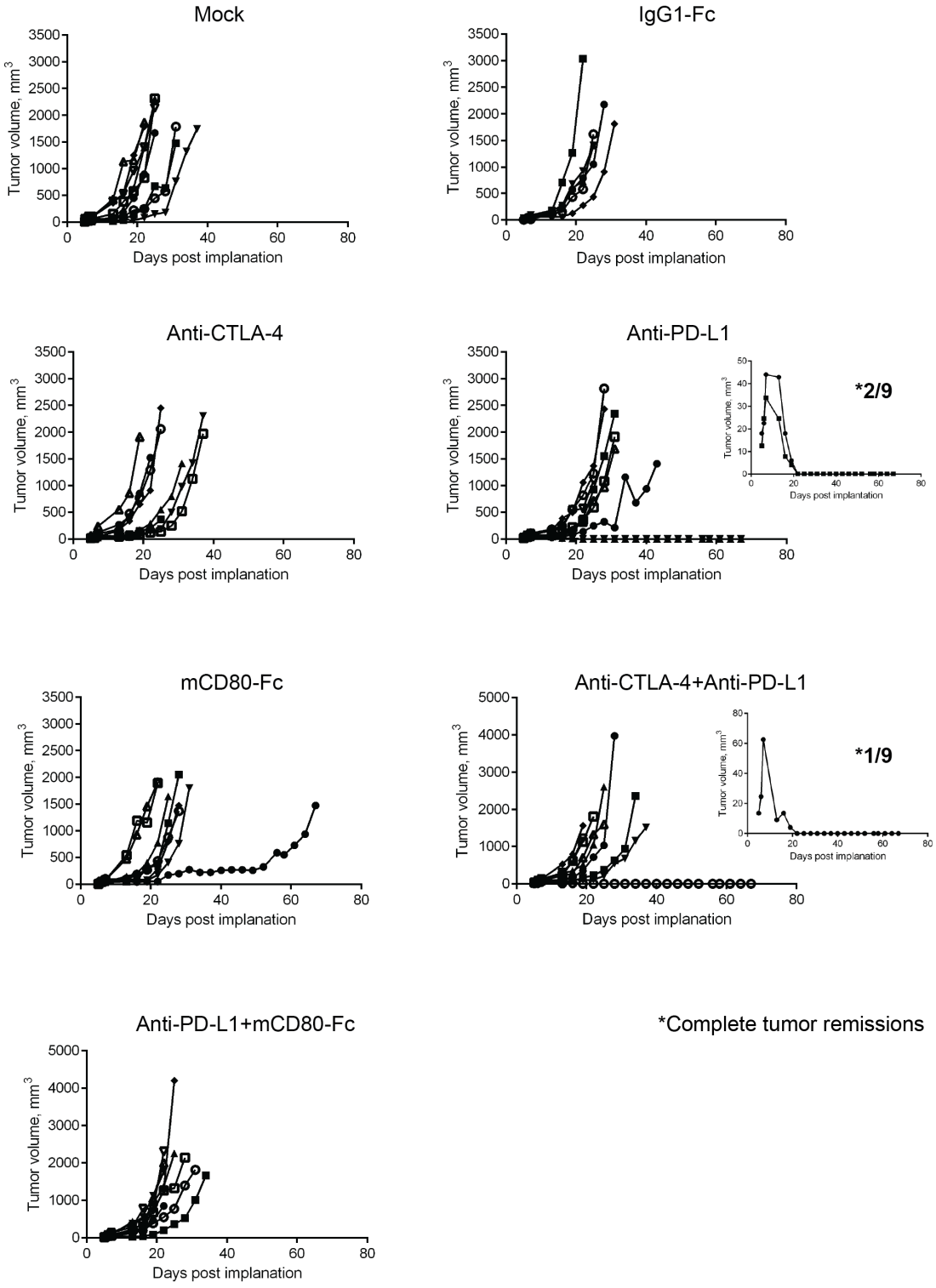

Figure A.7: **Individual tumor volume dynamics in the experiment comparing MeVac encoding immunomodulators targeting the immunosuppressive tumor environment.** MC38cea cells were implanted subcutaneously (s.c.) into the right flank of C57BL/6J mice (6 – 9 animals per group). When tumors reached an average volume of 70 mm^3 mice received intratumoral injections with 1×10^6 ciu or with MeVac vectors encoding the respective transgenes on four consecutive days in 100 µl virus suspension with carrier fluid (OptiMEM). Mice in the mock group received i.t. injections with 100 µl OptiMEM. Tumor volume dynamics for individual animals are shown. ciu — cell infectious units.

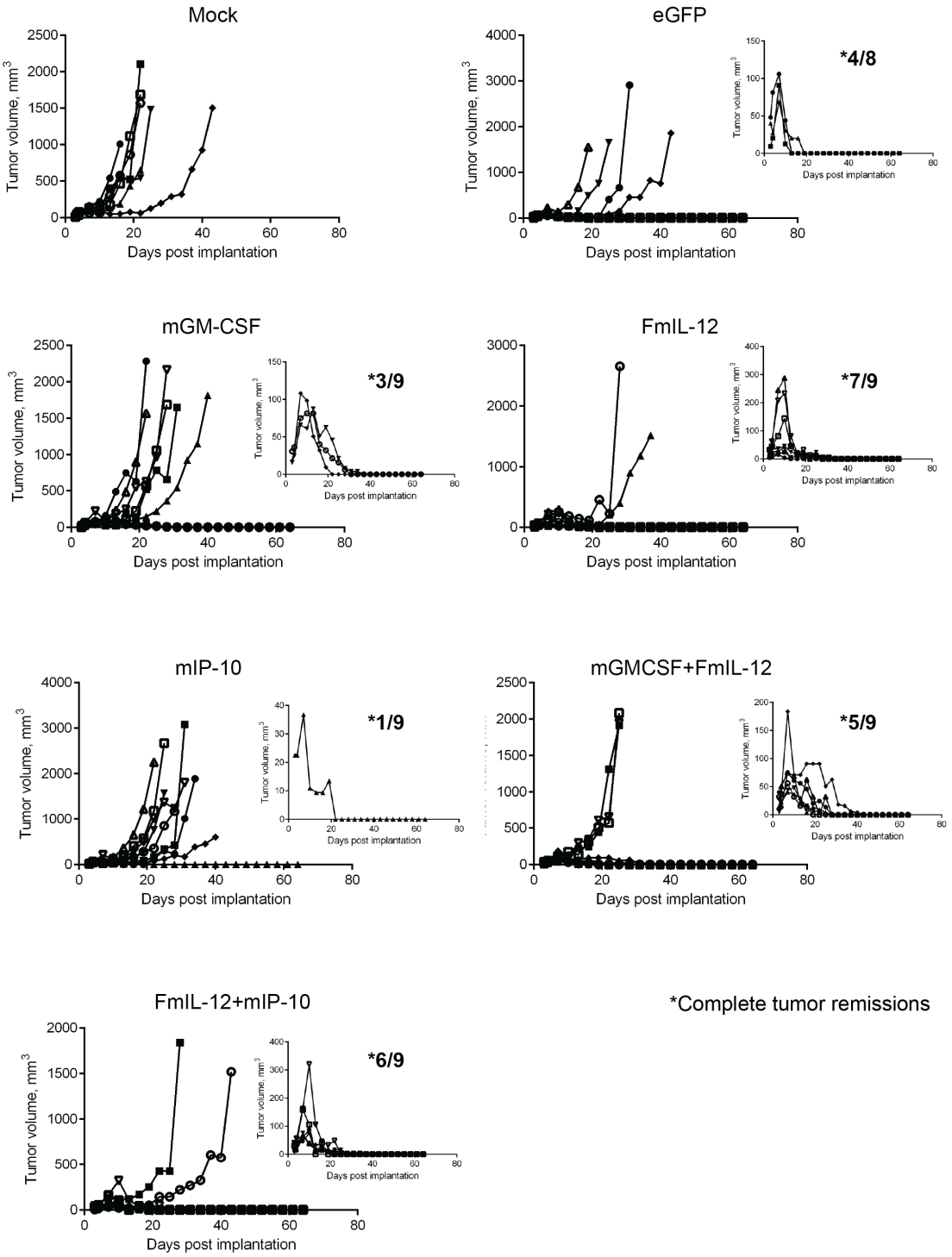

Figure A.8: **Individual tumor volume dynamics in the experiment comparing MeVac encoding immunomodulators targeting antigen presenting cell and effector cell responses.** MC38cea cells were implanted subcutaneously (s.c.) into the right flank of C57BL/6J mice (6 – 9 animals per group). When tumors reached an average volume of 40 mm^3 mice received intratumoral injections with 5×10^5 ciu with MeVac vectors encoding the respective transgenes on five consecutive days in 100 µl virus suspension with carrier fluid (OptiMEM). Mice in the mock group received i.t. injections with 100 µl OptiMEM. Tumor volume dynamics for individual animals are shown. ciu — cell infectious units.

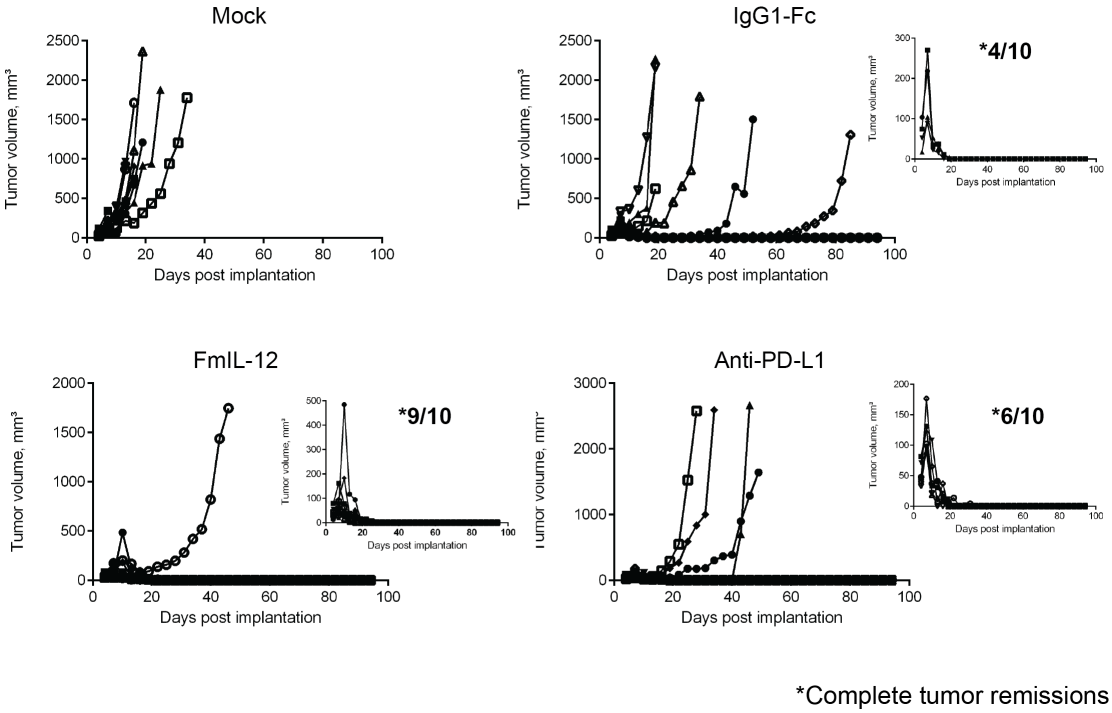

Figure A.9: **Individual tumor volume dynamics in the experiment comparing MeVac encoding FmIL-12 and anti-PD-L1.** MC38cea cells were implanted subcutaneously into the right flank of C57BL/6J mice (10 animals per group). When tumors reached an average volume of 40 mm^3 mice received intratumoral (i.t.) injections with 1×10^6 ciu of viruses encoding the respective transgenes on four consecutive days in 100 µl virus suspension with carrier fluid (OptiMEM). Mice in the mock group received i.t. injections with 100 µl OptiMEM. Tumor volume dynamics for individual animals are shown. ciu — cell infectious units

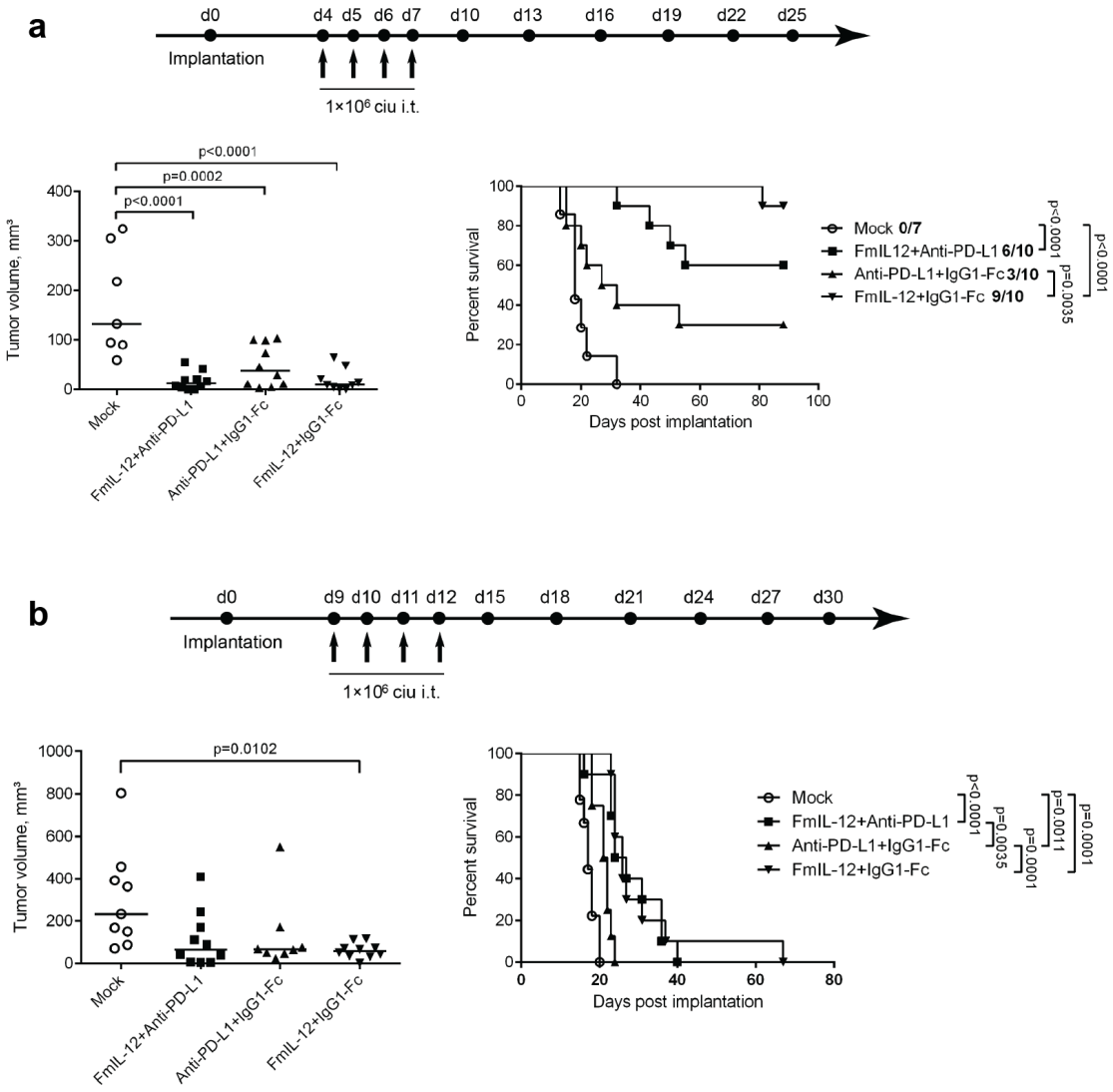

Figure A.10: **Therapeutic efficacy of FmIL-12 and anti-PD-L1 encoding MeVac combination.** MC38cea (**a**) or B16-CD20 (**b**) cells were implanted subcutaneously into the right flank of C57BL/6J mice (7 – 10 animals per group). When tumors reached an average volume of 40 mm^3 mice received intratumoral (i.t.) injections with 1×10^6 ciu of targeted viruses (Hbl-αCEA in **a** or Hbl-αCD20 in **b**) encoding the respective transgenes on four consecutive days in 100 µl virus suspension with carrier fluid (OptiMEM). Mice in the mock group received i.t. injections of 100 µl OptiMEM. Tumor volume distribution on day 13 (**a**) or day 15 (**b**) post implantation with median in each group and Kaplan-Meier analysis are shown. Dots represent individual mice. Complete tumor remission rates are shown in Kaplan-Meier plots. ciu — cell infectious units.

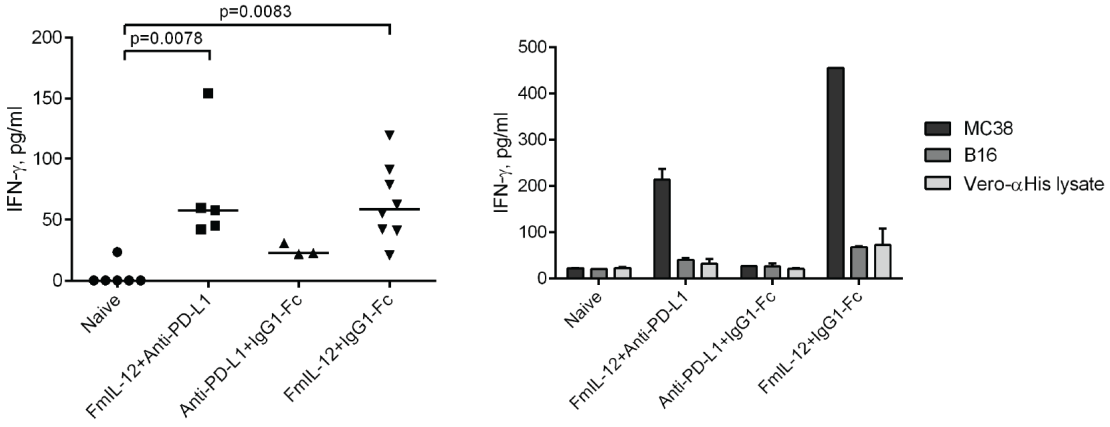

Figure A.11: **IFN-γ memory recall in long-term survivors of MeVac FmIL-12 and anti-PD-L1 combination treatments.** Splenocytes were collected from the animals two weeks after a rechallenge with MC38cea cells, stimulated with recombinant murine IL-2 and cocultivated with MC38cea cells (**a**) or MC38 and B16 cells and Vero-αHis cell lysate (**b**) for one mouse from each group at a ratio 10:1. Supernatants were collected after 48 h and IFN-γ concentration measured by ELISA. Dots representing individual mice and median in each group are shown in **a**. Mean values with standard errors of the mean from two replicate measurements per sample are shown in **b**

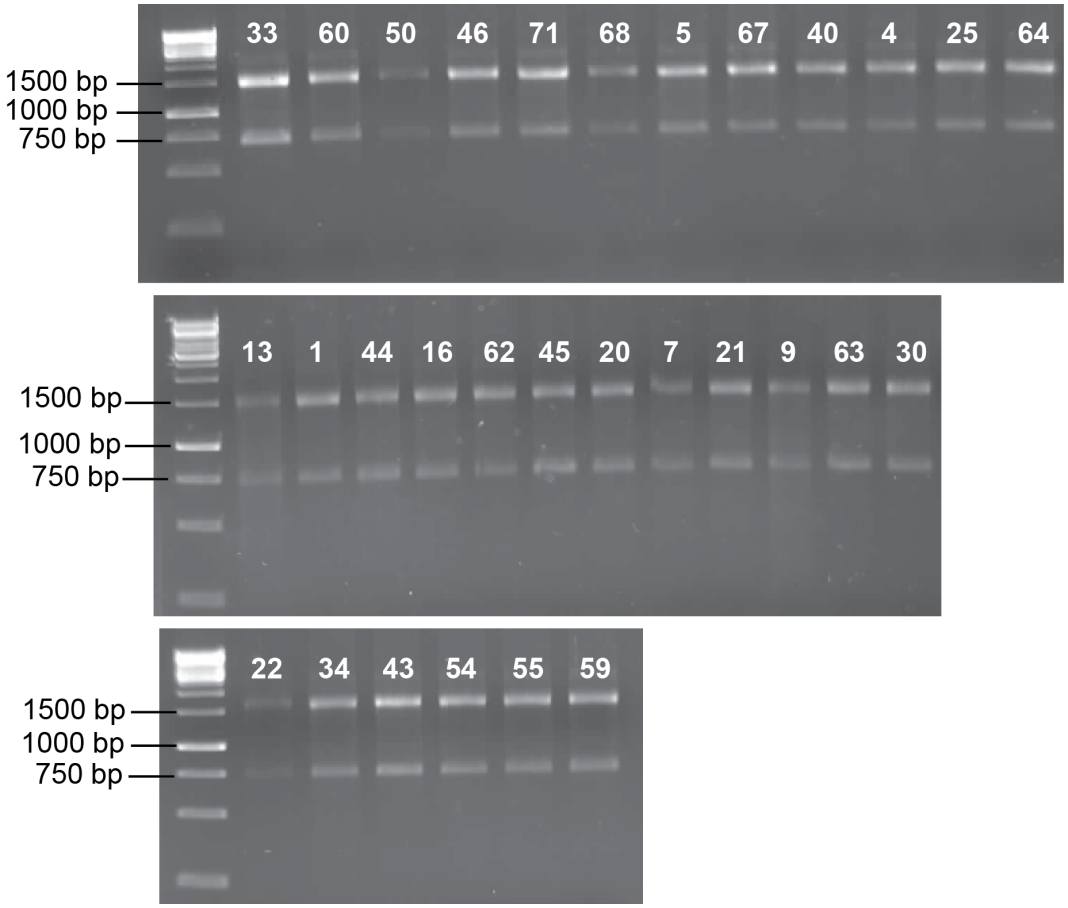

Figure A.12: **RNA integrity test.** MC38cea cells were implanted subcutaneously into C57BL/6J mice. When tumors reached an average volume of 120 mm^3 or 100 mm^3 mice received intratumoral treatment with MeVac encoding murine IL-12 fusion proteim, antibody against murine PD-L1 or antibody constant region IgG1-Fc. Mice in the mock group received i.t. injections with a respective amount of OptiMEM. Tumors were explanted one or four days after the last treatment. A part of the tumor was stored in an RNA stabilization reagent (RNA*later*) and total RNA was isolated subsequently. The RNA integrity was assessed by loading 300 ng RNA on 1% agarose gel. Numbers denote the individual samples.

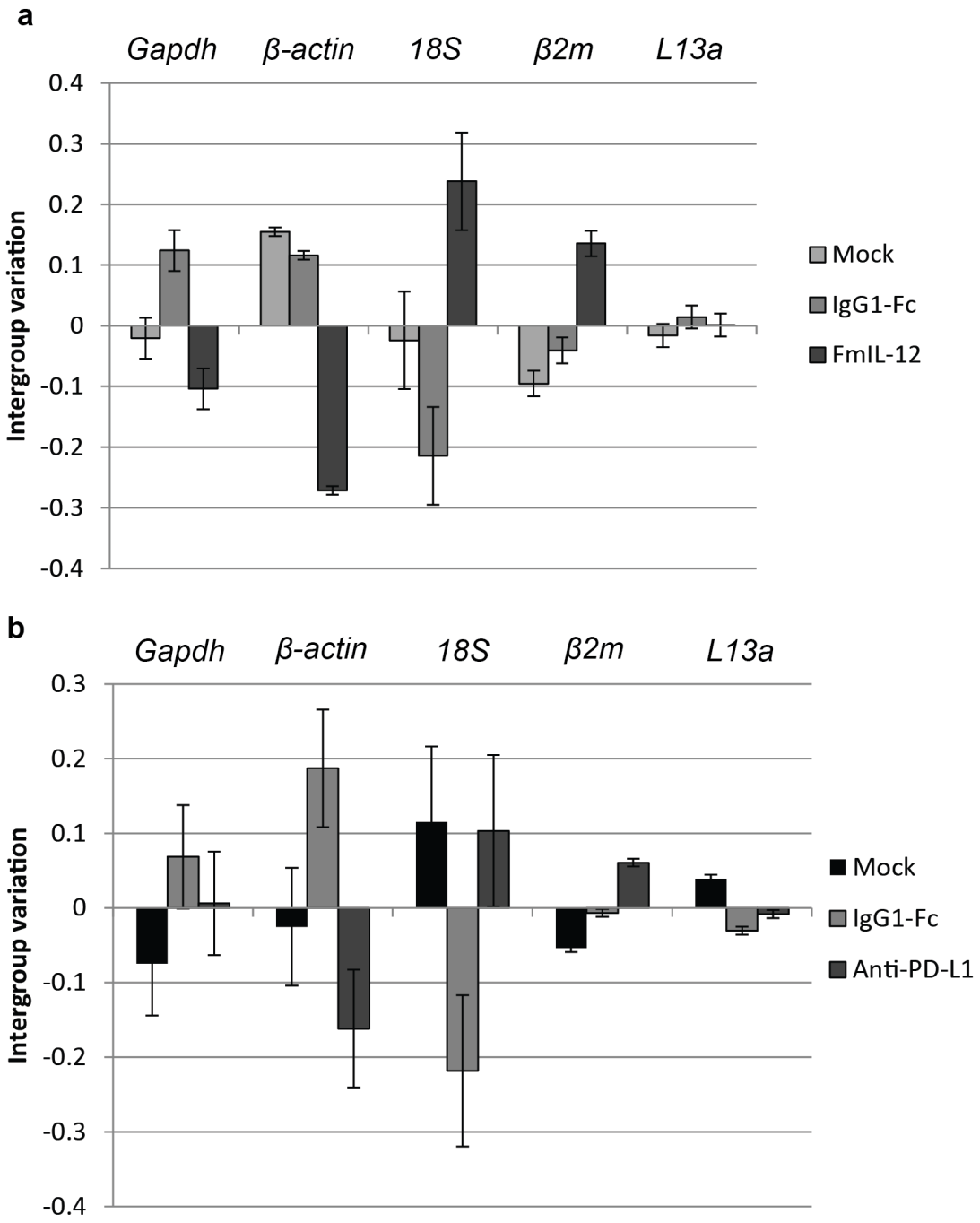

Figure A.13: **Validation of reference genes for reverse transcription quantitative PCR (RT-qPCR) analysis.** MC38cea cells were implanted subcutaneously into C57BL/6J mice. When tumors reached an average volume of 120 mm^3 (**a**) or 100 mm^3 (**b**) mice received intratumoral treatment with MeVac encoding the respective transgenes or the respective amount of OptiMEM (mock). RT-qPCR analysis for different potential reference genes was carried out using RNA from three tumors per group explanted one (**a**) or four (**b**) days after the last treatment. Results were analysed using the NormFinder software[219]. The gene having the lowest variation between conditions and samples was chosen for further use as a reference.

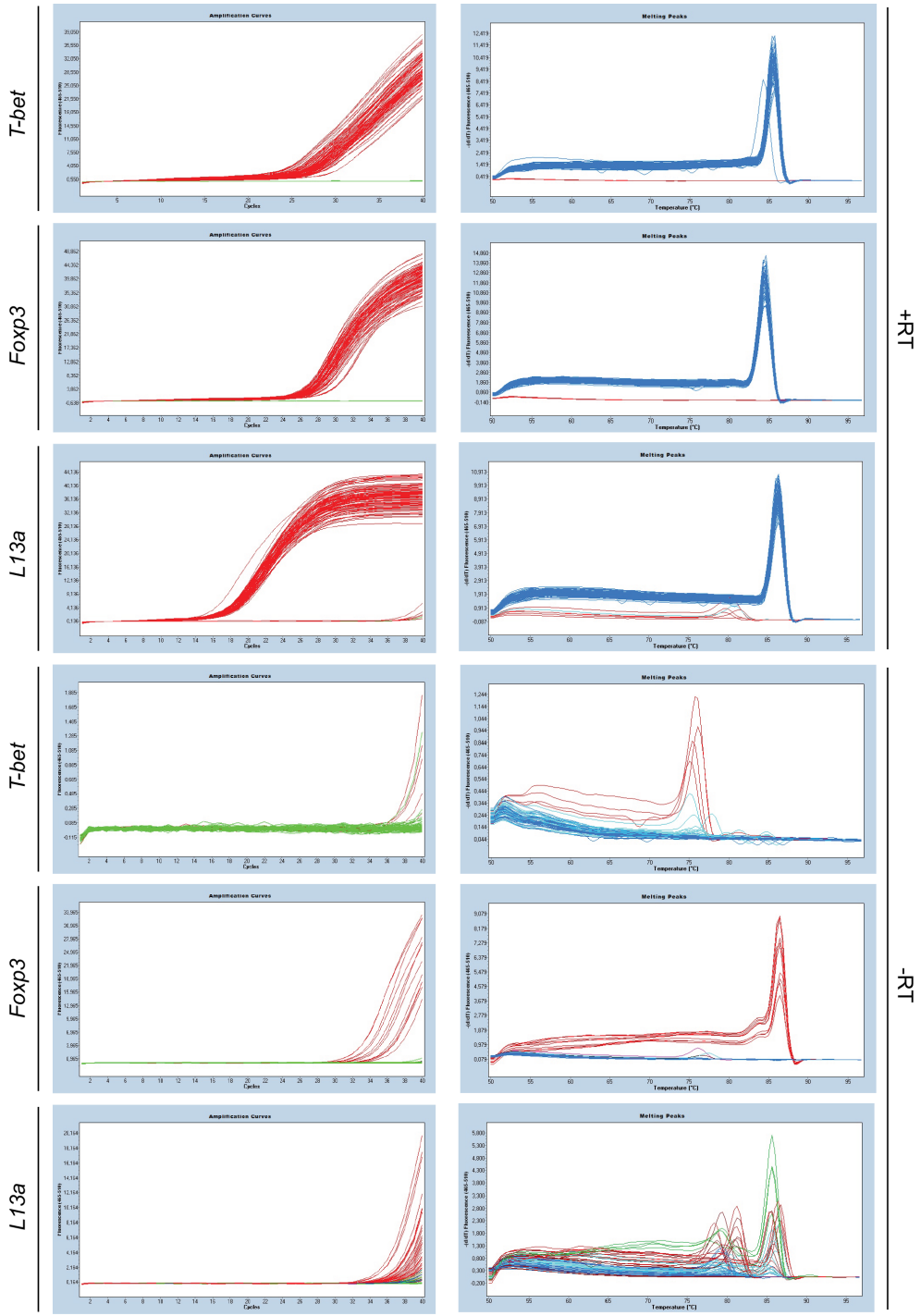

Figure A.14: **Amplification and melting curves in RT-qPCR analysis of *Foxp3* and *T-bet* mRNA levels.** MC38cea cells were implanted subcutaneously into C57BL/6J mice. When tumors reached an average volume of 120 mm^3 (**a**) or 100 mm^3 (**b**) mice received intratumoral (i.t.) treatment with MeVac encoding murine IL-12 fusion proteim, antibody against murine PD-L1 or antibody constant region IgG1-Fc. Mice in the mock group received i.t. injections with a respective amount of OptiMEM. Reverse transcription quantitative PCR (RT-qPCR) analysis for *Foxp3*, *T-bet* or *L13a* as a reference gene was carried out using RNA from tumors explanted one or four days after the last treatment. Amplification curves (left panels) and melting curves (right panels) for individual samples ar shown. +RT — cDNA samples; −RT — minus reverse transcriptase controls.

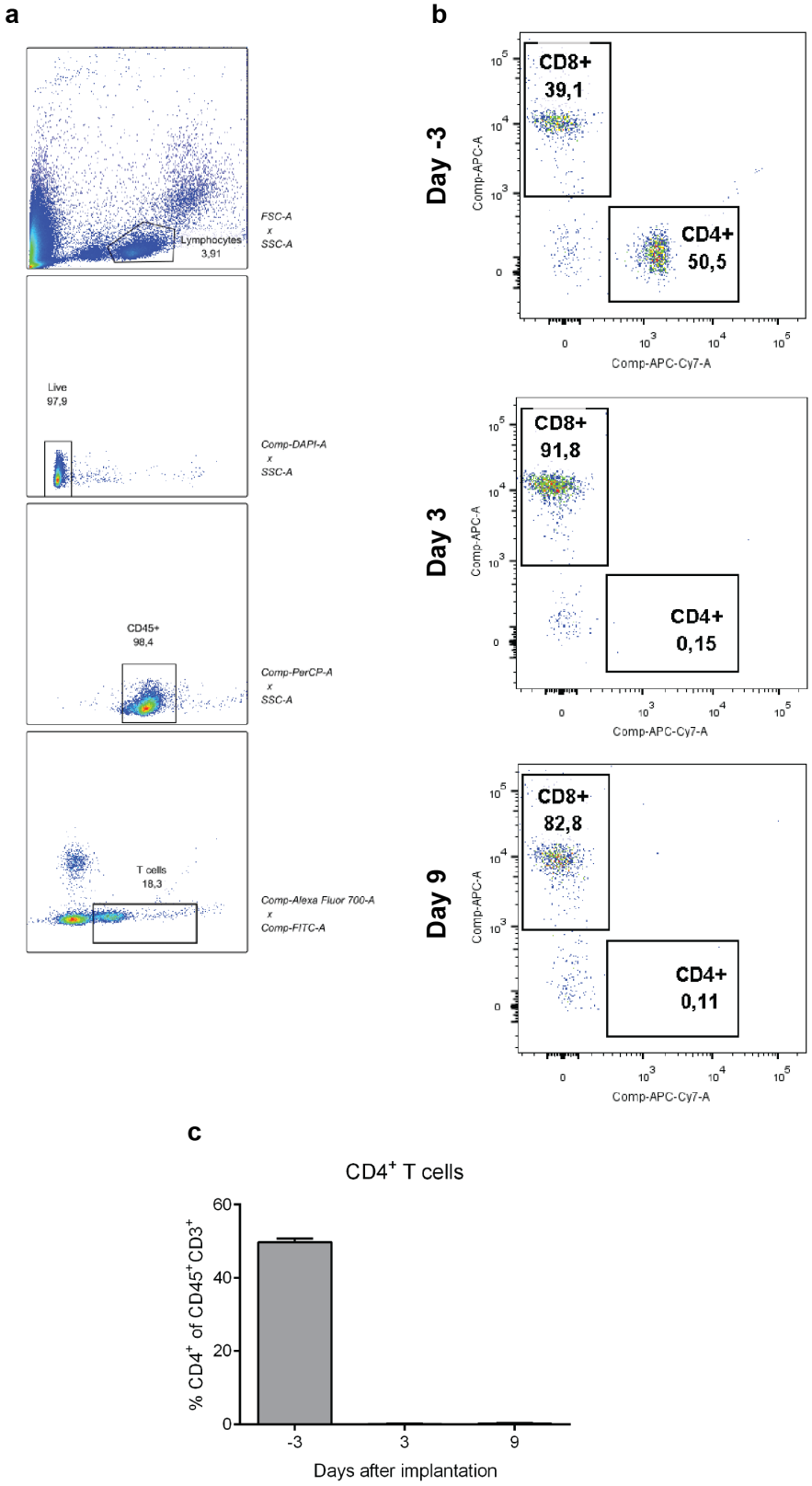

Figure A.15: **Depletion efficiency of CD4$^+$ T cells.** Flow cytometry analysis of peripheral blood was carried out to assess the depletion efficiency of CD4$^+$ T cells in selected mice. **a** — example of ancestry gating for the plots in **b**. **b** — frequencies of the CD8$^+$ and CD4$^+$ T cell populations for one selected animal on different time points prior to (day -3) and after (day 3 and 9) subcutaneous implantation of MC38cea tumor cells. **c** — average percentage with standard deviation of CD4$^+$ cells from all T cells from two animals at different time points.

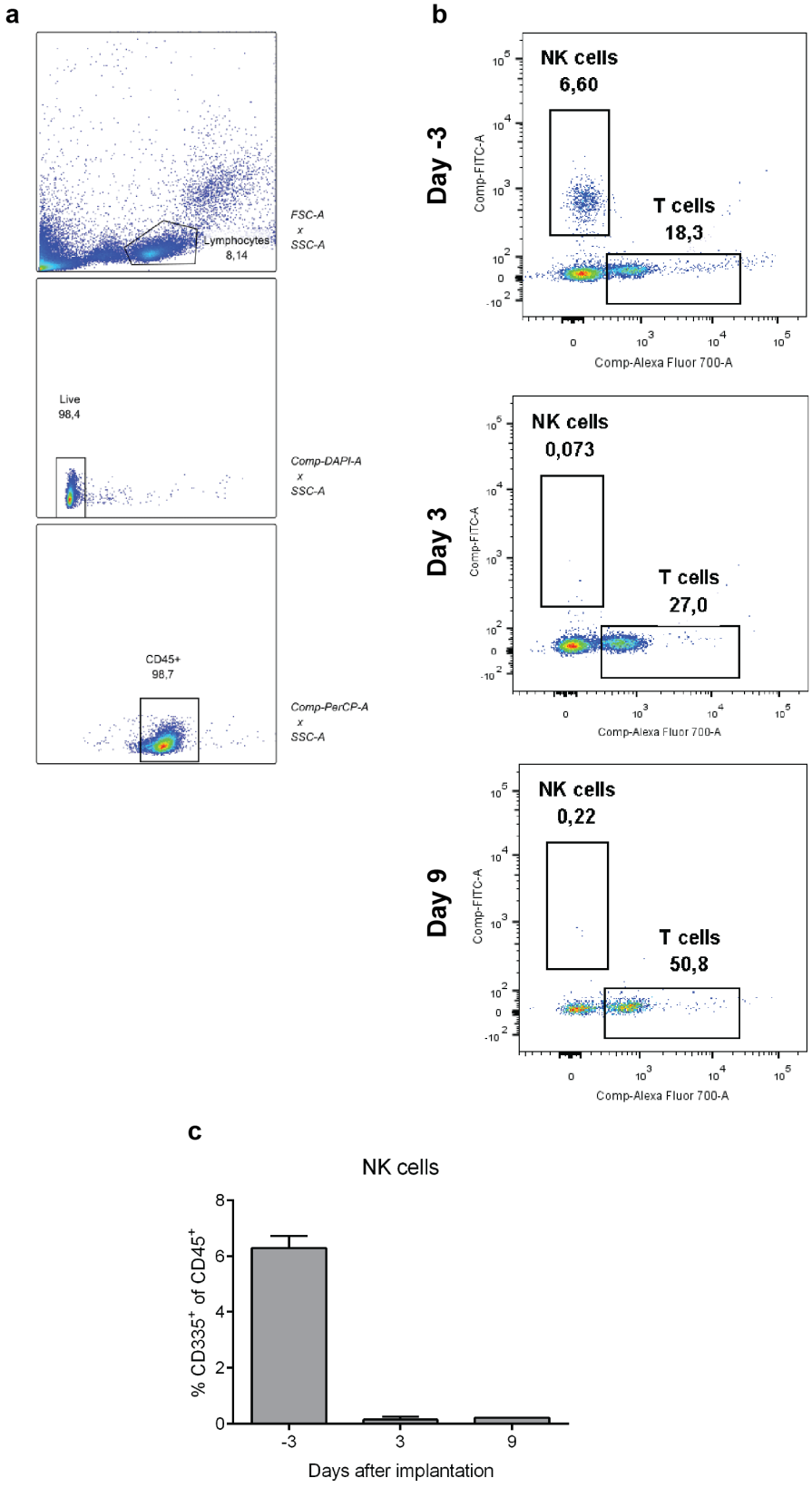

Figure A.16: **Depletion efficiency of NK cells.** Flow cytometry analysis of peripheral blood was carried out to assess the depletion efficiency of NK cells in selected mice. **a** — example of ancestry gating for the plots in **b**. **b** — frequencies of the NK and T cell populations for one selected animal on different time points prior to (day −3) and after (day 3 and 9) subcutaneous implantation of MC38cea tumor cells. **c** — average percentage with standard deviation of NK cells from all T cells from two animals at different time points.

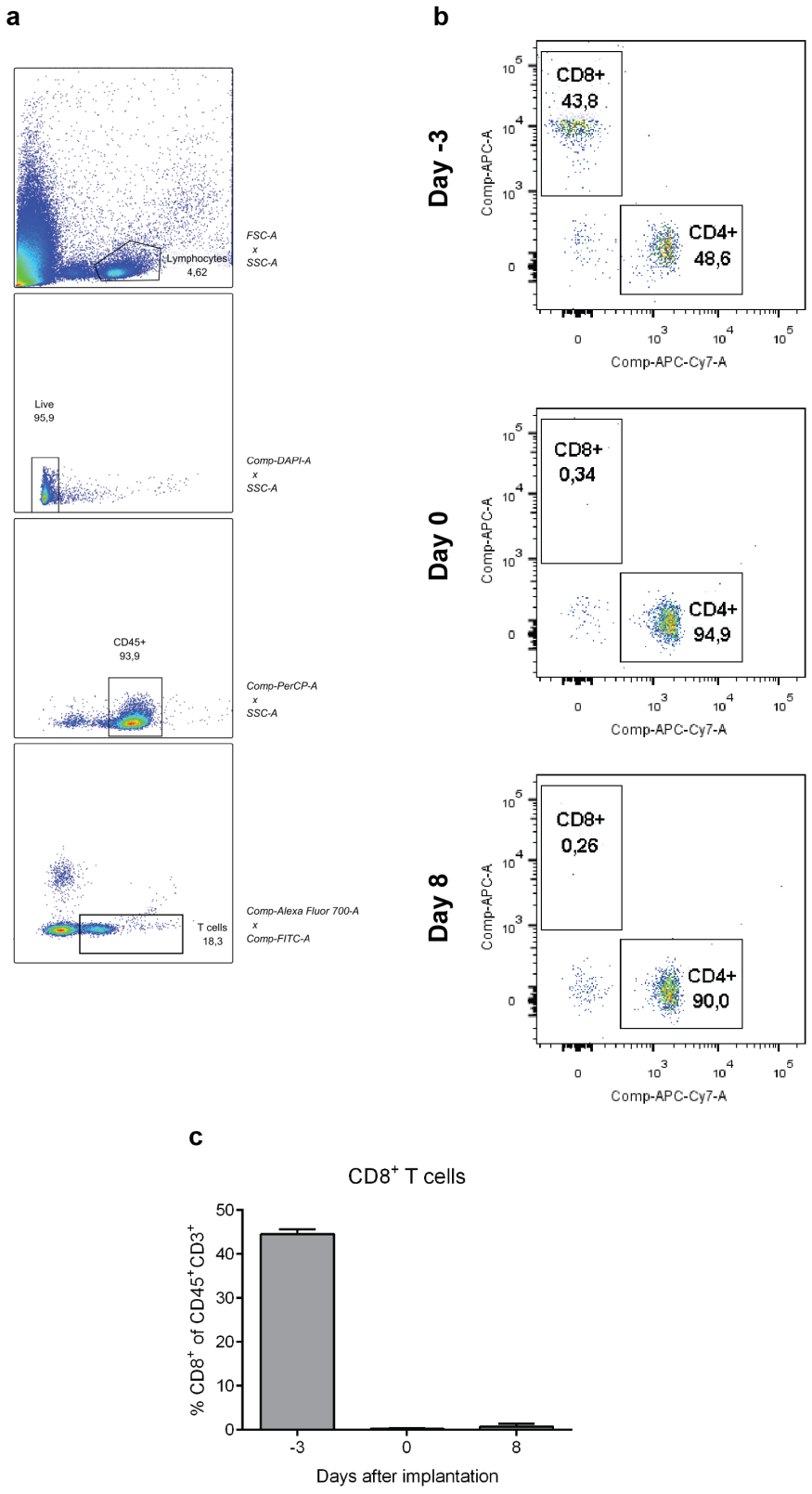

Figure A.17: **Depletion efficiency of CD8$^+$ T cells.** Flow cytometry analysis of peripheral blood was carried out to assess the depletion efficiency of CD8$^+$ T cells in selected mice. **a** — example of ancestry gating for the plots in **b**. **b** — frequencies of the CD8$^+$ and CD4$^+$ T cell populations for one selected animal on different time points prior to and after subcutaneous implantation of MC38cea tumor cells (day 0). **c** — average percentage with standard deviation of CD8$^+$ cells from all T cells from two animals at different time points.

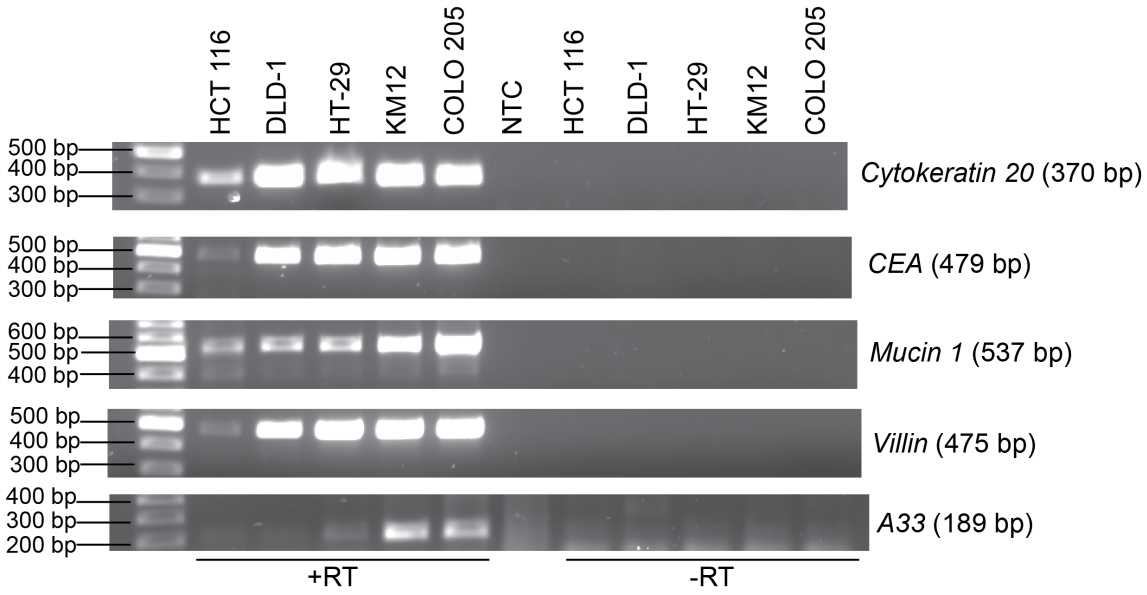

Figure A.18: **Validation of human colon cancer cell lines.** Colon cell specific markers in the respective cell lines were assessed by RT-PCR. +RT — cDNA samples; −RT — minus reverse transcriptase controls; NTC — no template control.

Bibliography

1. K. Murphy, "An introduction to immunobiology and innate immunity," in *Janeway's Immunobiology*, ch. I, pp. 1–125, New York: Garland Science, 8 ed., 2011.
2. D. L. Mueller, "Mechanisms maintaining peripheral tolerance," *Nature Immunology*, vol. 11, no. 1, pp. 21–27, 2010.
3. S. M. Kahan, E. J. Wherry, and A. J. Zajac, "T cell exhaustion during persistent viral infections," *Virology*, vol. 479-480, pp. 180–193, 2015.
4. M. D. Rosenblum, K. A. Remedios, and A. K. Abbas, "Mechanisms of human autoimmunity," *Journal of Clinical Investigation*, vol. 125, no. 6, pp. 2228–2233, 2015.
5. D. Hanahan and R. A. Weinberg, "Hallmarks of cancer: The next generation," *Cell*, vol. 144, no. 5, pp. 646–674, 2011.
6. S. M. Burnet, "Cancer — A biological approach. I. The processes of control," *British Medical Journal*, vol. 1, no. 5022, pp. 779–786, 1957.
7. V. Shankaran, H. Ikeda, A. T. Bruce, J. M. White, P. E. Swanson, L. J. Old, and R. D. Schreiber, "IFNγ and lymphocytes prevent primary tumour development and shape tumour immunogenicity," *Nature*, vol. 410, no. 6832, pp. 1107–1111, 2001.
8. G. P. Dunn, A. T. Bruce, H. Ikeda, L. J. Old, and R. D. Schreiber, "Cancer immunoediting: from immunosurveillance to tumor escape," *Nature Immunology*, vol. 3, no. 11, pp. 991–998, 2002.
9. D. Mittal, M. M. Gubin, R. D. Schreiber, and M. J. Smyth, "New insights into cancer immunoediting and its three component phases–elimination, equilibrium and escape," *Current Opinion in Immunology*, vol. 27, pp. 16–25, 2014.
10. I. Mellman, G. Coukos, and G. Dranoff, "Cancer immunotherapy comes of age," *Nature*, vol. 480, no. 7378, pp. 480–9, 2011.
11. L. M. Weiner, A. S. Belldegrun, J. Crawford, A. W. Tolcher, P. Lockbaum, R. H. Arends, L. Navale, R. G. Amado, G. Schwab, and R. A. Figlin, "Dose and schedule study of panitumumab monotherapy in patients with advanced solid malignancies," *Clinical Cancer Research*, vol. 14, no. 2, pp. 502–508, 2008.
12. P. J. Kaplan-Lefko, J. D. Graves, S. J. Zoog, Y. Pan, J. Wall, D. G. Branstetter, J. Moriguchi, A. Coxon, J. N. Huard, R. Xu, M. L. Peach, G. Juan, S. Kaufman, Q. Chen, A. Bianchi, J. J. Kordich, M. Ma, I. N. Foltz, and B. C. Gliniak, "Conatumumab, a fully human agonist antibody to death receptor 5, induces apoptosis via caspase activation in multiple tumor types," *Cancer Biology and Therapy*, vol. 9, no. 8, pp. 618–631, 2010.
13. S. A. Rosenberg and N. P. Restifo, "Adoptive cell transfer as personalized immunother-

apy for human cancer," *Science*, vol. 348, no. 6230, pp. 62–68, 2015.

14. E. Vacchelli, J. Pol, N. Bloy, A. Eggermont, I. Cremer, W. H. Fridman, J. Galon, A. Marabelle, H. Kohrt, L. Zitvogel, G. Kroemer, and L. Galluzzi, "Trial watch: Tumor-targeting monoclonal antibodies for oncological indications," *OncoImmunology*, vol. 4, no. 1, p. e985940, 2015.
15. L. Galluzzi, E. Vacchelli, J.-M. Bravo-San Pedro, A. Buqué, L. Senovilla, E. E. Baracco, N. Bloy, F. Castoldi, J.-P. Abastado, P. Agostinis, R. N. Apte, F. Aranda, M. Ayyoub, P. Beckhove, J.-Y. Blay, L. Bracci, A. Caignard, C. Castelli, F. Cavallo, E. Celis, V. Cerundolo, A. Clayton, M. P. Colombo, L. Coussens, M. V. Dhodapkar, A. M. Eggermont, D. T. Fearon, W. H. Fridman, J. Fučíková, D. I. Gabrilovich, J. Galon, A. Garg, F. Ghiringhelli, G. Giaccone, E. Gilboa, S. Gnjatic, A. Hoos, A. Hosmalin, D. Jäger, P. Kalinski, K. Kärre, O. Kepp, R. Kiessling, J. M. Kirkwood, E. Klein, A. Knuth, C. E. Lewis, R. Liblau, M. T. Lotze, E. Lugli, J.-P. Mach, F. Mattei, D. Mavilio, I. Melero, C. J. Melief, E. A. Mittendorf, L. Moretta, A. Odunsi, H. Okada, A. K. Palucka, M. E. Peter, K. J. Pienta, A. Porgador, G. C. Prendergast, G. A. Rabinovich, N. P. Restifo, N. Rizvi, C. Sautès-Fridman, H. Schreiber, B. Seliger, H. Shiku, B. Silva-Santos, M. J. Smyth, D. E. Speiser, R. Spisek, P. K. Srivastava, J. E. Talmadge, E. Tartour, S. H. Van Der Burg, B. J. Van Den Eynde, R. Vile, H. Wagner, J. S. Weber, T. L. Whiteside, J. D. Wolchok, L. Zitvogel, W. Zou, and G. Kroemer, "Classification of current anticancer immunotherapies," *Oncotarget*, vol. 5, no. 24, pp. 12472–508, 2014.
16. R. Medzhitov, "Recognition of microorganisms and activation of the immune response," *Nature*, vol. 449, no. 7164, pp. 819–26, 2007.
17. N. Goutagny, Y. Estornes, U. Hasan, S. Lebecque, and C. Caux, "Targeting pattern recognition receptors in cancer immunotherapy," *Targeted Oncology*, vol. 7, no. 1, pp. 29–54, 2012.
18. K. Kawai, J. Miyazaki, A. Joraku, H. Nishiyama, and H. Akaza, "Bacillus Calmette-Guerin (BCG) immunotherapy for bladder cancer: Current understanding and perspectives on engineered BCG vaccine," *Cancer Science*, vol. 104, no. 1, pp. 22–27, 2013.
19. C. Guo, M. Manjili, J. Subjeck, D. Sarkar, P. Fisher, and X. Wang, "Therapeutic Cancer Vaccines: Past, Present and Future," *Advances in Cancer Research*, vol. 119, pp. 421–475, 2013.
20. C. M. Pieczonka, D. Telonis, V. Mouraviev, and D. Albala, "Sipuleucel-T for the Treatment of Patients With Metastatic Castrate-resistant Prostate Cancer: Considerations for Clinical Practice," *Reviews in Urology*, vol. 17, no. 4, pp. 203–10, 2015.
21. S. Jarosławski and M. Toumi, "Sipuleucel-T (Provenge)-Autopsy of an Innovative Paradigm Change in Cancer Treatment: Why a Single-Product Biotech Company Failed to Capitalize on its Breakthrough Invention," *BioDrugs: clinical immunotherapeutic, biopharmaceuticals and gene therapy*, vol. 29, no. 5, pp. 301–307, 2015.

22. C. A. Dinarello, "Historical insights into cytokines," *European Journal of Immunology*, vol. 37, no. SUPPL. 1, pp. 34–45, 2007.
23. S. P. Commins, L. Borish, and J. W. Steinke, "Immunologic messenger molecules: cytokines, interferons, and chemokines," *The Journal of Allergy and Clinical Immunology*, vol. 125, no. 2 Suppl 2, pp. S53–72, 2010.
24. S. Lee and K. Margolin, "Cytokines in Cancer Immunotherapy," *Cancers*, vol. 3, no. 4, pp. 3856–3893, 2011.
25. A. Amin and R. J. White, "High-dose interleukin-2: is it still indicated for melanoma and RCC in an era of targeted therapies?," *Oncology (Williston park, N.Y.)*, vol. 27, no. 7, pp. 680–691, 2013.
26. S. A. Rosenberg, "IL-2: the first effective immunotherapy for human cancer," *The Journal of Immunology*, vol. 192, no. 12, pp. 5451–8, 2014.
27. G. Trinchieri, "Interleukin-12 and the regulation of innate resistance and adaptive immunity," *Nature Reviews. Immunology*, vol. 3, no. 2, pp. 133–146, 2003.
28. T. Kodama, K. Takeda, O. Shimozato, Y. Hayakawa, M. Atsuta, K. Kobayashi, M. Ito, H. Yagita, and K. Okumura, "Perforin-dependent NK cell cytotoxicity is sufficient for anti-metastatic effect of IL-12," *European Journal of Immunology*, vol. 29, no. 4, pp. 1390–1396, 1999.
29. E. E. Voest, B. M. Kenyon, M. S. O'Reilly, G. Truitt, R. J. D'Amato, and J. Folkman, "Inhibition of angiogenesis in vivo by interleukin 12," *Journal of the National Cancer Institute*, vol. 87, no. 8, pp. 581–586, 1995.
30. S. Li, X. Xia, F. M. Mellieon, J. Liu, and S. Steele, "Candidate genes associated with tumor regression mediated by intratumoral IL-12 electroporation gene therapy," *Molecular Therapy*, vol. 9, no. 3, pp. 347–354, 2004.
31. M. B. Atkins, M. J. Robertson, M. Gordon, M. T. Lotze, M. DeCoste, J. S. DuBois, J. Ritz, A. B. Sandler, H. D. Edington, P. D. Garzone, J. W. Mier, C. M. Canning, L. Battiato, H. Tahara, and M. L. Sherman, "Phase I evaluation of intravenous recombinant human interleukin 12 in patients with advanced malignancies," *Clinical Cancer Research*, vol. 3, no. 3, pp. 409–17, 1997.
32. J. Leonard, M. Sherman, G. Fisher, L. Buchanan, G. Larsen, M. Atkins, J. Sosman, J. Dutcher, N. Vogelzang, and J. Ryan, "Effects of single-dose interleukin-12 exposure on interleukin-12-associated toxicity and interferon-gamma production," *Blood*, vol. 90, no. 7, pp. 2541–2548, 1997.
33. E. Bajetta, M. Del Vecchio, R. Mortarini, R. Nadeau, A. Rakhit, L. Rimassa, C. Fowst, A. Borri, A. Anichini, and G. Parmiani, "Pilot study of subcutaneous recombinant human interleukin 12 in metastatic melanoma," *Clinical Cancer Research*, vol. 4, no. 1, pp. 75–85, 1998.
34. R. Lenzi, M. Rosenblum, C. Verschraegen, A. P. Kudelka, J. J. Kavanagh, M. E. Hicks, E. A. Lang, M. A. Nash, L. B. Levy, M. E. Garcia, C. D. Platsoucas, J. L. Abbruzzese,

and R. S. Freedman, "Phase I study of intraperitoneal recombinant human interleukin 12 in patients with Mullerian carcinoma, gastrointestinal primary malignancies, and mesothelioma," *Clinical Cancer Research*, vol. 8, no. 12, pp. 3686–3695, 2002.

35. A. I. Daud, R. C. DeConti, S. Andrews, P. Urbas, A. I. Riker, V. K. Sondak, P. N. Munster, D. M. Sullivan, K. E. Ugen, J. L. Messina, and R. Heller, "Phase I trial of interleukin-12 plasmid electroporation in patients with metastatic melanoma," *Journal of Clinical Oncology*, vol. 26, no. 36, pp. 5896–5903, 2008.
36. G. Linette, H. Omid, E. D. Whitman, J. J. Nemunaitis, J. Chesney, S. S. Agarwala, A. Starodub, J. A. Barrett, A. Marsh, L. A. Martell, A. Cho, T. D. Reed, H. Youssoufian, and A. Vergara-Silva, "A phase I open-label study of Ad-RTS-hIL-12, an adenoviral vector engineered to express hIL-12 under the control of an oral activator ligand, in subjects with unresectable stage III/IV melanoma," in *2013 ASCO Annual Meeting*, 2013.
37. M. Robertson, J. Kline, H. Struemper, K. Koch, J. Bauman, O. Gardner, S. Murray, F. Germaschewski, J. Weisenbach, Z. Jonak, and J. Toso, "A Dose-Escalation Study of Recombinant Human Interleukin-18 in Combination with Rituximab in Patients with Non-Hodgkin's Lymphoma," *Journal of Immunotherapy*, vol. 36, no. 6, pp. 331–341, 2013.
38. G. H. Windbichler, H. Hausmaninger, W. Stummvoll, A. H. Graf, C. Kainz, J. Lahodny, U. Denison, E. Müller-Holzner, and C. Marth, "Interferon-gamma in the first-line therapy of ovarian cancer: a randomized phase III trial," *British Journal of Cancer*, vol. 82, no. 6, pp. 1138–44, 2000.
39. R. Dreicer, W. See, and E. Klein, "Phase II trial of GM-CSF in advanced prostate cancer," *Investigational New Drugs*, vol. 19, no. 3, pp. 261–265, 2001.
40. M. Tominaga, Y. Iwashita, M. Ohta, K. Shibata, T. Ishio, N. Ohmori, T. Goto, S. Sato, and S. Kitano, "Antitumor effects of the MIG and IP-10 genes transferred with poly [D,L-2,4-diaminobutyric acid] on murine neuroblastoma," *Cancer Gene Therapy*, vol. 14, no. 8, pp. 696–705, 2007.
41. M. Ferrantini, I. Capone, and F. Belardelli, "Interferon-α and cancer: Mechanisms of action and new perspectives of clinical use," *Biochimie*, vol. 89, no. 6-7, pp. 884–893, 2007.
42. M. J. Smyth, E. Cretney, M. H. Kershaw, and Y. Hayakawa, "Cytokines in cancer immunity and immunotherapy," *Immunological Reviews*, vol. 202, pp. 275–293, 2004.
43. J. A. Bluestone, H. Bour-Jordan, M. Cheng, and M. Anderson, "Series Editor : Antonio La Cava T cells in the control of organ-specific autoimmunity," *Journal of Clinical Investigation*, vol. 125, no. 6, pp. 2250–2260, 2015.
44. D. M. Pardoll, "The blockade of immune checkpoints in cancer immunotherapy," *Nature Reviews. Cancer*, vol. 12, pp. 252–64, apr 2012.
45. D. S. Vinay, E. P. Ryan, G. Pawelec, W. H. Talib, J. Stagg, E. Elkord, T. Lichtor, W. K.

Decker, R. L. Whelan, H. M. C. S. Kumara, E. Signori, K. Honoki, A. G. Georgakilas, A. Amin, W. G. Helferich, C. S. Boosani, G. Guha, M. R. Ciriolo, S. Chen, S. I. Mohammed, A. S. Azmi, W. N. Keith, A. Bilsland, D. Bhakta, D. Halicka, H. Fujii, K. Aquilano, S. S. Ashraf, S. Nowsheen, X. Yang, B. K. Choi, and B. S. Kwon, "Immune evasion in cancer: Mechanistic basis and therapeutic strategies," *Seminars in Cancer Biology*, vol. 35, pp. S185–S198, 2015.

46. D. L. Mueller, M. K. Jenkins, and R. H. Schwartz, "Clonal expansion versus functional clonal inactivation: a costimulatory signalling pathway determines the outcome of T cell antigen receptor occupancy," *Annual Review of Immunology*, vol. 7, pp. 445–480, 1989.
47. L. Chen and D. B. Flies, "Molecular mechanisms of T cell co-stimulation and co-inhibition," *Nature Reviews. Immunology*, vol. 13, no. April, pp. 227–42, 2013.
48. J. L. Riley and C. H. June, "The CD28 family: A T-cell rheostat for therapeutic control of T-cell activation," *Blood*, vol. 105, no. 1, pp. 13–21, 2005.
49. L. S. K. Walker and D. M. Sansom, "The emerging role of CTLA4 as a cell-extrinsic regulator of T cell responses," *Nature Reviews. Immunology*, vol. 11, no. 12, pp. 852–863, 2011.
50. L. S. K. Walker and D. M. Sansom, "Confusing signals: recent progress in CTLA-4 biology," *Trends in Immunology*, vol. 36, no. 2, pp. 63–70, 2015.
51. P. Waterhouse, J. M. Penninger, E. Timms, A. Wakeham, A. Shahinian, K. P. Lee, C. B. Thompson, H. Griesser, and T. W. Mak, "Lymphoproliferative disorders with early lethality in mice deficient in Ctla-4," *Science*, vol. 270, no. 5238, pp. 985–988, 1995.
52. D. R. Leach, M. F. Krummel, and J. P. Allison, "Enhancement of antitumor immunity by CTLA-4 blockade," *Science*, vol. 271, no. 5256, pp. 1734–1736, 1996.
53. F. S. Hodi, S. J. O'Day, D. F. McDermott, R. W. Weber, J. A. Sosman, J. B. Haanen, R. Gonzalez, C. Robert, D. Schadendorf, J. C. Hassel, W. Akerley, A. J. M. van den Eertwegh, J. Lutzky, P. Lorigan, J. M. Vaubel, G. P. Linette, D. Hogg, C. H. Ottensmeier, C. Lebbé, C. Peschel, I. Quirt, J. I. Clark, J. D. Wolchok, J. S. Weber, J. Tian, M. J. Yellin, G. M. Nichol, A. Hoos, and W. J. Urba, "Improved survival with ipilimumab in patients with metastatic melanoma," *The New England Journal of Medicine*, vol. 363, no. 8, pp. 711–23, 2010.
54. Y. Agata, A. Kawasaki, H. Nishimura, Y. Ishida, T. Tsubata, H. Yagita, and T. Honjo, "Expression of the PD-1 antigen on the surface of stimulated mouse T and B lymphocytes," *International Immunology*, vol. 8, no. 5, pp. 765–772, 1996.
55. Y. Jiang, Y. Li, and B. Zhu, "T-cell exhaustion in the tumor microenvironment," *Cell Death & Disease*, vol. 6, p. e1792, 2015.
56. G. J. Freeman, A. J. Long, Y. Iwai, K. Bourque, T. Chernova, H. Nishimura, L. J. Fitz, N. Malenkovich, T. Okazaki, M. C. Byrne, H. F. Horton, L. Fouser, L. Carter, V. Ling,

M. R. Bowman, B. M. Carreno, M. Collins, C. R. Wood, and T. Honjo, "Engagement of the PD-1 immunoinhibitory receptor by a novel B7 family member leads to negative regulation of lymphocyte activation," *The Journal of Experimental Medicine*, vol. 192, no. 7, pp. 1027–34, 2000.

57. Y. Latchman, C. R. Wood, T. Chernova, D. Chaudhary, M. Borde, I. Chernova, Y. Iwai, A. J. Long, J. A. Brown, R. Nunes, E. A. Greenfield, K. Bourque, V. A. Boussiotis, L. L. Carter, B. M. Carreno, N. Malenkovich, H. Nishimura, T. Okazaki, T. Honjo, A. H. Sharpe, and G. J. Freeman, "PD-L2 is a second ligand for PD-1 and inhibits T cell activation," *Nature Immunology*, vol. 2, no. 3, pp. 261–268, 2001.
58. M. Terme, E. Ullrich, L. Aymeric, K. Meinhardt, M. Desbois, N. Delahaye, S. Viaud, B. Ryffel, H. Yagita, G. Kaplanski, A. Prévost-Blondel, M. Kato, J. L. Schultze, E. Tartour, G. Kroemer, N. Chaput, and L. Zitvogel, "IL-18 induces PD-1-dependent immunosuppression in cancer," *Cancer Research*, vol. 71, no. 16, pp. 5393–5399, 2011.
59. M. J. Butte, M. E. Keir, T. B. Phamduy, A. H. Sharpe, G. J. Freeman, and H. Sharpe, "PD-L1 interacts specifically with B7-1 to inhibit T cell proliferation," *Immunity*, vol. 27, no. 1, pp. 111–122, 2007.
60. H. Dong, S. E. Strome, D. R. Salomao, H. Tamura, F. Hirano, D. B. Flies, P. C. Roche, J. Lu, G. Zhu, K. Tamada, V. A. Lennon, E. Celis, and L. Chen, "Tumor-associated B7-H1 promotes T-cell apoptosis: a potential mechanism of immune evasion," *Nature Medicine*, vol. 8, no. 8, pp. 793–800, 2002.
61. J. M. Taube, R. a. Anders, G. D. Young, H. Xu, R. Sharma, T. L. McMiller, S. Chen, A. P. Klein, D. M. Pardoll, S. L. Topalian, and L. Chen, "Colocalization of inflammatory response with B7-h1 expression in human melanocytic lesions supports an adaptive resistance mechanism of immune escape," *Science Translational Medicine*, vol. 4, no. 127, p. 127ra37, 2012.
62. A. Rosenwald, G. Wright, K. Leroy, X. Yu, P. Gaulard, R. D. Gascoyne, W. C. Chan, T. Zhao, C. Haioun, T. C. Greiner, D. D. Weisenburger, J. C. Lynch, J. Vose, J. O. Armitage, E. B. Smeland, S. Kvaloy, H. Holte, J. Delabie, E. Campo, E. Montserrat, A. Lopez-Guillermo, G. Ott, H. K. Muller-Hermelink, J. M. Connors, R. Braziel, T. M. Grogan, R. I. Fisher, T. P. Miller, M. LeBlanc, M. Chiorazzi, H. Zhao, L. Yang, J. Powell, W. H. Wilson, E. S. Jaffe, R. Simon, R. D. Klausner, and L. M. Staudt, "Molecular diagnosis of primary mediastinal B cell lymphoma identifies a clinically favorable subgroup of diffuse large B cell lymphoma related to Hodgkin lymphoma," *The Journal of Experimental Medicine*, vol. 198, no. 6, pp. 851–62, 2003.
63. K. Abiko, N. Matsumura, J. Hamanishi, N. Horikawa, R. Murakami, K. Yamaguchi, Y. Yoshioka, T. Baba, I. Konishi, and M. Mandai, "IFN-γ from lymphocytes induces PD-L1 expression and promotes progression of ovarian cancer," *British Journal of Cancer*, vol. 112, no. 9, pp. 1501–1509, 2015.
64. R. Bellucci, A. Martin, D. Bommarito, K. Wang, S. H. Hansen, G. J. Freeman, and

J. Ritz, "Interferon-γ-induced activation of JAK1 and JAK2 suppresses tumor cell susceptibility to NK cells through upregulation of PD-L1 expression," *OncoImmunology*, vol. 4, no. 6, p. e1008824, 2015.

65. A. T. Parsa, J. S. Waldron, A. Panner, C. A. Crane, I. F. Parney, J. J. Barry, K. E. Cachola, J. C. Murray, T. Tihan, M. C. Jensen, P. S. Mischel, D. Stokoe, and R. O. Pieper, "Loss of tumor suppressor PTEN function increases B7-H1 expression and immunoresistance in glioma," *Nature Medicine*, vol. 13, no. 1, pp. 84–8, 2007.
66. E. A. Akbay, S. Koyama, J. Carretero, A. Altabef, H. Jeremy, C. L. Christensen, O. R. Mikse, A. D. Cherniack, M. Ellen, T. J. Pugh, M. D. Wilkerson, P. E. Fecci, M. Butaney, J. B. Reibel, M. Soucheray, T. J. Cohoon, P. A. Janne, D. N. Hayes, G. I. Shapiro, T. Shimamura, and M. Lynette, "Activation of the PD-1 pathway contributes to immune escape in EGFR-driven lung tumors," *Cancer Discovery*, vol. 3, no. 12, pp. 1355–1363, 2014.
67. J. Hamanishi, M. Mandai, M. Iwasaki, T. Okazaki, Y. Tanaka, K. Yamaguchi, T. Higuchi, H. Yagi, K. Takakura, N. Minato, T. Honjo, and S. Fujii, "Programmed cell death 1 ligand 1 and tumor-infiltrating CD8+ T lymphocytes are prognostic factors of human ovarian cancer," *Proceedings of the National Academy of Sciences of the United States of America*, vol. 104, no. 9, pp. 3360–5, 2007.
68. R. Hino, K. Kabashima, Y. Kato, H. Yagi, M. Nakamura, T. Honjo, T. Okazaki, and Y. Tokura, "Tumor cell expression of programmed cell death-1 ligand 1 is a prognostic factor for malignant melanoma," *Cancer*, vol. 116, no. 7, pp. 1757–1766, 2010.
69. J. Kiyasu, H. Miyoshi, A. Hirata, F. Arakawa, A. Ichikawa, D. Niino, Y. Sugita, Y. Yufu, I. Choi, Y. Abe, N. Uike, K. Nagafuji, T. Okamura, K. Akashi, R. Takayanagi, M. Shiratsuchi, and K. Ohshima, "Expression of programmed cell death ligand 1 is associated with poor overall survival in patients with diffuse large B-cell lymphoma," *Blood*, vol. 126, no. 19, pp. 2193–2202, 2015.
70. C. Robert, A. Ribas, J. D. Wolchok, F. S. Hodi, O. Hamid, R. Kefford, J. S. Weber, A. M. Joshua, W. J. Hwu, T. C. Gangadhar, A. Patnaik, R. Dronca, H. Zarour, R. W. Joseph, P. Boasberg, B. Chmielowski, C. Mateus, M. A. Postow, K. Gergich, J. Elassaiss-Schaap, X. N. Li, R. Iannone, S. W. Ebbinghaus, S. P. Kang, and A. Daud, "Anti-programmed-death-receptor-1 treatment with pembrolizumab in ipilimumab-refractory advanced melanoma: A randomised dose-comparison cohort of a phase 1 trial," *The Lancet*, vol. 384, no. 9948, pp. 1109–1117, 2014.
71. "U.S. Food and Drug Administration. Hematology/Oncology (Cancer) Approvals & Safety Notifications." `http://www.fda.gov/Drugs/InformationOnDrugs/ApprovedDrugs/ucm279174.htm`, last accessed: 09.02.2017.
72. C. Robert, J. Schachter, G. V. Long, A. Arance, J. J. Grob, L. Mortier, A. Daud, M. S. Carlino, C. McNeil, M. Lotem, J. Larkin, P. Lorigan, B. Neyns, C. U. Blank, O. Hamid, C. Mateus, R. Shapira-Frommer, M. Kosh, H. Zhou, N. Ibrahim, S. Ebbinghaus, and

A. Ribas, "Pembrolizumab versus Ipilimumab in Advanced Melanoma," *New England Journal of Medicine*, vol. 372, no. 26, pp. 2521–2532, 2015.

73. S. L. Topalian, J. M. Taube, R. A. Anders, and D. M. Pardoll, "Mechanism-driven biomarkers to guide immune checkpoint blockade in cancer therapy," *Nature Reviews. Cancer*, vol. 16, no. 5, pp. 275–87, 2016.
74. M. Swart, I. Verbrugge, and J. B. Beltman, "Combination Approaches with Immune-Checkpoint Blockade in Cancer Therapy," *Frontiers in Oncology*, vol. 6, p. 233, 2016.
75. J. Bell and G. McFadden, "Viruses for tumor therapy," *Cell Host and Microbe*, vol. 15, no. 3, pp. 260–265, 2014.
76. J. G. Pol, J. Rességuier, and B. D. Lichty, "Oncolytic viruses: A step into cancer immunotherapy," *Virus Adaptation and Treatment*, vol. 4, no. 1, pp. 1–21, 2011.
77. G. Dock, "The Influence of Complicating Diseases Upon Leukæmia," *The American Journal of the Medical Sciences*, vol. 127, no. 4, pp. 563–592, 1904.
78. H. R. Bierman, D. M. Crile, K. S. Dod, K. H. Kelly, N. I. Petrakis, L. P. White, and M. B. Shimkin, "Remissions in leukemia of childhood following acute infectious disease. Staphylococcus and streptococcus, varicella, and feline panleukopenias," *Cancer*, vol. 6, no. 3, pp. 591–605, 1953.
79. R. Alemany, C. Balagué, and D. Curiel, "Replicative adenoviruses for cancer therapy," *Nature Biotechnology*, vol. 18, no. 7, pp. 723–727, 2000.
80. S. Varghese and S. D. Rabkin, "Oncolytic herpes simplex virus vectors for cancer virotherapy," *Cancer Gene Therapy*, vol. 9, no. 12, pp. 967–978, 2002.
81. J. P. F. Nüesch, J. Lacroix, A. Marchini, and J. Rommelaere, "Molecular pathways: Rodent parvoviruses - Mechanisms of oncolysis and prospects for clinical cancer treatment," *Clinical Cancer Research*, vol. 18, no. 13, pp. 3516–3523, 2012.
82. J. Gong, E. Sachdev, A. C. Mita, and M. M. Mita, "Clinical development of reovirus for cancer therapy: An oncolytic virus with immune-mediated antitumor activity," *World Journal of Methodology*, vol. 6, no. 1, p. 25, 2016.
83. S. J. Russell and K. W. Peng, "Measles virus for cancer therapy," *Current Topics in Microbiology and Immunology*, vol. 330, pp. 213–41, 2009.
84. D. Zamarin and P. Palese, "Oncolytic Newcastle Disease Virus for cancer therapy: old challenges and new directions," *Future Microbiology*, vol. 7, no. 3, pp. 347–367, 2012.
85. D. H. Kirn and S. H. Thorne, "Targeted and armed oncolytic poxviruses: a novel multi-mechanistic therapeutic class for cancer," *Nature Reviews. Cancer*, vol. 9, no. 1, pp. 64–71, 2009.
86. E. Hastie and V. Z. Grdzelishvili, "Vesicular stomatitis virus as a flexible platform for oncolytic virotherapy against cancer," *Journal of General Virology*, vol. 93, no. PART 12, pp. 2529–2545, 2012.
87. M. G. Katze, Y. He, and M. Gale Jr., "Viruses and interferon: a fight for supremacy,"

Nature Reviews. Immunology, vol. 2, no. 9, pp. 675–687, 2002.

88. S. Naik and S. J. Russell, "Engineering oncolytic viruses to exploit tumor specific defects in innate immune signaling pathways," *Expert Opinion on Biological Therapy*, vol. 9, no. 9, pp. 1163–1176, 2009.
89. Y. Saito, M. Sunamura, F. Motoi, H. Abe, S. Egawa, D. G. Duda, T. Hoshida, S. Fukuyama, H. Hamada, and S. Matsuno, "Oncolytic replication-competent adenovirus suppresses tumor angiogenesis through preserved E1A region," *Cancer Gene Therapy*, vol. 13, no. 3, pp. 242–52, 2006.
90. C. J. Breitbach, J. M. Paterson, C. G. Lemay, T. J. Falls, A. McGuire, K. A. Parato, D. F. Stojdl, M. Daneshmand, K. Speth, D. Kirn, J. A. McCart, H. Atkins, and J. C. Bell, "Targeted Inflammation During Oncolytic Virus Therapy Severely Compromises Tumor Blood Flow," *Molecular Therapy*, vol. 15, no. 9, pp. 1686–1693, 2007.
91. T.-C. Liu, T. Hwang, B.-H. Park, J. C. Bell, and D. H. Kirn, "The targeted oncolytic poxvirus JX-594 demonstrates antitumoral, antivascular, and anti-HBV activities in patients with hepatocellular carcinoma," *Molecular Therapy*, vol. 16, no. 9, pp. 1637–42, 2008.
92. R. J. Prestwich, E. J. Ilett, F. Errington, R. M. Diaz, L. P. Steele, T. Kottke, J. Thompson, F. Galivo, K. J. Harrington, H. S. Pandha, P. J. Selby, R. G. Vile, and A. a. Melcher, "Immune-mediated antitumor activity of reovirus is required for therapy and is independent of direct viral oncolysis and replication," *Clinical Cancer Research*, vol. 15, no. 18, pp. 4374–4381, 2009.
93. B. D. Lichty, C. J. Breitbach, D. F. Stojdl, and J. C. Bell, "Going viral with cancer immunotherapy," *Nature Reviews. Cancer*, vol. 14, no. 8, pp. 559–567, 2014.
94. T. F. Gajewski, H. Schreiber, and Y.-X. Fu, "Innate and adaptive immune cells in the tumor microenvironment," *Nature Immunology*, vol. 14, no. 10, pp. 1014–1022, 2013.
95. O. Takeuchi and S. Akira, "Innate immunity to virus infection," *Immunological Reviews*, vol. 227, no. 1600-065X (Electronic), pp. 75–86, 2009.
96. S. A. Gujar, P. Marcato, D. Pan, and P. W. K. Lee, "Reovirus Virotherapy Overrides Tumor Antigen Presentation Evasion and Promotes Protective Antitumor Immunity," *Molecular Cancer Therapeutics*, vol. 9, no. 11, pp. 2924–2933, 2010.
97. M. Toda, S. D. Rabkin, H. Kojima, and R. L. Martuza, "Herpes simplex virus as an in situ cancer vaccine for the induction of specific anti-tumor immunity," *Human Gene Therapy*, vol. 10, no. 3, pp. 385–393, 1999.
98. Y. Endo, R. Sakai, M. Ouchi, H. Onimatsu, M. Hioki, S. Kagawa, F. Uno, Y. Watanabe, Y. Urata, N. Tanaka, and T. Fujiwara, "Virus-mediated oncolysis induces danger signal and stimulates cytotoxic T-lymphocyte activity via proteasome activator upregulation," *Oncogene*, vol. 27, no. 17, pp. 2375–2381, 2008.
99. C. L. White, K. R. Twigger, L. Vidal, J. S. De Bono, M. Coffey, L. Heinemann, R. Morgan, A. Merrick, F. Errington, R. G. Vile, A. A. Melcher, H. S. Pandha, and K. J. Har-

rington, "Characterization of the adaptive and innate immune response to intravenous oncolytic reovirus (Dearing type 3) during a phase I clinical trial," *Gene Therapy*, vol. 15, no. 12, pp. 911–20, 2008.

100. R. H. I. Andtbacka, H. L. Kaufman, F. Collichio, T. Amatruda, N. Senzer, J. Chesney, K. A. Delman, L. E. Spitler, I. Puzanov, S. S. Agarwala, M. Milhem, L. Cranmer, B. Curti, K. Lewis, M. Ross, T. Guthrie, G. P. Linette, G. A. Daniels, K. Harrington, M. R. Middleton, W. H. Miller, J. S. Zager, Y. Ye, B. Yao, A. Li, S. Doleman, A. Van Der Walde, J. Gansert, and R. S. Coffin, "Talimogene laherparepvec improves durable response rate in patients with advanced melanoma," *Journal of Clinical Oncology*, vol. 33, no. 25, pp. 2780–2788, 2015.
101. B. G. Derubertis, B. M. Stiles, A. Bhargava, N. J. Gusani, M. Hezel, M. D'Angelica, and Y. Fong, "Cytokine-secreting herpes viral mutants effectively treat tumor in a murine metastatic colorectal liver model by oncolytic and T-cell-dependent mechanisms," *Cancer Gene Therapy*, vol. 14, no. 6, pp. 590–7, 2007.
102. N. Lapteva, M. Aldrich, D. Weksberg, L. Rollins, T. Goltsova, S.-Y. Chen, and X. F. Huang, "Targeting the intratumoral dendritic cells by the oncolytic adenoviral vaccine expressing RANTES elicits potent antitumor immunity," *Journal of Immunotherapy*, vol. 32, no. 2, pp. 145–56, 2009.
103. D. Zamarin, R. B. Holmgaard, S. K. Subudhi, J. S. Park, M. Mansour, P. Palese, T. Merghoub, J. D. Wolchok, and J. P. Allison, "Localized Oncolytic Virotherapy Overcomes Systemic Tumor Resistance to Immune Checkpoint Blockade Immunotherapy," *Science Translational Medicine*, vol. 6, no. 226, pp. 226ra32–226ra32, 2014.
104. C. E. Engeland, C. Grossardt, R. Veinalde, S. Bossow, D. Lutz, J. K. Kaufmann, I. Shevchenko, V. Umansky, D. M. Nettelbeck, W. Weichert, D. Jäger, C. von Kalle, and G. Ungerechts, "CTLA-4 and PD-L1 Checkpoint Blockade Enhances Oncolytic Measles Virus Therapy," *Molecular Therapy*, vol. 22, no. 11, pp. 1949–1959, 2014.
105. F. Yu, X. Wang, Z. S. Guo, D. L. Bartlett, S. M. Gottschalk, and X.-T. Song, "T-cell engager-armed oncolytic vaccinia virus significantly enhances antitumor therapy.," *Molecular Therapy*, vol. 22, no. 1, pp. 102–11, 2014.
106. Y. S. Lee, J. H. Kim, K. J. Choi, I. K. Choi, H. Kim, S. Cho, B. C. Cho, and C. O. Yun, "Enhanced antitumor effect of oncolytic adenovirus expressing interleukin-12 and B7-1 in an immunocompetent murine model," *Clinical Cancer Research*, vol. 12, no. 19, pp. 5859–5868, 2006.
107. X. Fu, A. Rivera, L. Tao, and X. Zhang, "An HSV-2 based oncolytic virus can function as an attractant to guide migration of adoptively transferred T cells to tumor sites," *Oncotarget*, vol. 6, no. 2, pp. 902–914, 2015.
108. N. Nishio, I. Diaconu, H. Liu, V. Cerullo, I. Caruana, V. Hoyos, L. Bouchier-Hayes, B. Savoldo, and G. Dotti, "Armed Oncolytic Virus Enhances Immune Functions of Chimeric Antigen Receptor-Modified T Cells in Solid Tumors," *Cancer Research*,

vol. 74, no. 18, pp. 5195–5205, 2014.

109. J. G. Pol, L. Zhang, B. W. Bridle, K. B. Stephenson, J. Rességuier, S. Hanson, L. Chen, N. Kazdhan, J. L. Bramson, D. F. Stojdl, Y. Wan, and B. D. Lichty, "Maraba virus as a potent oncolytic vaccine vector," *Molecular Therapy*, vol. 22, no. 2, pp. 420–9, 2014.
110. J. M. Michot, C. Bigenwald, S. Champiat, M. Collins, F. Carbonnel, S. Postel-Vinay, A. Berdelou, A. Varga, R. Bahleda, A. Hollebecque, C. Massard, A. Fuerea, V. Ribrag, A. Gazzah, J. P. Armand, N. Amellal, E. Angevin, N. Noel, C. Boutros, C. Mateus, C. Robert, J. C. Soria, A. Marabelle, and O. Lambotte, "Immune-related adverse events with immune checkpoint blockade: A comprehensive review," *European Journal of Cancer*, vol. 54, pp. 139–148, 2016.
111. L. V. D. Laar, P. J. Coffer, and A. M. Woltman, "Review article Regulation of dendritic cell development by GM-CSF : molecular control and implications for immune homeostasis and therapy," *Development*, vol. 119, no. 15, pp. 3383–3393, 2012.
112. M. Robinson, B. Li, Y. Ge, D. Ko, S. Yendluri, T. Harding, M. VanRoey, K. R. Spindler, and K. Jooss, "Novel Immunocompetent Murine Tumor Model for Evaluation of Conditionally Replication-Competent (Oncolytic) Murine Adenoviral Vectors," *Journal of Virology*, vol. 83, no. 8, pp. 3450–3462, 2009.
113. R. J. Wong, S. G. Patel, S. Kim, R. P. DeMatteo, S. Malhotra, J. J. Bennett, M. St-Louis, J. P. Shah, P. a. Johnson, and Y. Fong, "Cytokine gene transfer enhances herpes oncolytic therapy in murine squamous cell carcinoma," *Human Gene Therapy*, vol. 12, no. 3, pp. 253–65, 2001.
114. C. Grossardt, C. E. Engeland, S. Bossow, N. Halama, K. Zaoui, M. F. Leber, C. Springfeld, D. Jaeger, C. von Kalle, and G. Ungerechts, "Granulocyte-Macrophage Colony-Stimulating Factor-Armed Oncolytic Measles Virus Is an Effective Therapeutic Cancer Vaccine," *Human Gene Therapy*, vol. 24, no. 7, pp. 644–654, 2013.
115. A. Vigil, M. S. Park, O. Martinez, M. A. Chua, S. Xiao, J. F. Cros, L. Martínez-Sobrido, S. L. C. Woo, and A. García-Sastre, "Use of reverse genetics to enhance the oncolytic properties of newcastle disease virus," *Cancer Research*, vol. 67, no. 17, pp. 8285–8292, 2007.
116. S. K. Chatterjee, H. Qin, S. Manna, and P. K. Tripathi, "Recombinant Vaccinia Virus Expressing Cytokine GM-CSF as Tumor Vaccine," *Anticancer Research*, vol. 19, pp. 2869–2874, 1999.
117. E. Ramsburg, J. Publicover, L. Buonocore, A. Poholek, M. Robek, A. Palin, and J. K. Rose, "A vesicular stomatitis virus recombinant expressing granulocyte-macrophage colony-stimulating factor induces enhanced T-cell responses and is highly attenuated for replication in animals," *Journal of Virology*, vol. 79, no. 24, p. 15043, 2005.
118. J. Carew, "A Novel Approach to Cancer Therapy Using an Oncolytic Herpes Virus to Package Amplicons Containing Cytokine Genes," *Molecular Therapy*, vol. 4, no. 3, pp. 250–256, 2001.

119. D. Post, E. Sandberg, M. Kyle, N. Devi, B. DJ, Z. Xu, M. Tighiouart, and E. Van Meir, "Targeted Cancer Gene Therapy Using a Hypoxia Inducible Factor– Dependent Oncolytic Adenovirus Armed with Interleukin-4," *Cancer Research*, vol. 67, no. 14, pp. 6872–6881, 2007.

120. K. Terada, H. Wakimoto, E. Tyminski, E. a. Chiocca, and Y. Saeki, "Development of a rapid method to generate multiple oncolytic HSV vectors and their in vivo evaluation using syngeneic mouse tumor models," *Gene Therapy*, vol. 13, no. 8, pp. 705–14, 2006.

121. Y.-S. Lee, J.-H. Kim, K.-J. Choi, I.-K. Choi, H. Kim, S. Cho, B. C. Cho, and C.-O. Yun, "Enhanced Antitumor Effect of Oncolytic Adenovirus Expressing Interleukin-12 and B7-1 in an Immunocompetent Murine Model," *Clinical Cancer Research*, vol. 12, no. 19, pp. 5859–5868, 2006.

122. Y. Ino, Y. Saeki, H. Fukuhara, and T. Todo, "Triple combination of oncolytic herpes simplex virus-1 vectors armed with interleukin-12, interleukin-18, or soluble B7-1 results in enhanced antitumor efficacy," *Clinical Cancer Research*, vol. 12, no. 2, pp. 643–52, 2006.

123. E. J. Shin, G. B. Wanna, B. Choi, D. Aguila, O. Ebert, E. M. Genden, and S. L. Woo, "Interleukin-12 expression enhances vesicular stomatitis virus oncolytic therapy in murine squamous cell carcinoma," *The Laryngoscope*, vol. 117, no. 2, pp. 210–4, 2007.

124. D. C. Gaston, C. I. Odom, L. Li, J. M. Markert, J. C. Roth, K. A. Cassady, R. J. Whitley, and J. N. Parker, "Production of bioactive soluble interleukin-15 in complex with interleukin-15 receptor alpha from a conditionally-replicating oncolytic HSV-1," *PLoS ONE*, vol. 8, no. 11, pp. 1–13, 2013.

125. M. van Rikxoort, M. Michaelis, M. Wolschek, T. Muster, A. Egorov, J. Seipelt, H. W. Doerr, and J. Cinatl, "Oncolytic effects of a novel influenza a virus expressing interleukin-15 from the NS reading frame," *PLoS ONE*, vol. 7, no. 5, 2012.

126. K. Stephenson, N. Barra, E. Davies, A. Ashkar, and B. Lichty, "Expressing human interleukin-15 from oncolytic vesicular stomatitis virus improves survival in a murine metastatic colon adenocarcinoma model through the enhancement of anti-tumor immunity," *Cancer Gene Therapy*, vol. 19, no. 4, pp. 238–246, 2012.

127. I.-k. Choi, J.-s. Lee, S.-n. Zhang, J. Park, K.-m. Lee, C. H. Sonn, and C.-o. Yun, "Oncolytic adenovirus co-expressing IL-12 and IL-18 improves tumor-specific immunity via differentiation of T cells expressing IL-12Rb2 or IL-18Ra," *Gene Therapy*, vol. 18, no. 9, pp. 898–909, 2011.

128. C. Su, L. Peng, J. Sham, X. Wang, Q. Zhang, D. Chua, C. Liu, Z. Cui, H. Xue, H. Wu, Q. Yang, B. Zhang, X. Liu, M. Wu, and Q. Qian, "Immune gene-viral therapy with triplex efficacy mediated by oncolytic adenovirus carrying an interferon-gamma gene yields efficient antitumor activity in immunodeficient and immunocompetent mice," *Molecular Therapy*, vol. 13, no. 5, pp. 918–27, 2006.

129. M.-C. Bourgeois-Daigneault, D. G. Roy, T. Falls, K. Twumasi-Boateng, L. E. St-Germain, M. Marguerie, V. Garcia, M. Selman, V. A. Jennings, J. Pettigrew, S. Amos, J.-S. Diallo, B. Nelson, and J. C. Bell, "Oncolytic vesicular stomatitis virus expressing interferon-γ has enhanced therapeutic activity," *Molecular Therapy — Oncolytics*, vol. 3, no. December 2015, p. 16001, 2016.

130. E. V. Shashkova, J. F. Spencer, W. S. M. Wold, and K. Doronin, "Targeting interferon-alpha increases antitumor efficacy and reduces hepatotoxicity of E1A-mutated spread-enhanced oncolytic adenovirus," *Molecular Therapy*, vol. 15, no. 3, pp. 598–607, 2007.

131. H. Li, K.-W. Peng, D. Dingli, R. a. Kratzke, and S. J. Russell, "Oncolytic measles viruses encoding interferon beta and the thyroidal sodium iodide symporter gene for mesothelioma virotherapy," *Cancer gene therapy*, vol. 17, no. 8, pp. 550–8, 2010.

132. D. H. Kirn, Y. Wang, F. Le Boeuf, J. Bell, and S. H. Thorne, "Targeting of interferon-beta to produce a specific, multi-mechanistic oncolytic vaccinia virus," *PLoS Medicine*, vol. 4, no. 12, p. e353, 2007.

133. C. L. Willmon, V. Saloura, Z. G. Fridlender, P. Wongthida, R. M. Diaz, J. Thompson, T. Kottke, M. Federspiel, G. Barber, S. M. Albelda, and R. G. Vile, "Expression of IFN-beta enhances both efficacy and safety of oncolytic vesicular stomatitis virus for therapy of mesothelioma," *Cancer Research*, vol. 69, no. 19, pp. 7713–20, 2009.

134. R. Edukulla, E. Ramakrishna, N. Woller, B. Mundt, S. Knocke, E. Gürlevik, M. Saborowski, N. Malek, M. P. Manns, T. Wirth, F. Kühnel, and S. Kubicka, "Antitumoral immune response by recruitment and expansion of dendritic cells in tumors infected with telomerase-dependent oncolytic viruses," *Cancer Research*, vol. 69, no. 4, pp. 1448–58, 2009.

135. S. Leveille, M.-L. Goulet, B. D. Lichty, and J. Hiscott, "Vesicular stomatitis virus oncolytic treatment interferes with tumor-associated dendritic cell functions and abrogates tumor antigen presentation.," *Journal of Virology*, vol. 85, no. 23, pp. 12160–9, 2011.

136. B. Huang, R. Sikorski, D. H. Kirn, and S. H. Thorne, "Synergistic anti-tumor effects between oncolytic vaccinia virus and paclitaxel are mediated by the IFN response and HMGB1," *Gene Therapy*, vol. 18, no. 2, pp. 164–172, 2010.

137. H. S. Kim, S. Kim-Schulze, D. W. Kim, and H. L. Kaufman, "Host lymphodepletion enhances the therapeutic activity of an oncolytic vaccinia virus expressing 4-1BB ligand," *Cancer Research*, vol. 69, no. 21, pp. 8516–25, 2009.

138. F. Galivo, R. M. Diaz, U. Thanarajasingam, D. Jevremovic, P. Wongthida, J. Thompson, T. Kottke, G. N. Barber, A. Melcher, and R. G. Vile, "Interference of CD40L-mediated tumor immunotherapy by oncolytic vesicular stomatitis virus," *Human Gene Therapy*, vol. 21, no. 4, pp. 439–50, 2010.

139. D. E. Griffin, "Measles Virus," in *Fields Virology* (D. M. Knipe and P. M. Howley, eds.), ch. 36, pp. 1042–1069, Philadelphia, PA: Lippincott Williams & Wilkins, 6 ed.,

2013.

140. P. C. Dowling, B. M. Blumberg, J. Menonna, J. E. Adamus, P. Cook, J. C. Crowley, D. Kolakofsky, and S. D. Cook, "Transcriptional map of the measles virus genome," *Journal of General Virology*, vol. 67, no. 9, pp. 1987–1992, 1986.
141. W. W. Hall and S. J. Martin, "Purification and characterization of measles virus," *Journal of General Virology*, vol. 19, pp. 175–188, 1973.
142. W. J. Bellini, G. Englund, S. Rozenblatt, H. Arnheiter, and C. D. Richardson, "Measles virus P gene codes for two proteins," *Journal of Virology*, vol. 53, no. 3, pp. 908–19, 1985.
143. R. Cattaneo, K. Kaelin, K. Baczko, and M. A. Billeter, "Measles virus editing provides an additional cysteine-rich protein," *Cell*, vol. 56, no. 5, pp. 759–764, 1989.
144. C. L. Parks, R. A. Lerch, P. Walpita, H.-P. Wang, M. S. Sidhu, and S. A. Udem, "Analysis of the Noncoding Regions of Measles Virus Strains in the Edmonston Vaccine Lineage," *Journal of Virology*, vol. 75, no. 2, pp. 921–933, 2001.
145. R. W. H. Ruigrok, T. Crépin, and D. Kolakofsky, "Nucleoproteins and nucleocapsids of negative-strand RNA viruses," *Current Opinion in Microbiology*, vol. 14, no. 4, pp. 504–510, 2011.
146. R. Cox and R. K. Plemper, "The paramyxovirus polymerase complex as a target for next-generation anti-paramyxovirus therapeutics," *Frontiers in Microbiology*, vol. 6, no. MAY, pp. 1–14, 2015.
147. R. K. Plemper, A. L. Hammond, and R. Cattaneo, "Measles virus envelope glycoproteins hetero-oligomerize in the endoplasmic reticulum," *The Journal of Biological Chemistry*, vol. 276, no. 47, pp. 44239–44246, 2001.
148. J. M. Fontana, B. Bankamp, W. J. Bellini, and P. a. Rota, "Regulation of interferon signaling by the C and V proteins from attenuated and wild-type strains of measles virus," *Virology*, vol. 374, no. 1, pp. 71–81, 2008.
149. K. M. J. Sparrer, C. K. Pfaller, and K.-K. Conzelmann, "Measles Virus C Protein Interferes with Beta Interferon Transcription in the Nucleus," *Journal of Virology*, vol. 86, no. 2, pp. 796–805, 2012.
150. M. E. Davis, M. K. Wang, L. J. Rennick, F. Full, S. Gableske, A. W. Mesman, S. I. Gringhuis, T. B. H. Geijtenbeek, W. P. Duprex, and M. U. Gack, "Antagonism of the phosphatase PP1 by the measles virus v protein is required for innate immune escape of MDA5," *Cell Host and Microbe*, vol. 16, no. 1, pp. 19–30, 2014.
151. R. Cattaneo, G. Rebmann, A. Schmid, K. Baczkol, V. Ter Meulen ', and M. A. Billeter, "Altered transcription of a defective measles virus genome derived from a diseased human brain," *The EMBO Journal*, vol. 6, no. 3, pp. 681–688, 1987.
152. W. J. Moss and D. E. Griffin, "Global measles elimination," *Nature reviews. Microbiology*, vol. 4, no. 12, pp. 900–908, 2006.
153. M. D. Muhlebach, M. Mateo, P. L. Sinn, S. Prufer, K. M. Uhlig, V. H. Leonard,

C. K. Navaratnarajah, M. Frenzke, X. X. Wong, B. Sawatsky, S. Ramachandran, P. B. McCray Jr., K. Cichutek, V. von Messling, M. Lopez, and R. Cattaneo, "Adherens junction protein nectin-4 is the epithelial receptor for measles virus," *Nature*, vol. 480, no. 7378, pp. 530–533, 2011.

154. R. S. Noyce, D. G. Bondre, M. N. Ha, L.-T. Lin, G. Sisson, M.-S. Tsao, and C. D. Richardson, "Tumor cell marker PVRL4 (nectin 4) is an epithelial cell receptor for measles virus," *PLoS Pathogens*, vol. 7, no. 8, p. e1002240, 2011.
155. H. Tatsuo, N. Ono, K. Tanaka, and Y. Yanagi, "SLAM (CDw150) is a cellular receptor for measles virus," *Nature*, vol. 406, no. 6798, pp. 893–897, 2000.
156. N. Reymond, S. Fabre, E. Lecocq, J. Adelaide, P. Dubreuil, and M. Lopez, "Nectin4/PRR4, a New Afadin-associated Member of the Nectin Family that Trans-interacts with Nectin1/PRR1 through V Domain Interaction," *The Journal of Biological Chemistry*, vol. 276, no. 46, pp. 43205–43215, 2001.
157. C. S. Ferreira, M. Frenzke, V. H. Leonard, G. G. Welstead, C. D. Richardson, and R. Cattaneo, "Measles virus infection of alveolar macrophages and dendritic cells precedes spread to lymphatic organs in transgenic mice expressing human signaling lymphocytic activation molecule (SLAM, CD150)," *Journal of Virology*, vol. 84, no. 6, pp. 3033–3042, 2010.
158. K. Lemon, R. D. de Vries, A. W. Mesman, S. Mcquaid, G. van Amerongen, S. Yuksel, M. Ludlow, L. J. Rennick, T. Kuiken, B. K. Rima, T. B. H. Geijtenbeek, A. D. M. E. Osterhaus, W. P. Duprex, and R. L. de Swart, "Early target cells of measles virus after aerosol infection of non-human primates," *PLoS Pathogens*, vol. 7, no. 1, 2011.
159. T. R. Moench, D. E. Griffin, C. R. Obriecht, A. J. Vaisberg, and R. T. Johnson, "Acute measles in patients with and without neurological involvement: distribution of measles virus antigen and RNA," *The Journal of Infectious Diseases*, vol. 158, no. 2, pp. 433–442, 1988.
160. D. E. Griffin, "Measles virus-induced suppression of immune responses," *Immunological Reviews*, vol. 236, pp. 176–189, 2010.
161. R. K. Garg, "Subacute sclerosing panencephalitis," *Journal of Neurology*, vol. 255, no. 12, pp. 1861–1871, 2008.
162. "Weekly epidemiological record: relevé épidémiologique hebdomadaire," *The Weekly Epidemiological Record*, vol. 90, no. 46, pp. 617–632, 2015.
163. J. J. Ryon, W. J. Moss, M. Monze, and D. E. Griffin, "Functional and phenotypic changes in circulating lymphocytes from hospitalized zambian children with measles," *Clinical and Diagnostic Laboratory Immunology*, vol. 9, no. 5, pp. 994–1003, 2002.
164. D. E. Griffin and B. J. Ward, "Differential CD4 T cell activation in measles," *The Journal of Infectious Diseases*, vol. 168, no. 2, pp. 275–281, 1993.
165. V. A. Hirsch, RL, Griffin DE, Johnson RT, Cooper SJ, Lindo de Soriano I, Roedenbeck S, "Cellular immune responses during complicated and uncomplicated measles virus

infections of man," *Clinical Immunology and Immunopathology*, vol. 31, no. 1, pp. 1–12, 1984.

166. J. F. Enders and Peebles T. C., "Propagation in tissue cultures of cytopathogenic agents from patients with measles," *Proceedings of the Society for Experimetal Biology and Medicine*, vol. 86, no. 2, pp. 277–286, 1954.
167. J. F. Enders, S. L. Katz, M. V. Milovanovic, and A. Holloway, "Studies on an attenuated measles-virus vaccine. I. Development and preparations of the vaccine: technics for assay of effects of vaccination," *New England Journal of Medicine*, vol. 263, pp. 153–159, 1960.
168. B. Bankamp, M. Takeda, Y. Zhang, W. Xu, and P. A. Rota, "Genetic Characterization of Measles Vaccine Strains," *Journal of Infectious Diseases*, vol. 204, no. Supplement 1, pp. S533–S548, 2011.
169. A. J. Schwarz, "Preliminary tests of a highly attenuated measles vaccine," *American Journal of Diseases of Children*, vol. 103, pp. 386–389, 1962.
170. R. E. Dorig, a. Marcil, a. Chopra, and C. D. Richardson, "The human CD46 molecule is a receptor for measles virus (Edmonston strain)," *Cell*, vol. 75, no. L, pp. 295–305, 1993.
171. E. C. Hsu, F. Sarangi, C. Iorio, M. S. Sidhu, S. a. Udem, D. L. Dillehay, W. Xu, P. a. Rota, W. J. Bellini, and C. D. Richardson, "A single amino acid change in the hemagglutinin protein of measles virus determines its ability to bind CD46 and reveals another receptor on marmoset B cells," *Journal of Virology*, vol. 72, no. 4, pp. 2905–2916, 1998.
172. H. Yamamoto, A. F. Fara, P. Dasgupta, and C. Kemper, "CD46: The 'multitasker' of complement proteins," *International Journal of Biochemistry and Cell Biology*, vol. 45, no. 12, pp. 2808–2820, 2013.
173. A. Maciejczyk, J. Szelachowska, B. Szynglarewicz, R. Szulc, A. Szulc, T. Wysocka, E. Jagoda, H. Lage, and P. Surowiak, "CD46 Expression is an unfavorable prognostic factor in breast cancer cases," *Applied Immunohistochemistry & Molecular Morphology*, vol. 19, no. 6, pp. 540–6, 2011.
174. A. Gorter, V. T. Blok, W. H. Haasnoot, N. G. Ensink, M. R. Daha, and G. J. Fleuren, "Expression of CD46, CD55, and CD59 on renal tumor cell lines and their role in preventing complement-mediated tumor cell lysis," *Laboratory Investigation; a Journal of Technical Methods and Pathology*, vol. 74, no. 6, pp. 1039–49, 1996.
175. R. Buettner, M. Huang, T. Gritsko, J. Karras, S. Enkemann, T. Mesa, S. Nam, H. Yu, and R. Jove, "Activated signal transducers and activators of transcription 3 signaling induces CD46 expression and protects human cancer cells from complement-dependent cytotoxicity," *Molecular Cancer Research*, vol. 5, no. 8, pp. 823–32, 2007.
176. S. Gross, "Measles and Leukemia," *The Lancet*, vol. 1, no. 7695, pp. 397–298, 1971.
177. A. Bluming and J. Ziegler, "Regression of Burkitt's lymphoma in association with

measles infection," *The Lancet*, vol. 298, no. 7715, pp. 105–106, 1971.

178. H. C. Mota, "Infantile Hodgkin's Disease: Remission after Measles," *British Medical Journal*, vol. 2, no. 5863, p. 421, 1973.
179. B. D. Anderson, T. Nakamura, S. J. Russell, and K. W. Peng, "High CD46 receptor density determines preferential killing of tumor cells by oncolytic measles virus," *Cancer Research*, vol. 64, no. 14, pp. 4919–4926, 2004.
180. N. K. Rushmere, J. M. Knowlden, J. M. W. Gee, M. E. Harper, J. F. Robertson, B. P. Morgan, and R. I. Nicholson, "Analysis of the level of mRNA expression of the membrane regulators of complement, CD59, CD55 and CD46, in breast cancer," *International Journal of Cancer*, vol. 108, no. 6, pp. 930–936, 2004.
181. V. T. Blok, M. R. Daha, O. M. Tijsma, M. G. Weissglas, L. J. van den Broek, and A. Gorter, "A possible role of CD46 for the protection in vivo of human renal tumor cells from complement-mediated damage," *Laboratory Investigation; a Journal of Technical Methods and Pathology*, vol. 80, no. 3, pp. 335–44, 2000.
182. N. Kinugasa, T. Higashi, K. Nouso, H. Nakatsukasa, M. Kobayashi, M. Ishizaki, N. Toshikumi, K. Yoshida, S. Uematsu, and T. Tsuji, "Expression of membrane cofactor protein (MCP, CD46) in human liver diseases," *British Journal of Cancer*, vol. 80, no. 11, pp. 1820–1825, 1999.
183. J. C. Varela, C. Atkinson, R. Woolson, and T. E. Keane, "Upregulated expression of complement inhibitory proteins on bladder cancer cells and anti-MUC1 antibody immune selection," *Internation Journal of Cancer*, vol. 123, no. 6, pp. 1357–1363, 2008.
184. H. Juhl, F. Helmig, K. Baltzer, H. Kalthoff, D. Henne-bruns, and B. Kremer, "Frequent Expression of Complement on Gastrointestinal Cancer Cells Limits the Therapeutic Potential of Monoclonal Antibody 17-1A," *Journal of Surgical Oncology*, vol. 64, no. December 1996, pp. 222–230, 1997.
185. T. Seya, M. Matsumoto, T. Hara, M. Hatanaka, T. Masaoka, and H. Akedo, "Distribution of C3-step regulatory proteins of the complement system, CD35 (CR1), CD46 (MCP), and CD55 (DAF), in hematological malignancies," *Leukemia & Lymphoma*, vol. 12, no. 5-6, pp. 395–400, 1994.
186. D. Grote, S. J. Russell, T. I. Cornu, R. Cattaneo, R. Vile, G. A. Poland, and A. K. Fielding, "Live attenuated measles virus induces regression of human lymphoma xenografts in immunodeficient mice," *Blood*, vol. 97, no. 12, pp. 3746–3754, 2001.
187. K. W. Peng, G. J. Ahmann, L. Pham, P. R. Greipp, R. Cattaneo, and S. J. Russell, "Systemic therapy of myeloma xenografts by an attenuated measles virus," *Blood*, vol. 98, no. 7, pp. 2002–2007, 2001.
188. F. Radecke, P. Spielhofer, H. Schneider, K. Kaelin, M. Huber, C. Dötsch, G. Christiansen, and M. a. Billeter, "Rescue of measles viruses from cloned DNA," *The EMBO journal*, vol. 14, no. 23, pp. 5773–84, 1995.

189. U. Schneider, F. Bullough, S. Vongpunsawad, S. J. Russell, and R. Cattaneo, "Recombinant measles viruses efficiently entering cells through targeted receptors," *Journal of Virology*, vol. 74, no. 21, pp. 9928–9936, 2000.

190. A. L. Hammond, R. K. Plemper, J. Zhang, U. Schneider, S. J. Russell, and R. Cattaneo, "Single-Chain Antibody Displayed on a Recombinant Measles Virus Confers Entry through the Tumor-Associated Carcinoembryonic Antigen," *Journal of Virology*, vol. 75, no. 5, pp. 2087–2096, 2001.

191. K. W. Peng, K. A. Donovan, U. Schneider, R. Cattaneo, J. A. Lust, and S. J. Russell, "Oncolytic measles viruses displaying a single-chain antibody against CD38, a myeloma cell marker," *Blood*, vol. 101, no. 7, pp. 2557–2562, 2003.

192. A. Bucheit, S. Kumar, D. Grote, Y. Lin, V. von Messling, R. Cattaneo, and A. Fielding, "An oncolytic measles virus engineered to enter cells through the CD20 antigen," *Molecular Therapy*, vol. 7, no. 1, pp. 62–72, 2003.

193. K. Friedrich, J. R. Hanauer, S. Prüfer, R. C. Münch, I. Völker, C. Filippis, C. Jost, K.-M. Hanschmann, R. Cattaneo, K.-W. Peng, A. Plückthun, C. J. Buchholz, K. Cichutek, and M. D. Mühlebach, "DARPin-targeting of measles virus: unique bispecificity, effective oncolysis, and enhanced safety," *Molecular Therapy*, vol. 21, no. 4, pp. 849–59, 2013.

194. K. W. Peng, P. D. Holler, B. A. Orr, D. M. Kranz, and S. J. Russell, "Targeting virus entry and membrane fusion through specific peptide/MHC complexes using a high-affinity T-cell receptor," *Gene Therapy*, vol. 11, no. 15, pp. 1234–1239, 2004.

195. S. Vongpunsawad, N. Oezgun, W. Braun, and R. Cattaneo, "Selectively receptor-blind measles viruses: Identification of residues necessary for SLAM- or CD46-induced fusion and their localization on a new hemagglutinin structural model," *Journal of Virology*, vol. 78, no. 1, pp. 302–13, 2004.

196. T. Nakamura, K.-W. Peng, S. Vongpunsawad, M. Harvey, H. Mizuguchi, T. Hayakawa, R. Cattaneo, and S. J. Russell, "Antibody-targeted cell fusion," *Nature Biotechnology*, vol. 22, no. 3, pp. 331–6, 2004.

197. M. F. Leber, S. Bossow, V. H. J. Leonard, K. Zaoui, C. Grossardt, M. Frenzke, T. Miest, S. Sawall, R. Cattaneo, C. von Kalle, and G. Ungerechts, "MicroRNA-sensitive oncolytic measles viruses for cancer-specific vector tropism," *Molecular Therapy*, vol. 19, no. 6, pp. 1097–1106, 2011.

198. M. Baertsch, M. Leber, S. Bossow, M. Singh, C. Engeland, J. Albert, C. Grossardt, D. Jäger, C. von Kalle, and G. Ungerechts, "MicroRNA-mediated multi-tissue detargeting of oncolytic measles virus," *Cancer Gene Therapy*, vol. 21, no. 9, pp. 373–380, 2014.

199. I. D. Iankov, C. Allen, M. J. Federspiel, R. M. Myers, K. W. Peng, J. N. Ingle, S. J. Russell, and E. Galanis, "Expression of Immunomodulatory Neutrophil-activating Protein of Helicobacter pylori Enhances the Antitumor Activity of Oncolytic Measles Virus,"

Molecular Therapy, vol. 20, no. 6, pp. 1139–1147, 2012.

200. D. Grote, R. Cattaneo, and A. K. Fielding, "Neutrophils Contribute to the Measles Virus-induced Antitumor Effect : Enhancement by Granulocyte Macrophage Colony-stimulating Factor Expression Neutrophils Contribute to the Measles Virus-induced Antitumor Effect : Enhancement by Granulocyte Macrophage," *Cancer Research*, vol. 63, pp. 6463–6468, 2003.
201. J. Weber, "Ipilimumab: Controversies in its development, utility and autoimmune adverse events," *Cancer Immunology, Immunotherapy*, vol. 58, no. 5, pp. 823–830, 2009.
202. J. Naidoo, D. B. Page, B. T. Li, L. C. Connell, K. Schindler, M. E. Lacouture, M. A. Postow, and J. D. Wolchok, "Toxicities of the anti-PD-1 and anti-PD-L1 immune checkpoint antibodies," *Annals of Oncology*, vol. 26, no. 12, pp. 2375–2391, 2015.
203. K.-W. Peng, S. Facteau, T. Wegman, D. O'Kane, and S. J. Russell, "Non-invasive in vivo monitoring of trackable viruses expressing soluble marker peptides," *Nature Medicine*, vol. 8, no. 5, pp. 527–531, 2002.
204. D. Dingli, K.-w. Peng, M. E. Harvey, P. R. Greipp, M. K. O. Connor, R. Cattaneo, J. C. Morris, and S. J. Russell, "Image-guided radiovirotherapy for multiple myeloma using a recombinant measles virus expressing the thyroidal sodium iodide symporter," *Blood*, vol. 103, no. 5, pp. 1641–1646, 2004.
205. A. R. Penheiter, S. J. Russell, and S. K. Carlson, "The sodium iodide symporter (NIS) as an imaging reporter for gene, viral, and cell-based therapies," *Current Gene Therapy*, vol. 12, no. 1, pp. 33–47, 2012.
206. L. Heinzerling, V. Künzi, P. a. Oberholzer, T. Kündig, H. Naim, and R. Dummer, "Oncolytic measles virus in cutaneous T-cell lymphomas mounts antitumor immune responses in vivo and targets interferon-resistant tumor cells," *Blood*, vol. 106, no. 7, pp. 2287–94, 2005.
207. E. Galanis, "Therapeutic potential of oncolytic measles virus: promises and challenges," *Clinical Pharmacology and Therapeutics*, vol. 88, no. 5, pp. 620–5, 2010.
208. E. Galanis, P. J. Atherton, M. J. M. Maurer, K. L. Knutson, S. C. Dowdy, W. a. Cliby, P. Haluska, H. J. Long, A. Oberg, I. Aderca, M. S. Block, J. Bakkum-Gamez, M. J. Federspiel, S. J. Russell, K. R. Kalli, G. Keeney, K. W. Peng, and L. C. Hartmann, "Oncolytic Measles Virus Expressing the Sodium Iodide Symporter to Treat Drug-Resistant Ovarian Cancer," *Cancer Research*, vol. 75, no. 1, pp. 22–30, 2014.
209. S. J. Russell, M. J. Federspiel, K.-W. Peng, C. Tong, D. Dingli, W. G. Morice, V. Lowe, M. K. O'Connor, R. A. Kyle, N. Leung, F. K. Buadi, S. V. Rajkumar, M. A. Gertz, M. Q. Lacy, and A. Dispenzieri, "Remission of disseminated cancer after systemic oncolytic virotherapy," *Mayo Clinic Proceedings*, vol. 89, no. 7, pp. 926–33, 2014.
210. J. Ye, G. Coulouris, I. Zaretskaya, I. Cutcutache, S. Rozen, and T. L. Madden, "Primer-BLAST: A tool to design target-specific primers for polymerase chain reaction," *BMC*

Bioinformatics, vol. 13, no. 1, p. 134, 2012.

211. C. Yanisch-Perron, J. Vieira, and J. Messing, "Improved M13 phage cloning vectors and host strains: nucleotide sequences of the M13mp18 and pUC19 vectors," *Gene*, vol. 33, no. 1, pp. 103–19, 1985.
212. C. Grossardt, *Engineering Targeted and Cytokine-armed Oncolytic Measles Viruses*. PhD thesis, Ruperto-Carola University of Heidelberg, 2013.
213. C. E.Engeland, *Immune Checkpoint Modulation Enhances Oncolytic Virotherapy*. PhD thesis, Ruperto-Carola University of Heidelberg, 2014.
214. C. Combredet, V. Labrousse, L. Mollet, C. Lorin, F. Delebecque, B. Hurtrel, M. B. Feinberg, M. Brahic, and H. Mcclure, "A Molecularly Cloned Schwarz Strain of Measles Virus Vaccine Induces Strong Immune Responses in Macaques and Transgenic Mice A Molecularly Cloned Schwarz Strain of Measles Virus Vaccine Induces Strong Immune Responses in Macaques and Transgenic Mice," *Journal of Virology*, vol. 77, no. 21, pp. 11546–11554, 2003.
215. A. Martin, P. Staeheli, and U. Schneider, "RNA polymerase II-controlled expression of antigenomic RNA enhances the rescue efficacies of two different members of the Mononegavirales independently of the site of viral genome replication," *Journal of Virology*, vol. 80, no. 12, pp. 5708–15, 2006.
216. T. Nakamura, K.-W. Peng, M. Harvey, S. Greiner, I. a. J. Lorimer, C. D. James, and S. J. Russell, "Rescue and propagation of fully retargeted oncolytic measles viruses," *Nature Biotechnology*, vol. 23, no. 2, pp. 209–14, 2005.
217. S. A. Rosenberg, P. Spiess, and R. Lafreniere, "a New Approach To the Adoptive Immunotherapy of Cancer With Tumor-Infiltrating Lymphocytes," *Science*, vol. 233, no. 4770, pp. 1318–1321, 1986.
218. P. F. Robbins, J. A. Kantor, M. Salgaller, P. H. Hand, P. D. Fernsten, and J. Schlom, "Transduction and expression of the human carcinoembryonic antigen gene in a murine colon carcinoma cell line," *Cancer Research*, vol. 51, no. 14, pp. 3657–62, 1991.
219. C. L. Andersen, J. L. Jensen, and T. F. Ørntoft, "Normalization of real-time quantitative reverse transcription-PCR data: A model-based variance estimation approach to identify genes suited for normalization, applied to bladder and colon cancer data sets," *Cancer Research*, vol. 64, no. 15, pp. 5245–5250, 2004.
220. T. T. D. Amsen, K. E. de Visser, "Approaches to Determine Expression of Inflammatory Cytokines," *Methods Molecular Biology*, vol. 511, pp. 61–73, 2009.
221. P. Calain and L. Roux, "The rule of six, a basic feature for efficient replication of Sendai virus defective interfering RNA," *Journal of Virology*, vol. 67, no. 8, pp. 4822–4830, 1993.
222. G. J. Lieschke, P. K. Rao, M. K. Gately, and R. C. Mulligan, "Bioactive murine and human interleukin-12 fusion proteins which retain antitumor activity in vivo," *Nature Biotechnology*, vol. 15, no. 1, pp. 35–40, 1997.

223. C. E. Rudd, A. Taylor, and H. Schneider, "CD28 and CTLA-4 coreceptor expression and signal transduction," *Immunological Reviews*, vol. 229, no. 1, pp. 12–26, 2009.

224. S. T. Haile, S. P. Dalal, V. Clements, K. Tamada, and S. Ostrand-Rosenberg, "Soluble CD80 restores T cell activation and overcomes tumor cell programmed death ligand 1-mediated immune suppression," *The Journal of Immunology*, vol. 191, no. 5, pp. 2829–36, 2013.

225. B. K. Rima and W. P. Duprex, "New concepts in measles virus replication: Getting in and out in vivo and modulating the host cell environment," *Virus Research*, vol. 162, no. 1-2, pp. 47–62, 2011.

226. G. Ungerechts, C. Springfeld, M. E. Frenzke, J. Lampe, W. B. Parker, E. J. Sorscher, and R. Cattaneo, "An immunocompetent murine model for oncolysis with an armed and targeted measles virus," *Molecular Therapy*, vol. 15, no. 11, pp. 1991–7, 2007.

227. J. K. Kaufmann, S. Bossow, C. Grossardt, S. Sawall, J. Kupsch, P. Erbs, J. C. Hassel, C. von Kalle, A. H. Enk, D. M. Nettelbeck, and G. Ungerechts, "Chemovirotherapy of malignant melanoma with a targeted and armed oncolytic measles virus," *Journal of Investigative Dermatology*, vol. 133, no. 4, pp. 1034–1042, 2013.

228. M. Iwasaki and Y. Yanagi, "Expression of the Sendai (murine parainfluenza) virus C protein alleviates restriction of measles virus growth in mouse cells," *Proceedings of the National Academy of Sciences of the United States of America*, vol. 108, no. 37, pp. 15384–15389, 2011.

229. T. Whistler, W. J. Bellini, and P. A. Rota, "Generation of defective interfering particles by two vaccine strains of measles virus," *Virology*, vol. 220, no. 2, pp. 480–484, 1996.

230. C. K. Pfaller, G. M. Mastorakos, W. E. Matchett, X. Ma, C. E. Samuel, and R. Cattaneo, "Measles Virus Defective Interfering RNAs Are Generated Frequently and Early in the Absence of C Protein and Can Be Destabilized by Adenosine Deaminase Acting on RNA-1-Like Hypermutations," *Journal of Virology*, vol. 89, no. 15, pp. 7735–47, 2015.

231. J. I. Quetglas, S. Labiano, M. A. Aznar, E. Bolanos, A. Azpilikueta, I. Rodriguez, E. Casales, A. Rodriguez, V. Segura, C. Smerdou, and I. Melero, "Virotherapy with a Semliki Forest Virus-based Vector encoding IL-12 synergizes with PD-1/PD-L1 Blockade," *Cancer Immunology Research*, pp. 10–16, 2015.

232. S. F. Wolf, P. A. Temple, M. Kobayashi, D. Young, M. Dicig, L. Lowe, R. Dzialo, L. Fitz, C. Ferenz, and R. M. Hewick, "Cloning of cDNA for natural killer cell stimulatory factor, a heterodimeric cytokine with multiple biologic effects on T and natural killer cells," *The Journal of Immunology*, vol. 146, no. 9, pp. 3074–81, 1991.

233. A. E. Moore, "Viruses with oncolytic properties and their adaptation to tumors," *Annals of the New York Academy of Sciences*, vol. 54, no. 6, pp. 945–52, 1952.

234. W. M. Hammon, D. S. Yohn, B. C. Casto, and R. W. Atchison, "Oncolytic Potentials of Nonhuman Viruses for Human Cancer. I. Effects of Twenty-Four Viruses on Human

Cancer Cell Lines," *Journal of the National Cancer Institute*, vol. 31, no. 2, pp. 329–45, 1963.

235. D. L. Bartlett, Z. Liu, M. Sathaiah, R. Ravindranathan, Z. Guo, Y. He, and Z. S. Guo, "Oncolytic viruses as therapeutic cancer vaccines," *Molecular Cancer*, vol. 12, no. 1, p. 103, 2013.
236. V. Cerullo, I. Diaconu, V. Romano, M. Hirvinen, M. Ugolini, S. Escutenaire, S. L. Holm, A. Kipar, A. Kanerva, and A. Hemminki, "An oncolytic adenovirus enhanced for toll-like receptor 9 stimulation increases antitumor immune responses and tumor clearance," *Molecular Therapy*, vol. 20, no. 11, pp. 2076–2086, 2012.
237. J. J. Rojas, P. Sampath, B. Bonilla, A. Ashley, W. Hou, D. Byrd, and S. H. Thorne, "Manipulating TLR Signaling Increases the Anti-tumor T Cell Response Induced by Viral Cancer Therapies," *Cell Reports*, vol. 15, no. 2, pp. 264–273, 2016.
238. "European Medicines Agency. Summary of European public assessment report (EPAR) for Imlygic (Talimogene Laherparepvec)," 2017. `http://www.ema.europa.eu/ema/index.jsp?curl=pages/medicines/human/medicines/002771/human_med_001941.jsp&mid=WC0b01ac058001d124`, last accessed: 09.02.2017.
239. A. Gauvrit, S. Brandler, C. Sapede-Peroz, N. Boisgerault, F. Tangy, and M. Gregoire, "Measles virus induces oncolysis of mesothelioma cells and allows dendritic cells to cross-prime tumor-specific CD8 response," *Cancer Research*, vol. 68, no. 12, pp. 4882–92, 2008.
240. J.-B. Guillerme, N. Boisgerault, D. Roulois, J. Ménager, C. Combredet, F. Tangy, J.-F. Fonteneau, and M. Gregoire, "Measles virus vaccine-infected tumor cells induce tumor antigen cross-presentation by human plasmacytoid dendritic cells," *Clinical Cancer Research*, vol. 19, no. 5, pp. 1147–58, 2013.
241. O. G. Donnelly, F. Errington-mais, L. Steele, E. Hadac, K. Scott, H. Peach, R. M. Phillips, J. Bond, K. Harrington, R. Vile, S. Russell, P. Selby, and A. Alan, "Measles virus causes immunogenic cell death in human melanoma," *Gene Therapy*, vol. 20, no. 1, pp. 7–15, 2013.
242. C. Neumeister, R. Nanan, T. I. Cornu, C. G. K. L??der, V. ter Meulen, H. Naim, and S. Niewiesk, "Measles virus and canine distemper virus target proteins into a TAP-independent MHC class I-restricted antigen-processing pathway," *Journal of General Virology*, vol. 82, no. 2, pp. 441–447, 2001.
243. A. Zuniga, Z. Wang, M. Liniger, L. Hangartner, M. Caballero, J. Pavlovic, P. Wild, J. F. Viret, R. Glueck, M. A. Billeter, and H. Y. Naim, "Attenuated measles virus as a vaccine vector," *Vaccine*, vol. 25, no. 16, pp. 2974–2983, 2007.
244. S. Russell, "CD46: A complement regulator and pathogen receptor that mediates links between innate and acquired immune function," *Tissue Antigens*, vol. 64, no. 2, pp. 111–118, 2004.
245. M. Liu, S. Guo, and J. K. Stiles, "The emerging role of CXCL10 in cancer," *Oncology*

Letters, vol. 2, no. 4, pp. 583–589, 2011.

246. Q. Wu, R. Dhir, and A. Wells, "Altered CXCR3 isoform expression regulates prostate cancer cell migration and invasion," *Molecular Cancer*, vol. 11, p. 3, 2012.
247. T. Utsumi, T. Suyama, Y. Imamura, M. Fuse, S. Sakamoto, N. Nihei, T. Ueda, H. Suzuki, N. Seki, and T. Ichikawa, "The Association of CXCR3 and Renal Cell Carcinoma Metastasis," *The Journal of Urology*, vol. 192, no. 2, pp. 567–574, 2014.
248. G. S. V. Campanella, R. A. Colvin, and A. D. Luster, "CXCL10 can inhibit endothelial cell proliferation independently of CXCR3," *PLoS ONE*, vol. 5, no. 9, pp. 1–10, 2010.
249. W. Peng, C. Liu, C. Xu, Y. Lou, J. Chen, Y. Yang, H. Yagita, W. W. Overwijk, G. Lizeé, L. Radvanyi, and P. Hwu, "PD-1 blockade enhances T-cell migration to tumors by elevating IFN-γ inducible chemokines," *Cancer Research*, vol. 72, no. 20, pp. 5209–5218, 2012.
250. X. Yang, Y. Chu, Y. Wang, R. Zhang, and S. Xiong, "Targeted in vivo expression of IFN-gamma-inducible protein 10 induces specific antitumor activity," *Journal of Leukocyte Biology*, vol. 80, no. 6, pp. 1434–44, 2006.
251. J. Keyser, J. Schultz, K. Ladell, L. Elzaouk, L. Heinzerling, J. Pavlovic, and K. Moelling, "IP-10-encoding plasmid DNA therapy exhibits anti-tumor and anti-metastatic efficiency," *Experimental Dermatology*, vol. 13, no. 6, pp. 380–90, 2004.
252. S. C. Wightman, a. Uppal, S. P. Pitroda, S. Ganai, B. Burnette, M. Stack, G. Oshima, S. Khan, X. Huang, M. C. Posner, R. R. Weichselbaum, and N. N. Khodarev, "Oncogenic CXCL10 signalling drives metastasis development and poor clinical outcome," *British Journal of Cancer*, vol. 113, no. April, pp. 1–9, 2015.
253. M. J. Brunda, L. Luistro, R. R. Warrier, R. B. Wright, B. R. Hubbard, M. Murphy, S. F. Wolf, and M. K. Gately, "Antitumor and antimetastatic activity of interleukin 12 against murine tumors," *The Journal of Experimental Medicine*, vol. 178, no. 4, pp. 1223–30, 1993.
254. W. Su, T. Kitagawa, T. Ito, T. Oyama, C. M. Lee, Y. K. Kim, and H. Matsuda, "Antitumor effect to IL-12 administration into the portal vein on murine liver metastasis," *Journal of Hepato-Biliary-Pancreatic Surgery*, vol. 9, no. 4, pp. 503–510, 2002.
255. A. Gambotto, T. Tüting, D. L. McVey, I. Kovesdi, H. Tahara, M. T. Lotze, and P. D. Robbins, "Induction of antitumor immunity by direct intratumoral injection of a recombinant adenovirus vector expressing interleukin-12," *Cancer Gene Therapy*, vol. 6, no. 1, pp. 45–53, 1999.
256. S. Runge, K. M. J. Sparrer, C. Lässig, K. Hembach, A. Baum, A. García-Sastre, J. Söding, K. K. Conzelmann, and K. P. Hopfner, "In Vivo Ligands of MDA5 and RIG-I in Measles Virus-Infected Cells," *PLoS Pathogens*, vol. 10, no. 4, 2014.
257. Y. Kai Chan and M. U. Gack, "Viral evasion of intracellular DNA and RNA sensing," *Nature Reviews. Microbiology*, vol. 14, no. 6, pp. 360–373, 2016.
258. J.-I. Eguchi, K. Hiroishi, S. Ishii, and K. Mitamura, "Interferon-alpha and interleukin-

12 gene therapy of cancer: interferon-alpha induces tumor-specific immune responses while interleukin-12 stimulates non-specific killing," *Cancer Immunology, immunotherapy*, vol. 52, no. 6, pp. 378–86, 2003.

259. P. Ketzer, J. K. Kaufmann, S. Engelhardt, S. Bossow, C. von Kalle, J. S. Hartig, G. Ungerechts, and D. M. Nettelbeck, "Artificial riboswitches for gene expression and replication control of DNA and RNA viruses," *Proceedings of the National Academy of Sciences of the United States of America*, vol. 111, no. 5, pp. E554–62, 2014.
260. M. Wieland and J. S. Hartig, "Artificial riboswitches: Synthetic mRNA-based regulators of gene expression," *ChemBioChem*, vol. 9, no. 12, pp. 1873–1878, 2008.
261. S. Pilon-Thomas, A. Mackay, N. Vohra, and J. J. Mule, "Blockade of PD-L1 Enhances the Therapeutic Efficacy of Combination Immunotherapy Against Melanoma," *The Journal of Immunology*, vol. 184, no. 7, pp. 3442–3449, 2010.
262. A. Prodeus, A. Abdul-Wahid, N. W. Fischer, E. H.-B. Huang, M. Cydzik, and J. Gariépy, "Targeting the PD-1/PD-L1 Immune Evasion Axis With DNA Aptamers as a Novel Therapeutic Strategy for the Treatment of Disseminated Cancers," *Molecular Therapy — Nuclear Acids*, vol. 4, no. April, p. e237, 2015.
263. J. R. Brahmer, C. G. Drake, I. Wollner, J. D. Powderly, J. Picus, W. H. Sharfman, E. Stankevich, A. Pons, T. M. Salay, T. L. McMiller, M. M. Gilson, C. Wang, M. Selby, J. M. Taube, R. Anders, L. Chen, A. J. Korman, D. M. Pardoll, I. Lowy, and S. L. Topalian, "Phase I study of single-agent anti-programmed death-1 (MDX-1106) in refractory solid tumors: Safety, clinical activity, pharmacodynamics, and immunologic correlates," *Journal of Clinical Oncology*, vol. 28, no. 19, pp. 3167–3175, 2010.
264. C. Roach, N. Zhang, E. Corigliano, M. Jansson, G. Toland, G. Ponto, M. Dolled-Filhart, K. Emancipator, D. Stanforth, and K. Kulangara, "Development of a Companion Diagnostic PD-L1 Immunohistochemistry Assay for Pembrolizumab Therapy in Non-Small-cell Lung Cancer," *Applied Immunohistochemistry & Molecular Morphology*, vol. 00, no. 00, pp. 1–6, 2016.
265. S. Koyama, E. A. Akbay, Y. Y. Li, G. S. Herter-Sprie, K. A. Buczkowski, W. G. Richards, L. Gandhi, A. J. Redig, S. J. Rodig, H. Asahina, R. E. Jones, M. M. Kulkarni, M. Kuraguchi, S. Palakurthi, P. E. Fecci, B. E. Johnson, P. A. Janne, J. A. Engelman, S. P. Gangadharan, D. B. Costa, G. J. Freeman, R. Bueno, F. S. Hodi, G. Dranoff, K.-K. Wong, and P. S. Hammerman, "Adaptive resistance to therapeutic PD-1 blockade is associated with upregulation of alternative immune checkpoints," *Nature Communications*, vol. 7, pp. 1–9, 2016.
266. C. Blank, I. Brown, A. C. Peterson, T. C. R. Transgenic, C. D. T. Cells, M. Spiotto, Y. Iwai, T. Honjo, and T. F. Gajewski, "PD-L1 / B7H-1 Inhibits the Effector Phase of Tumor Rejection by T Cell Receptor (TCR) Transgenic CD8 + T Cells PD-L1 / B7H-1 Inhibits the Effector Phase of Tumor Rejection by T Cell Receptor," *Cancer Research*, no. Il, pp. 1140–1145, 2004.

267. J. Chang, J.-H. Cho, S.-W. Lee, S.-Y. Choi, S.-J. Ha, and Y.-C. Sung, "IL-12 priming during in vitro antigenic stimulation changes properties of CD8 T cells and increases generation of effector and memory cells," *The Journal of Immunology*, vol. 172, no. 5, pp. 2818–2826, 2004.

268. V. Lazarevic, L. H. Glimcher, and G. M. Lord, "T-bet: a bridge between innate and adaptive immunity," *Nature Reviews. Immunology*, vol. 13, no. 11, pp. 777–89, 2013.

269. M. Kobayashi, L. Fitz, M. Ryan, R. M. Hewick, S. C. Clark, S. Chan, R. Loudon, F. Sherman, B. Perussia, and G. Trinchieri, "Identification and purification of natural killer cell stimulatory factor (NKSF), a cytokine with multiple biologic effects on human lymphocytes," *The Journal of Experimental Medicine*, vol. 170, no. 3, pp. 827–45, 1989.

270. F. Gerosa, M. Tommasi, C. Benati, G. Gandini, M. Libonati, G. Tridente, G. Carra, and G. Trinchieri, "Differential effects of tyrosine kinase inhibition in CD69 antigen expression and lytic activity induced by rIL-2, rIL-12, and rIFN-alpha in human NK cells," *Cellular Immunology*, vol. 150, no. 2, pp. 382–90, 1993.

271. J. Chehimi, N. M. Valiante, A. D'Andrea, M. Rengaraju, Z. Rosado, M. Kobayashi, B. Perussia, S. F. Wolf, S. E. Starr, and G. Trinchieri, "Enhancing effect of natural killer cell stimulatory factor (NKSF/interleukin-12) on cell-mediated cytotoxicity against tumor-derived and virus-infected cells," *European Journal of Immunology*, vol. 23, no. 8, pp. 1826–1830, 1993.

272. E. Marcenaro, M. Della Chiesa, F. Bellora, S. Parolini, R. Millo, L. Moretta, and A. Moretta, "IL-12 or IL-4 prime human NK cells to mediate functionally divergent interactions with dendritic cells or tumors," *The Journal of Immunology*, vol. 174, no. 7, pp. 3992–3998, 2005.

273. M. E. Ross and M. A. Caligiuri, "Cytokine-induced apoptosis of human natural killer cells identifies a novel mechanism to regulate the innate immune response," *Blood*, vol. 89, no. 3, pp. 910–8, 1997.

274. B. B. Desai, P. M. Quinn, A. G. Wolitzky, P. K. Mongini, R. Chizzonite, and M. K. Gately, "IL-12 receptor. II. Distribution and regulation of receptor expression," *The Journal of Immunology*, vol. 148, no. 10, pp. 3125–32, 1992.

275. J. M. Farber, "Mig and IP-10: CXC chemokines that target lymphocytes," *Journal of Leukocyte Biology*, vol. 61, no. 3, pp. 246–57, 1997.

276. C. S. Tannenbaum, R. Tubbs, D. Armstrong, J. H. Finke, R. M. Bukowski, and T. a. Hamilton, "The CXC chemokines IP-10 and Mig are necessary for IL-12-mediated regression of the mouse RENCA tumor," *The Journal of Immunology*, vol. 161, pp. 927–932, 1998.

277. C. L. Nastala, H. D. Edington, T. G. McKinney, H. Tahara, M. A. Nalesnik, M. J. Brunda, M. K. Gately, S. F. Wolf, R. D. Schreiber, and W. J. Storkus, "Recombinant IL-12 administration induces tumor regression in association with IFN-gamma production," *The Journal of Immunology*, vol. 153, no. 4, pp. 1697–706, 1994.

278. M. J. Smyth, M. Taniguchi, and S. E. A. Street, "The antitumor activivty of IL-12: Mechanism of Innate Immunity that are model and dose dependent," *The Journal of Immunology*, vol. 165, no. 5, pp. 2665–2670, 2000.

279. D. L. Barber, E. Wherry, D. Masopust, B. Zhu, J. P. Allison, A. H. Sharpe, G. J. Freeman, and R. Ahmed, "Restoring function in exhausted CD8 T cells during chronic viral infection," *Nature*, vol. 439, no. 7077, pp. 682–687, 2006.

280. C. Blank, J. Kuball, S. Voelkl, H. Wiendl, B. Becker, B. Walter, O. Majdic, T. F. Gajewski, M. Theobald, R. Andreesen, and A. Mackensen, "Blockade of PD-L1 (B7-H1) augments human tumor-specific T cell responses in vitro," *International Journal of Cancer*, vol. 119, no. 2, pp. 317–327, 2006.

281. P. C. Tumeh, C. L. Harview, J. H. Yearley, I. P. Shintaku, E. J. M. Taylor, L. Robert, B. Chmielowski, M. Spasic, G. Henry, V. Ciobanu, A. N. West, M. Carmona, C. Kivork, E. Seja, G. Cherry, A. J. Gutierrez, T. R. Grogan, C. Mateus, G. Tomasic, J. A. Glaspy, R. O. Emerson, H. Robins, R. H. Pierce, D. A. Elashoff, C. Robert, and A. Ribas, "PD-1 blockade induces responses by inhibiting adaptive immune resistance," *Nature*, vol. 515, no. 7528, pp. 568–571, 2014.

282. J. T. Harty and V. P. Badovinac, "Shaping and reshaping CD8+ T-cell memory," *Nature Reviews. Immunology*, vol. 8, no. 2, pp. 107–19, 2008.

283. R. Bhat and C. Watzl, "Serial killing of tumor cells by human natural killer cells–enhancement by therapeutic antibodies," *PloS ONE*, vol. 2, no. 3, p. e326, 2007.

284. K. Taga, A. Yamauchi, K. Kabashima, E. T. Bloom, J. Muller, and G. Tosato, "Target-induced death by apoptosis in human lymphokine-activated natural killer cells," *Blood*, vol. 87, no. 6, pp. 2411–8, 1996.

285. H. Ida, T. Nakashima, N. L. Kedersha, S. Yamasaki, M. Huang, Y. Izumi, T. Miyashita, T. Origuchi, A. Kawakami, K. Migita, P. I. Bird, P. Anderson, and K. Eguchi, "Granzyme B leakage-induced cell death: A new type of activation-induced natural killer cell death," *European Journal of Immunology*, vol. 33, no. 12, pp. 3284–3292, 2003.

286. J. D. Brandstadter and Y. Yang, "Natural killer cell responses to viral infection," *Journal of Innate Immunity*, vol. 3, no. 3, pp. 274–279, 2011.

287. D. M. Benson, C. E. Bakan, A. Mishra, C. C. Hofmeister, Y. Efebera, B. Becknell, R. a. Baiocchi, J. Zhang, J. Yu, M. K. Smith, C. N. Greenfield, P. Porcu, S. M. Devine, R. Rotem-yehudar, G. Lozanski, J. C. Byrd, and M. a. Caligiuri, "The PD-1 / PD-L1 axis modulates the natural killer cell versus multiple myeloma effect : a therapeutic target for CT-011 , a novel monoclonal anti – PD-1 antibody," *Blood*, vol. 116, no. 13, pp. 2286–2294, 2010.

288. I. W. Mak, N. Evaniew, and M. Ghert, "Lost in translation: animal models and clinical trials in cancer treatment," *American Journal of Translational Research*, vol. 6, no. 2, pp. 114–8, 2014.

289. J. J. Zou, D. S. Schoenhaut, D. M. Carvajal, R. R. Warrier, D. H. Presky, M. K. Gately, and U. Gubler, "Structure-function analysis of the p35 subunit of mouse interleukin 12," *The Journal of Biological Chemistry*, vol. 270, no. 11, pp. 5864–71, 1995.

290. N. Boisgerault, J.-B. Guillerme, D. Pouliquen, M. Mesel-Lemoine, C. Achard, C. Combredet, J.-F. Fonteneau, F. Tangy, and M. Grégoire, "Natural oncolytic activity of live-attenuated measles virus against human lung and colorectal adenocarcinomas," *BioMed Research International*, vol. 2013, p. 387362, 2013.

291. R. H. Shoemaker, "The NCI60 human tumour cell line anticancer drug screen," *Nature Reviews. Cancer*, vol. 6, no. 10, pp. 813–823, 2006.

292. B. Jabri and V. Abadie, "IL-15 functions as a danger signal to regulate tissue-resident T cells and tissue destruction," *Nature Reviews. Immunology*, vol. 15, no. 12, pp. 771–83, 2015.

Publications

R. Veinalde, C. Grossardt, L. Hartmann, M.-C. Bourgeois-Daigneault, J. C. Bell, D. Jäger, C. von Kalle, G. Ungerechts,
"Oncolytic measles virus encoding interleukin-12 mediates potent anti-tumor effects through T cell activation," *OncoImmunology*, in press, 2017.*

C. E. Engeland., C. Grossardt, **R. Veinalde**, S. Bossow, D. Lutz, J. K. Kaufmann, I. Shevchenko, V. Umansky, D. M. Nettelbeck, W. Weichert, D. Jäger, C. von Kalle, G. Ungerechts,
"CTLA-4 and PD-L1 checkpoint blockade enhances oncolytic measles virus therapy," *Molecular Therapy*, vol. 22, no. 11, pp. 1949 – 1959, 2014.

R. Veinalde, R. Petrovska, R. Brūvere, G. Feldmane, D. Pjanova,
"*Ex vivo* cytokine production in peripheral blood mononuclear cells after their stimulation with dsRNA of natural origin," *Biotechnology and Applied Biochemistry*, vol. 61, no. 1, pp. 65 – 73, 2013.

R. Veinalde, A. Ozola, K. Azarjana, A. Molven, L. A. Akslen, S. Doniņa, G. Proboka, I. Čēma, A. Baginskis, D. Pjanova,
"Analysis of Latvian familial melanoma patients reveals novel variants in the non-coding regions of *CDKN2A* and that the *CDK4* mutation R24H is a founder mutation,", *Melanoma Research*, vol. 23, no. 3, pp. 221 – 226, 2013.

H. E. Puntervoll, X. Rang, H. H. Vetti, I. M. Bachmann, M. F. Avril, M. Benfodda, C. Catricalà, S. Dalle, A. B. Duval-Modeste, P. Ghiorzo, P. Grammatico, M. Harland, N. K. Hayward, H. H. Hu, T. Jouary, T. Martin-Denavit, A. Ozola, J. M. Palmer, L. Pastorino, D. Pjanova, N. Soufir, S. J. Steine, A. J. Stratigos, L. Thomas, J. Tinat, H. Tsao, **R. Veinalde**, M. A. Tucker, B. Bressac de Paillerets, J. A. Newton-Bishop, A. M. Goldstein, L. A. Akslen,
"Melanoma prone families with *CDK4* germline mutation: phenotypic profile and associations with *MC1R* variants," *Journal of Medical Genetics*, vol. 50, no. 4, pp. 264 – 270, 2013.

*Main results of this study are summarized in this publication.

Congress Contributions

R. Veinalde, L. Hartmann, C. von Kalle, D. Jäger, G. Ungerechts, C. E. Engeland.
Development of rational immunomodulation strategies for virotherapy.
Short talk. EMBL-Cancer Core Europe Conference on Cancer Immunotherapy,
February 2 – 4, 2017, Heidelberg, Germany.

R. Veinalde, C. Grossardt, M-C. Bourgeois-Daigneault, J. C. Bell, C. von Kalle, D. Jäger, G. Ungerechts, C. E. Engeland.
Determinants of efficacy in immunovirotherapy.
Short talk. Tenth International Meeting on Replicating Oncolytic Virus Therapeutics,
October 1 – 4, 2016, Vancouver, British Columbia, Canada.

R. Veinalde, C. Grossardt, M-C. Bourgeois-Daigneault, C. von Kalle, D. Jäger, G. Ungerechts, C. E. Engeland.
Determinants of efficacy in cancer immunovirotherapy.
Poster presentation. Second CRI-CIMT-EATI-AACR International Cancer Immunotherapy Conference: Translating Science Into Survival,
September 25 – 28, 2016, New York, New York, USA.

R. Veinalde, C. Grossardt, M-C. Bourgeois-Daigneault, C. von Kalle, D. Jäger, G. Ungerechts, C. E. Engeland.
Exploring determinants of efficacy in immunovirotherapy.
Poster presentation. XXII Annual Meeting of German Society for Gene Therapy,
September 14 – 16, 2016, Heidelberg, Germany.

R. Veinalde, C. E. Engeland, C. Grossardt, D. Jäger, C. von Kalle, G. Ungerechts.
Development of oncolytic measles virus with immunomodulatory transgenes.
Poster presentation. XXI Annual Meeting of German Society for Gene Therapy,
February 26 – 28, 2015, Vienna, Austria.

Acknowledgements

I would like to express my gratitude to everyone who supported me throughout the preparation of this study:

Prof. Dr. Dr. Guy Ungerechts for his trust, giving the opportunity to work on this exciting project;

Dr. Dr. Christine E. Engeland for her excellent supervision, constructive criticism, valuable advice, optimism and friendly help at all times;

Prof. Dr. Harald zur Hausen for the Melanie and Eduard zur Hausen fellowship;

Prof. Dr. Christof von Kalle as a referee for my PhD thesis and a member of my Thesis Advisory Committee (TAC), Prof. Dr. Ralf Bartenschlager as a Chairperson of my Examining Committee and member of my TAC, PD Dr. Dr. Angelika Riemer as a member of my TAC;

Dr. Dirk Grimm and PD Dr. Karin Müller-Decker as members of my Examining Committee;

Dr. Marie-Claude Bourgeois-Daigneault for her support with CBA experiments;

All present and former members of AG Ungerechts for creating a productive, but most importantly always friendly working atmosphere.

Thesis Declaration

I hereby declare that I have written the submitted dissertation myself and in this process I have used no other sources or materials than those expressly indicated. I hereby declare that I have not applied to be examined at any other institution, nor have I used the dissertation in this or any other form at any other institution as an examination paper, nor submitted it to any other faculty as a dissertation.

Heidelberg, February 28, 2017 Rūta Veinalde